EXPERIMENTAL IN SITU INVESTIGATION OF THE EFFECTS OF PROTONS, ULTRAVIOLET RADIATION, AND TEMPERATURE ON THERMOPHYSICAL PROPERTIES OF SOLAR CELL FILTERS AND OTHER SPACECRAFT MATERIALS

Prepared by

Lawrence B. Fogdall and Sheridan S. Cannaday

The Boeing Company

Research and Engineering Division

Final Report for Jet Propulsion Laboratory Program HF 525908

Radiation Effects on Optical Properties of Solar Cells and Filters

February 1971

EXPERIMENTAL *IN SITU* INVESTIGATION OF THE EFFECTS OF PROTONS, ULTRAVIOLET RADIATION, AND TEMPERATURE ON THERMOPHYSICAL PROPERTIES OF SOLAR CELL FILTERS AND OTHER SPACECRAFT MATERIALS

Prepared by

Lawrence B. Fogdall and Sheridan S. Cannaday

The Boeing Company

Research and Engineering Division

Final Report for Jet Propulsion Laboratory Program HF 525908

Radiation Effects on Optical Properties of Solar Cells and Filters

February 1971

This work was performed for the Jet Propulsion Laboratory, California Institute of Technology, sponsored by the National Aeronautics and Space Administration under Contract NAS7-100.

ABSTRACT

An investigation was conducted to determine *in situ* the effects of ultraviolet radiation and solar wind protons on materials considered for use on the 1973 Venus-Mercury flyby vehicle. The experimental program involved more than 2400 hours of continuous radiation-facility testing, preceded, interrupted, and followed by *in situ* thermophysical property measurements on transmissive solar cell filters, opaque solar cell-filter stacks, adhesives, 7940 fused silica, and Kapton film. Sun rate, solar wind rate, and sample temperature were all increased with time during the 2400 hours, providing an accurate simulation of radiation conditions along the planned flyby trajectory. Final exposure levels of 12,000 ESH and 10^{16} protons/cm^2 were reached. Solar absorptance increased and solar transmittance decreased in most solar cell filters. The solar absorptance of solar cell-filter stacks also increased. Changes measured in solar cell filters were generally less than changes measured on solar cell-filter stacks. Both ultraviolet and proton exposure reduced the effectiveness of the ultraviolet rejection coatings in the solar cell filters. In some materials, simultaneous exposure to protons and ultraviolet radiation yielded synergistic damage greater than the sum of proton degradation and ultraviolet degradation in separate samples. Thermal damage in unbonded Kapton film was catastrophically large.

TABLE OF CONTENTS

LIST OF FIGURES

LIST OF FIGURES (Continued)

LIST OF FIGURES (Continued)

LIST OF FIGURES (Continued)

LIST OF FIGURES (Continued)

LIST OF TABLES

INTRODUCTION

A flyby of the planets Venus and Mercury during the 1973-1974 time period is planned as part of the National Aeronautics and Space Administration's continuing unmanned planetary exploration program. Successful completion of a space flight to within 0.4 astronomical unit (the approximate radius of Mercury's orbit about the sun) raises new requirements for temperature control of the flyby vehicle. At 0.4 AU the solar intensity is some six times that at Earth (1 AU). Temperature control of a flyby vehicle's solar array is particularly critical, for whereas the more intense solar radiation closer to the sun can provide increased conversion energy for electrical power generation, definite temperature control is required to limit any drop in conversion efficiency and, indeed, to forestall system failure from the high temperatures anticipated. Such solar array materials as state-of-the-art solders used heretofore would be expected to melt, raising the likelihood of loss of electrical continuity while the flight is in progress.

Typical temperature regimes expected during a Venus-Mercury flyby have been discussed elsewhere (Reference 1 is an example) and several feasible methods of reducing temperature extremes have been proposed. Variable-geometry solar panels have been designed, for example, so that their effective projected area exposed to the sun can be reduced at will as solar intensity rises. Various ratios of active cell areas to inactive reflector areas on a solar panel have been studied with the idea of rejecting as much incident solar energy as possible with a "mirror mosaic". Another solar panel design concept for spacecraft bound inward toward the sun involves transmitting only certain wavelengths of the sun's energy to solar cells — wavelengths the cells can utilize most efficiently for conversion to electrical power — and rejection (reflection) of as much as possible of the untransmitted energy. In any investigation of such spectrally selective "bandpass" filters for solar cells, an emphasis is placed on trading off filter thermophysical properties (such as solar absorptance, solar transmittance, and thermal emittance) for energy conversion properties. State-of-the-art solar cells (such as 18-mil-thick n/p 2 ohm-cm cells used in recent NASA space flights) accomplish energy conversion with light between

0.4 and 1.2 micron wavelength, and utilize 0.6 to 1.0 micron wavelength radiation most efficiently. Therefore, on the missions where incident radiation is abundant, the objective in employing bandpass filters is to transmit and allow a solar cell to utilize photon energy within the wavelength region stated above, while simultaneously reflecting unwanted radiation outside that wavelength region. This calls for filter design of infrared rejection capability as well as ultraviolet rejection.

Rejection of ultraviolet radiation has become a standard feature for solar cell filters, since ultraviolet radiation often is a cause of component degradation in space. Ultraviolet rejection is normally accomplished by an appropriate coating on a solar cell "cover glass". The glass (or quartz) stops damaging low energy space particulate radiation while transmitting radiation useful for energy conversion; the cover glass also provides a substrate for a first surface anti-reflection coating to maximize such useful radiation. Previous surveys and experiments (such as References 2 and 3) have uncovered degradation in both coatings and substrates. The entire spectrum of radiation effects must thus be examined: surface effects in the first and second surface coatings; bulk effects in the substrate and bonding agent between filter and cell. This program has spanned a broad investigation to increase understanding of anticipated effects during the upcoming Venus-Mercury mission. Radiation sources of concern included solar ultraviolet radiation and solar wind protons. Solar wind protons have an exceedingly short range in most materials, so that their displacement and ionization damage is anticipated only in first surface coatings, or in the first thousand or so Ångstroms of an uncoated substrate or other material. Outside the scope of the program were alpha particles, "heavy" ions from the sun, neutralizing "thermal" electrons in the solar wind, and high energy solar and a galactic cosmic ray particles. It is widely felt that this listing of included and excluded interplanetary radiation sources is roughly in the order of decreasing importance, taking into account relative abundances, damage mechanisms, and relative effectiveness for damage.

Thermophysical properties investigated within the scope of this program have included spectral and total absorption, transmission, and reflection properties of several candidate spacecraft materials including solar cell filters (discussed in detail hereinafter), and, of course, the effects of solar proton and ultraviolet radiation on these properties. Beyond the scope of the program and left to be determined in the future are the effects of solar ultraviolet and particle radiation on the thermal emittance of spacecraft materials and components.

EXPERIMENTAL PROGRAM

An experimental program to investigate the effects of space radiation on components and materials aboard the 1973 Venus-Mercury spacecraft was initiated at the Jet Propulsion Laboratory (JPL) in 1969. This document constitutes the final report to JPL of work done within that program framework at the Boeing Radiation Effects Laboratory (BREL) during 1970. The Boeing Company was asked to do experimental work including a 2400-hour simulation of the Venus-Mercury mission. This interplanetary flight calls for a transit of a space vehicle to the neighborhood of Venus over a real-time period of approximately 2900 hours. Gravitational attraction during the Venus flyby will alter the spacecraft trajectory so that Mercury is approached some 1400 hours later. The mission concludes with a post-Mercury-encounter phase on the order of 500 hours long.

The 2400-hour experimental investigation constitutes a minimal test acceleration factor of 2 over the real-time mission. Figure 1 shows the basic test exposure plan insofar as simulated ultraviolet radiation and solar wind intensity are concerned. A five-fold increase from 2 to 10 suns and solar wind intensities (relative to Earth orbit at 1 AU) assumes Mercury encounter at aphelion (0.43 AU).

Accurate simulation of temperature excursions expected in various materials tested was also included in the experimental plan. The importance of providing for this is discussed later in this document. Figure 2 represents the temperature of test sample substrates as a function of time (test hours) during the simulated mission. The predicted temperature profile with time, as calculated assuming certain absorption and emission properties of solar panel components, without radiation degradation being considered, is compared in Figure 2 with the actual temperature "schedule" employed during the 2400-hour radiation exposure test.

Test Materials

Emphasis during this experimental program has been placed on 3 "bandpass" solar cell filters that are candidates for the 1973 Venus-Mercury space flight. These filters have been evaluated alone and in combination with n/p 2 ohm-cm cells.

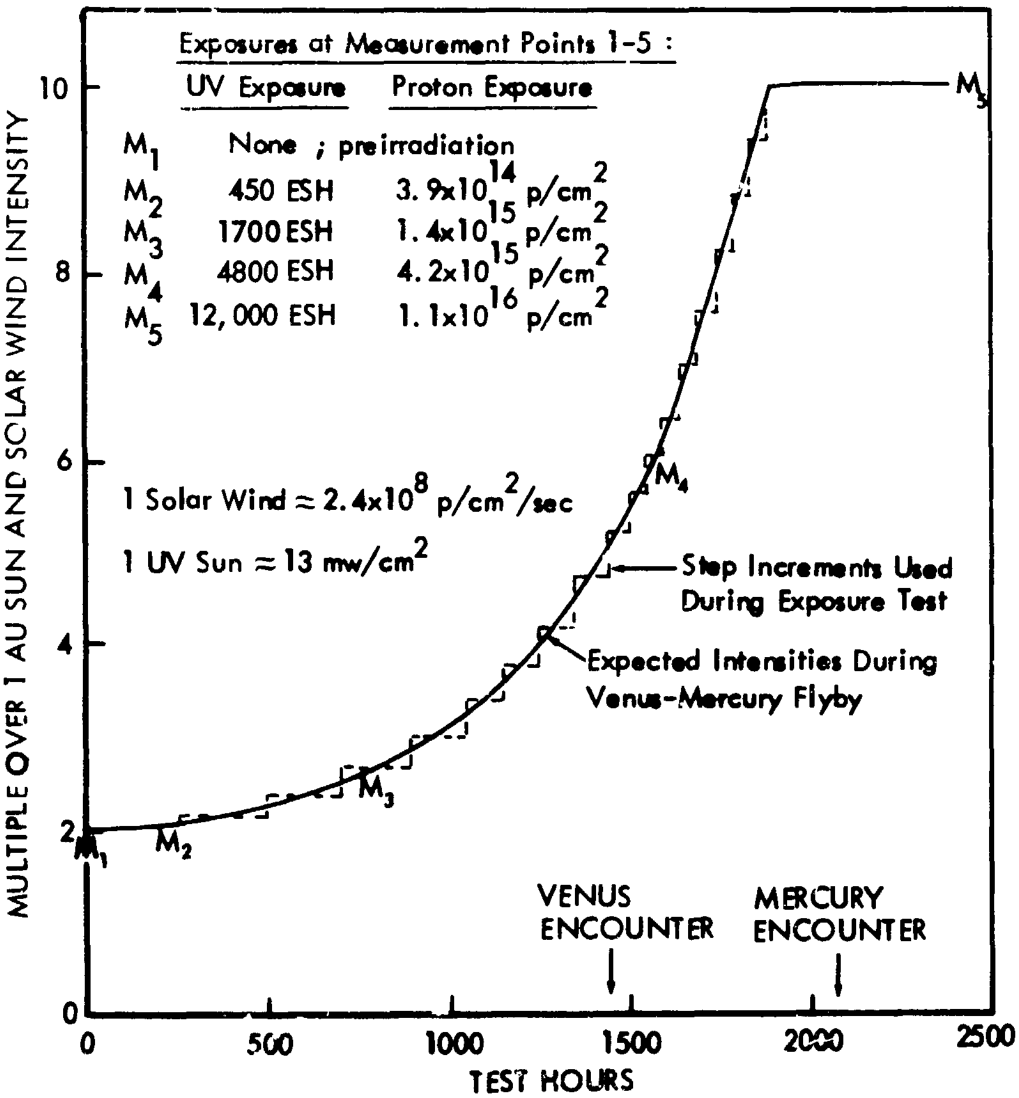

Figure 1. Increase in Ultraviolet Sun and Solar Wind Rates During Simulated Venus-Mercury Mission

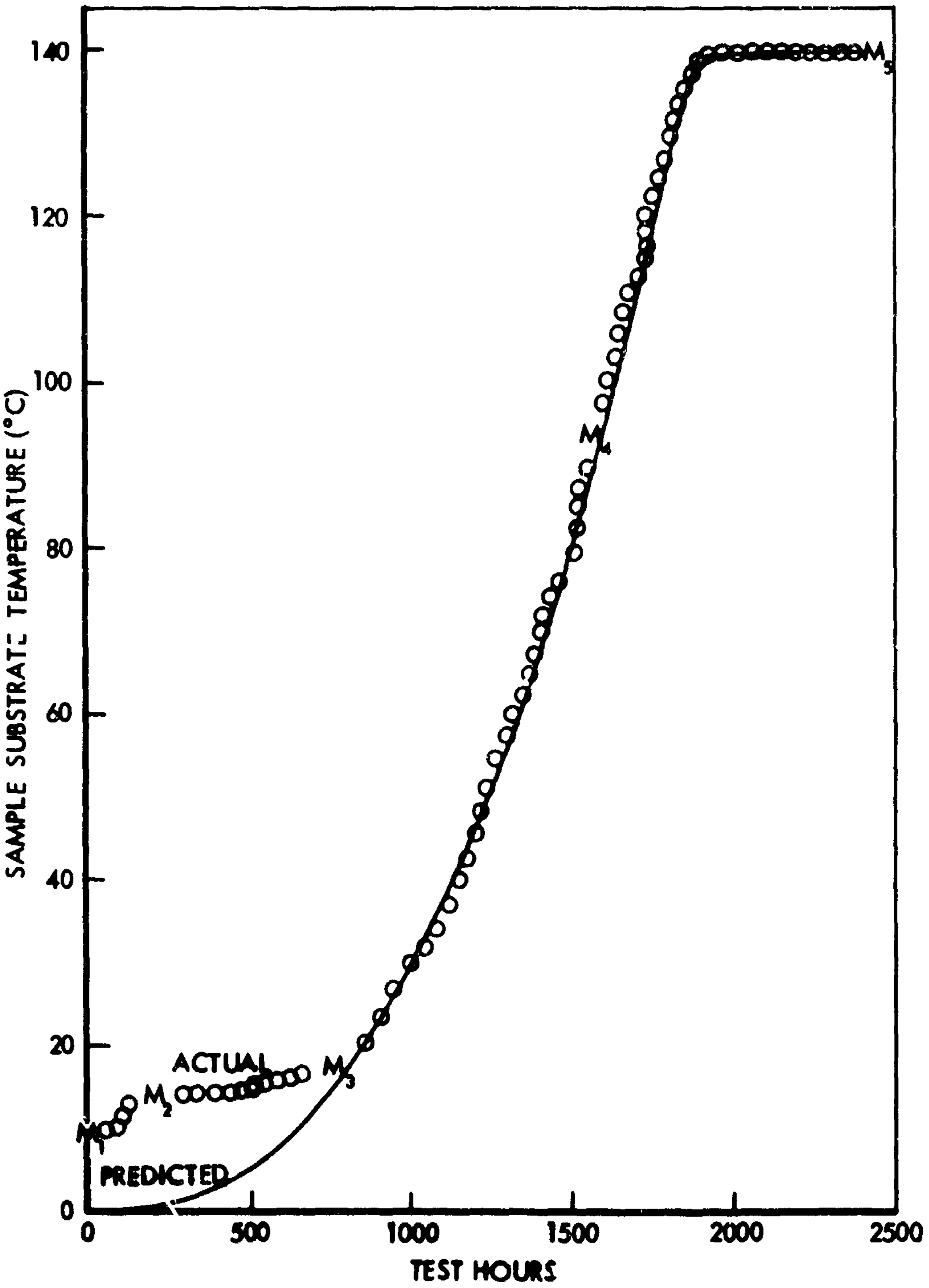

Figure 2. Sample Substrate Temperatures During Simulated Venus-Mercury Mission

Other materials investigated include uncoated 20-mil Corning 7940 fused silica substrates employed for the filter coatings, adhesives between 7940 quartz and aluminum reflectors, and Kapton polyimide film being evaluated for possible use as a thermal shield over much of the Venus-Mercury spacecraft. All these types of materials are listed in Table 1.

Table 1 also delineates the type of exposure (ultraviolet-only, proton-only, or simultaneous proton/ultraviolet radiation exposure) received by each sample coded with a JPL-assigned number. The table identifies the numbers assigned to samples evaluated during the 2400-hour exposure, and during a preliminary 500-hour exposure discussed later under "Temperature Effects." Sample sizes of 2 cm by 2 cm (the size chosen for space flight use), in combination with the total number of samples and material types to be exposed, placed a severe constraint on available beam size. Program schedule did not provide for development of technical ways to alleviate this constraint (such as multiple runs, beam expansion, or defocusing beyond that already available), but reduction of filters in the 2400-hour test to a 1 cm by 1 cm size did provide some relief as to total sample array size.

Significant pre-irradiation sample-to-sample differences were noted, especially in the infrared-wavelength-region reflectance characteristics of several types of materials. The silicone adhesives investigated exhibited appreciable sample-to-sample variations in infrared absorption bands centered at 1.7 and 2.3 microns. Likewise, cell/filter combinations as received had different pre-irradiation reflectance values at wavelengths longer than about one micron. Smaller reflectance value variations were measured at shorter wavelengths (visible and ultraviolet regions) in the various cells, filters, and adhesives tested. These measured sample-to-sample differences are shown in spectral plots included later in the "Experimental Results" section.

Table 1. Solar Panel and Other Materials Investigated and Type and Amount of Radiation Exposure Received.

Type of Test Sample	Sample Number and Exposure Received					
	2400 hr Test			500-hr Test		
	UV	p+	UV/p+	UV	p+	UV/p+
Blue filter on 2 Ω-cm cell	2074	2092	2083	2035	2047	2041
Modified 4026 filter on cell	2075	2093	2084	2036	2048	2042
Blue-Red filter on cell	2076	2094	2085	2040	2052	2046
Blue filter alone	2077	2095	2086	2038	2050	2044
Modified 4026 filter alone	2078	2096	2087	2039	2051	2045
Blue-Red filter alone	2079	2097	2088	—	—	—
Clear glass (7940 fused silica)	2080	2098	2089	—	—	—
Clear glass/RTV-602 adhesive/polished aluminum	2081	2099	2090	—	—	—
Clear glass/XR6-3489 adhesive/polished aluminum	2082	2100	2091	—	—	—
Blue-Red filter/adhesive/ polished aluminum substrate	—	—	—	2037	2049	2043
3-mil Kapton polyimide film	—	one sample	one sample	—	—	—

Initial transmission properties were found to exhibit less variation from sample to sample, with the exception of the type 4026 bandpass filter, in which cuton and cutoff wavelengths changed slightly (up to 10 mμ) from sample to sample. This caused only slight variances in measured thermophysical properties (solar-weighted values), but created significant yet solvable problems in computer-processing of separate spectral reflectance and spectral transmittance data to determine spectral absorptance properties of the 4026 filter (see Data Acquisition and Processing section below).

Table 2 and Figure 3 give additional details about characteristics of the filter samples investigated during this program. Table 2 lists reflection and transmission characteristics for the 3 filters (blue, blue-red, and 4026) that were evaluated both alone and in stack combinations with solar cells. Included are cuton and cutoff wavelengths of each filter alone, and an indication of the spectral selectiveness achieved by the multilayer interference designs. Figure 3 shows "exploded" views of each of the 3 filters tested in two configurations — alone (both reflectance and transmittance properties measured) and cemented to cells (reflectance/absorptance properties determined). A comparison of filter-only and filter/cell reflectance curves in Appendix A shows that certain wavelength shifts occur as a result of cementing filters to solar cells. Two of the largest shifts are (a) the "red peak" in blue-red filters, which is shifted approximately 20 millimicrons toward longer wavelengths, and (b) the 4026 filter cuton wavelength near 0.6 micron, which shifts approximately 10 millimicrons toward longer wavelengths.

Exposure Apparatus

Further development of the existing and proven Boeing combined radiation effects test chamber (CRETC) has taken place in support of this solar cell/filter effects program. The principal capability expansion has been the installation of an <u>in situ</u> transmission measurement system, together with an optical adjustment mechanism making possible the measurement of various sample sizes in both reflectance and transmittance modes.

Principal features of the CRETC facility have been described in earlier reports (References 4-6) for similar radiation effects investigations. Description of those portions of the facility applicable to this program is repeated here. Figure 4 is an overall view of the CRETC and its associated low energy particle accelerator (LEPA). The LEPA is capable of delivering positive ions extracted from its RF-

Table 2. Spectral Transmission Characteristics of Three Solar Cell Filters Investigated

2a. Blue Filter Characteristics:

1. Antireflection coating. To produce reflection of less than 2% in the region 600 to 800 millimicrons.
2. Cuton. 410 mμ at 50% transmission ± 15 mμ.
3. Ultraviolet rejection. Less than 1%.
4. Transmission characteristics. The mini..ıum transmittance measured at normal incidence in air is as follows:

   500 mμ to 600 mμ - 85 %
   600 mμ to 1100 mμ - 90 %
   600 mμ to 800 mμ - Not less than 94% average
   450 mμ to 1100 mμ - Not less than 94% average

2b. 4026 (Modified design) Filter Characteristics:

1. Antireflection coating - None
2. Cuton. 650 mμ at 50% transmission ± 20 mμ.
3. Ultraviolet rejection. Less than 1 %.
4. Cutoff. 1000 mμ at 50 % transmission ± 40 mμ.
5. Transmission characteristics. The minimum transmittance measured at normal incidence in air is as follows:

   700 mμ to 950 mμ - Not less than 75 % average.

6. Infrared cuton. 1900 mμ at 50% transmission ± 40 mμ.
7. Infrared rejection. 1050 mμ to 1800 mμ - Not less than 95% average.

2c. Blue-Red Filter Characteristics:

1. Antireflection coating. To produce reflection of less than 2% in the region 600 to 800 millimicrons.
2. Cuton. 400 mμ at 50% transmission ± 15 mμ.
3. Ultraviolet rejection. Less than 1% .
4. Cutoff. 1130 mμ at 50% transmission ± 40 mμ.
5. Transmission characteristics. The minimum transmittance measured at normal incidence in air is as follows:

   600 mμ - 800 mμ - Not less than 92% average

6. Infrared rejection. 1165 mμ to 1450 mμ - Not less than 95% .

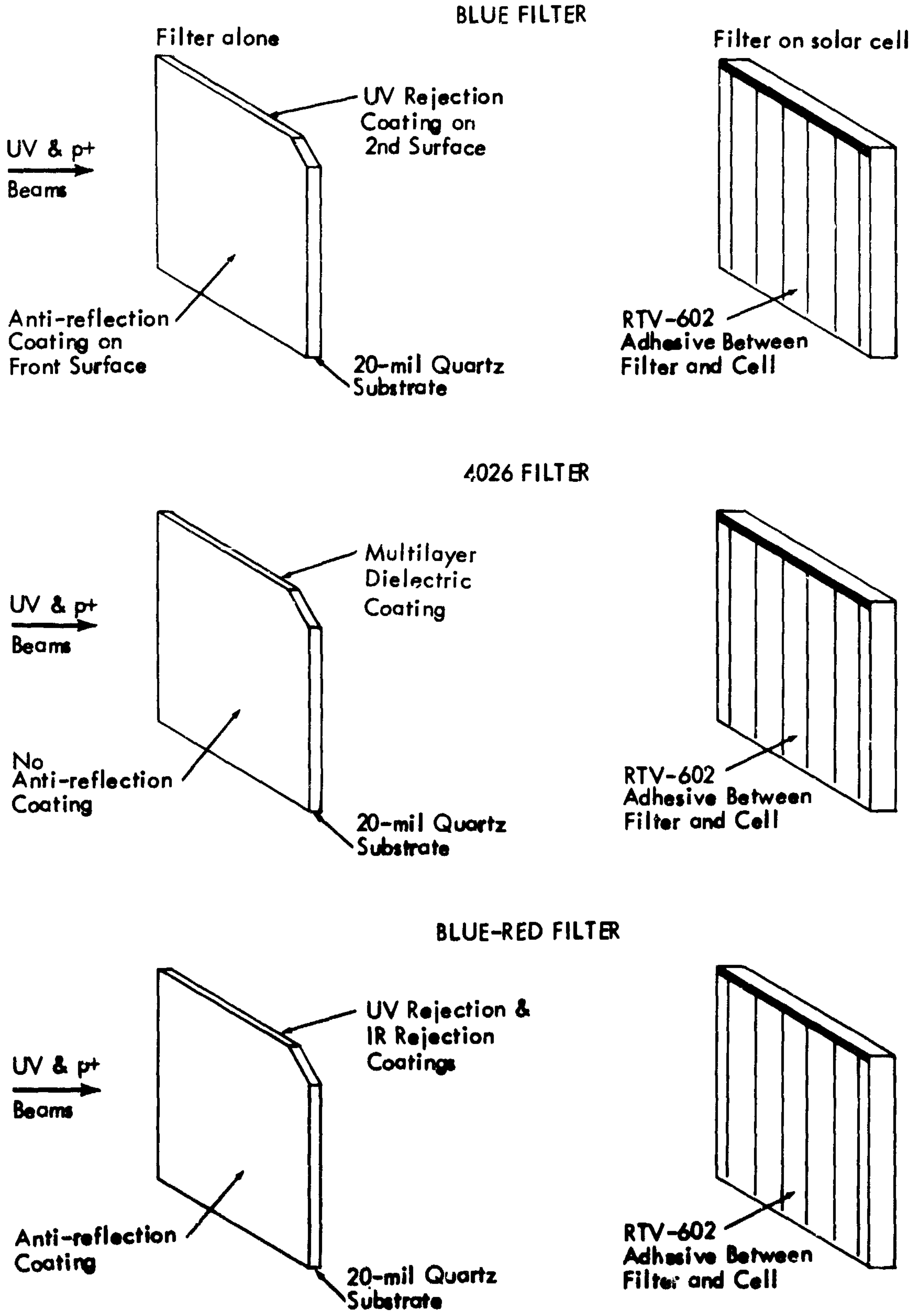

Figure 3. Exploded View of Three Filters Investigated and the Two Configurations Tested

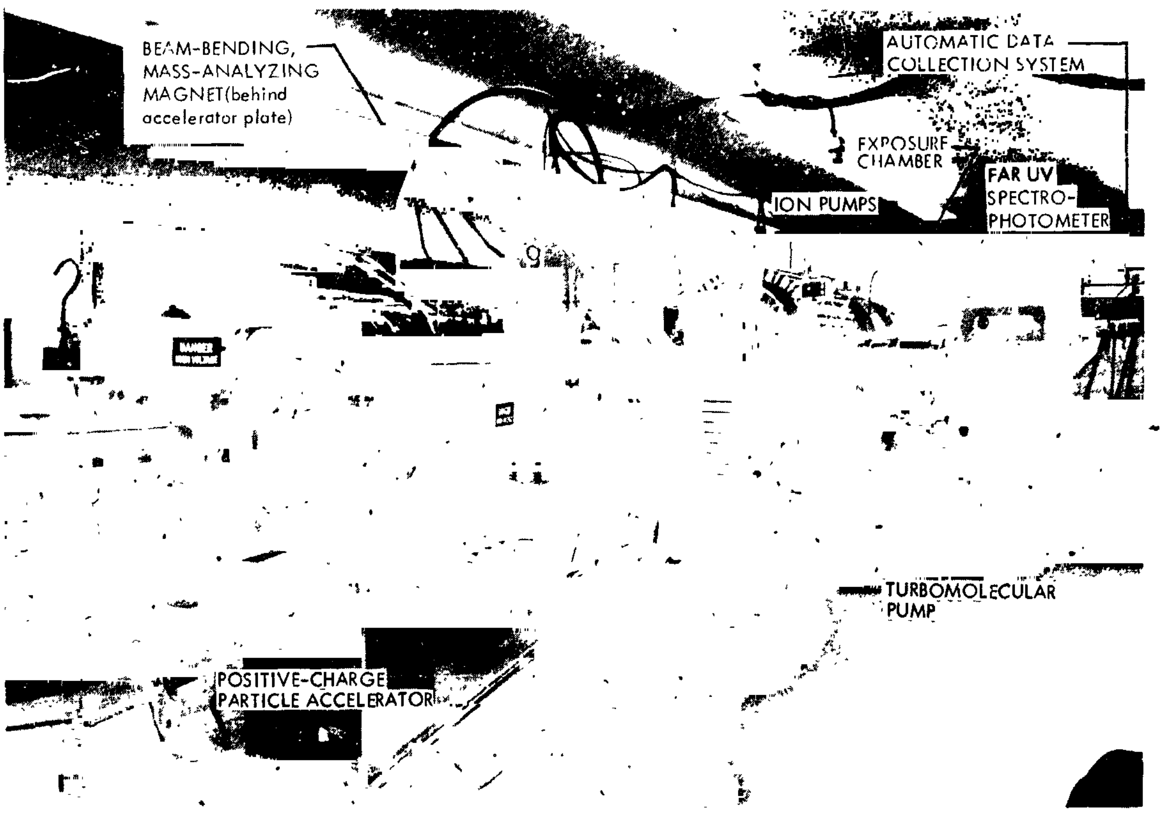

Figure 4. Experimental Facility for Combined Radiation Effects Studies and Evaluation in Situ

excited plasma to the CRETC, with particle energies selectable within the range 0.5 to 100 keV (kilo electron volts). For this program, 3-keV protons were extracted from the LEPA source and separated from other hydrogen species by a bending and mass-analyzing magnet between the LEPA and CRETC. The proton beam, with further defocusing inside the CRETC, was delivered on the sample plane at anticipated solar wind rates (10^8 - 10^9 protons/cm^2-second).

Figure 5 is a view of the opposite end of the CRETC facility. With the chamber door open, sample positions and interior equipment are apparent. The sample and dosimetry arrays are positioned in Figure 5 so that, were the chamber door closed, the sample holder would be adjacent to the integrating sphere, and the particle dosimetry tabs would be in the exposure position. More precisely, the lower group of dosimetry tabs seen within a dashed rectangle at the extreme left of Figure 5 would be adjacent to the rectangular proton channel and UV baffle.

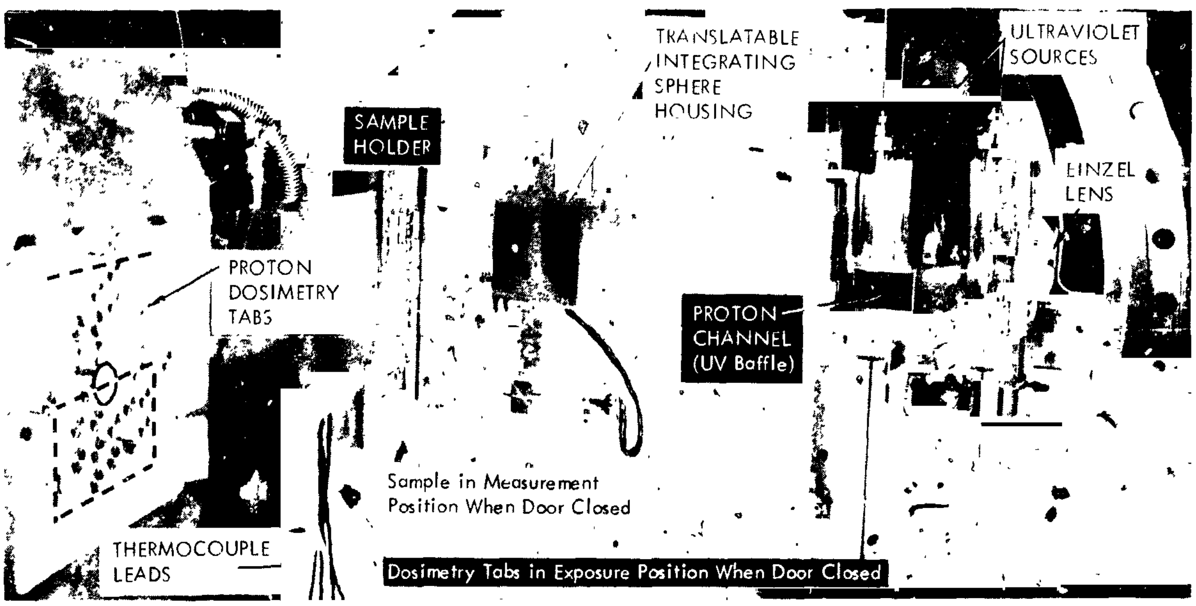

Figure 5. CRETC Ultraviolet Sources, Integrating Sphere, Sample Holder, and Other Interior Equipment

This baffle is positioned so that none of the lamp radiation (whether ultraviolet or longer wavelengths) can directly reach sample positions inside this rectangularly shaped area. The charged particle beam (protons in this program), however, is on a line of sight from the LEPA beam port through the defocusing Einzel lens to samples placed within the rectangular area. Thus, samples placed there are denoted the "proton only" array, but it should be kept in mind that energy from the ultraviolet source lamp(s) is scattered and reflected throughout the chamber, and a small amount can enter the proton channel. The intensity involved is a minute fraction of one sun, and due to the poor reflectance of stainless steel in the ultraviolet, the wavelengths involved are almost entirely in the visible and near-infrared wavelength regions.

Samples placed just above the proton channel, anywhere throughout an area the size and shape of the proton channel cross-section, receive both proton exposure and ultraviolet radiation exposure. On the dosimetry tab array at the left of Figure 5, this proton plus UV region extends above the dashed-line rectangle to the single dashed line which is near the uppermost proton tab. Thus, the entire array of some two dozen dosimetry tabs serves to map the uniformity of the proton beam at any given time. Absolute proton intensity is measured with a Faraday cup behind an aperture in the center of the dosimetry tab array. The uniformity and absolute measurements are correlated when the entire sample holder and dosimetry arm is moved, which rotates the tab just above or just below the aperture into the space usually occupied by the aperture. For the relatively large arrays of samples exposed to protons (and protons plus ultraviolet radiation) during this program, spatial uniformity has been maintained within plus or minus 20 percent. The LEPA has a deliverable proton flux range much in excess of the 2-solar wind to 10-solar wind variation with time called for in Figure 1, so that appropriate selection of LEPA controls provides the various proton intensities indicated.

The ultraviolet radiation for the simulated Venus-Mercury mission exposure is emitted by arc discharges in either or both of two long-arc xenon lamp sources seen at the right in Figure 5. Selection of one lamp or both, coupled with the large wattage range over which each lamp maintains its arc discharge, has provided a sun rate selection range large enough to encompass the 2-sun to 10-sun variation with time called for in Figure 1. Sun rates have been determined from radiometer output levels taken with and without a UV-absorbing filter over the radiometer detector. Uniformity of ultraviolet radiation intensity over the sample array is determined by "mapping" with the radiometer held in a precision jig. For the relatively large arrays of samples exposed to ultraviolet radiation during this program, spatial uniformity has been maintained within plus or minus 10 percent.

The temperature control system used during this program is diagrammed in Figure 6. The system was used in a mode wherein incoming nitrogen gas was always heated or used at its ambient temperature. This resulted in the temperature range +10°C to +140°C previously depicted in Figure 2. (A different configuration would be used to cool gas or even supply liquid nitrogen to simulate conditions during space flight to the outer planets.) During much of the testing period the controlled temperature was virtually without fluctuation, and within one degree Celsius of the desired value. On occasion, such as during UV lamp wattage changes or at times of changing temperature "set point", excursions up to ±5°C occurred while the proportional controller adjusted to the new value. The sample holder in the CRETC constitutes a relatively large thermal mass. Consequently temperature changes

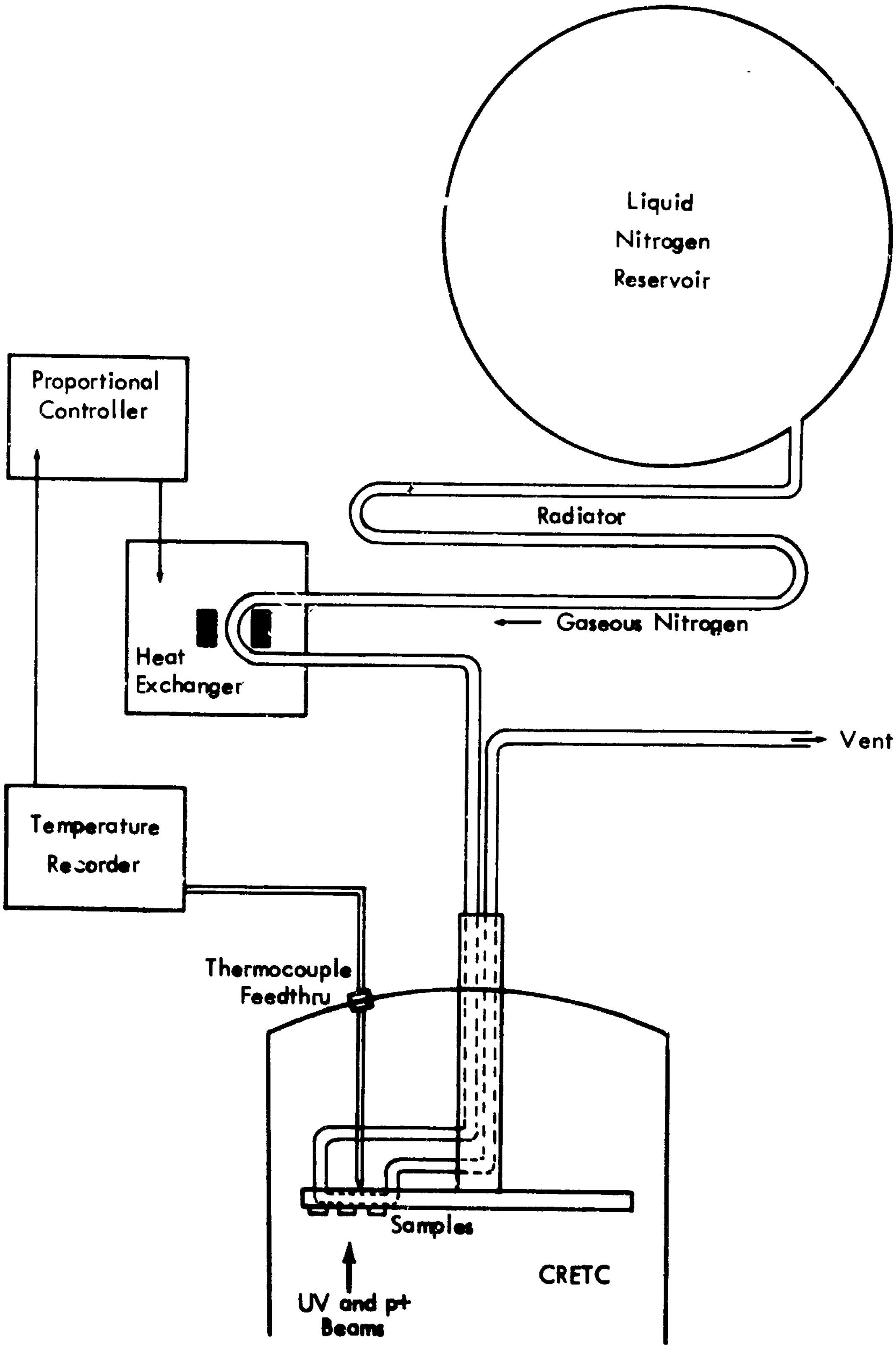

Figure 6. CRETC Sample Substrate Temperature Control System

occur at relatively low rates. (An additional example is that approximately one hour is needed to elevate sample holder and samples from room temperature to +140°C.) In evaluating results of the 2400-hour and preliminary 500-hour exposure tests, it should be remembered that, including measurement periods, samples were "at temperature" somewhat longer than the indicated hour periods. For the 2400-hour test, the time was approximately 2600 hours, spread fairly evenly over the test period and concentrated during measurement periods. During the preliminary 500-hour test equipment problems were encountered and consequently the samples were at +140°C for a total time of approximately 900 hours, including measurement periods.

Vacuum levels of 1×10^{-7} torr and better were achieved during exposure periods, using combinations of ion, cryogenic, and turbomolecular pumping. During times of sample measurement, vacuum levels of 3×10^{-8} torr were typically reached.

Sample Measurement Apparatus

Apparatus used to evaluate in situ spectral reflectance, transmittance, and absorptance properties of solar cell filters, adhesives, and Kapton film during this program is shown in Figure 7. The equipment external to the CRETC vacuum chamber includes a double-beam, ratio-recording far UV spectrophotometer, a data encoder and readout system, and a card punch. This sample measurement system enables spectral data to be recorded in the normal way as raw data on spectrophotometer charts, and simultaneously to be punched on cards for subsequent computer processing.

The in situ portion of the measurement system can be described in the following way. An integrating sphere reflectometer is situated in vacuo such that a translational movement of the sphere (Figure 5), coupled with a rotational movement of the sample holder on its "arm" (Figures 5 and 8) will bring any desired sample into position for measurement at the sphere's sample port. In Figure 8b the sample and dosimetry arrays are rotationally in transit from measurement and exposure positions (respectively) to their exposure and measurement positions (respectively). The camera angle in Figure 8b exposes to view the fixed Faraday cup described

Figure 7. Reflectance Measurement and Data Collection Systems

earlier, and the in situ sample transmission measurement source. Filter samples are mounted at a common radial distance from the sample arm pivot point, so that with one translational setting of the integrating sphere port, all filters can be measured by bringing each in turn in front of the sphere sample port with a rotational movement of the sample arm. The larger solar cell samples and adhesive samples are similarly mounted along common radii, most clearly shown in Figure 8c. Figure 8c also shows the grouping of samples into horizontal rows for proton-only exposure, ultraviolet-only exposure, and simultaneous proton/ultraviolet exposure.

Figure 8a. Sample Arm in Measurement Position and Dosimetry Arm in Exposure Position

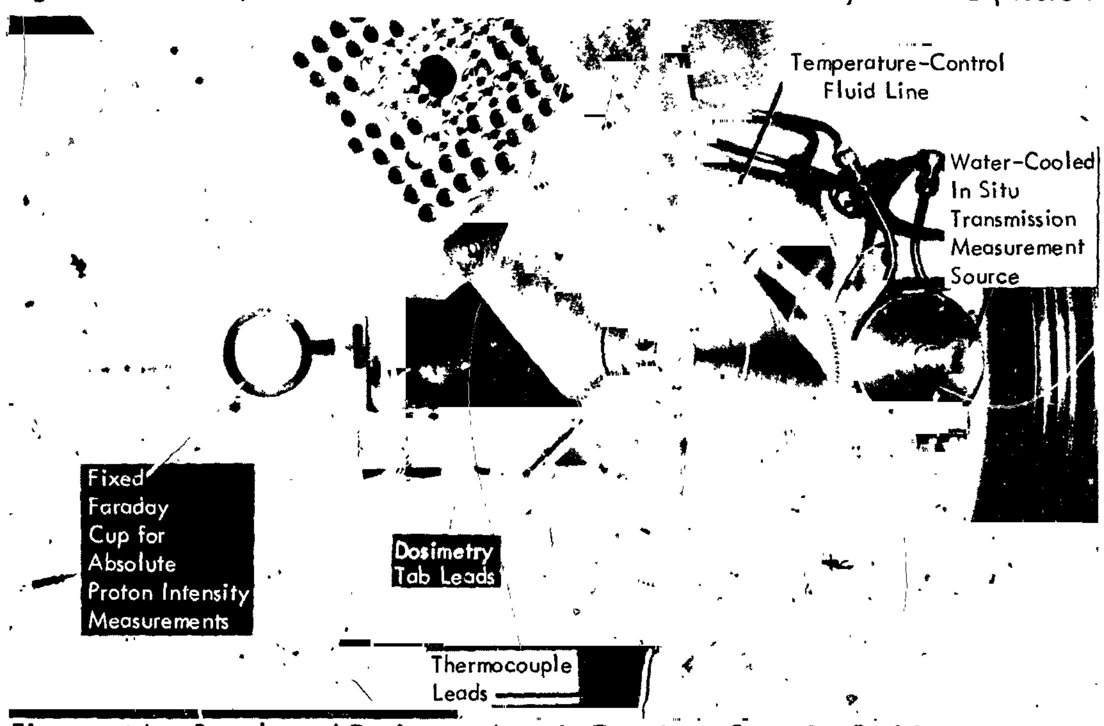

Figure 8b. Sample and Dosimetry Arms in Transit to Opposite Positions

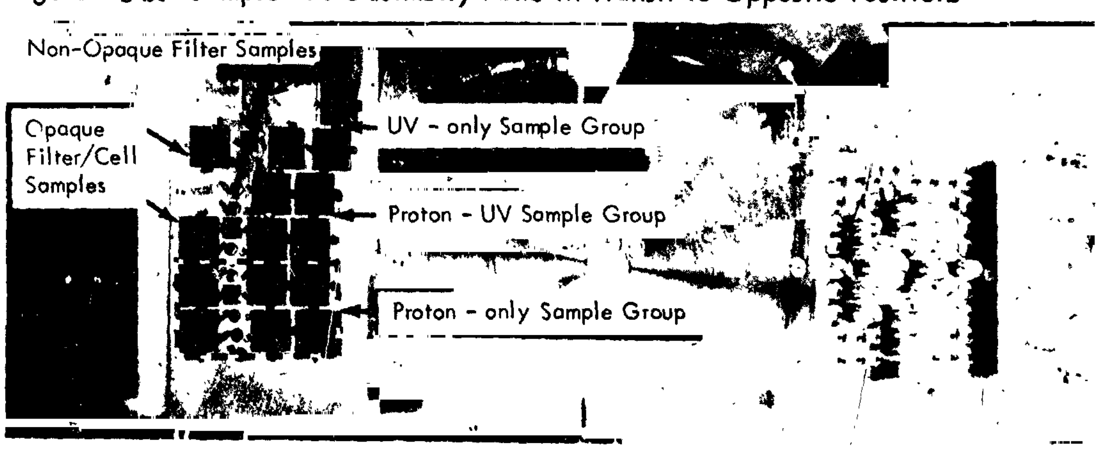

Figure 8c. Sample Arm in Exposure Position

Figure 9 represents a top-view, line diagram of the in situ sample measurement system. The double-beam configuration for reflectance measurements has been proven on numerous programs over the past 4 years. It provides reflectance data with high precision and repeatability (± 1/2 percent or better) which is only possible by using a double-beam-type reference. The reference is the magnesium oxide/Z-93 coating on the integrating sphere wall. In making a measurement, a reference curve is produced by (1) pivoting the sample beam mirror away from the sample port (using a solenoid in vacuo) so that the sample beam also strikes the MgO wall (dashed line inside the integrating sphere in Figure 9a), and (2) scaling the chart to the proper value with the spectrophotometer 100 percent potentiometer. Then sample reflectance is measured by returning the sample beam to the sample port. Being a continuous-scan instrument, the Beckman DK-2A spectrophotometer includes (when operating double-beam) an internal program to adjust slit width as source energy and detector sensitivity change with wavelength.

Because of limited time during this program, addition of transmission measurement capability to the CRETC facility has been restricted to an interim configuration utilizing a lamp source in vacuo, optically coupled to the sample beam path discussed above, and terminating with the appropriate detectors mounted beyond the monochromator (Figure 9b). Thus, for determining transmission properties during this program, single-beam directional measurements have been made, the sample beam passing through the integrating sphere, but not impinging on its walls. In the single-beam (energy) mode, the DK-2A provides for manual selection of slit width, source energy, and detector/amplifier gain. Then pen response between zero and 100 percent is a function of all these three parameters times percent transmittance. Normalization to display percent transmittance alone simply requires a different form of reference curve than the one generated for reflectance measurements. This is done with a reference port adjacent to (i.e., in the same row as) the filter samples (a total of 13 ports in Figure 8c). The optical equivalence of the 13 ports was determined before mounting samples; among all 13 ports there is less than one-tenth of one percent variation in effective transmittance. Thus only one port not covered with a sample validly serves as a reference for all 12 filter samples.

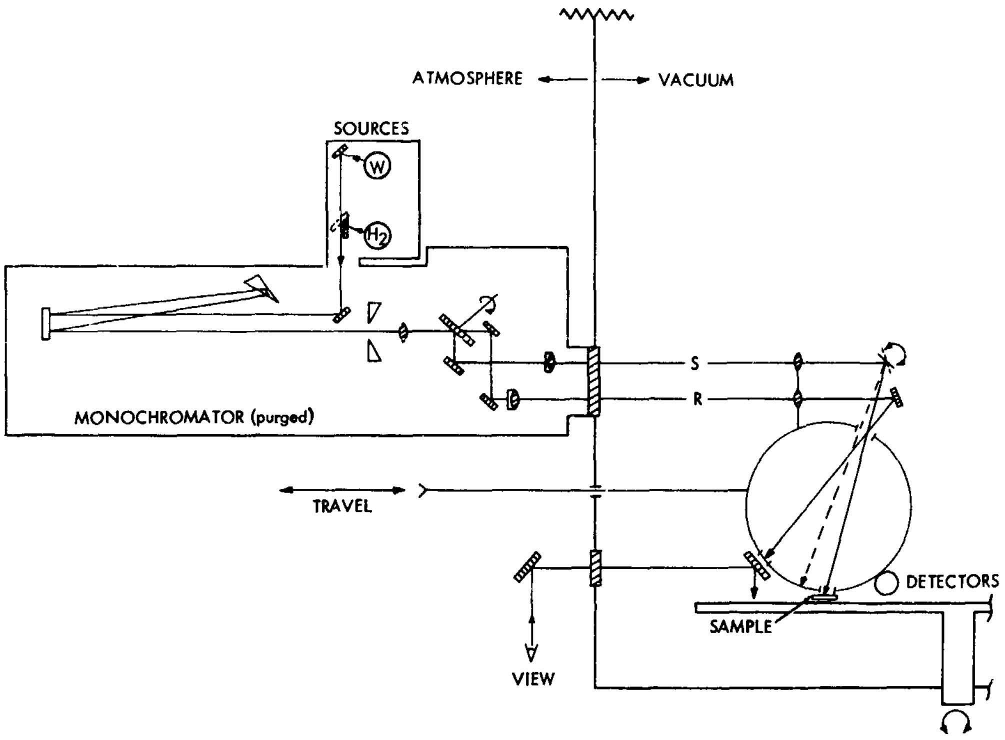

Figure 9a. CRETC Reflectance Measurement System

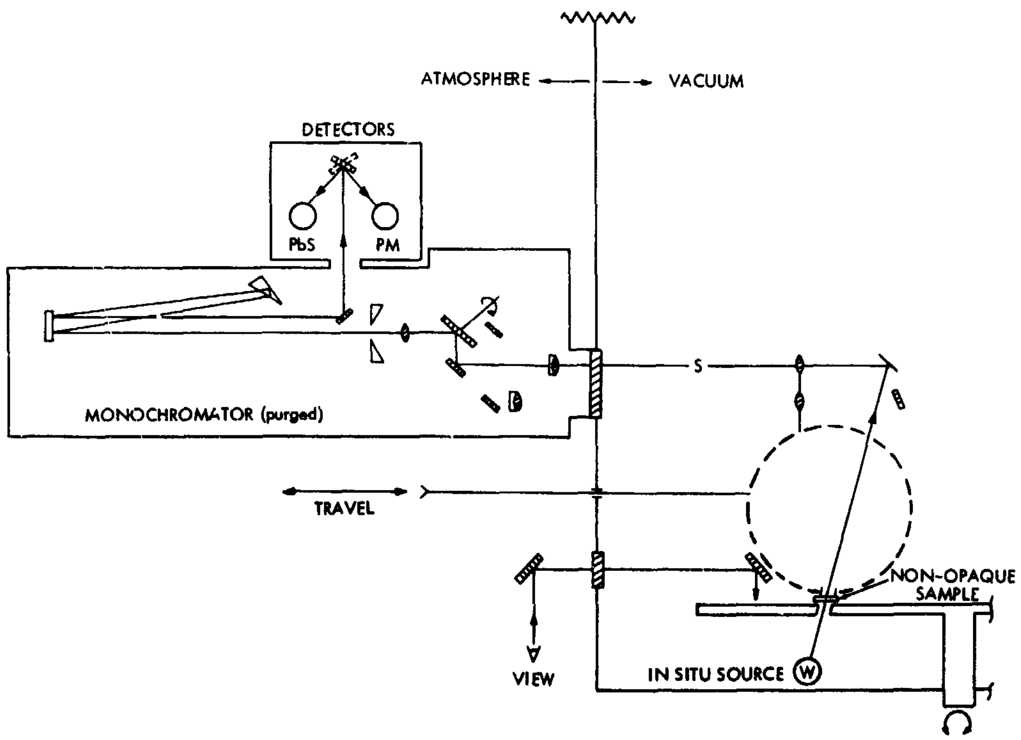

Figure 9b. CRETC Transmission Measurement System

Precision or repeatability of measurement is another matter. As with all single-beam measurement configurations, the passage of time between reference curve scan and sample curve scan, whether seconds or minutes, can and does introduce subtle percent variations in displayed transmittance percentages due to source strength changes and other variables along the optical/electronic train. Spectral variations of 2 percent are within experimental error.

At the beginning of the program there were two concerns about directional transmittance measurements; these were quickly resolved. One involves the fact that the transmission measurement source (in situ tungsten-iodine lamp) is mounted "behind" the filters, opposite the side on which protons and ultraviolet radiation are incident. Separate bench measurements using a Beckman DK-2A and Gier-Dunkle integrating sphere yield identical hemispherical transmittance curves, no matter which side of a filter sample faces the measurement source. These same transmittance curves also resolve the second concern, whether directional and hemispherical transmittance measurements are equivalent. The blue and blue-red filter designs result in virtually no scattering, and further examination after irradiation reveals no inducement of scattering or diffuse appearances; transmission remains directional. The many dielectric layers of the 4026 filter design offer increased possibilities for scattering and inducement of diffuse qualities during irradiation, yet examination of the 4026 filters after testing likewise shows no changes. Cuton/cutoff wavelengths do shift somewhat as an unirradiated 4026 filter is viewed from different angles (both by eye and by turning a sample with respect to its measurement beam). The 20-degree angle already in use for reflectance measurements has also been used for transmittance measurements during this program. In summary, it is felt that if any directional effects or differences exist in any filter types investigated, they are acceptably small.

Data Acquisition and Processing

The experimental apparatus necessary to align and measure both opaque and non-opaque samples has been described and discussed above. This section discusses the measurement and data processing procedures used during this program.

Reflectance measurements have been made on each sample, whether opaque (cell/filter stacks, adhesive/quartz, Kapton film) or non-opaque (filters and uncoated quartz), with high resolution of spectral data in mind. A separate Beckman chart and set of punched cards is made for each of three wavelength regions — 0.28 to 0.36, 0.36 to 0.71, and 0.71 to 2.5 microns — at scan speeds sufficiently slow to resolve all important spectral structure. Sample curves thus made are divided, wavelength by wavelength, by the values on reference curves (discussed in the previous section) so that the normalized result is invariant to the DK-2A 100 percent potentiometer setting. At the beginning of the program, a comparison of these normalized CRETC reflectance curves was made with comparable reflectance curves (of the same types of samples) generated using a bench DK-2A and sample-at-the-center integrating sphere. The latter integrating sphere is more widely regarded as approximating absolute reflectance more accurately, if imperfections in sphere wall uniformity and diffusivity are ignored. A spectrally dependent function expressing decimally the ratio of curves obtained with the two sphere configurations was thus determined, and incorporated into the existing data processing program. This program, working with reflectance data on all samples, has been used to compute solar reflectance of each sample and solar absorptance of opaque samples, and to control spectral plotting of processed data. Thermophysical property values obtained during this program appear to be in very good agreement with values obtained elsewhere previously, and have updated some earlier data.

During the course of the program this data processing program has also been modified and extended to treat sample transmittance data. The single-beam, continuous-scan transmittance measurement procedure, including as it does the manual selection of gain, slit width, and wavelength scan speed, requires further breakdown of spectral regions scanned at a time. Seven regions — two in the ultraviolet, three in the visible, and two in the infrared — have been employed, with wavelength scanning at reduced speeds for greater accuracy. Division of sample scan values by reference scan values, wavelength by wavelength, directly yields absolute spectral transmittance. Minor problems arise when manual slit settings different from automatic slit program settings are used (the former for transmittance measurements, the latter for reflectance measurements), especially on filters with steep spectral dependences. The 4026 filter in this program is probably a "worst case". A curve made with relatively wide monochromator slit settings has less spectral resolution and steepness than a curve made with relatively narrow slits. A displayed reflectance plot is not identically like an inverted transmittance plot. unless additional data treatment is undertaken to compensate for the slit width differences just mentioned. This is, in short, the procedure that has been established during the course of this program: by reiterative trials to determine spectral equivalence factors to compensate for different color bandpasses in separate reflectance and transmittance measurements. This is especially necessary in order to add computer-processed reflectance values and computer-processed transmittance values of filter samples, obtaining the spectral absorptance (and solar absorptance) from unity minus the computer-added sum of R and T.

The majority of the remainder of this report consists of formal reporting of spectral reflectance, transmittance, and absorptance data obtained on eleven types of solar panel and other spacecraft materials and components. The most significant results are summarized in the next section, "Experimental Results." Detailed spectral plots are gathered in the appendices.

EXPERIMENTAL RESULTS

As stated before, the principal experimental effort during this program has been conducting a 2400-hour in situ simulation of the 1973 Venus-Mercury flyby mission. Degradation of reflectance and transmittance properties due to radiation exposure occurs in both transmitting and non-transmitting materials. Both protons and ultraviolet radiation contribute to the measured degradation, with relative contributions varying from material to material. There are synergistic effects contributing to combined radiation damage greater than separate proton and UV damage amounts in several materials, and less than additive degradation in others.

Solar Cell Filters

Results for the most widely used solar cell and filter combination (blue filter) are summarized in Figure 10. The effect of ultraviolet radiation, and to a lesser extent protons, is to reduce the effectiveness of the UV rejection filter coating, and to reduce the effective transmittance of the blue filter at wavelengths important for conversion by the solar cell into electrical energy. In the near infrared wavelength region, initial sample-to-sample differences before exposure are as important a consideration as any changes induced by radiation exposure.

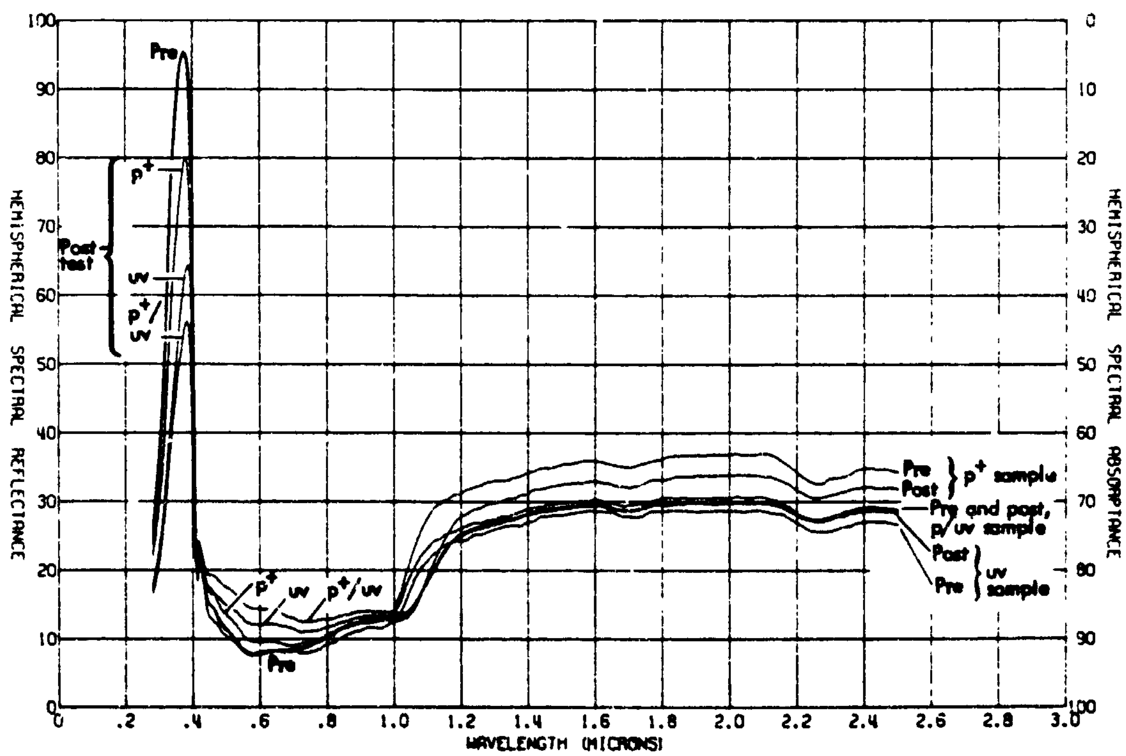

Figure 10. In Situ Effects of Protons and Ultraviolet Radiation on Blue Filter/2 ohm-cm Cell Stack

Degradation of the UV rejection filter by simultaneous exposure to protons and ultraviolet radiation is less than the sum of individual proton and ultraviolet damage amounts. On the other hand, combined proton/UV damage at wavelengths between 0.4 and 1.0 microns is approximately additive. Complete spectral data including mid-exposure results is given in Appendix A in Figures 24, 25, and 26.

Figure 10 indicates amounts by which protons, ultraviolet, and simultaneous exposure to protons and ultraviolet degrade solar cell properties as indicated by spectral reflectance measurements. Measurement of the transmittance of the blue filter alone, before and after the 3 types of exposure, give results summarized in Figure 11. It should be noted from Figure 11 that loss in energy reaching the solar cell from reduced transmittance occurs over a narrower wavelength region (0.4 to 0.8 microns) than loss in energy due to increased filter surface reflectance (Figure 10, 0.4 to 1.0 microns). Data is displayed in Figure 11 and in later transmittance plots in this report, exactly as computer processed. Smoothing and other widely practiced audio-visual efforts have not been employed. Thus, as indicated earlier, small variations, perhaps 2 percent due to single-beam precision limits, may be observed in these computer-plotted transmittance curves at one wavelength or another. In Figure 11 an example is at 0.72 microns, where transmittance changes are indicated to be much smaller than at wavelengths slightly longer and shorter than 0.72 microns. Such spectrally narrow variations should be discounted in any further analysis of transmittance data, since real transmittance changes are those that are apparent in this document's transmittance plots at more than one wavelength point. Wavelength points that are connected by computer-controlled plotting occur every 0.02 microns in the infrared, every 0.005 microns in the visible, and every 0.002 microns in the ultraviolet.

Complete spectral transmittance data for the blue filter, including mid-exposure results, is given in Figures 30, 31, and 32 of Appendix A.

Figure 12 summarizes reflectance degradation measured in 4026 filters over 2 ohm-cm solar cells. The dielectric interference coatings on the 4026 filter broaden the UV rejection feature to reject wavelengths as long as approximately 0.6 micron before exposure. The relative contributions of ultraviolet radiation

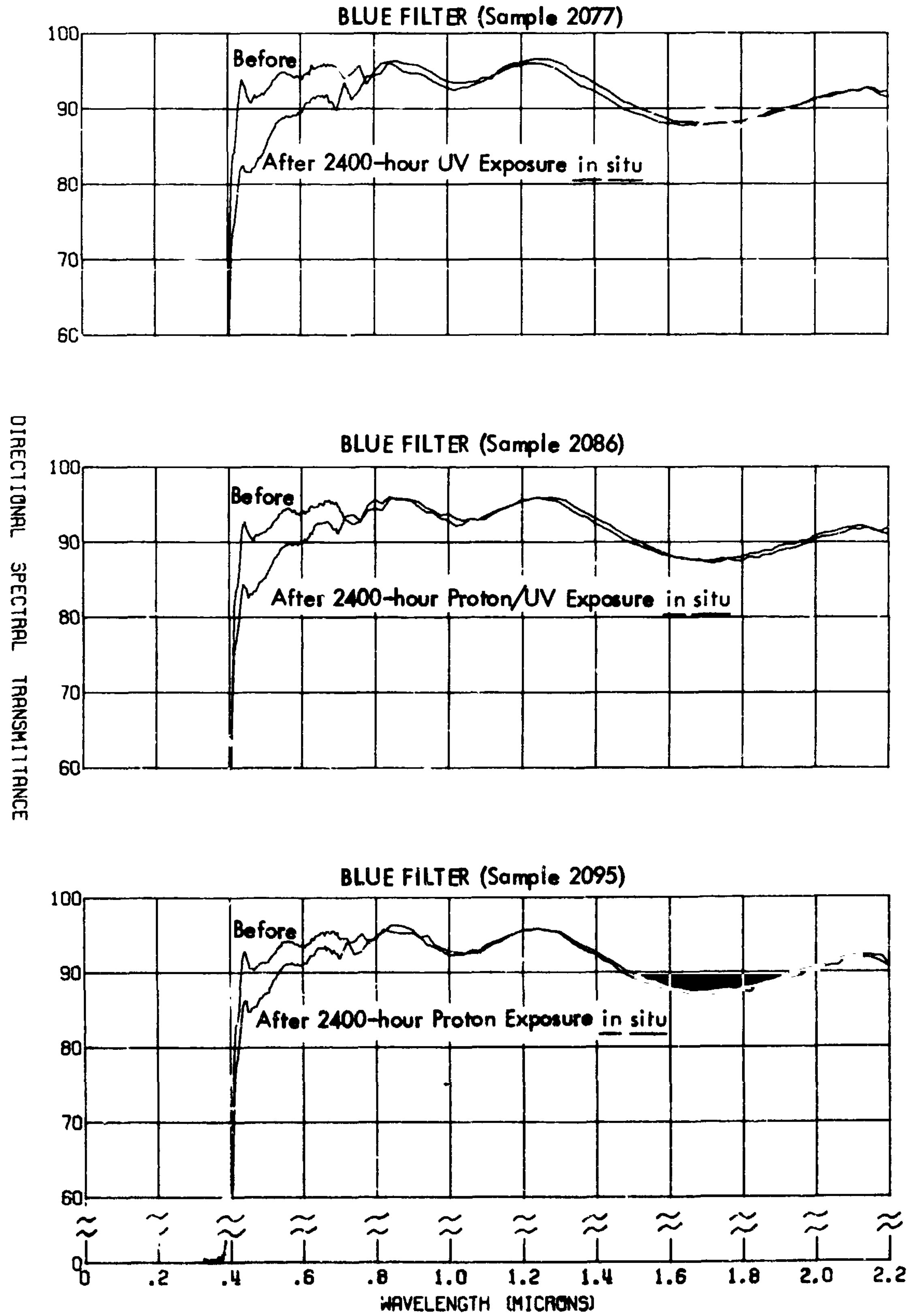

Figure 11. Decrease in in Situ Spectral Transmittance of Blue Filter After 2400-Hour Exposure

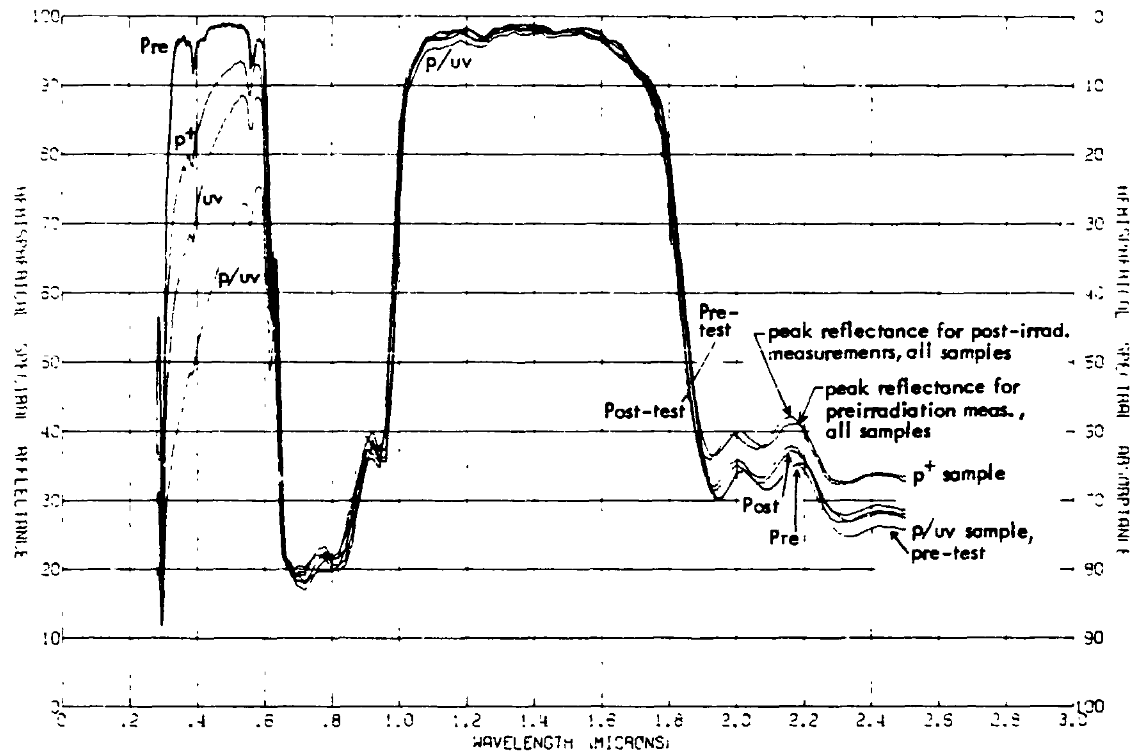

Figure 12. In Situ Effects of Protons and Ultraviolet Radiation on Modified 4026 Filter/2 ohm-cm Cell Stack

and protons, and the greater-than-additive combined proton/UV damage, are evident at the shorter wavelengths in Figure 12. Cuton and cutoff wavelengths (0.6, 1.0, and 1.8 microns) shift toward shorter wavelength values during exposure. In Figure 12 this wavelength shift is labelled near 2.2 microns, where local reflectance peaks shift noticeably toward shorter wavelenths. At 0.9 and 0.8 microns the tendency is for peak-and-valley structure to be attenuated along with the wavelength shifts during exposure.

Complete spectral data for the 4026 filter/cell combination, including mid-exposure results is contained in Appendix A as Figures 36, 37, and 38.

The third filter/cell combination investigated involves a blue-red filter over 2 ohm-cm solar cells. Reflectance changes in this combination are summarized in Figure 13. Besides initial sample-to-sample variations in the infrared, the principal result displayed in Figure 13 is that combined proton/UV damage is less than either proton damage or ultraviolet damage considered alone. This is true both for the UV rejection filter and at longer wavelengths surrounding the red peak.

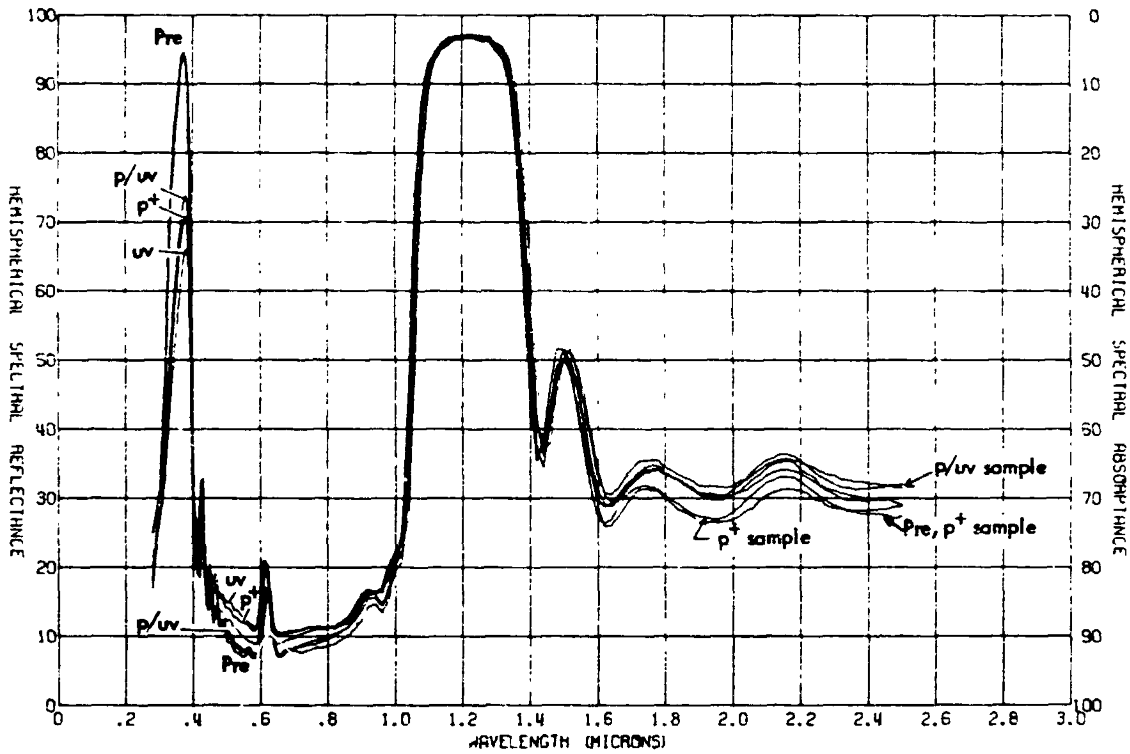

Figure 13. In Situ Effects of Protons and Ultraviolet Radiation on Blue-Red Filter/2 ohm-cm Cell Stack

Complete spectral data for the blue-red filter on 2 ohm-cm cells, including mid-exposure results, is shown in Figures 48, 49, and 50 of Appendix A. Spectral transmittance curves of the blue-red filter alone show losses at wavelengths surrounding the red peak. Complete spectral transmittance data including mid-exposure results, is shown in Figures 54, 55, and 56 of Appendix A.

Adhesives and Quartz

Included in this program was an evaluation of solar cell adhesives. Reflectance changes in quartz/RTV-602/polished aluminum samples are summarized in Figure 14. The appreciable differences from sample to sample, evidently in thickness of RTV-602 "cement" used to prepare each sample, as indicated by infrared absorption properties, should be noted. The samples exposed to ultraviolet radiation for 2400 hours in accordance with Figure 1 degraded severely. After the 2400-hour test their visual appearance was a deep tan. Complete spectral results, including mid-exposure data, are shown in Appendix A, Figures 60, 61, and 62.

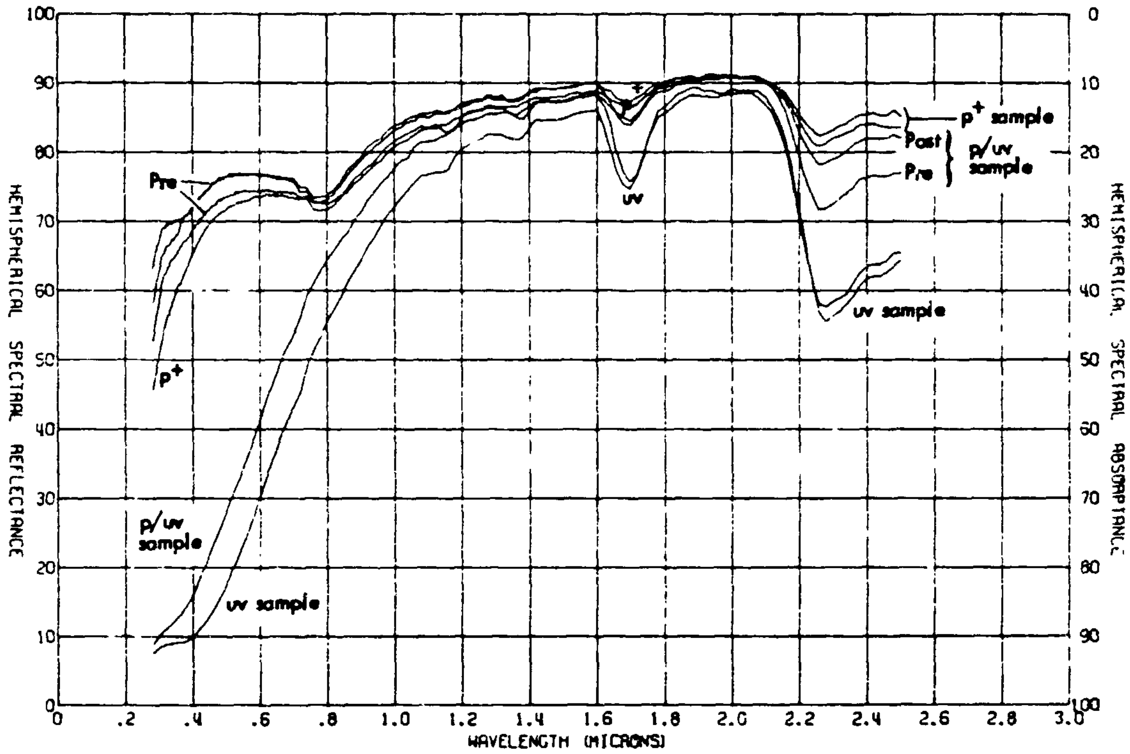

Figure 14. In Situ Effects of Protons and Ultraviolet Radiation on Clear Glass (Fused Silica)/RTV-602/Polished Aluminum

Similar pre-irradiation variations and post-irradiation reflectance changes are summarized in Figure 15 for quartz/XR6-3489/polished aluminum samples. Complete spectral results, including mid-exposure data, are presented in Appendix A, Figures 63, 64, and 65. Both XR6 and RTV adhesives exposed under quartz (7940 fused silica) received much higher ultraviolet ESH exposure, of course, than would have been the case for adhesives under quartz with a UV rejection coating. Some of the degradation is, in fact, in the "unscreened" quartz, as verified by transmittance losses in uncoated quartz substrates exposed to protons and ultraviolet radiation, separately and simultaneously (Figure 16). Complete spectral results for quartz, including mid-exposure data, are presented in Figures 66 through 74 in Appendix A.

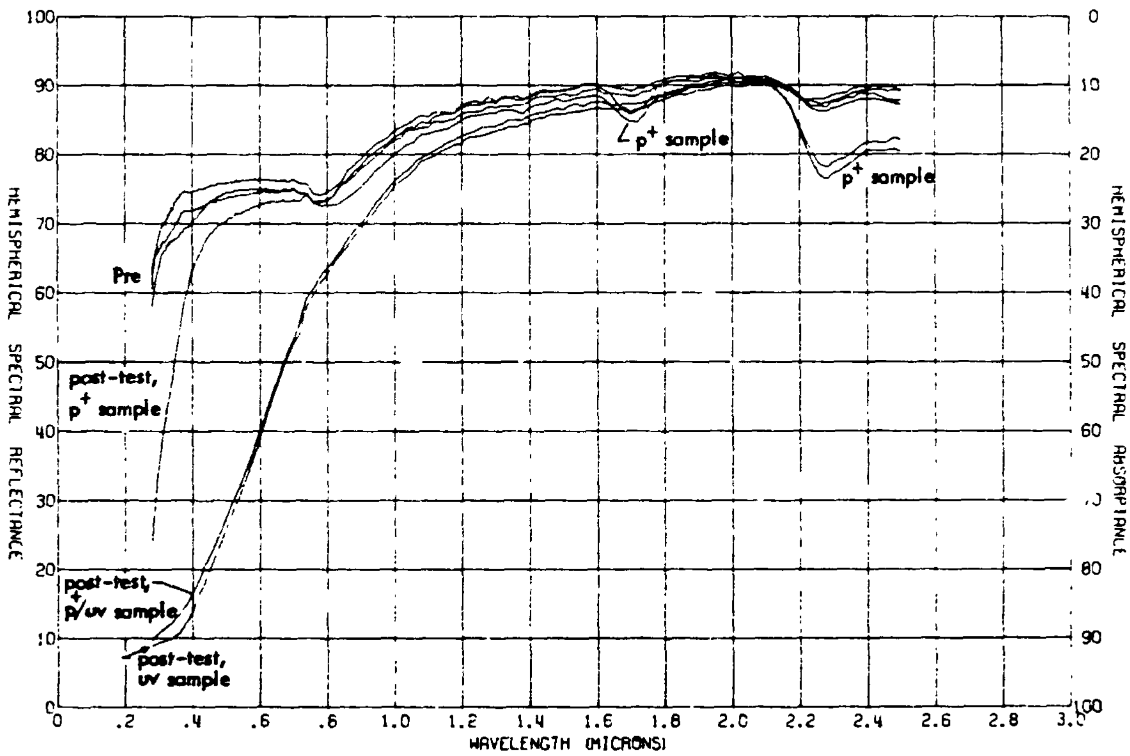

Figure 15. In Situ Effects of Protons and Ultraviolet Radiation on Clear Glass (Fused Silica)/XR6-3489/Polished Aluminum

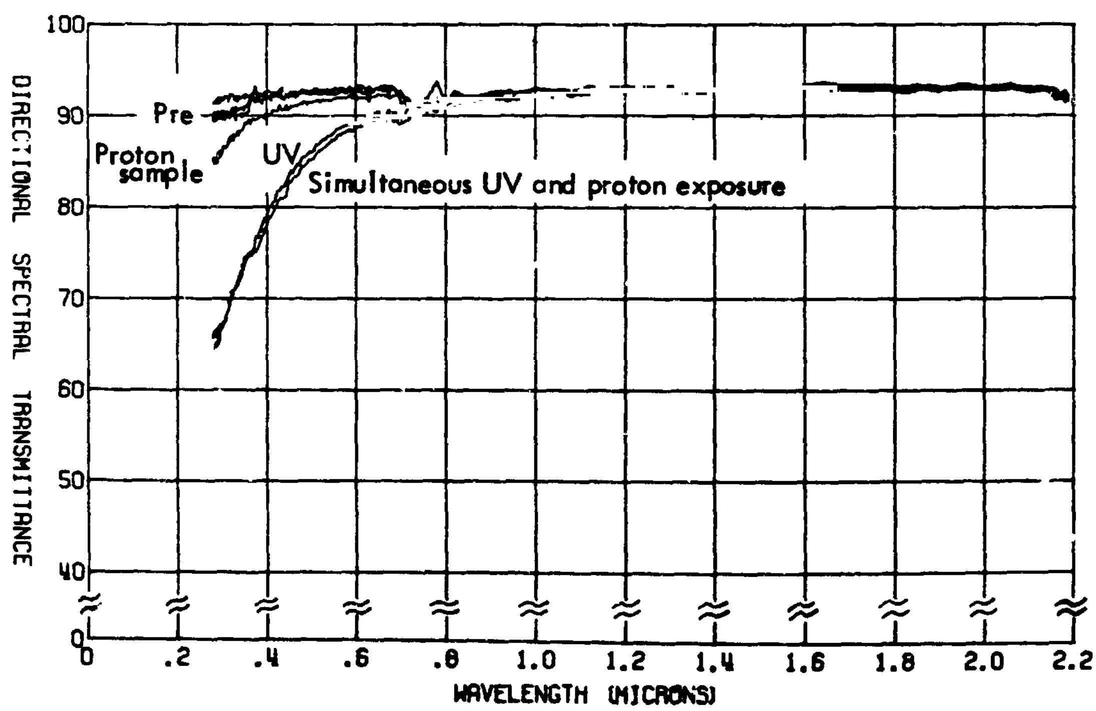

Figure 16. In Situ Effects of Protons and Ultraviolet Radiation on the Spectral Transmittance of 7940 Fused Silica

Kapton Film

Kapton film was also evaluated during the 2400-hour test for application as a "thermal shield" on the Venus-Mercury spacecraft. Preliminary design calls for the film to stand off, away from the spacecraft; hence, there would be no conducted heat to a substrate or spacecraft skin underneath (except along periodic support mechanisms). To simulate this, Kapton samples were mounted in the CRETC without being bonded to their substrates; on two sides of the 2 cm by 2 cm samples, the film was wrapped underneath the substrates. In the middle of a sample, the film was separated from its substrate by at least several mils, and in places perhaps 50 mils. The sample exposed to protons and ultraviolet radiation simultaneously (up to 10 suns by the end of the test) rose to an equilibrium temperature high enough to alter its chemical structure fundamentally, verified by a dark brown appearance after the exposure and by a corresponding reflectance curve (Figure 17). The sample exposed to protons alone remained relatively close to the temperature profile shown in Figure 2.

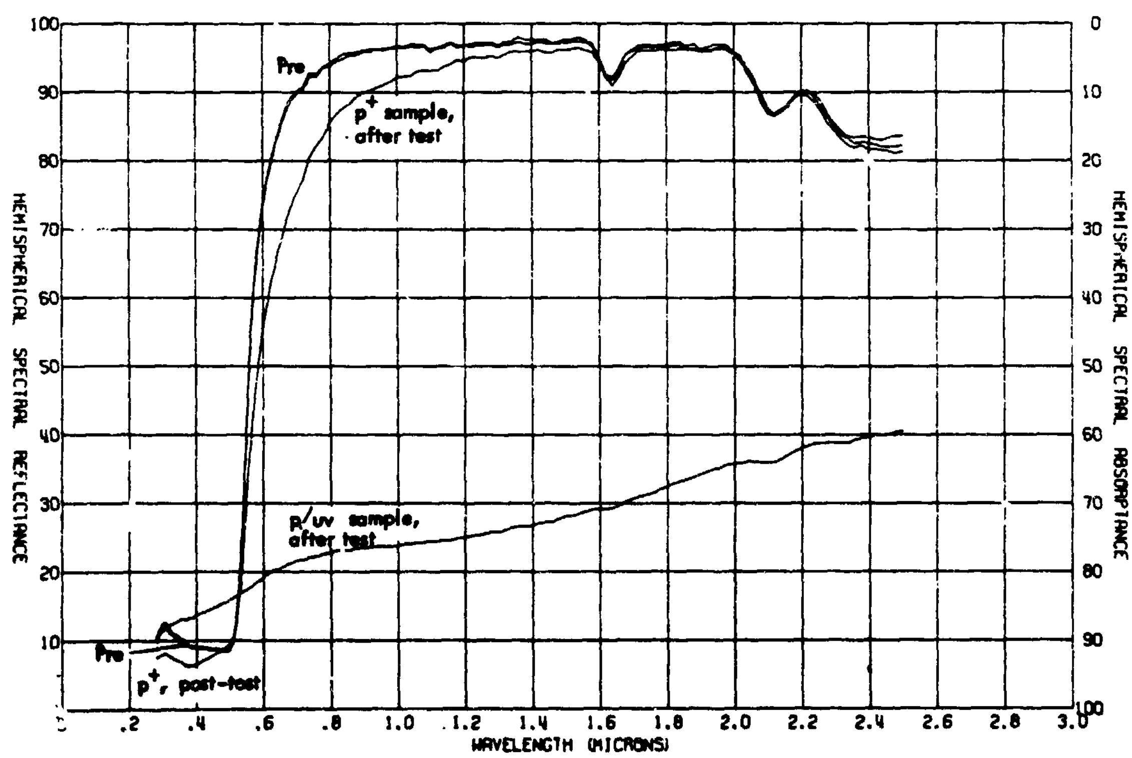

Figure 17. *In Situ* Effects of Protons and Ultraviolet Radiation on Gold-Backed Kapton Film

The amount of 3-keV proton damage indicated in Figure 17 is consistent with results obtained with Kapton during an earlier program using 40-keV protons (Reference 5). Complete spectral data, including mid-exposure results, are shown in Figures 75 and 76 of Appendix A.

ANALYSIS AND DISCUSSION

As indicated in the previous section, presentation of complete spectral results, the highlights of which have been summarized in Figures 10 through 17, is reserved for the Appendices to this report, due to the large number of spectral plots. Table 3 summarizes the combination of material type, thermophysical properties derived, and kind of exposure that corresponds to each figure number to be found in Appendix A, the location of complete spectral data plots from the 2400-hour test.

Thermophysical Properties

Thermophysical properties derived from computer-processed spectral data are also gathered in Tables 4 and 5, for opaque and non-opaque materials, respectively. The equations defining the thermophysical quantities of interest are

$$\text{Solar reflectance, } R_s = \frac{\int I_s(\lambda) R(\lambda)\, d\lambda}{\int I_s(\lambda)\, d\lambda}$$

and

$$\text{Solar transmittance, } \tau_s = \frac{\int I_s(\lambda)\, \tau(\lambda)\, d\lambda}{\int I_s(\lambda)\, d\lambda}$$

where $I_s(\lambda)$ is the solar irradiance as a function of wavelength λ, and $R(\lambda)$ and $\tau(\lambda)$ are sample reflectance and transmittance functions (respectively), generally varying with λ. For transmissive (non-opaque) samples, solar absorptance is, by definition, unity minus the sum of R_s and τ_s, namely

$$\alpha_s = 1 - (R_s + \tau_s)$$

Of course, for opaque samples this reduces to

$$\alpha_s = 1 - R_s .$$

The integral $\int I_s(\lambda)\, d\lambda$ is an expression of the solar "constant". With computerized data processing available, it is appropriate to replace the other integral evaluations with numerical summations, so that

Table 3. Figure Number in Appendix A for Each Material Investigated in 2400-hour Test, Thermophysical Property Derived, and Type of Exposure Received

Type of Material	Figure Number in Appendix A								
	Solar Reflectance			Solar Transmittance			Solar Absorptance		
	UV	UV/p+	p+	UV	UV/p+	p+	UV	UV/p+	p+
Blue filter on 2Ω -cm cell	--	--	--	--	--	--	24	25	26
Blue filter alone	27	28	29	30	31	32	33	34	35
4026 filter on cell	--	--	--	--	--	--	36	37	38
4026 filter alone	39	40	41	42	43	44	45	46	47
Blue-red filter on 2Ω-cm cell	--	--	--	--	--	--	48	49	50
Blue-red filter alone	51	52	53	54	55	56	57	58	59
Clear glass (quartz)/ RTV-602 adhesive/ polished aluminum	--	--	--	--	--	--	60	61	62
Clear glass(quartz)/ XR6-3489 adhesive/ polished aluminum	--	--	--	--	--	--	63	64	65
7940 fused silica (clear glass)	66	67	68	69	70	71	72	73	74
Kapton film	--	--	--	--	--	--	--	75	76

Table 4. Solar Absorptance of Opaque Samples Under Various Exposure Conditions

Kind of Exposure	Sample Type and Number	Before Exposure	After Exposure for a Duration of			
			222 hrs	753 hrs	1573 hrs	2400 hrs
Simultaneous Exposure to Protons and Ultraviolet Radiation	Blue Filter on cell, 2083	0.78	0.79	0.79	0.78	0.79
	4026 Filter on cell, 2084	0.31	0.34	0.36	0.41	0.44
	Blue Red Filter on cell, 2085	0.70	0.71	0.71	0.70	0.70
	Quartz/RTV/ Aluminum, 2090	0.22	0.26	0.29	0.36	0.46
	Quartz/XR6/ Aluminum, 2091	0.22	0.26	0.28	0.34	0.47
	Kapton Film	0.35	0.37	0.40	0.67	0.78
Exposure to Ultraviolet Radiation	Blue Filter on cell, 2074	0.79	0.79	0.79	0.80	0.80
	4026 Filter on cell, 2075	0.31	0.34	0.34	0.35	0.37
	Blue Red Filter on cell, 2076	0.70	0.70	0.70	0.70	0.70
	Quartz/RTV/ Aluminum, 2081	0.25	0.32	0.36	0.46	0.54
	Quartz/XR6/ Aluminum, 2082	0.22	0.27	0.28	0.33	0.48
Exposure to Protons	Blue Filter on cell, 2092	0.77	0.78	0.78	0.77	0.79
	4026 Filter on cell, 2093	0.30	0.32	0.32	0.32	0.34
	Blue Red Filter on cell, 2094	0.70	0.70	0.70	0.70	0.70
	Quartz/RTV/ Aluminum, 2099	0.22	0.23	0.23	0.23	0.25
	Quartz/XR6 Aluminum, 2100	0.21	0.23	0.23	0.24	0.26
	Kapton Film	0.34	0.35	0.36	0.38	0.40

Table 5. Solar Transmittance, Reflectance, and Absorptance Parameters of Four Filters Under Various Exposure Conditions

Kind of Exposure	Sample Type and Number	Parameter	Before Exposure	After Exposure for a Duration of			
				222 hrs	753 hrs	1573 hrs	2400 hrs
Simultaneous Exposure to Protons and Ultraviolet Radiation	Blue Filter, 2086	τ_s	0.84	0.84	0.84	0.83	0.82
		R_s	0.12	0.11	0.11	0.11	0.11
		α_s	0.04	0.05	0.05	0.06	0.07
	4026 Filter, 2087	τ_s	0.29	0.29	0.29	0.29	0.29
		R_s	0.67	0.65	0.64	0.61	0.58
		α_s	0.04	0.06	0.07	0.10	0.13
	Blue/Red Filter, 2088	τ_s	0.71	0.70	0.69	0.68	0.66
		R_s	0.23	0.23	0.23	0.23	0.23
		α_s	0.06	0.07	0.08	0.09	0.11
	Clear Glass (Quartz), 2089	τ_s	0.92	0.92	0.91	0.89	0.88
		R_s	0.06	0.06	0.07	0.07	0.07
		α_s	0.02	0.02	0.02	0.04	0.05
Exposure to Ultraviolet Radiation	Blue Filter, 2077	τ_s	0.85	0.84	0.83	0.83	0.82
		R_s	0.12	0.11	0.11	0.11	0.10
		α_s	0.03	0.05	0.06	0.06	0.08
	4026 Filter, 2078	τ_s	0.29	0.30	0.30	0.30	0.30
		R_s	0.66	0.65	0.64	0.63	0.62
		α_s	0.05	0.05	0.06	0.07	0.08
	Blue/Red Filter, 2079	τ_s	0.71	0.71	0.70	0.69	0.69
		R_s	0.23	0.23	0.23	0.23	0.23
		α_s	0.06	0.06	0.07	0.08	0.08
	Clear Glass (Quartz), 2080	τ_s	0.92	0.92	0.91	0.89	0.88
		R_s	0.07	0.07	0.07	0.07	0.07
		α_s	0.01	0.01	0.02	0.04	0.05
Exposure to Protons	Blue Filter, 2095	τ_s	0.84	0.85	0.85	0.84	0.83
		R_s	0.12	0.12	0.11	0.11	0.11
		α_s	0.04	0.03	0.04	0.05	0.06
	4026 Filter, 2096	τ_s	0.29	0.29	0.29	0.29	0.30
		R_s	0.67	0.66	0.65	0.65	0.64
		α_s	0.04	0.05	0.06	0.06	0.06
	Blue/Red Filter, 2097	τ_s	0.71	0.70	0.70	0.70	0.70
		R_s	0.23	0.23	0.23	0.23	0.23
		α_s	0.06	0.07	0.07	0.07	0.07
	Clear Glass (Quartz), 2098	τ_s	0.92	0.92	0.92	0.92	0.91
		R_s	0.06	0.06	0.07	0.07	0.07
		α_s	0.01	0.01	0.01	0.01	0.02

$$R_s = \frac{\sum^{100} R_i}{100}$$

and

$$T_s = \frac{\sum^{100} T_i}{100}$$

and $\alpha_s = 1 - R_s - T_s$ or $\alpha_s = 1 - R_s$ as the case may be. These simplified R_s and T_s equations are valid when weighting the wavelengths used in specifying R_i and T_i in accordance with the spectral intensity of the solar output function. In other words, of 100 wavelengths used in making summations, there is an appropriate concentration in the visible and near infrared wavelength regions.

Comparison of Filter-only and Filter-on-Cell Results

One of the more consistent observations of data from this program is that damage to the reflectance property of filters over cells is greater than damage to the reflectance of filters alone. Modified 4026 filter spectral data at 360 mμ, for example, displayed in Appendix A in figures listed in Table 3, is reduced to change-in-reflectance values and presented in Figure 18. Values of ΔR are negative since pre-irradiation reflectance at 360 mμ is greater than reflectance after various exposure times (horizontal axis). In agreement with the summary plot presented earlier (Figure 12), reflectance changes after combined proton/ultraviolet exposure are greater than those after ultraviolet-only exposure and those are greater than measured reflectance changes after proton-only exposure. But considering each type of exposure by itself, measured damage is nearly always greater in the filter-over-cell sample than in the filter-only sample. In both types of samples there are, presumably, contributions to sample reflectance from front and back surfaces of the filter, and any absorption induced in bulk in the quartz substrate can contribute, but again, presumably in both sample cases (filter over cell, and filter alone). [Results presented earlier for 7940 quartz do indicate loss of transmission (Figure 16) and increased absorption (Figures 72 through 74 in Appendix A for 7940 fused silica after exposure).] The only other physical differences between filter/cell samples

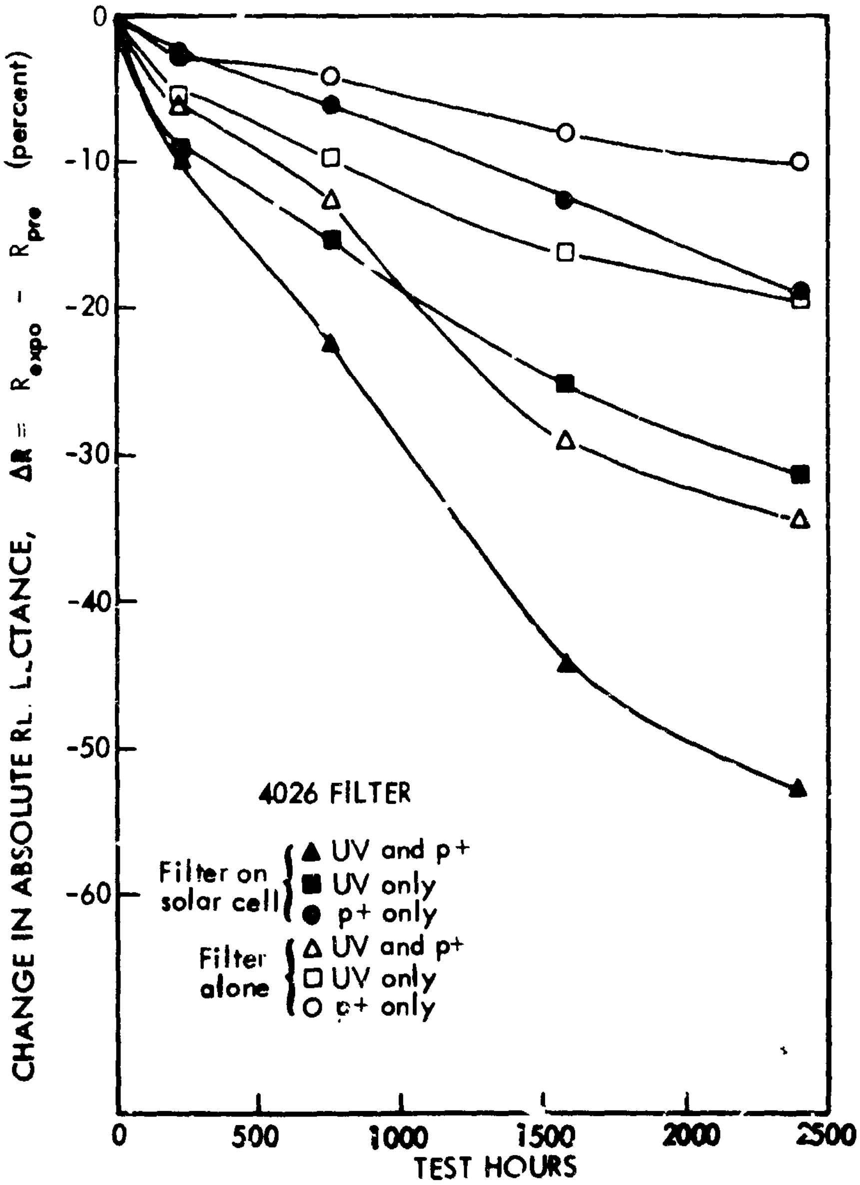

Figure 18. Degradation of UV Rejection in 4026 Filter at 360 mμ.

and filter-only samples, of course, are the highly absorbing cell underneath and the adhesive between filter and cell. Both adhesives evaluated do degrade heavily, at least by "worst case", "accelerated" exposure with low-loss quartz instead of a partially reflecting filter on top.

An analysis of the same kind using $\Delta\alpha_s$ values instead of ΔR values would show similar effects — that α_s damage is greater in 4026 filter/cell combinations than in 4026 filters alone; and that simultaneous proton/ultraviolet damage is greater than ultraviolet or proton damage, and, in fact, even greater than their sum.

Relative changes similar to those presented in Figure 18, but lesser in extent, exist at wavelengths out to about 0.6 micron on the 4026 filter. At longer wavelengths, near 0.8 microns and 1.2 microns, reflectance changes after exposure are measured, but are too small and inconsistent in 4026 filter samples to present in this kind of plot.

Such is not the case with blue filter samples, though. At 580 mμ the blue filter, whether alone or bonded to a cell, initially has a low reflectance that rises with exposure. This is shown in Figure 19 for 6 blue filter samples, 3 over cells and 3 alone. Both protons and ultraviolet radiation are capable of reducing the effectiveness of the antireflection coating on the front surface of the blue filter (and blue-red filter). Absolute changes are smaller than in Figure 18 (note expanded scale on the vertical axis), but the data consistently shows that reflectance changes (increases) in blue filters over cells are greater than reflectance increases in blue filters alone.

In Figure 20 reflectance degradation at 360 mμ is likewise more extensive in blue filters over cells than in blue filters alone. In filters over cells, Figures 19 and 20 show combined proton-ultraviolet damage to be greater, generally, than damage from ultraviolet radiation only, as anticipated. However, in samples of the blue filter alone, both figures (19 and 20) indicate greater changes from ultraviolet-only exposure than from simultaneous proton-ultraviolet exposure. This is consistent with measured transmittance results for blue filters alone; Figure 11

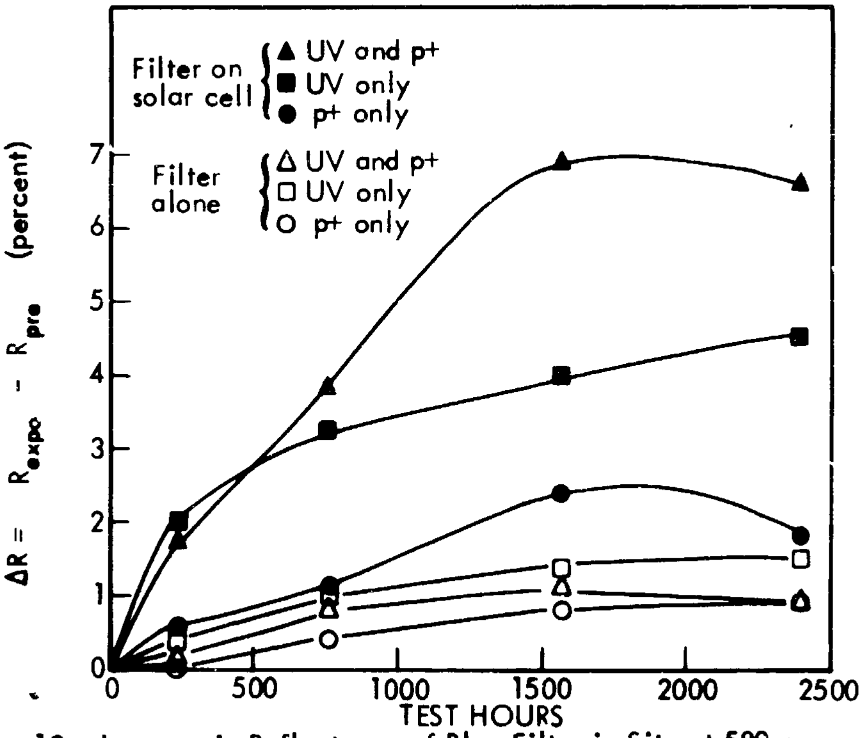

Figure 19. Increase in Reflectance of Blue Filter *in Situ* at 580 mμ

Figure 20. Degradation of UV Rejection in Blue Filter at 360 mμ

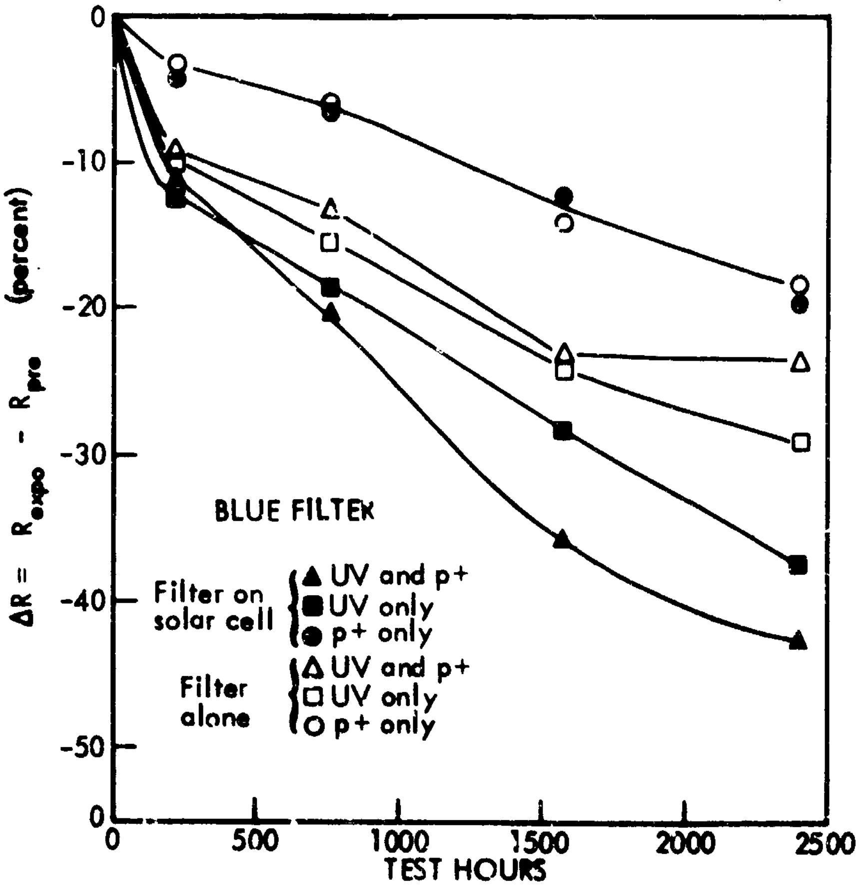

indicates that ultraviolet-only exposure results in greater transmittance losses in the blue filter than does exposure to protons and ultraviolet radiation simultaneously.

A similar analysis of data shows less consistent results for the blue-red filter than for either of the preceding two filters. At 580 mμ (near the red peak) degradation due to increased reflectance is generally more extensive in blue-red filters over cells, than in blue-red filters alone (Figure 21). Consistent with Figure 13, changes after proton-ultraviolet exposure are less than either ultraviolet or proton-induced changes by themselves. In Figure 22 for data at 360 mμ, filter-only damage is sometimes heavier than, sometimes less than, damage in blue-red filters over cells, depending on type of radiation exposure and length of exposure.

Temperature Effects

The importance of adequate and accurate temperature control of samples has been shown by this program to be of great significance. Mention has already been made of the results observed in Kapton film from the intentional lack of thermal contact between samples and substrates during exposure (results summarized in Figure 17).

Beyond this "failure" of Kapton film are lesser, non-catastrophic effects measured in other materials. The fact that filters having UV rejection coatings continue to degrade throughout exposure — whether early in the 2400-hour period with the adjacent sample-holding block maintained at relatively low temperatures, or whether later in the 2400-hour test at higher temperatures — has already been discussed. On the other hand, those filters having infrared rejection or "stopband" coatings (blue-red and 4026) sustain degradation to those coatings at low temperatures and exposure values, but recover at higher exposure values when substrate temperature rises sufficiently high. Examples are found in Appendix A, such as Figure 51 for the blue-red filter, Figure 49 for the blue-red filter on a cell, and Figure 3? for the 4026 filter bonded to a cell.

Prior to conducting the 2400-hour simulation of the entire Venus-Mercury flyby mission, a 500-hour test was conducted simulating the constant-temperature,

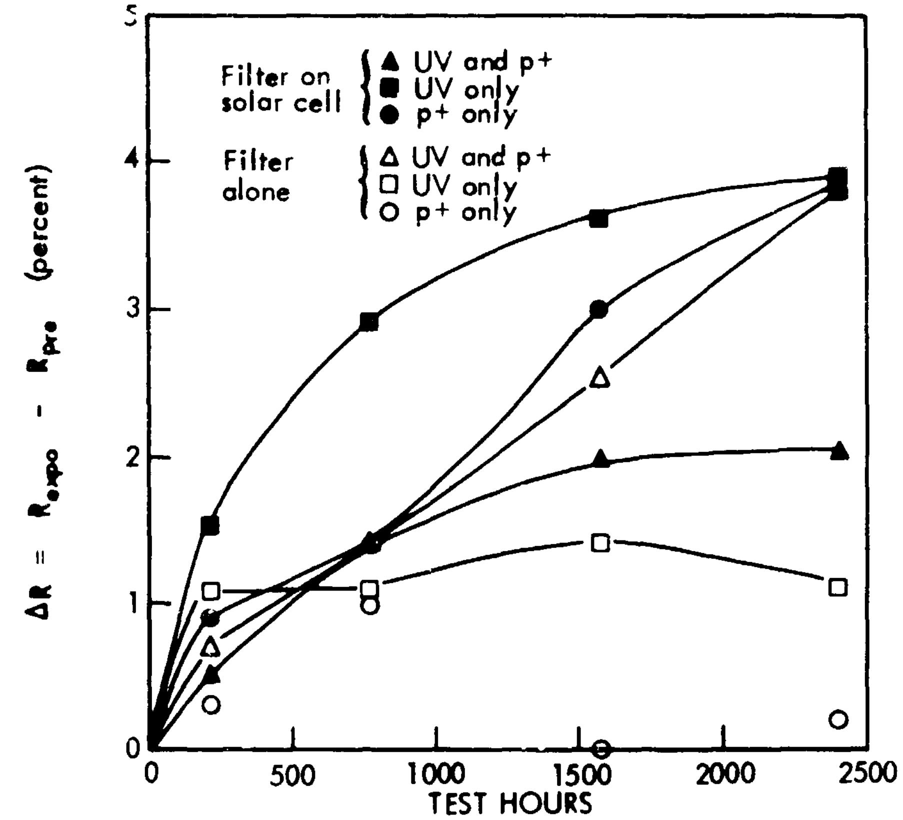

Figure 21. Increase in Reflectance of Blue-Red Filter in Situ at 580 mμ.

Figure 22. Degradation of UV Rejection in Blue-Red Filter at 360 mμ

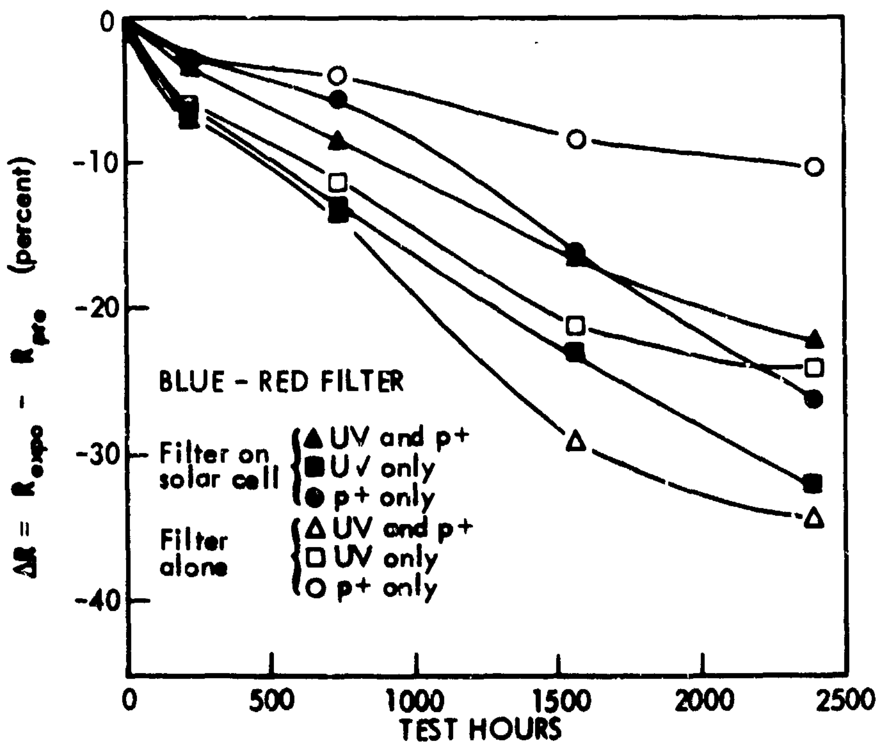

constant-exposure-rate portion of the 2400-hour test (note Figures 1 and 2). Many of the same materials were investigated in this preliminary test. Table 1 lists definitively the samples exposed. Sample substrate temperature was maintained at 140°C throughout the exposure and measurement periods. Exposure levels at the end of 500 hours of 5 sun rate, 5 solar wind rate testing were 2500 equivalent sun hours (ESH) of ultraviolet radiation, and 2.2×10^{15} protons/cm^2 (3-keV). Thus these maximum exposure values from the 500-hour test are some 50 percent greater in amount than exposure levels on samples in the 2400-hour test at measurement point 3 (see Figures 1 and 2). Most samples in the 2400-hour test sustained appreciable degradation at measurement point 3 (753 hours, temperature still relatively low) and underwent substantial additional changes after measurement point 3, as temperature and exposure rates increased. In contrast, however, sample property changes in the 500-hour test were in nearly all cases very small. Except for one anomaly discussed later at the beginning of Appendix B, even the largest 500-hour test changes with exposure were less than changes at 222 hours (measurement point 2) in the 2400-hour test. It appears, then, that high temperature radiation exposure alone is insufficient to simulate degradation anticipated in solar panel materials during a Venus-Mercury-type flyby.

Table 6 lists the figure numbers in Appendix B that present spectral results for the several materials investigated during the 500-hour test. The small thermophysical property value changes derived from small spectral changes are gathered as Table 7 at the beginning of Appendix B.

Another effect related to sample temperature has been observed in modified 4026 filters. Striations running nearly the length of the filter, and shorter, localized "gouge-like" defects develop in the dielectric coating layers of 4026 filters (whether alone or in cell stacks) as a result of the sample being elevated to temperatures approximately +140°C. These defects are observed whether or not radiation exposure follows the temperature excursion. At the beginning of this program, for instance, spare samples were pumped down in the CRETC vacuum chamber, and their temperatures raised to +140°C by the method depicted in Figure 6 for the purpose of checking out sample transmittance measurement procedures. Samples were "at

Table 6. Figure Number in Appendix B for Each Material Investigated in 500-hour Test, Thermophysical Property Plotted, and Type of Exposure Received

Type of Material	Figure Number in Appendix B								
	Reflectance			Transmittance			Absorptance		
	UV	UV/p+	p+	UV	UV/p+	p+	UV	UV/p+	p+
Blue filter on 2 Ω-cm cell	77	78	79	--	--	--	77	78	79
Blue filter alone	80	81	82	83	84	85	86	87	88
4026 filter on cell	89	90	91	--	--	--	89	90	91
4026 filter alone	92	93	94	95	96	97	98	99	100
Blue-red filter on 2 Ω-cm cell	101	102	103	--	--	--	101	102	103
Blue-red filter/adhesive/aluminum	104	105	106	--	--	--	104	105	106

temperature" approximately 4 hours. When returned to room temperature and brought back into air, both the short and long striation defects were apparent. They were similarly evident, and on some samples were more abundant, after the longer 500-hour and 2400-hour tests (which of course included radiation exposure). Figure 23 is an oblique view of JPL samples 2075 and 2078 in air following exposure to ultraviolet radiation during the 2400-hour test. The larger sample, a 4026 filter over a 2 x 2 cm cell, shows the long striations primarily, whereas in the 1 x 1 cm filter (sample 2078) the shorter defects predominate. Tables 5 and 7 indicate that solar transmittance (τ_s) is unaffected by the inducement of these defects in 4026 filters.

Figure 23. Defects in Multilayer Dielectric Coating of Modified 4026 Filter After 2400-Hour Test

CONCLUSIONS

1. Adequate temperature simulation in combination with simultaneous exposure to solar wind protons and ultraviolet radiation is the minimum necessary to allow an accurate prediction of effects of a Venus-Mercury flyby on solar panel and other spacecraft materials. In particular, a simulation of a Venus-Mercury flyby employing constant radiation exposure rates and the constant maximum temperature anticipated is a poor simulation, falsely predicting only small amounts of degradation when in fact heavy damage occurs.

2. Solar ultraviolet radiation dominates solar wind protons as the major damage source in solar panel and spacecraft materials investigated in this program. Yet because of apparent synergistic effects from these two types of radiation, they must be used in simultaneous combination to result in an accurate prediction of space radiation effects.

3. In general, thermophysical property value changes in transmissive solar cell filters after radiation exposure are quantitatively less than changes measured on solar cell-filter stacks.

4. The 4026 filter is presumably the only viable choice for use on a solar panel remaining substantially perpendicular to the sun's direction throughout a Venus-Mercury flyby if temperatures below +140°C are to be maintained. Though its solar absorptance increases due to exposure to protons and ultraviolet radiation, the 4026 filter appears to be suitable for use on a normal solar panel.

5. The blue filter and blue-red filter are suitable candidates for use on a Venus-Mercury tiltable solar panel. The blue-red filter appears to be slightly more resistant than the blue filter to increase in solar absorptance due to radiation exposure.

APPENDIX A

This appendix consists of computer-processed spectral plots of reflectance, transmittance, and/or absorptance of samples exposed to protons and/or ultraviolet radiation during the 2400-hour test simulating the 1973 Venus-Mercury spacecraft mission. Derived thermophysical properties that apply are also shown on each spectral plot.

FIGURE 24. IN SITU ULTRAVIOLET EFFECTS ON THE REFLECTANCE OF J P L SAMPLE 2074 BLUE FILTER ON 2 OHM-CM CELL 2400-HOUR TEST

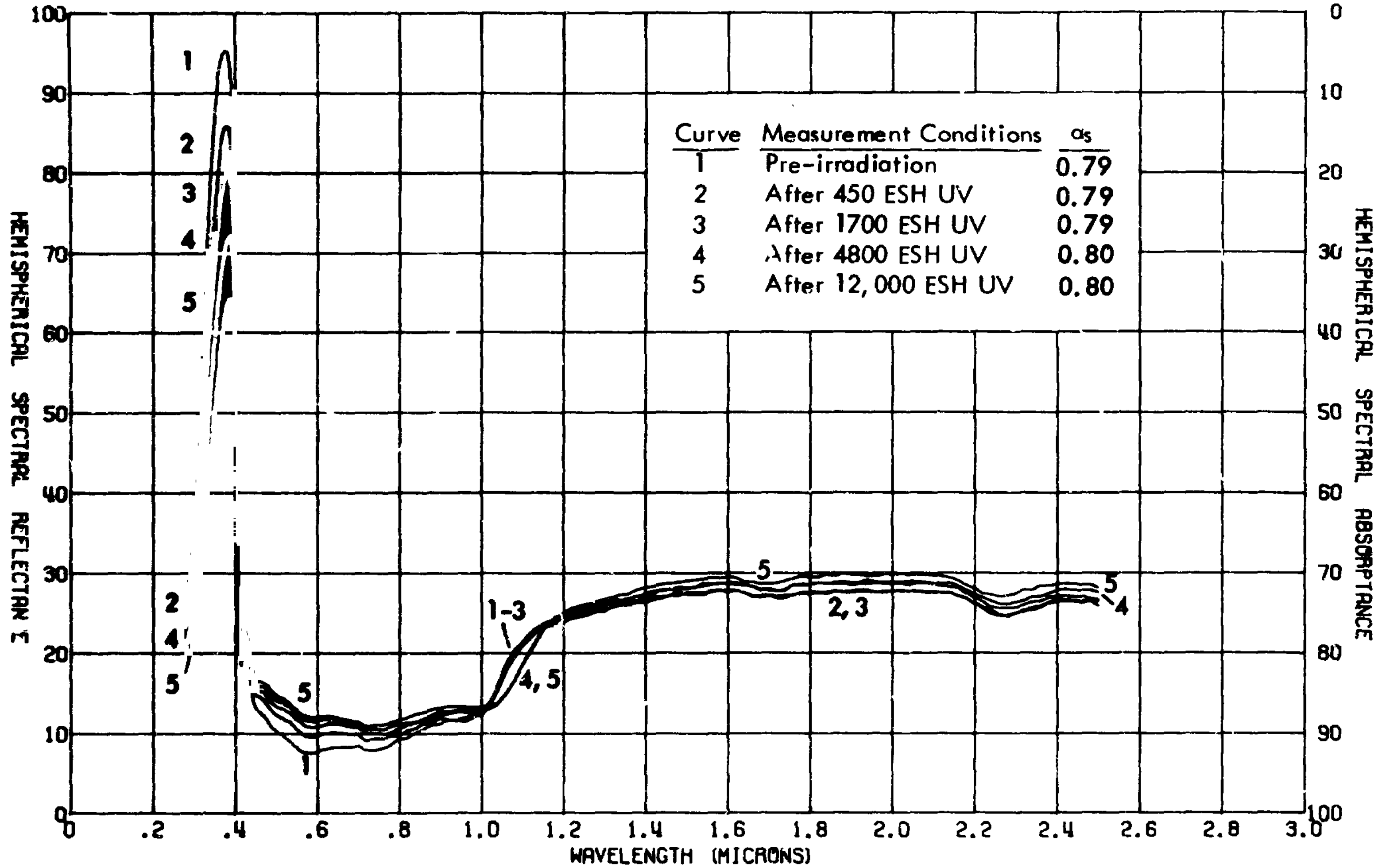

FIGURE 25

IN SITU PROTON-ULTRAVIOLET EFFECTS ON THE REFLECTANCE OF J P L SAMPLE 2083
BLUE FILTER ON 2 OHM-CM CELL 2400-HOUR TEST

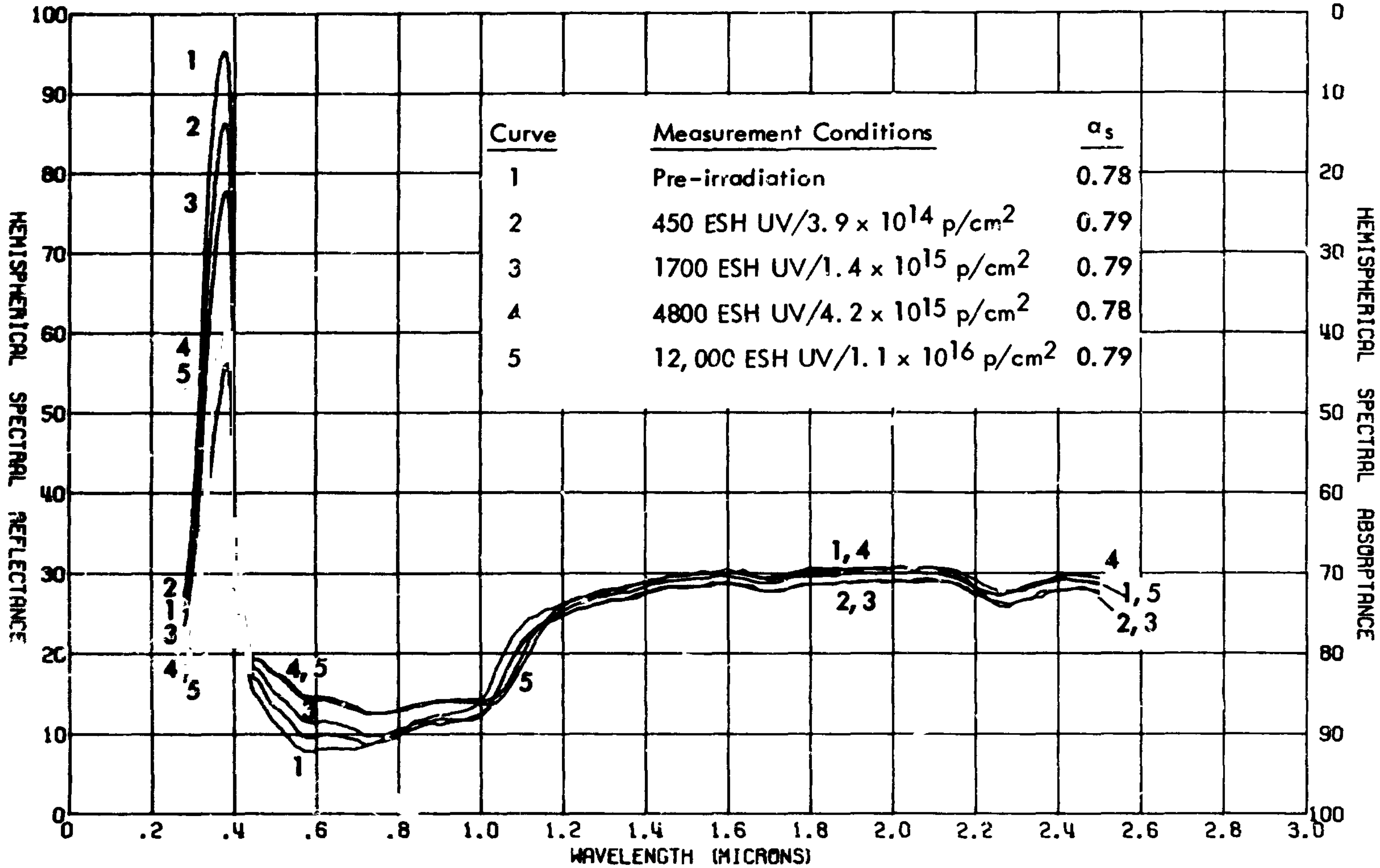

FIGURE 26. IN SITU PROTON EFFECTS ON THE REFLECTANCE OF J P L SAMPLE 2092 BLUE FILTER ON 2 OHM-CM CELL 2400-HOUR TEST

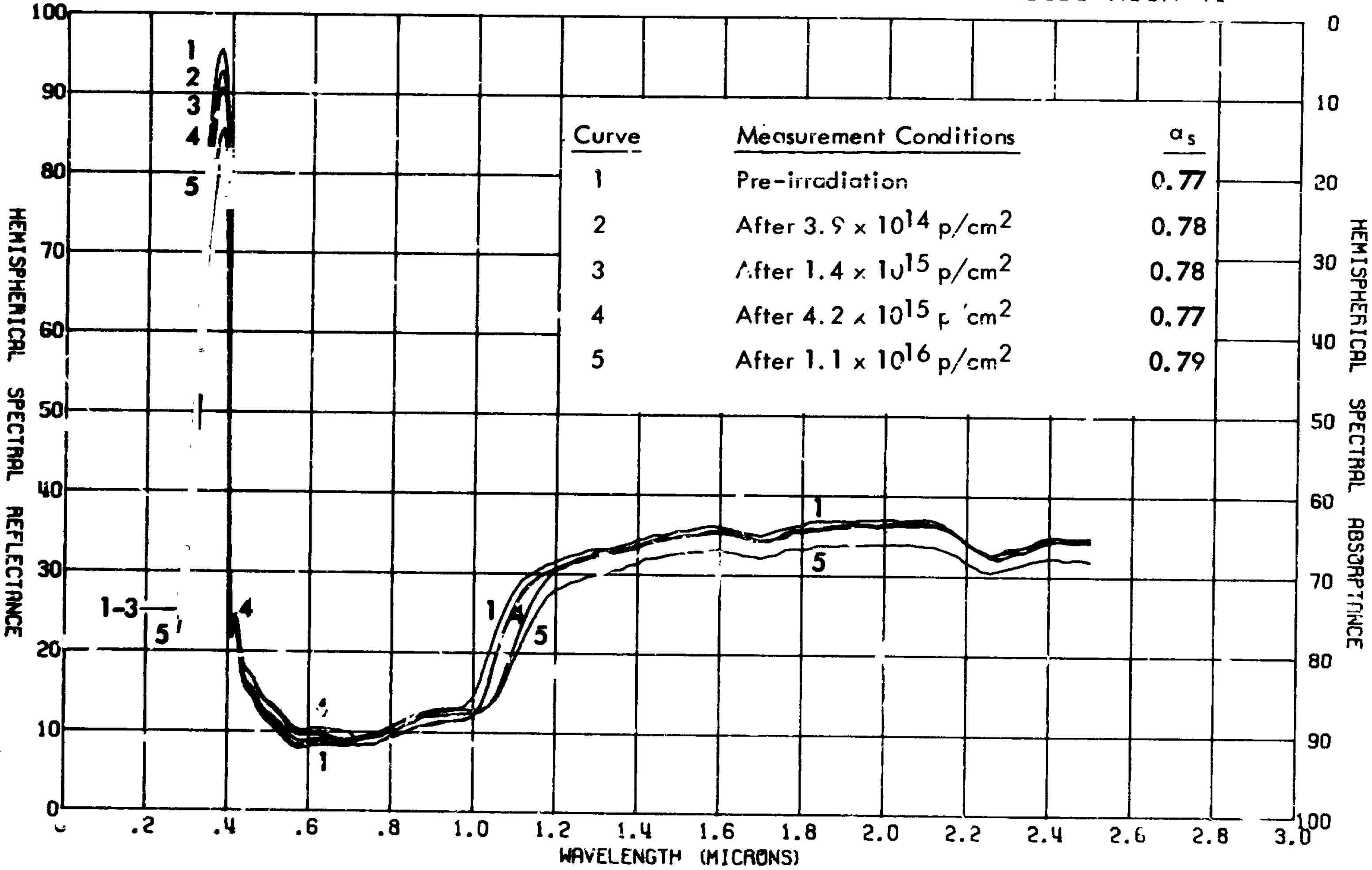

FIGURE 27. IN SITU ULTRAVIOLET EFFECTS ON THE REFLECTANCE OF J P L SAMPLE 2077
BLUE FILTER 2400-HOUR TEST

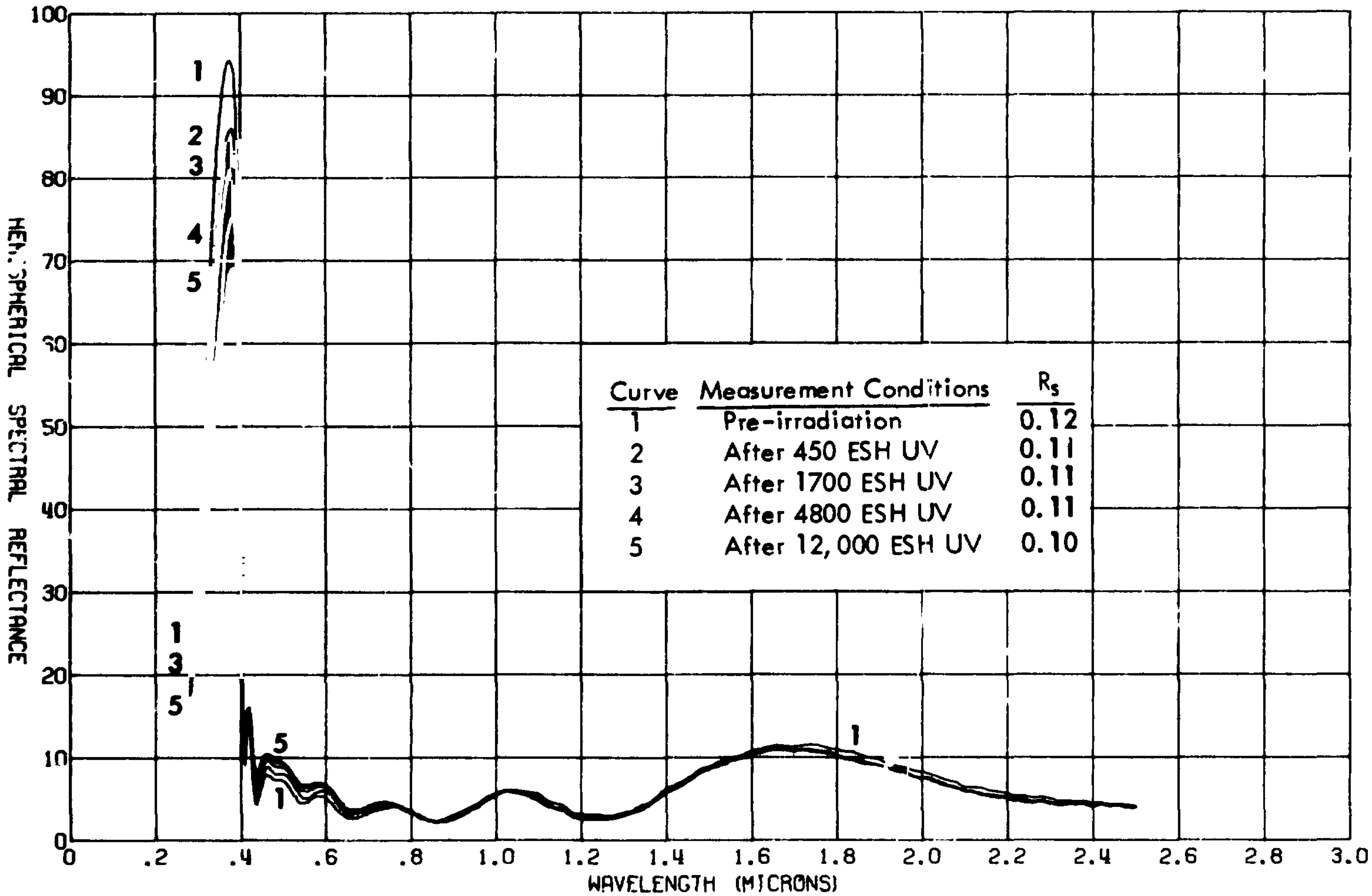

FIGURE 28.

IN SITU PROTON-ULTRAVIOLET EFFECTS ON THE REFLECTANCE OF J P L SAMPLE 2086
BLUE FILTER 2400-HOUR TEST

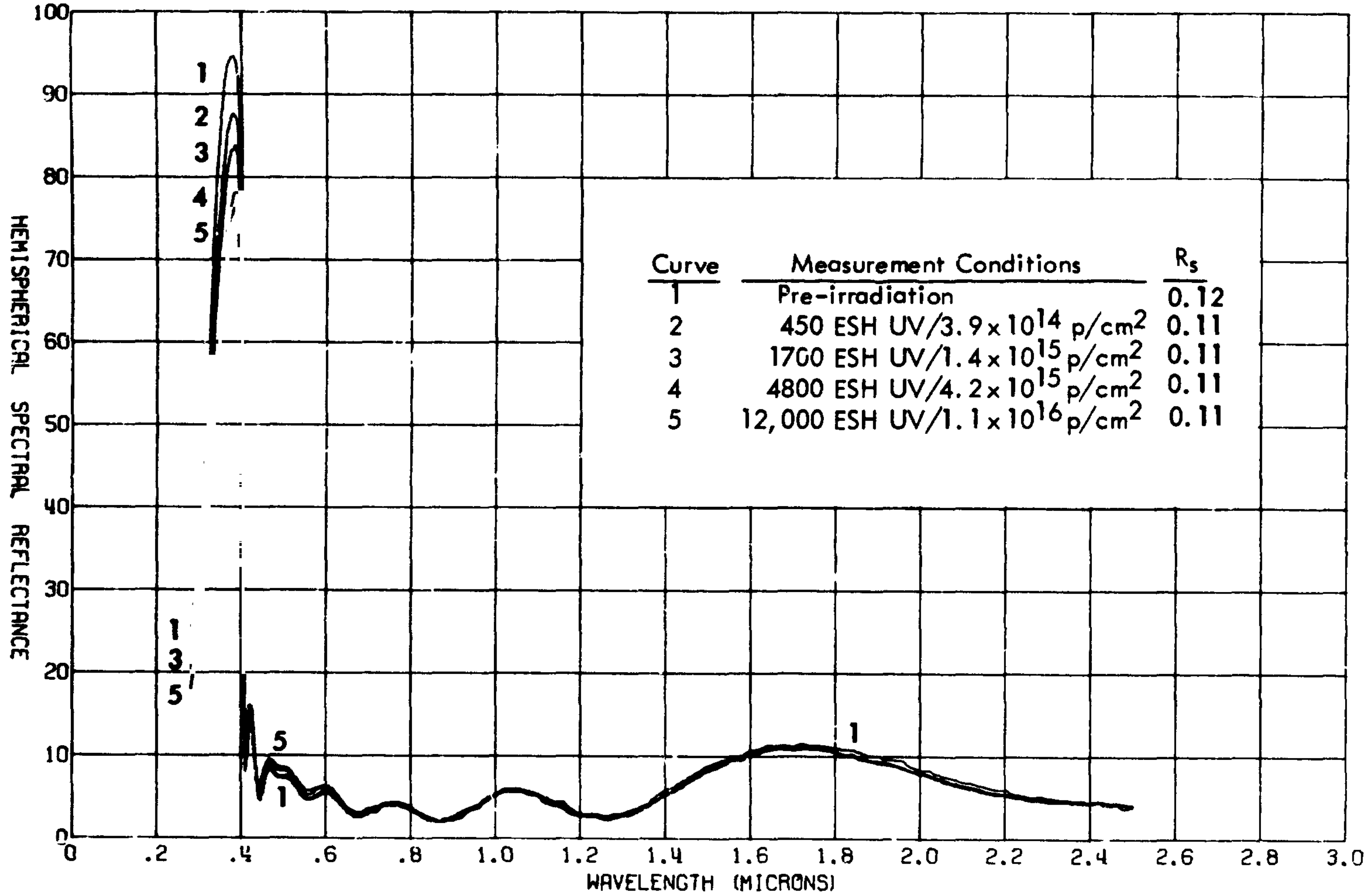

FIGURE 29. IN SITU PROTON EFFECTS ON THE REFLECTANCE OF J P L SAMPLE 2095
BLUE FILTER 2400-HOUR TEST

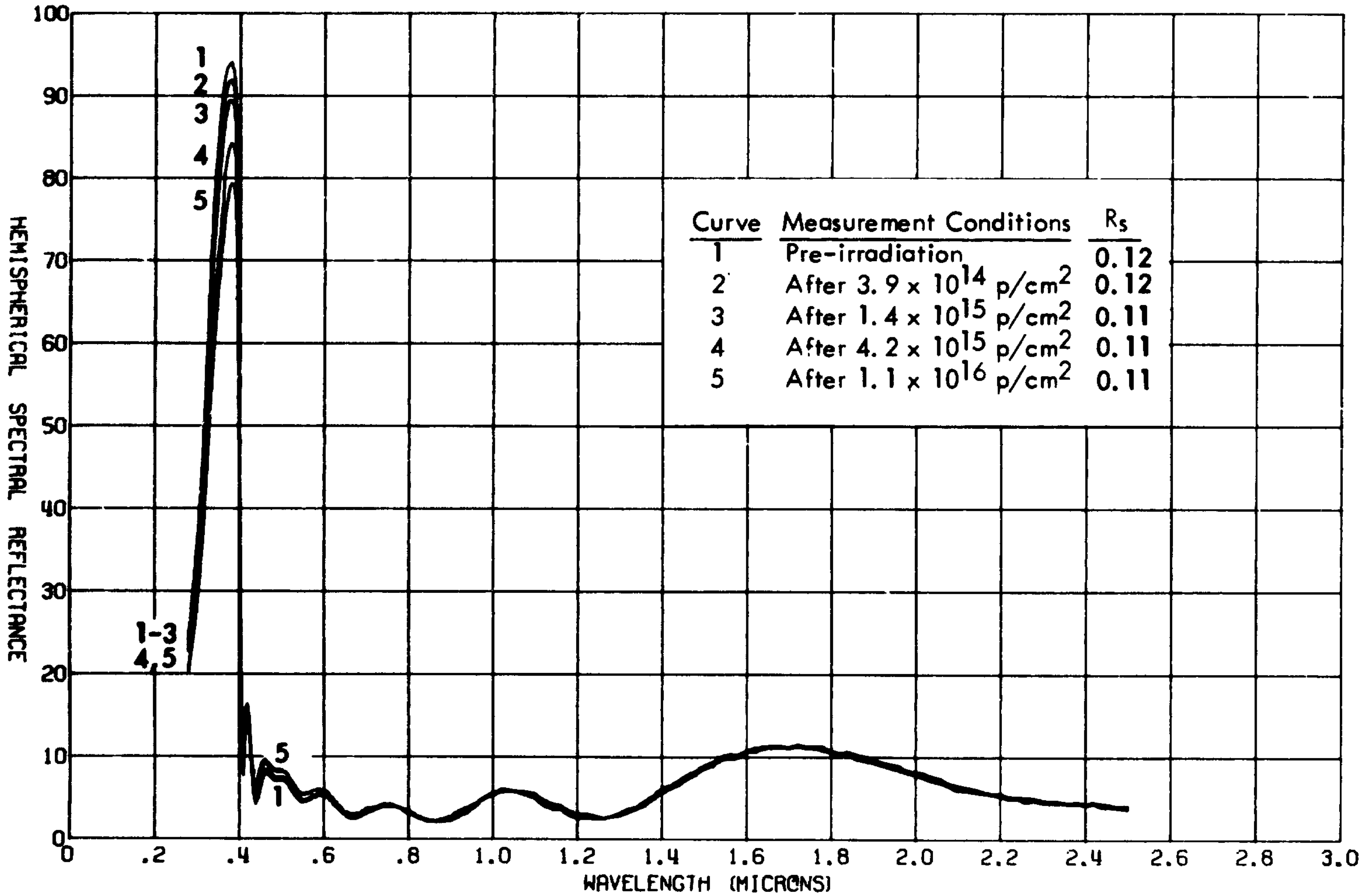

FIGURE 30. IN SITU ULTRAVIOLET EFFECTS ON THE TRANSMITTANCE OF J P L SAMPLE 2077 BLUE FILTER 2400-HOUR TEST

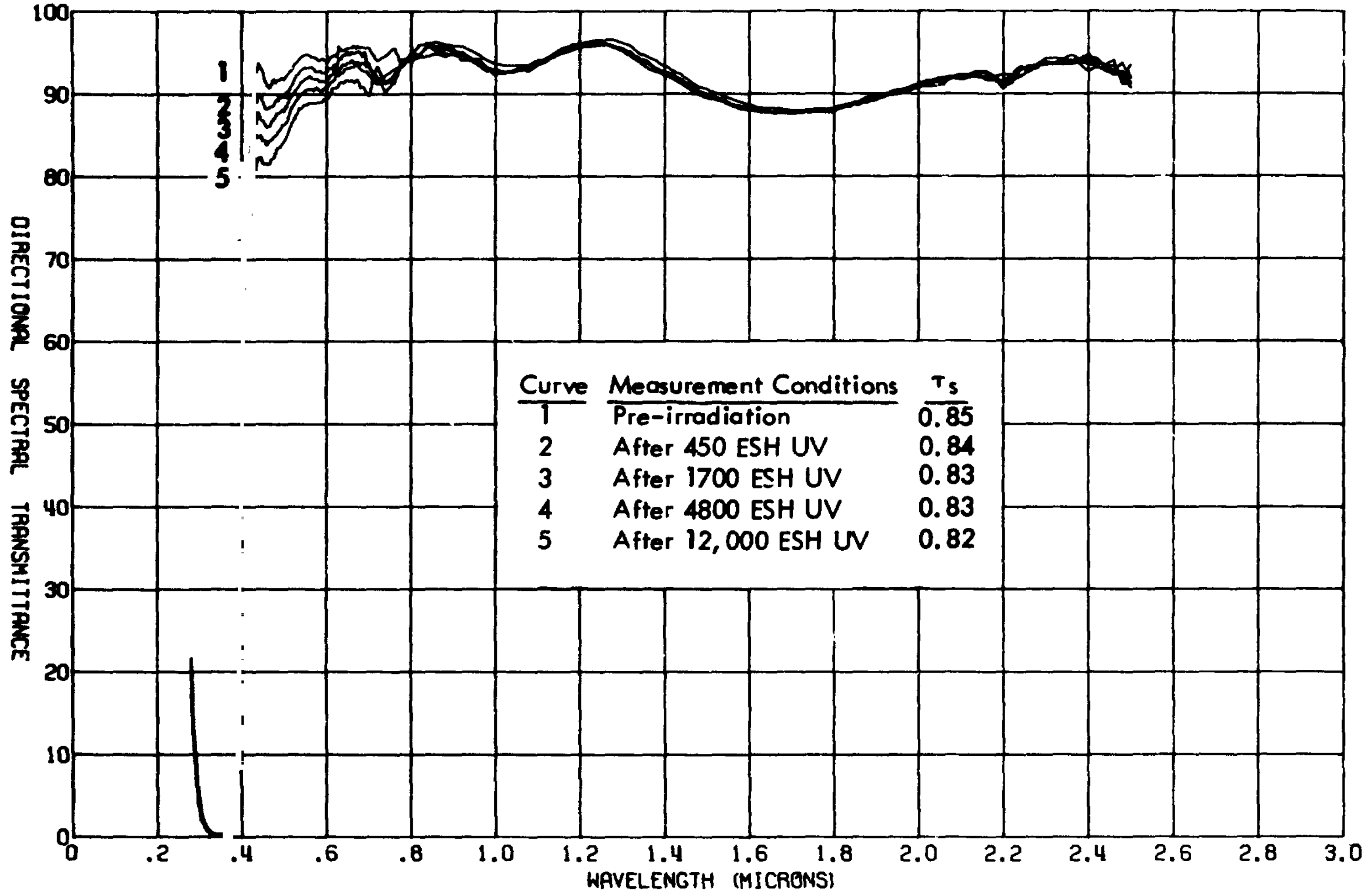

FIGURE 31.

IN SITU PROTON-ULTRAVIOLET EFFECTS ON THE TRANSMITTANCE OF J P L SAMPLE 2086
BLUE FILTER 2400-HOUR TEST

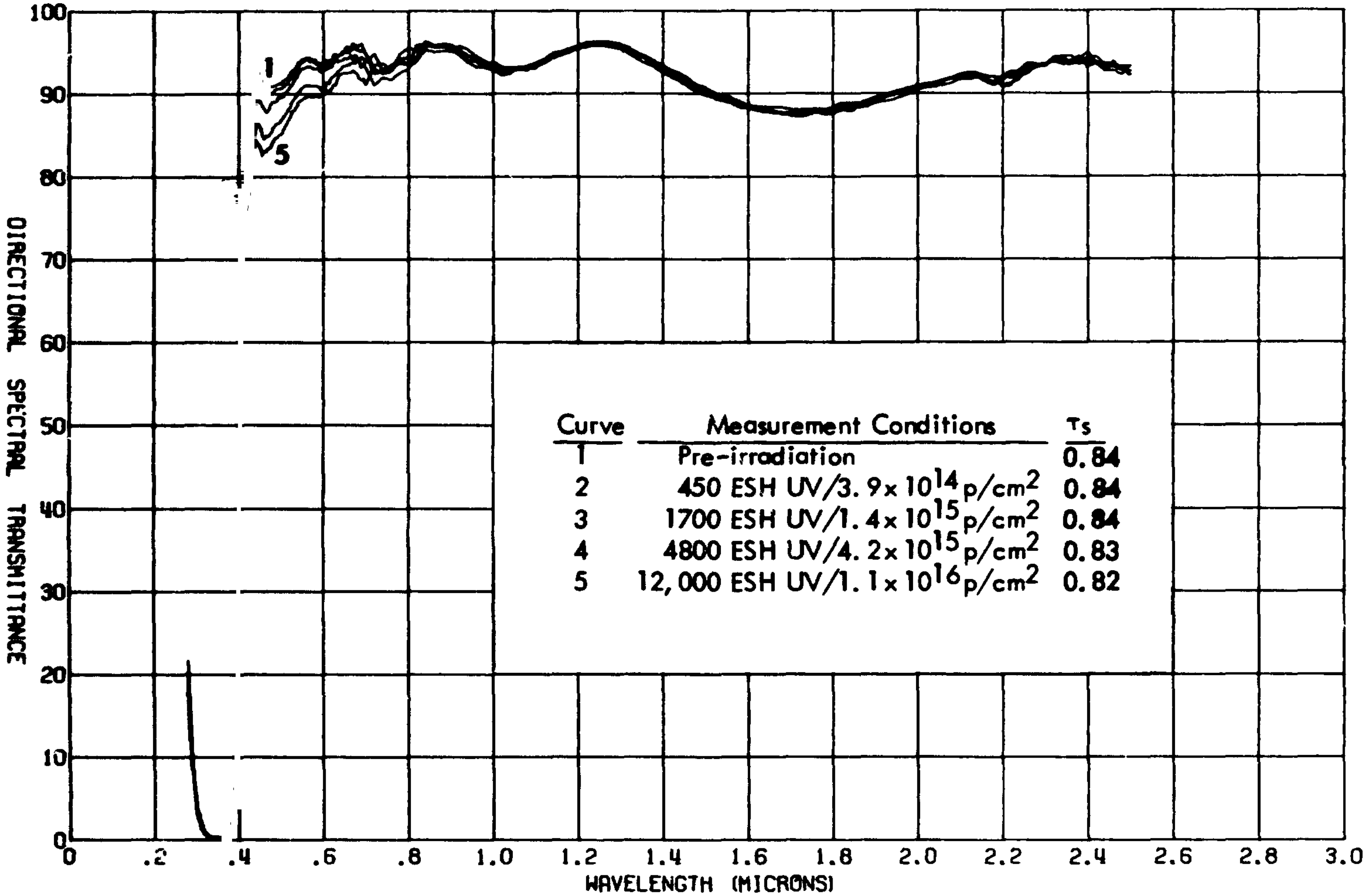

FIGURE 32. IN SITU PROTON EFFECTS ON THE TRANSMITTANCE OF J P L SAMPLE 2095 BLUE FILTER 2400-HOUR TEST

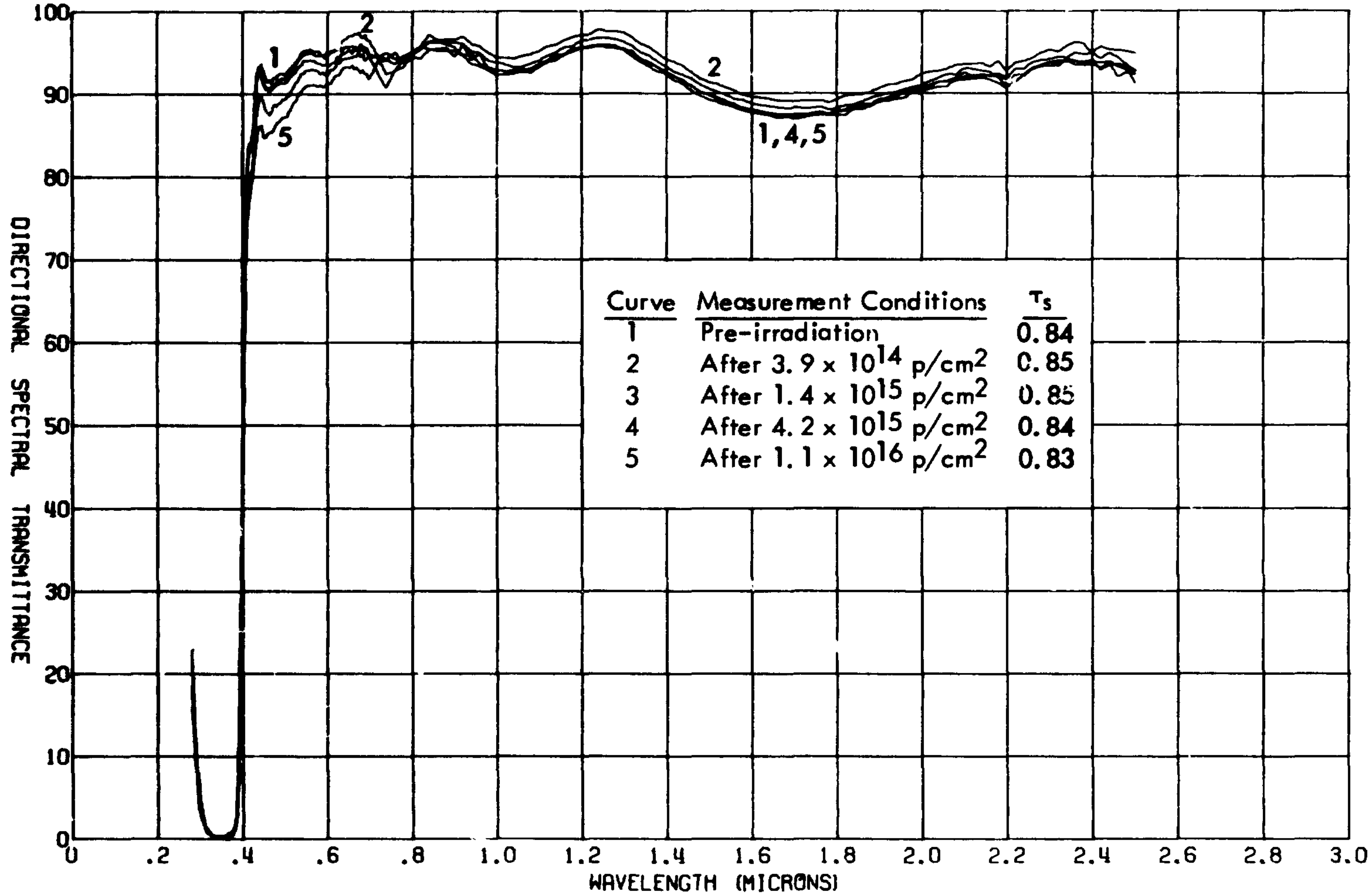

FIGURE 33. IN SITU ULTRAVIOLET EFFECTS ON THE ABSORPTANCE OF J P L SAMPLE 2077
BLUE FILTER 2400-HOUR TEST

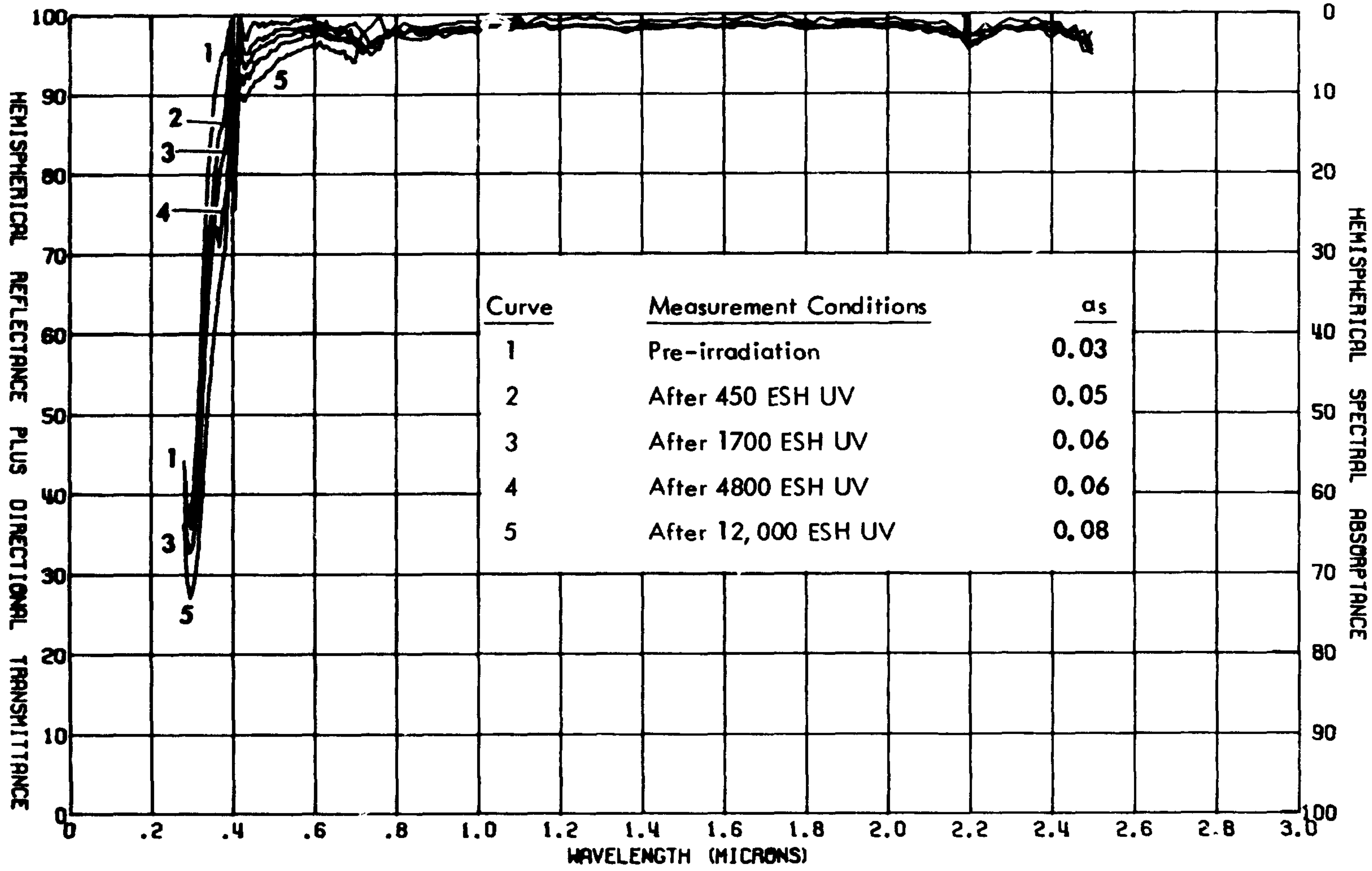

FIGURE 34.

IN SITU PROTON-ULTRAVIOLET EFFECTS ON THE ABSORPTANCE OF J P L SAMPLE 2086
BLUE FILTER 2400-HOUR TEST

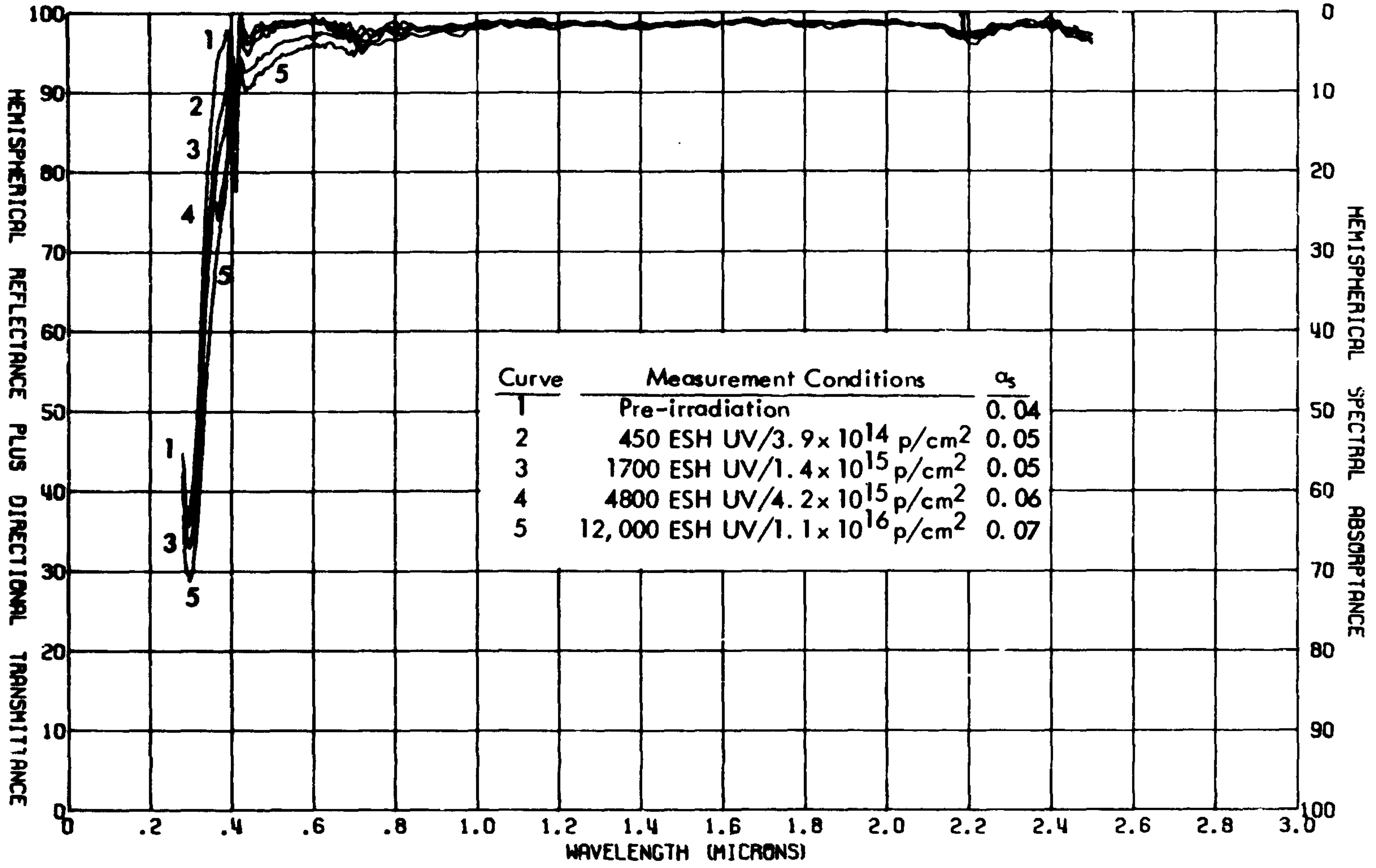

FIGURE 35. IN SITU PROTON EFFECTS ON THE ABSORPTANCE OF J P L SAMPLE 2095
BLUE FILTER 2400-HOUR TEST

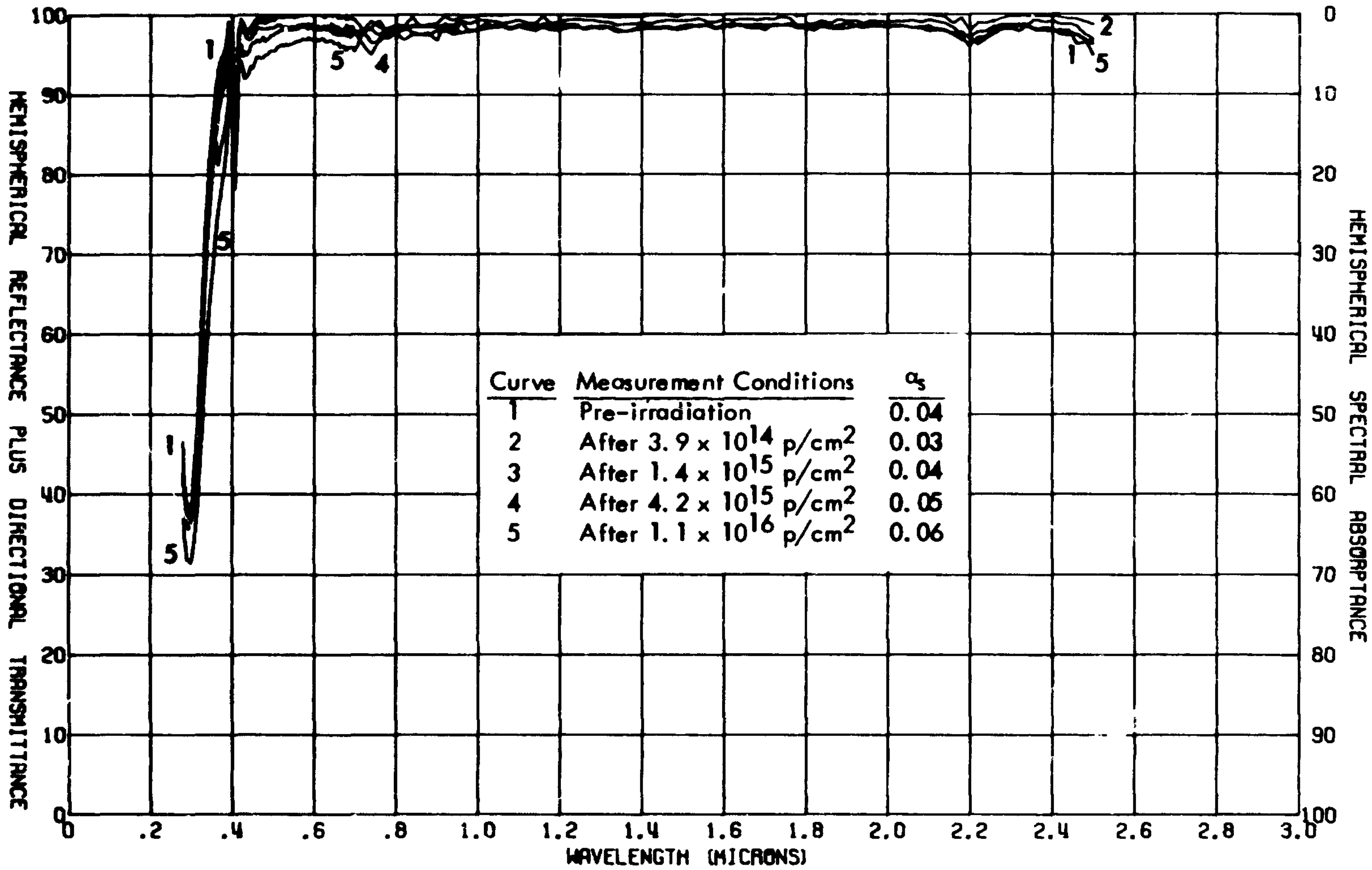

FIGURE 36. IN SITU ULTRAVIOLET EFFECTS ON THE REFLECTANCE OF J P L SAMPLE 2075
MODIFIED 4026 FILTER ON 2 OHM-CM CELL 2400-HOUR TEST

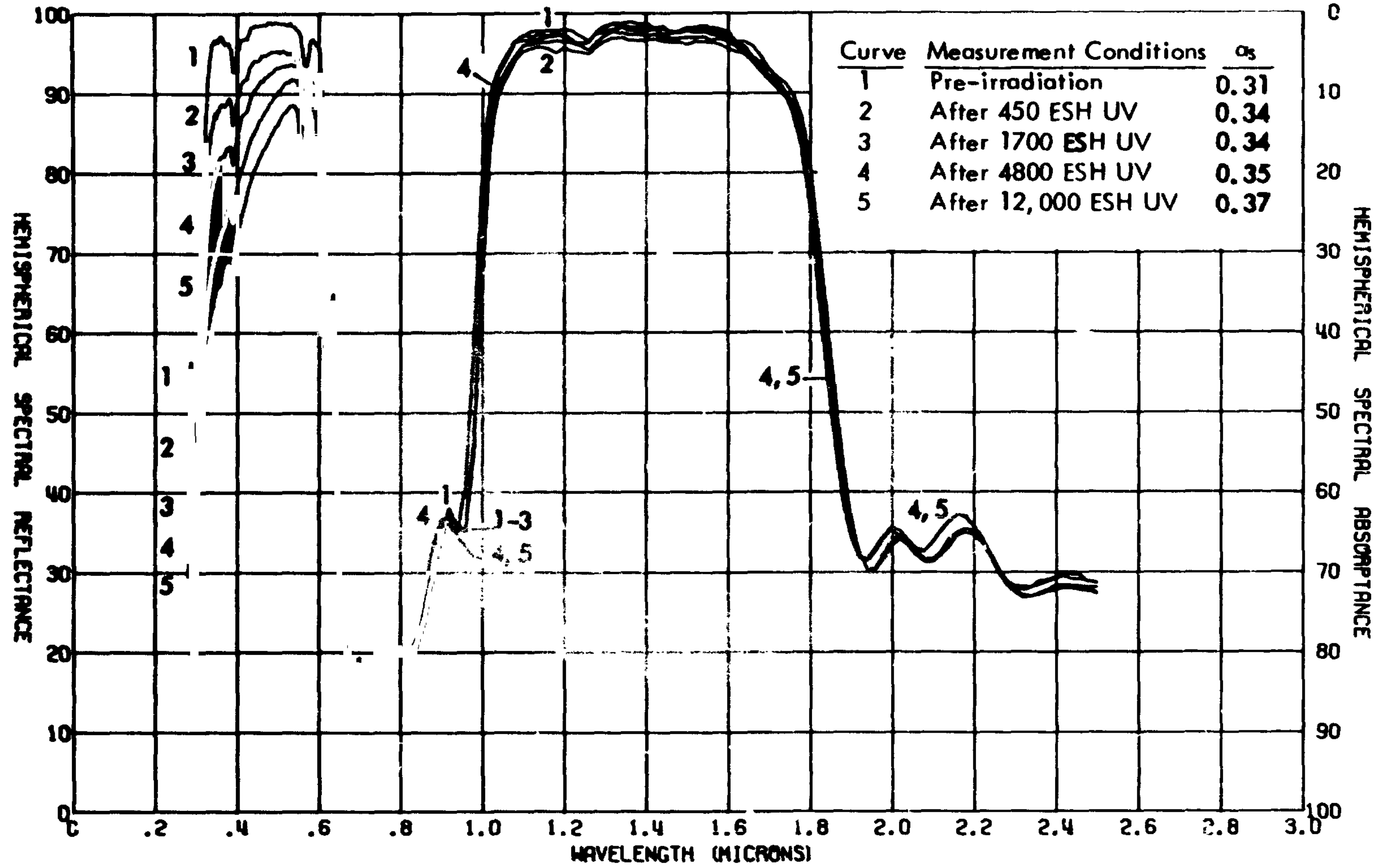

FIGURE 37.

IN SITU PROTON-ULTRAVIOLET EFFECTS ON THE REFLECTANCE OF J P L SAMPLE 2084
MODIFIED 4026 FILTER ON 2 OHM-CM CELL 2400-HOUR TEST

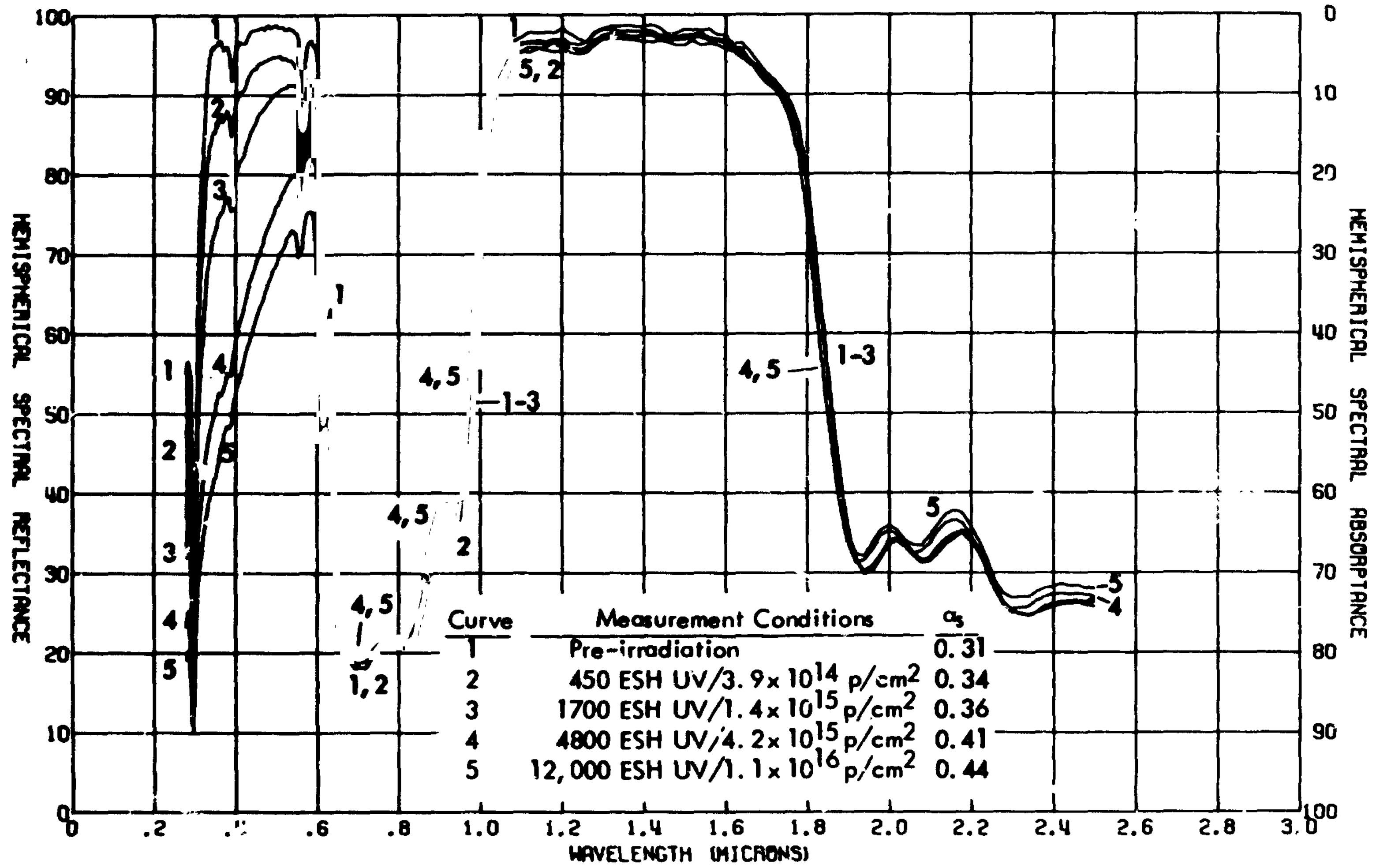

FIGURE 38. IN SITU PROTON EFFECTS ON THE REFLECTANCE OF J P L SAMPLE 2093 MODIFIED 4026 FILTER ON 2 OHM-CM CELL 2400-HOUR TEST

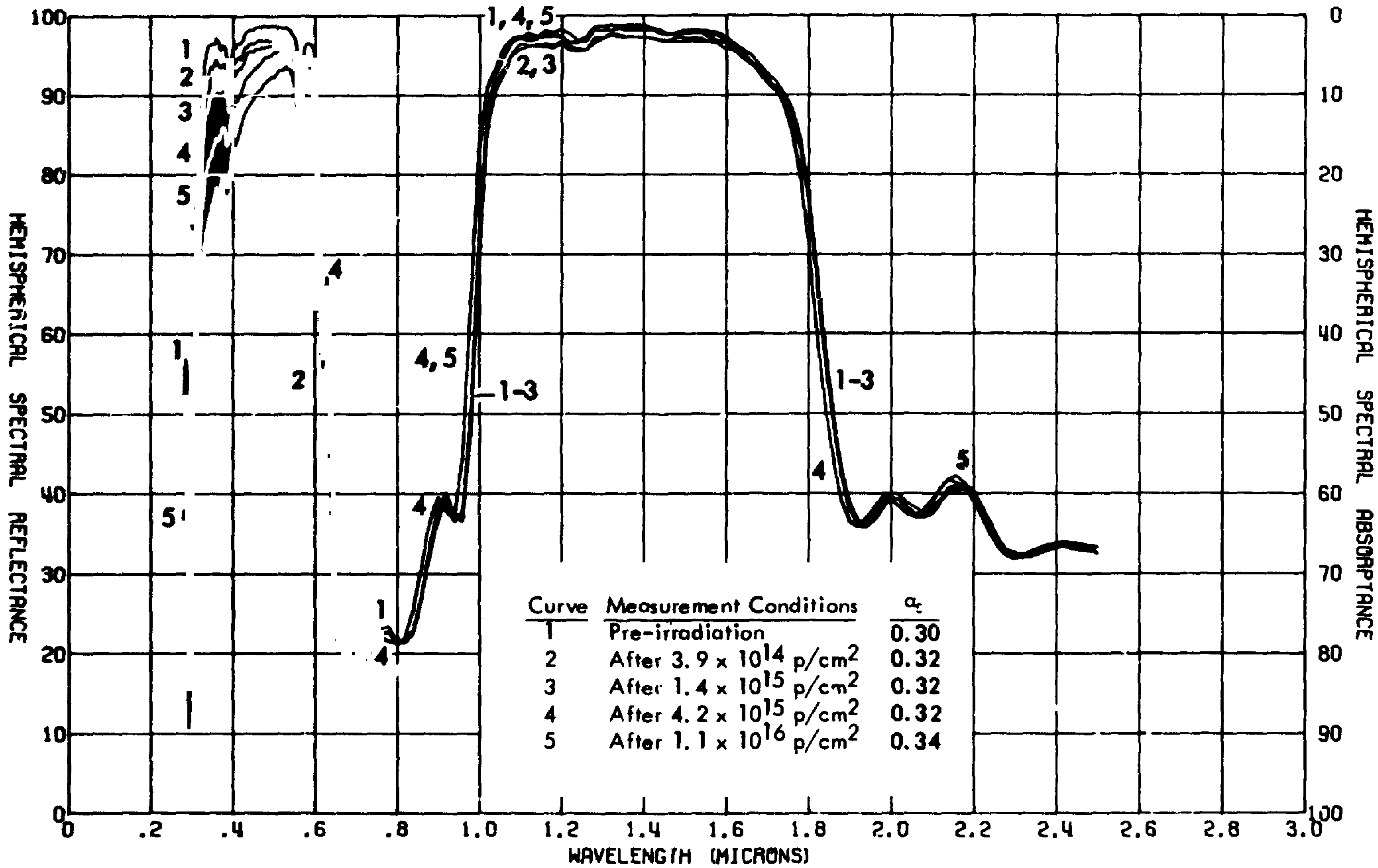

FIGURE 39. IN SITU ULTRAVIOLET EFFECTS ON THE REFLECTANCE OF J P L SAMPLE 2078 MODIFIED 4026 FILTER 2400-HOUR TEST

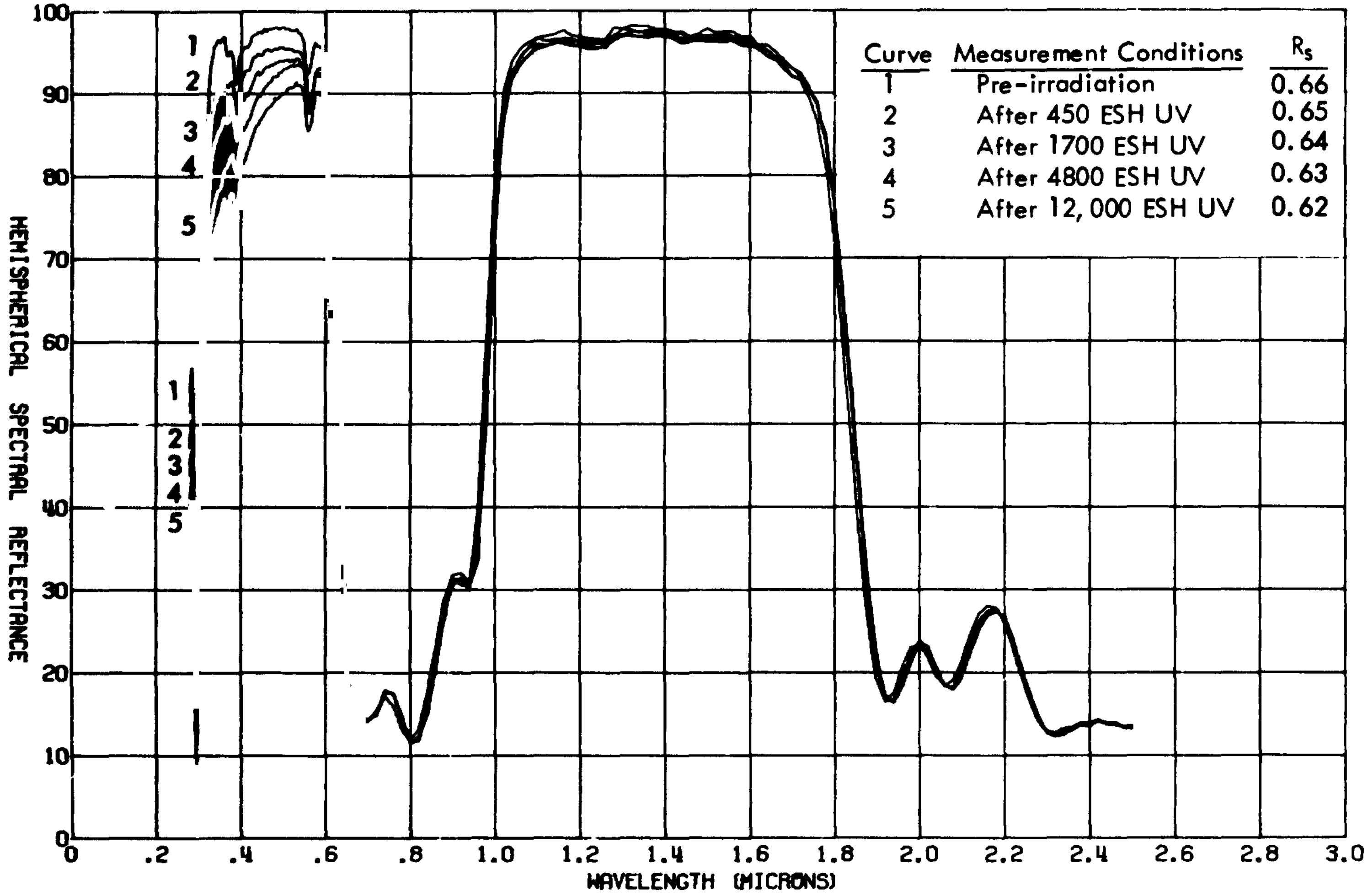

F: ЭURE 40.

IN SITU PROTON-ULTRAVIOLET EFFECTS ON THE REFLECTANCE OF J P L SAMPLE 2087
MODIFIED 4026 FILTER 2400-HOUR TEST

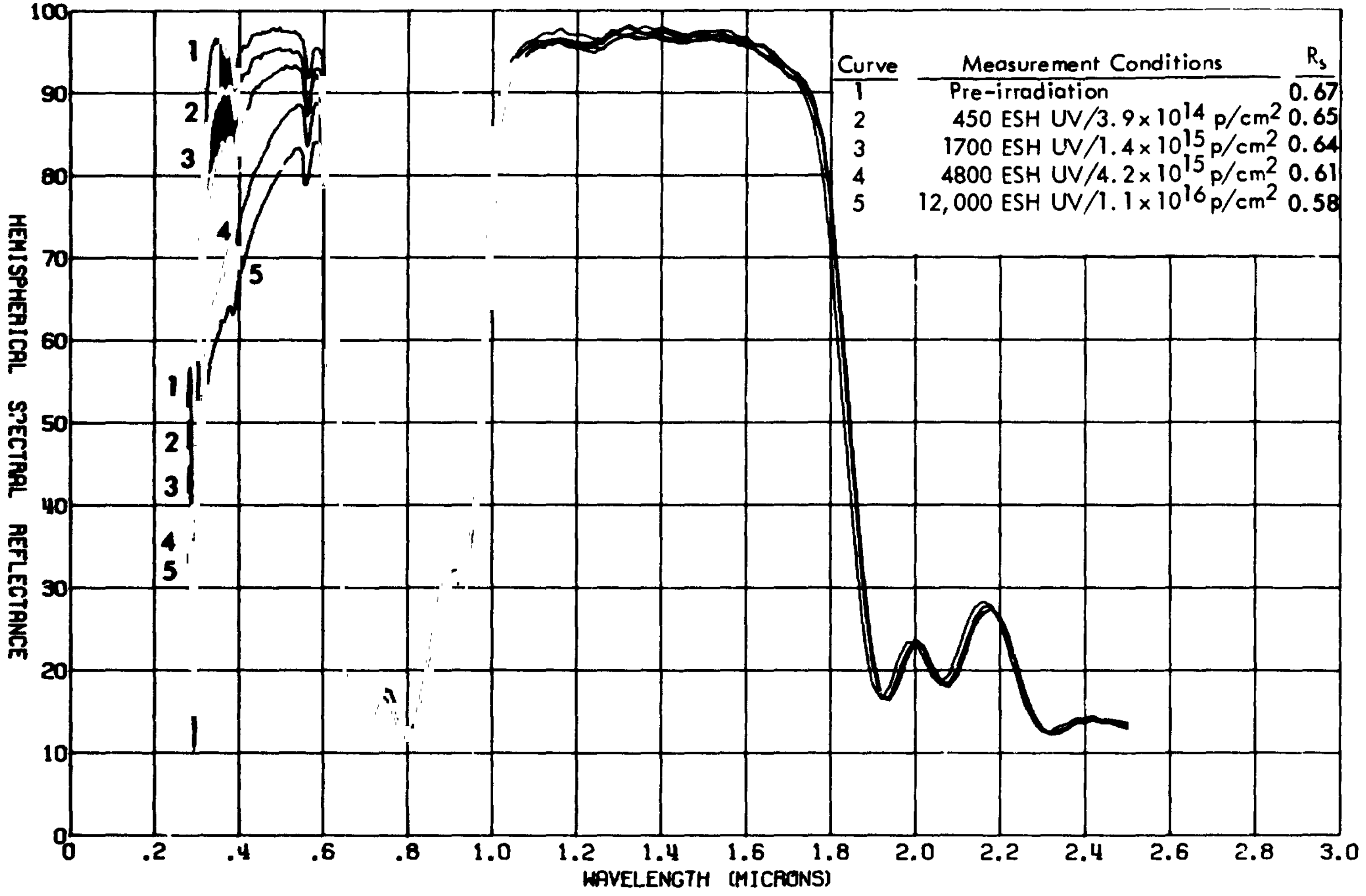

FIGURE 41. IN SITU PROTON EFFECTS ON THE REFLECTANCE OF J P L SAMPLE 2096 MODIFIED 4026 FILTER 2400-HOUR TEST

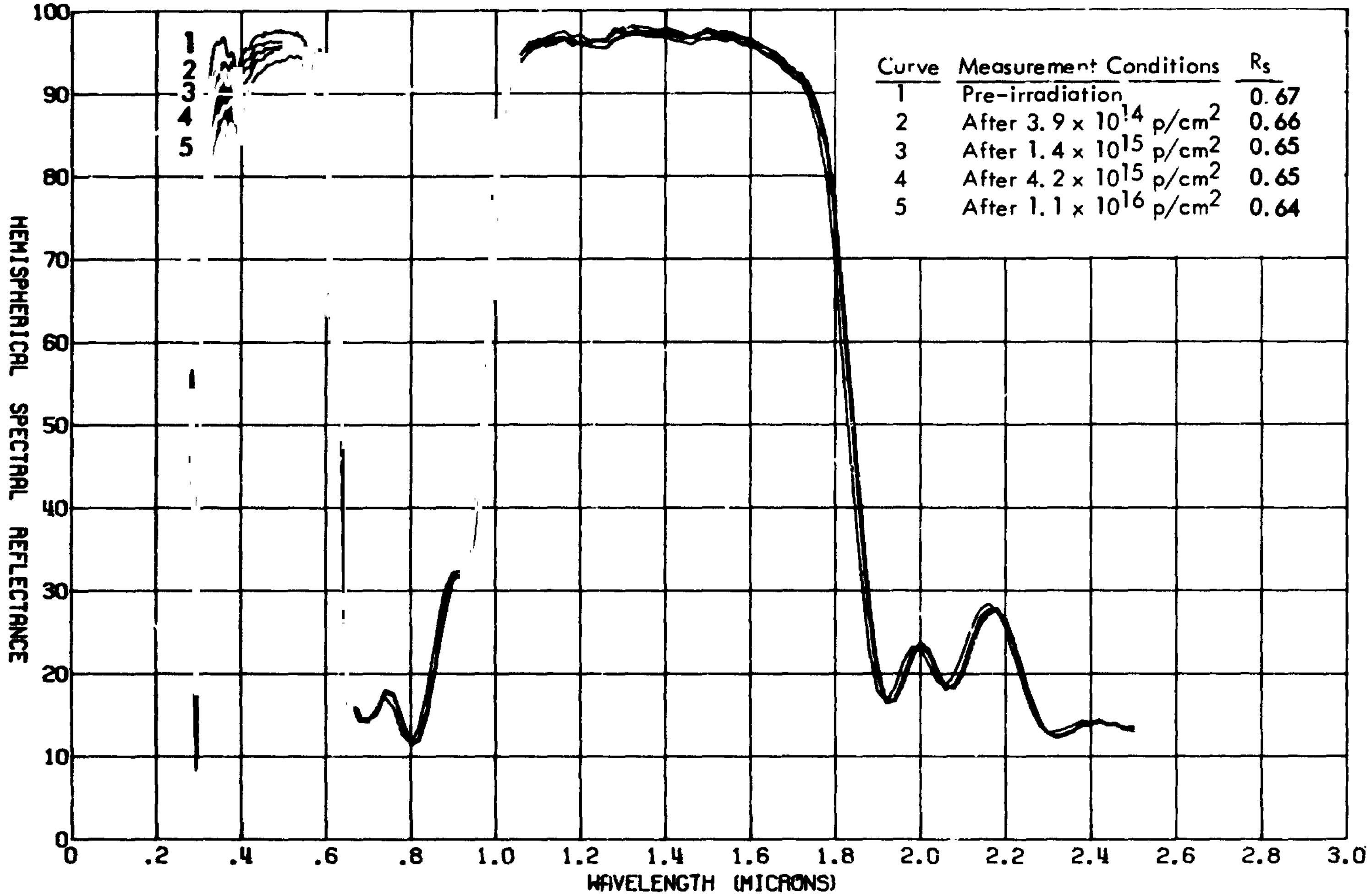

FIGURE 42. IN SITU ULTRAVIOLET EFFECTS ON THE TRANSMITTANCE OF J P L SAMPLE 2078
MODIFIED 4026 FILTER 2400-HOUR TEST

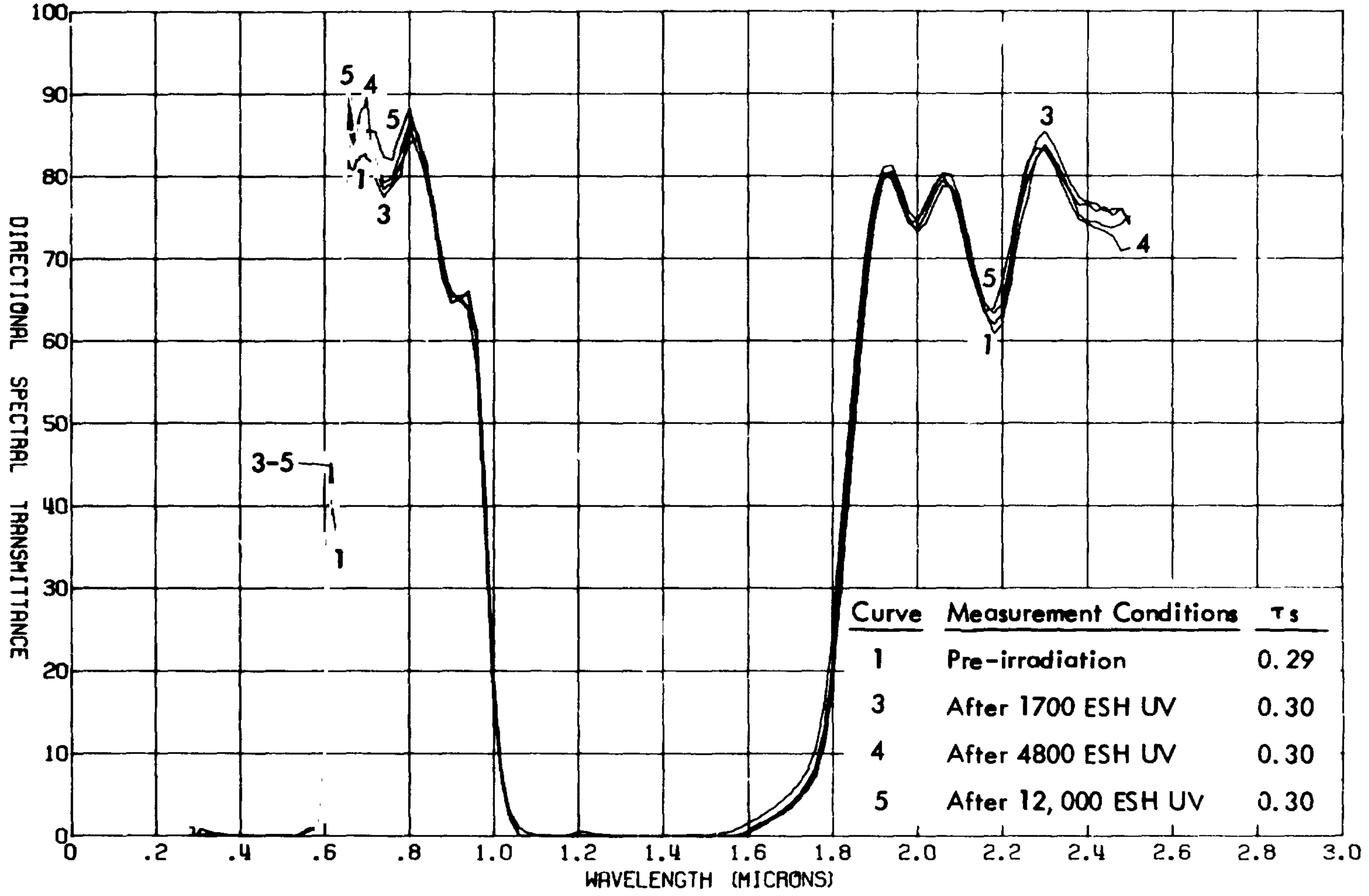

FIGURE 43.

IN SITU PROTON-ULTRAVIOLET EFFECTS ON THE TRANSMITTANCE OF J P L SAMPLE 2087
MODIFIED 4026 FILTER 2400-HOUR TEST

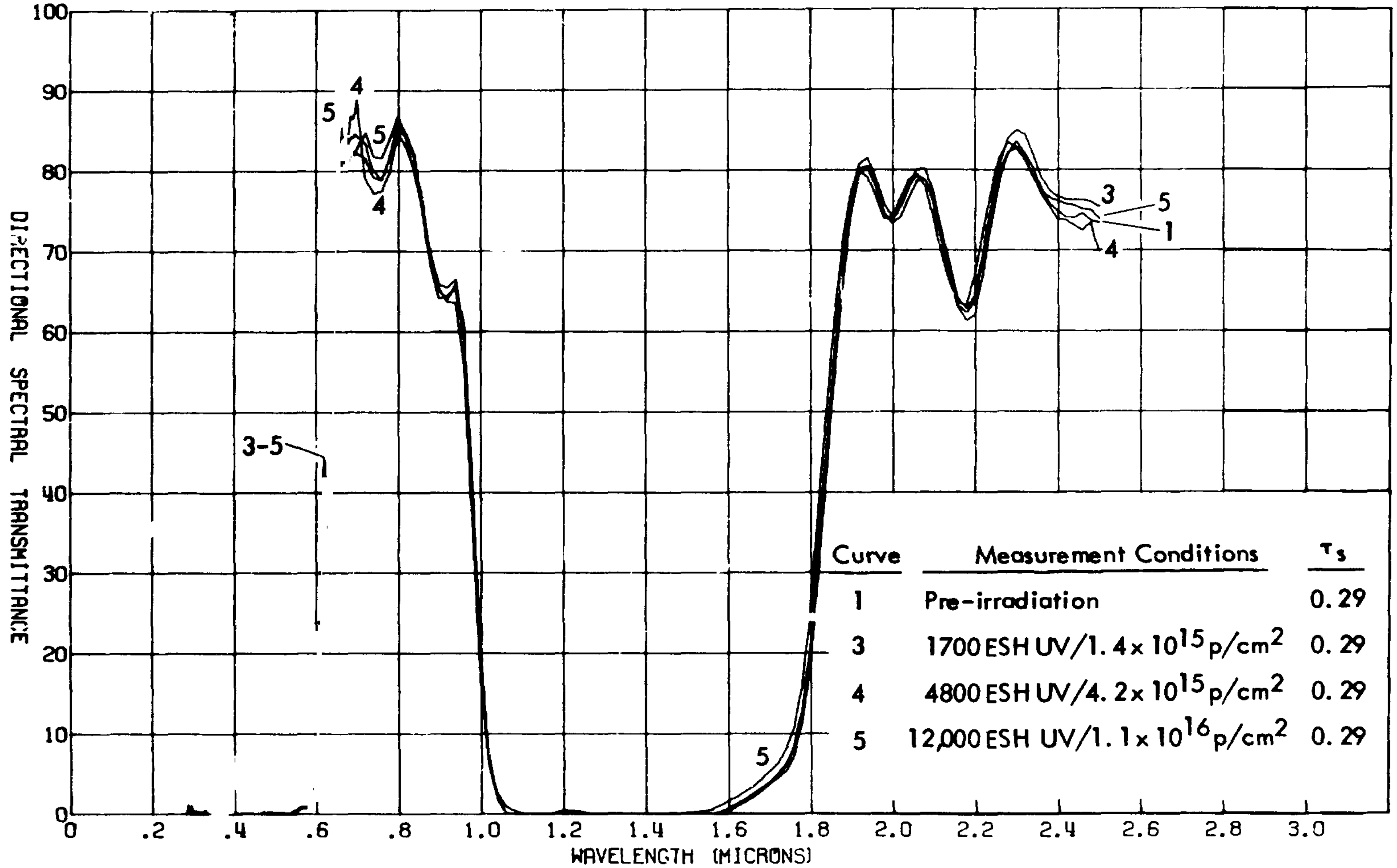

FIGURE 44. IN SITU PROTON EFFECTS ON THE TRANSMITTANCE OF J P L SAMPLE 2096 MODIFIED 4026 FILTER 2400-HOUR TEST

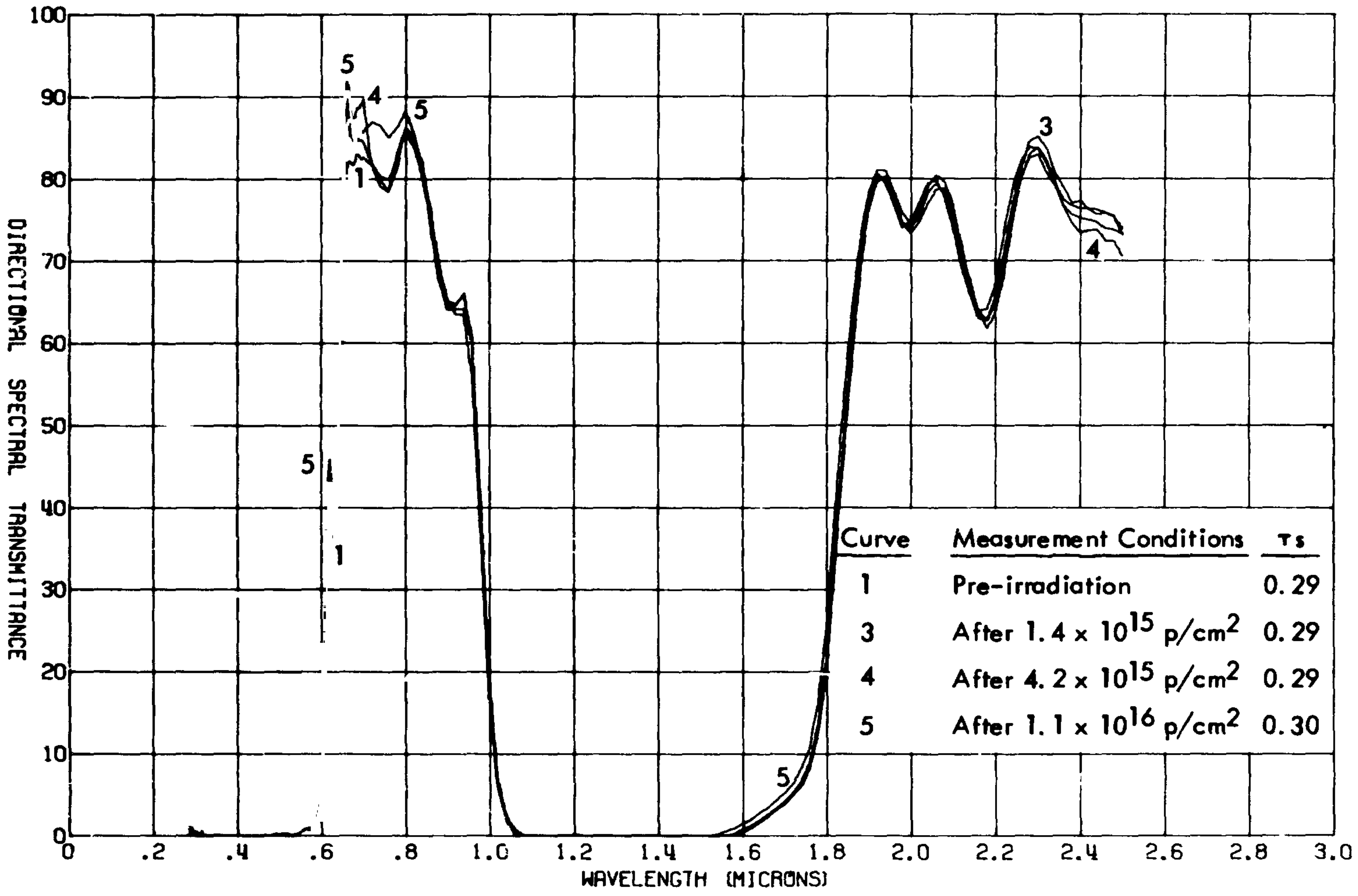

FIGURE 45. IN SITU ULTRAVIOLET EFFECTS ON THE ABSORPTANCE OF J P L SAMPLE 2078 MODIFIED 4026 FILTER 2400-HOUR TEST

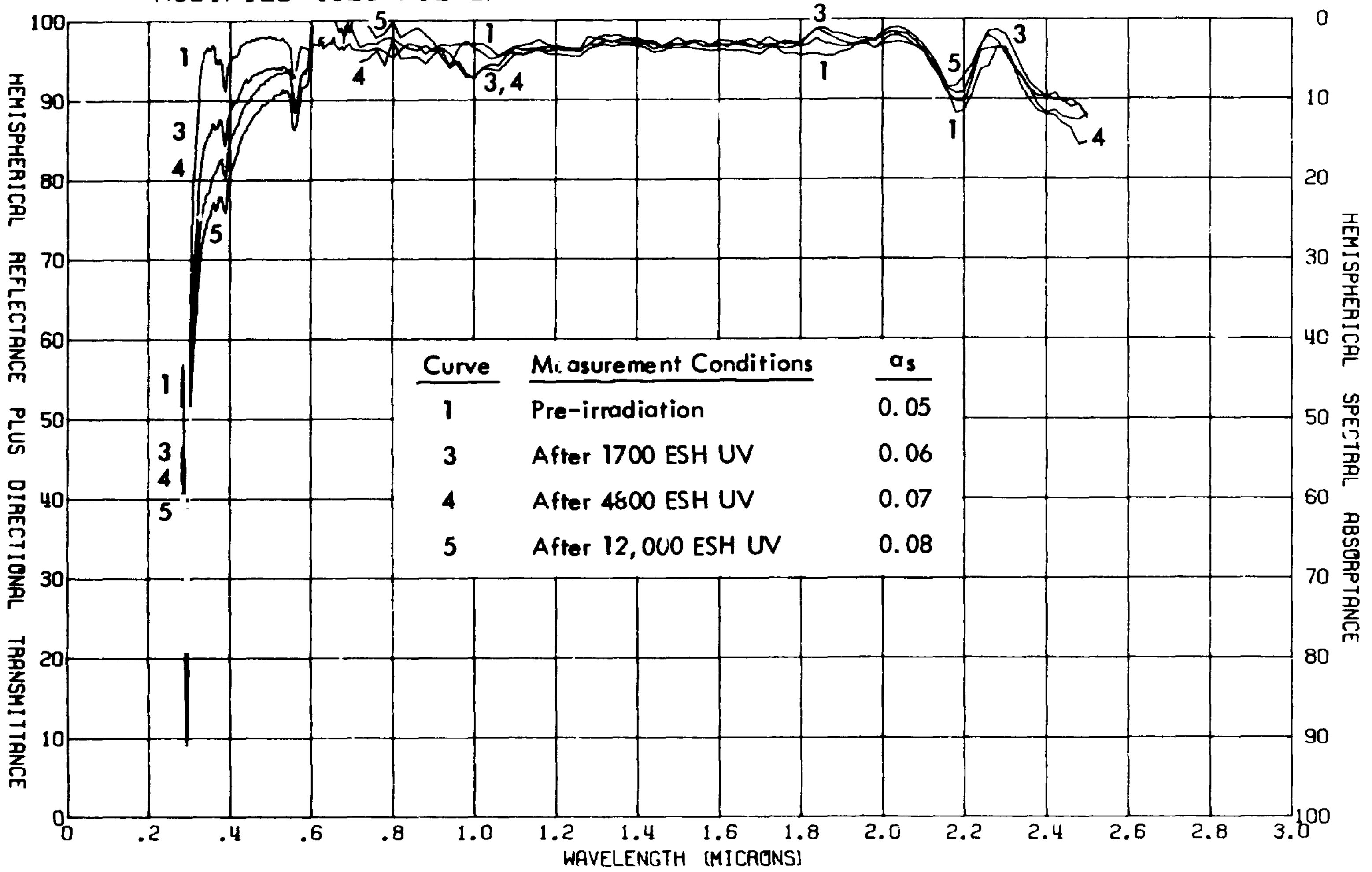

Curve	Measurement Conditions	α_s
1	Pre-irradiation	0.05
3	After 1700 ESH UV	0.06
4	After 4600 ESH UV	0.07
5	After 12,000 ESH UV	0.08

FIGURE 46.

IN SITU PROTON-ULTRAVIOLET EFFECTS ON THE ABSORPTANCE OF J P L SAMPLE 2087
MODIFIED 4026 FILTER 2400-HOUR TEST

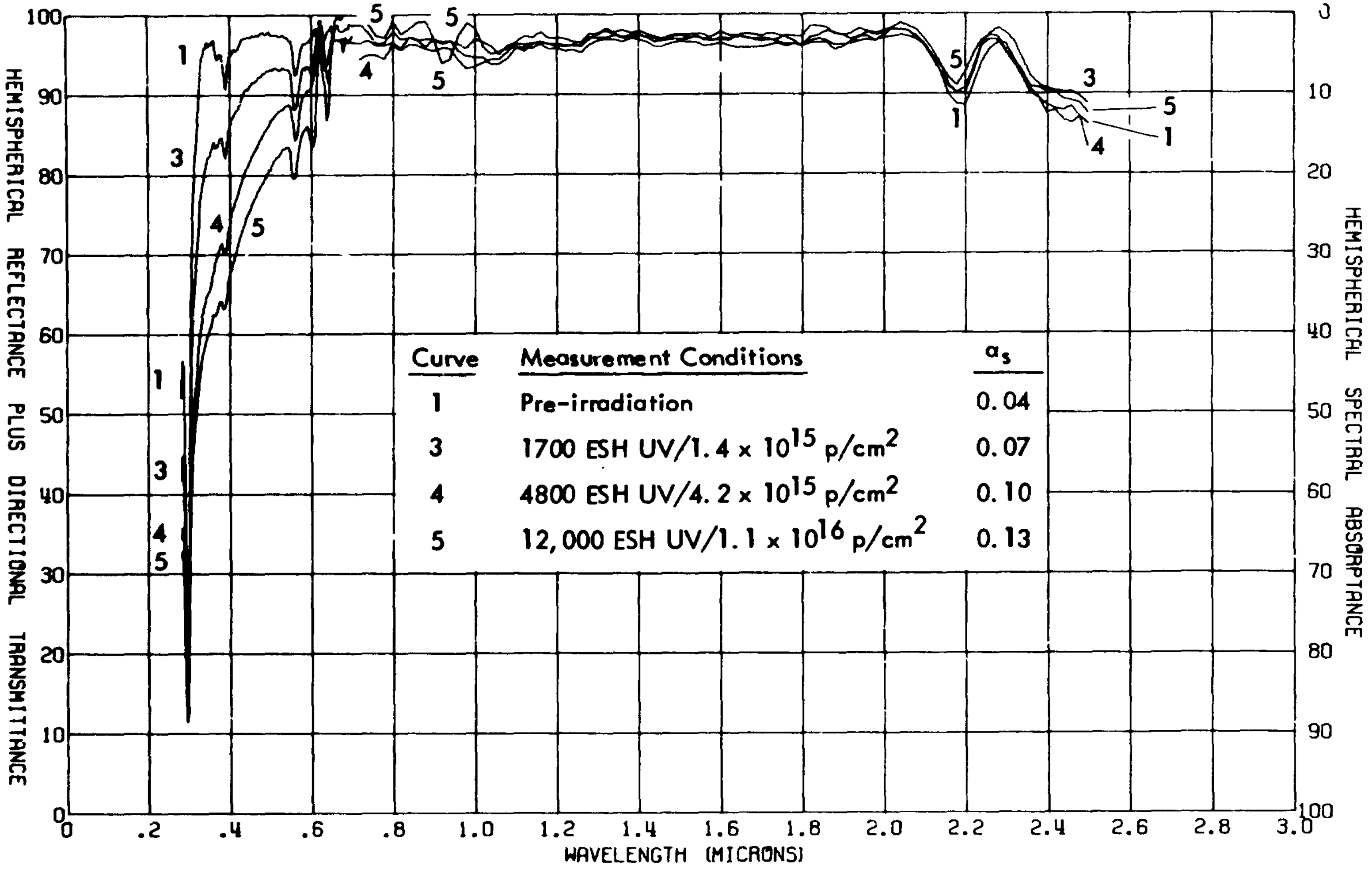

Curve	Measurement Conditions	α_s
1	Pre-irradiation	0.04
3	1700 ESH UV/1.4 x 10^{15} p/cm^2	0.07
4	4800 ESH UV/4.2 x 10^{15} p/cm^2	0.10
5	12,000 ESH UV/1.1 x 10^{16} p/cm^2	0.13

FIGURE 47. IN SITU PROTON EFFECTS ON THE ABSORPTANCE OF J P L SAMPLE 2096
MODIFIED 4026 FILTER 2400-HOUR TEST

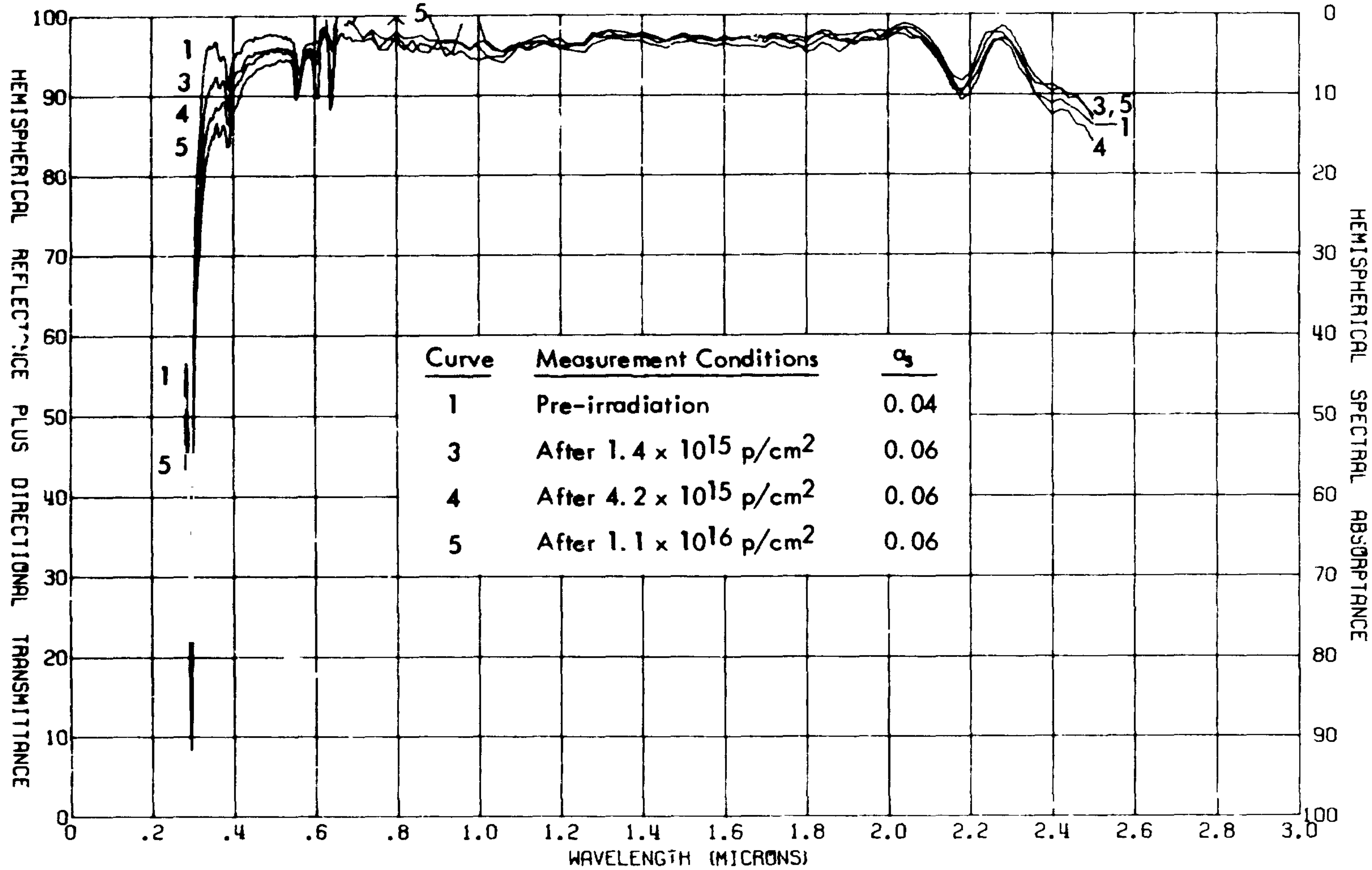

FIGURE 48. IN SITU ULTRAVIOLET EFFECTS ON THE REFLECTANCE OF J P L SAMPLE 2076 BLUE-RED FILTER ON 2 OHM-CM CELL 2400-HOUR TEST

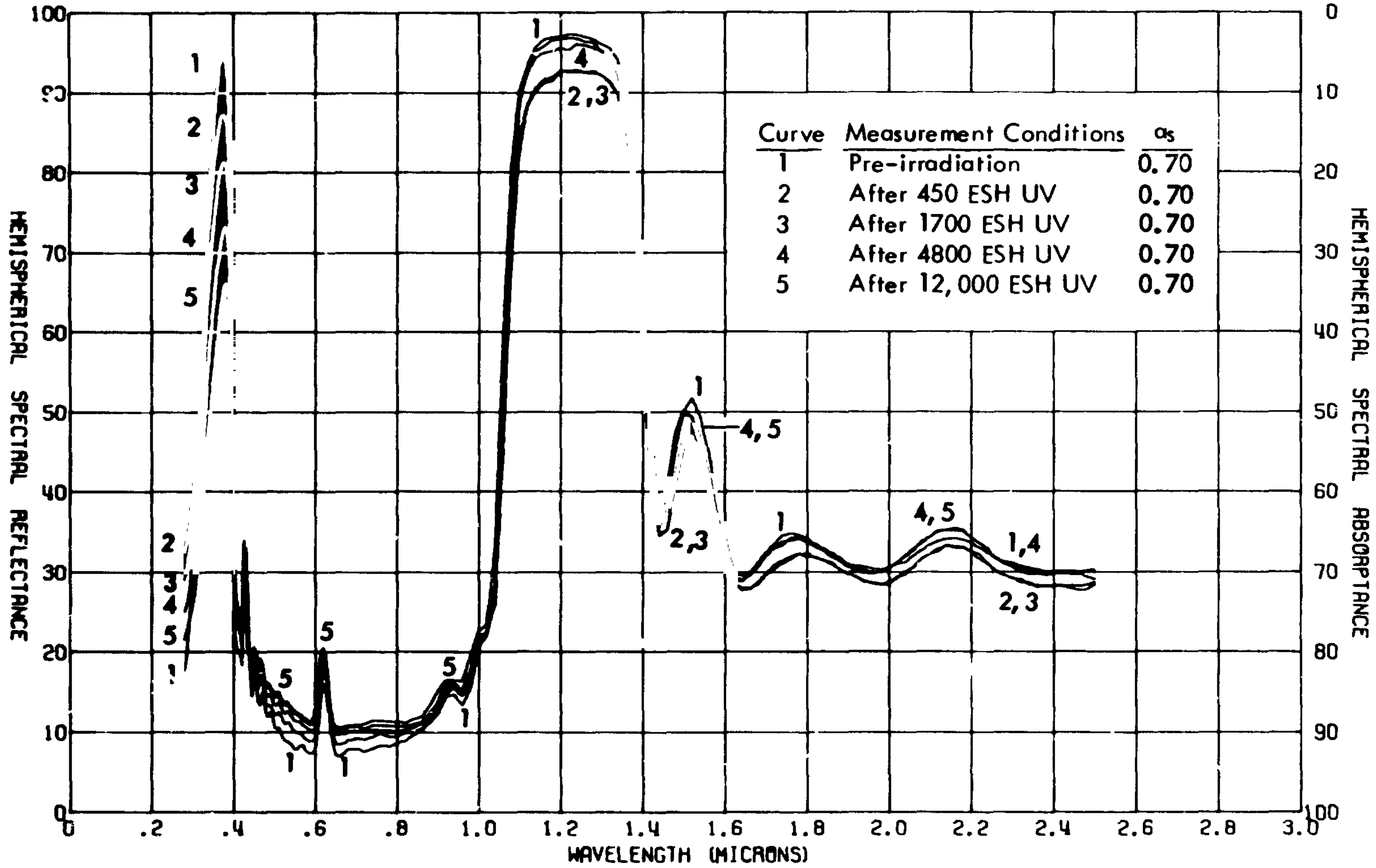

FIGURE 49.

IN SITU PROTON-ULTRAVIOLET EFFECTS ON THE REFLECTANCE OF J P L SAMPLE 2085
BLUE-RED FILTER ON 2 OHM-CM CELL 2400-HOUR TEST

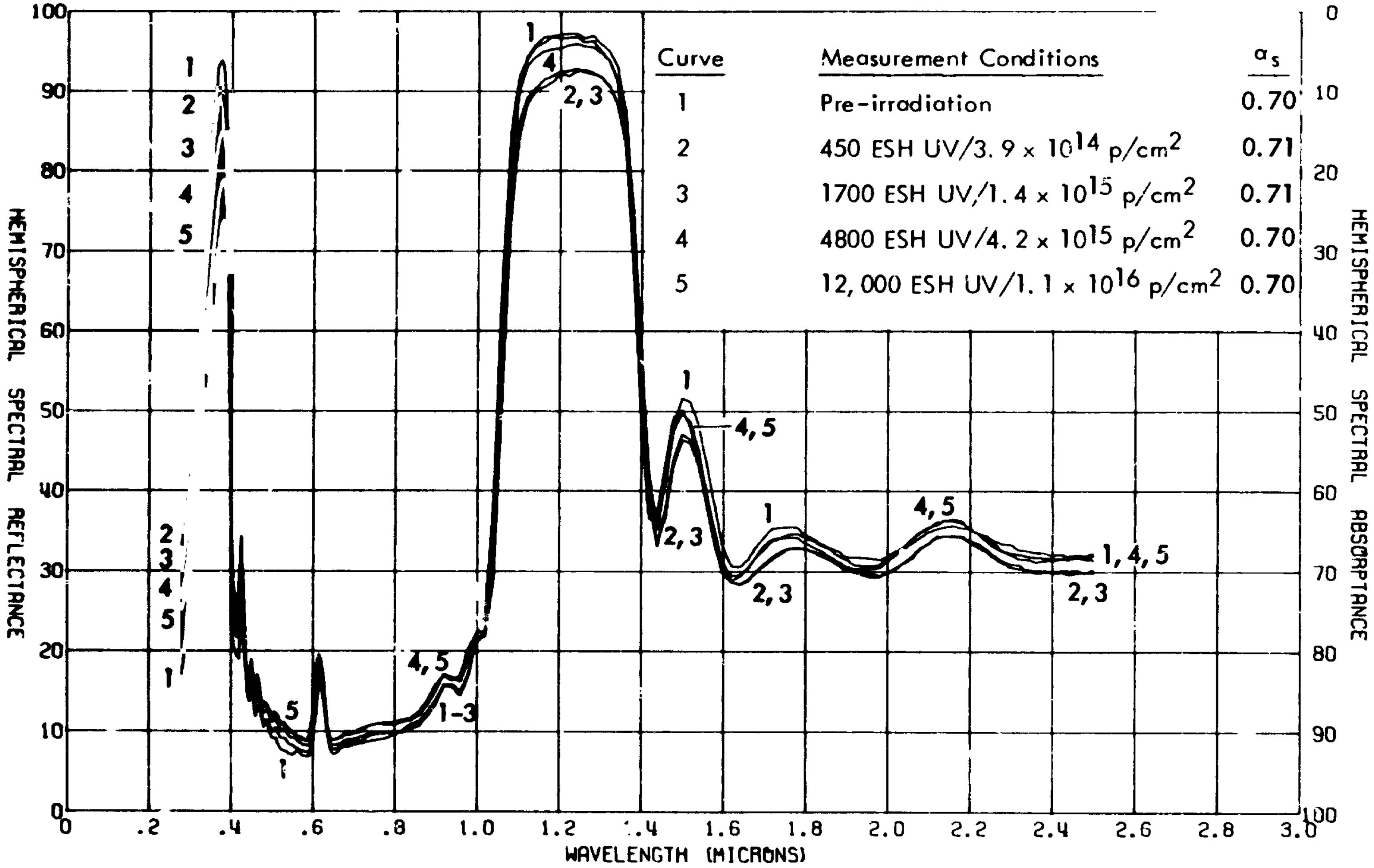

FIGURE 50.

IN SITU PROTON EFFECTS ON THE REFLECTANCE OF J P L SAMPLE 2094
BLUE-RED FILTER ON 2 OHM-CM CELL 2400-HOUR TEST

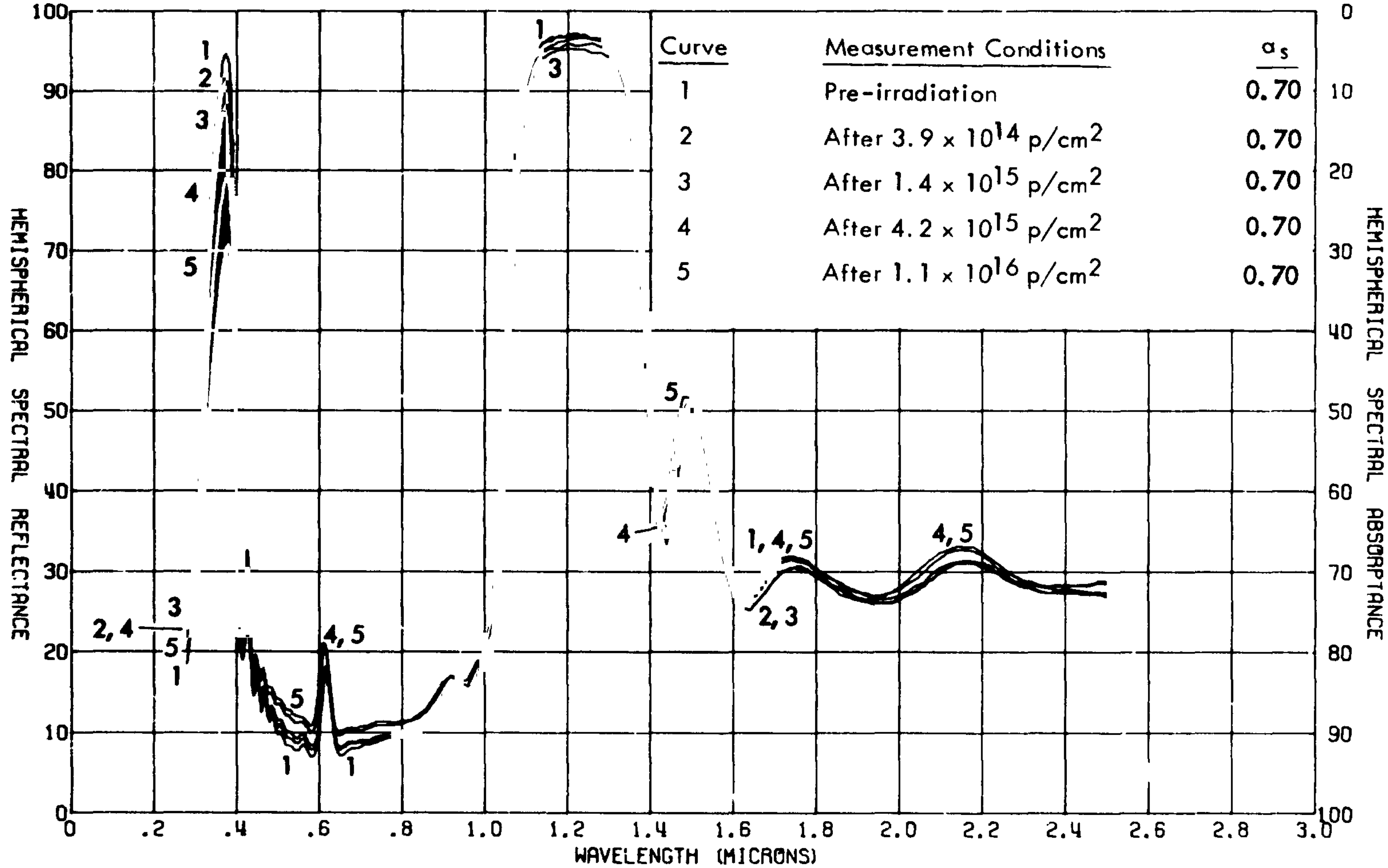

Curve	Measurement Conditions	α_s
1	Pre-irradiation	0.70
2	After 3.9×10^{14} p/cm^2	0.70
3	After 1.4×10^{15} p/cm^2	0.70
4	After 4.2×10^{15} p/cm^2	0.70
5	After 1.1×10^{16} p/cm^2	0.70

FIGURE 51. IN SITU ULTRAVIOLET EFFECTS ON THE REFLECTANCE OF J P L SAMPLE 2079
BLUE-RED FILTER 2400-HOUR TEST

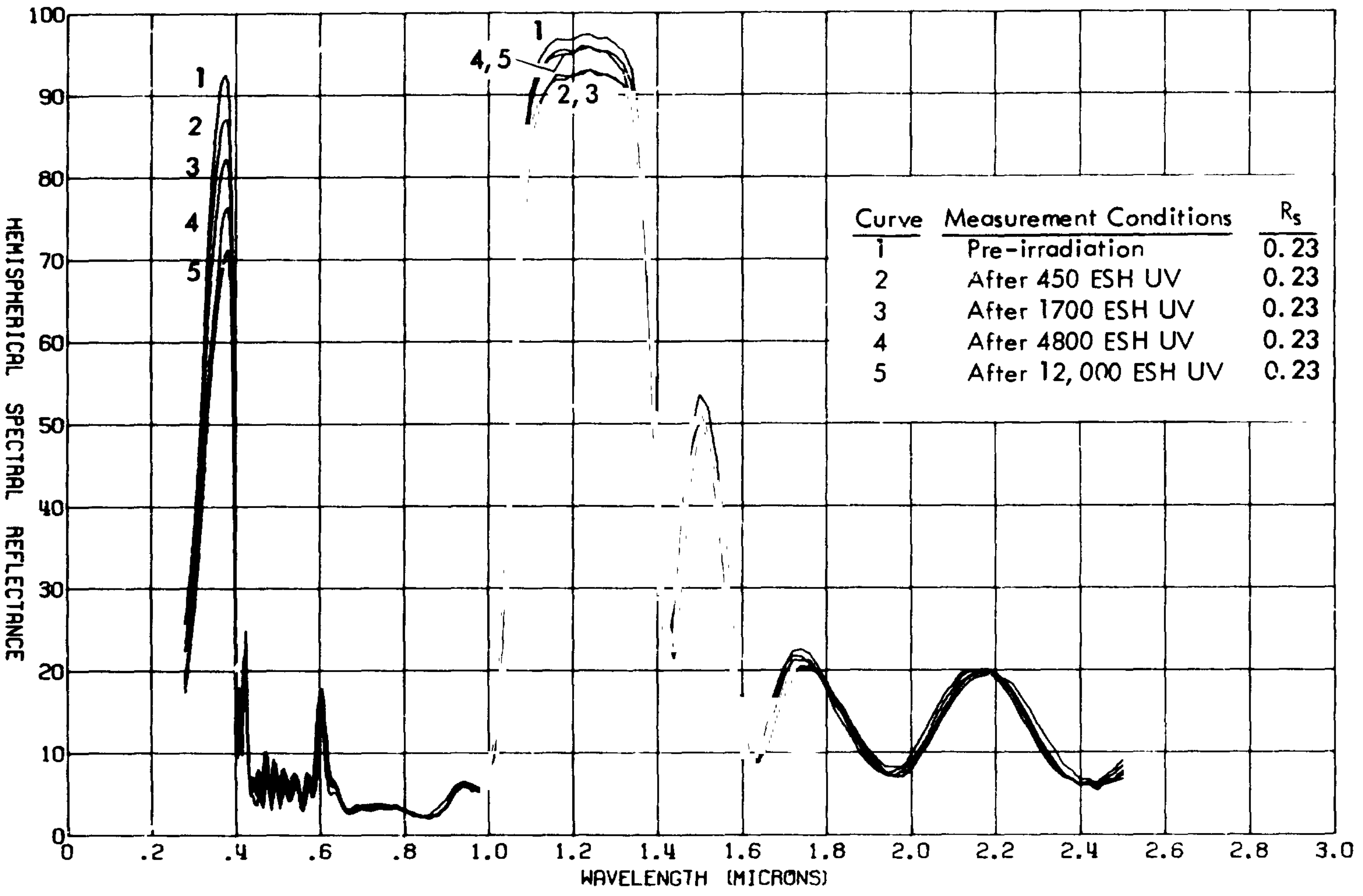

FIGURE 52.

IN SITU PROTON-ULTRAVIOLET EFFECTS ON THE REFLECTANCE OF J P L SAMPLE 2088
BLUE-RED FILTER 2400-HOUR TEST

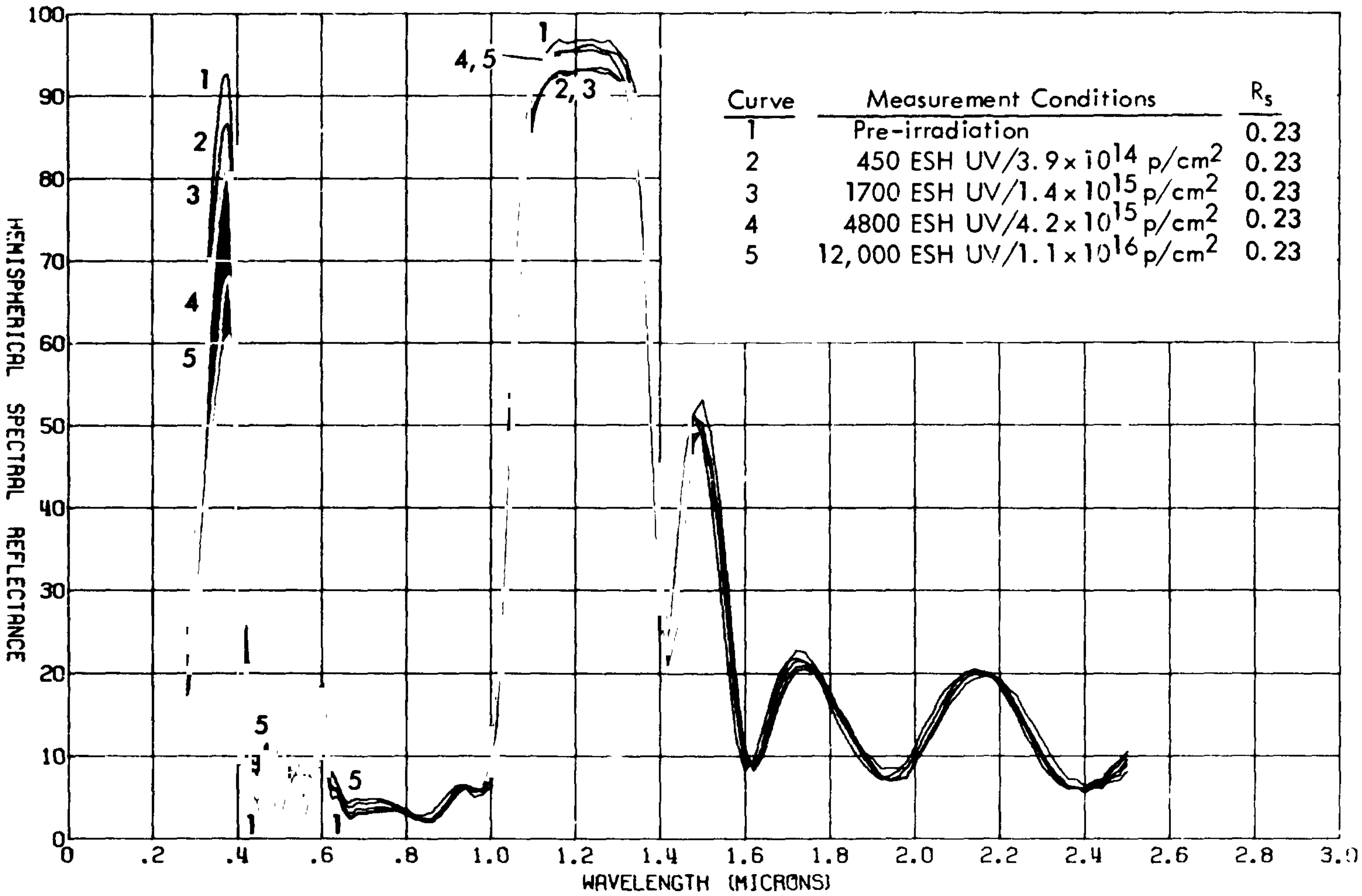

FIGURE 53. IN SITU PROTON EFFECTS ON THE REFLECTANCE OF J P L SAMPLE 2097
BLUE-RED FILTER 2400-HOUR TEST

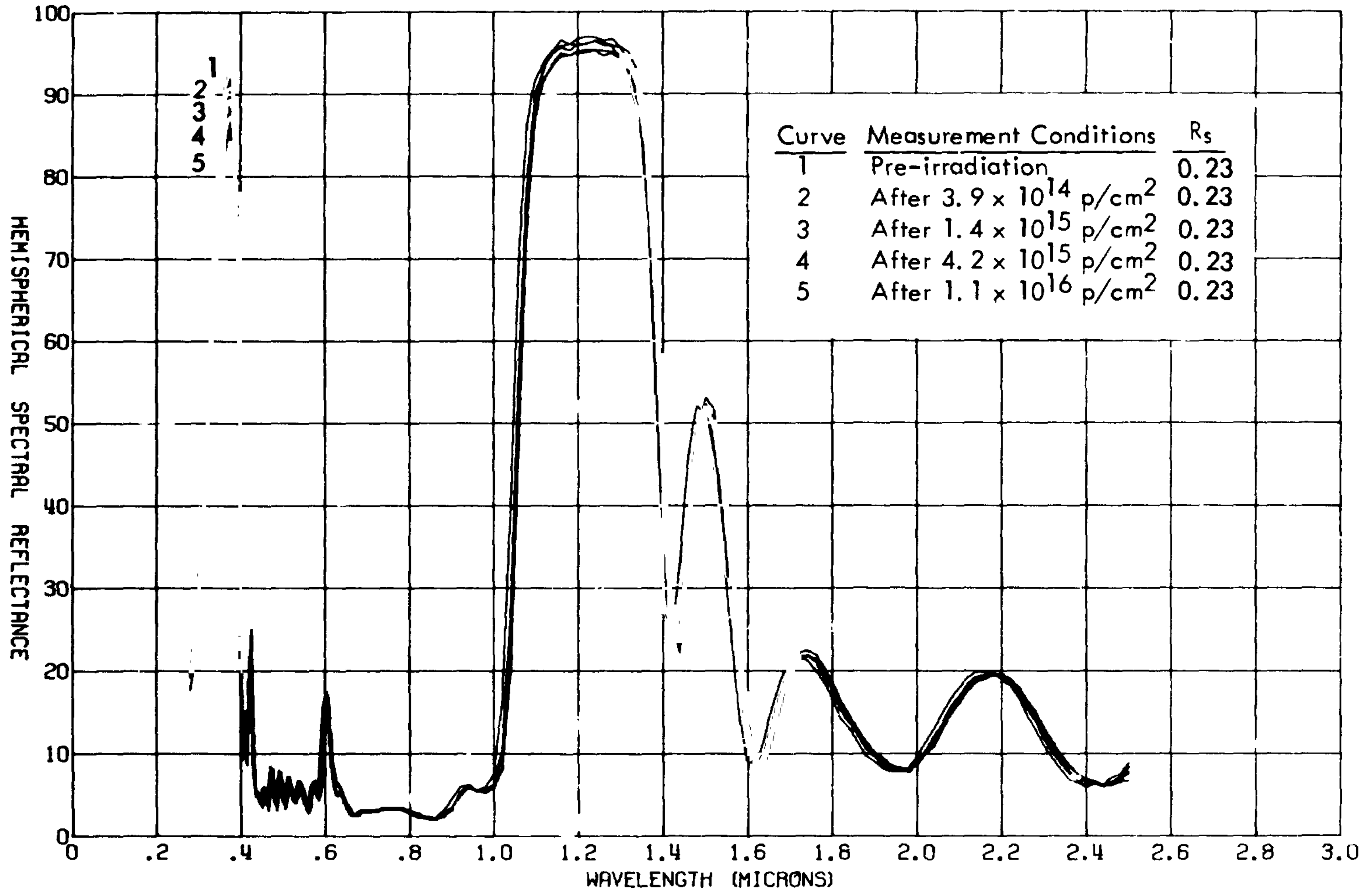

FIGURE 54. IN SITU ULTRAVIOLET EFFECTS ON THE TRANSMITTANCE OF J P L SAMPLE 2079 BLUE-RED FILTER 2400-HOUR TEST

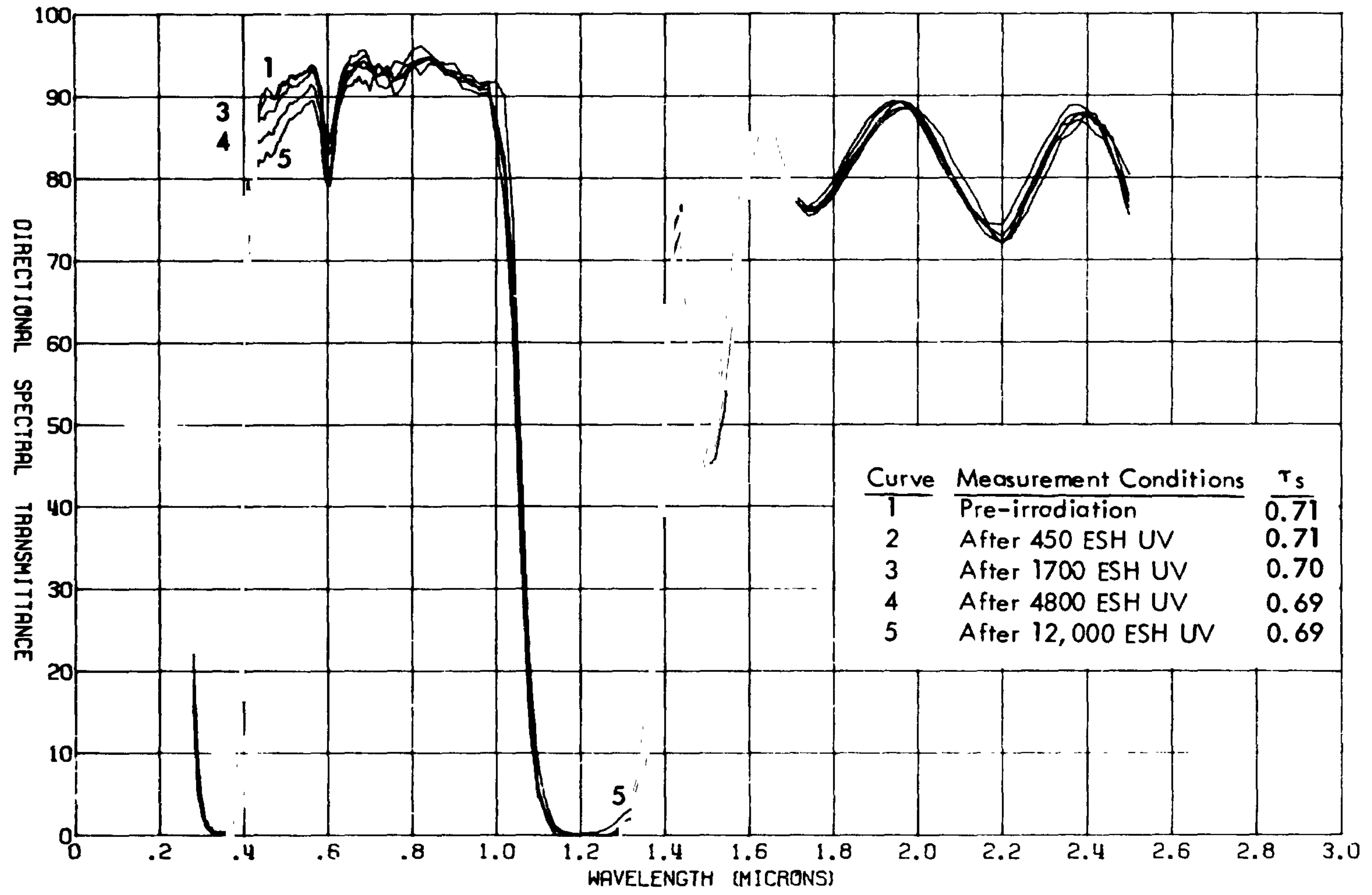

FIGURE 55.

IN SITU PROTON-ULTRAVIOLET EFFECTS ON THE TRANSMITTANCE OF J P L SAMPLE 2088
BLUE-RED FILTER 2400-HOUR TEST

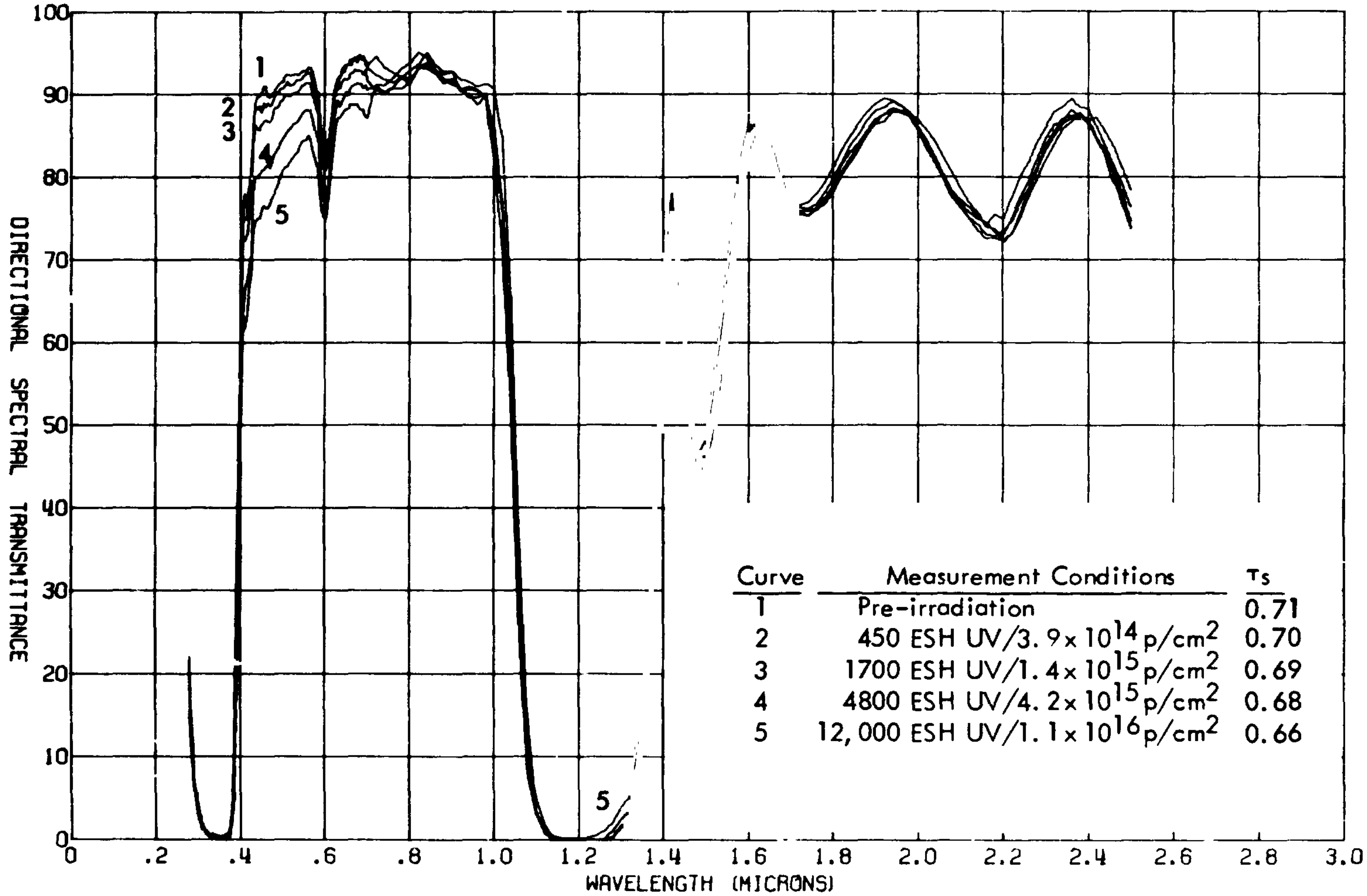

FIGURE 56. IN SITU PROTON EFFECTS ON THE TRANSMITTANCE OF J P L SAMPLE 2097
BLUE-RED FILTER 2400-HOUR TEST

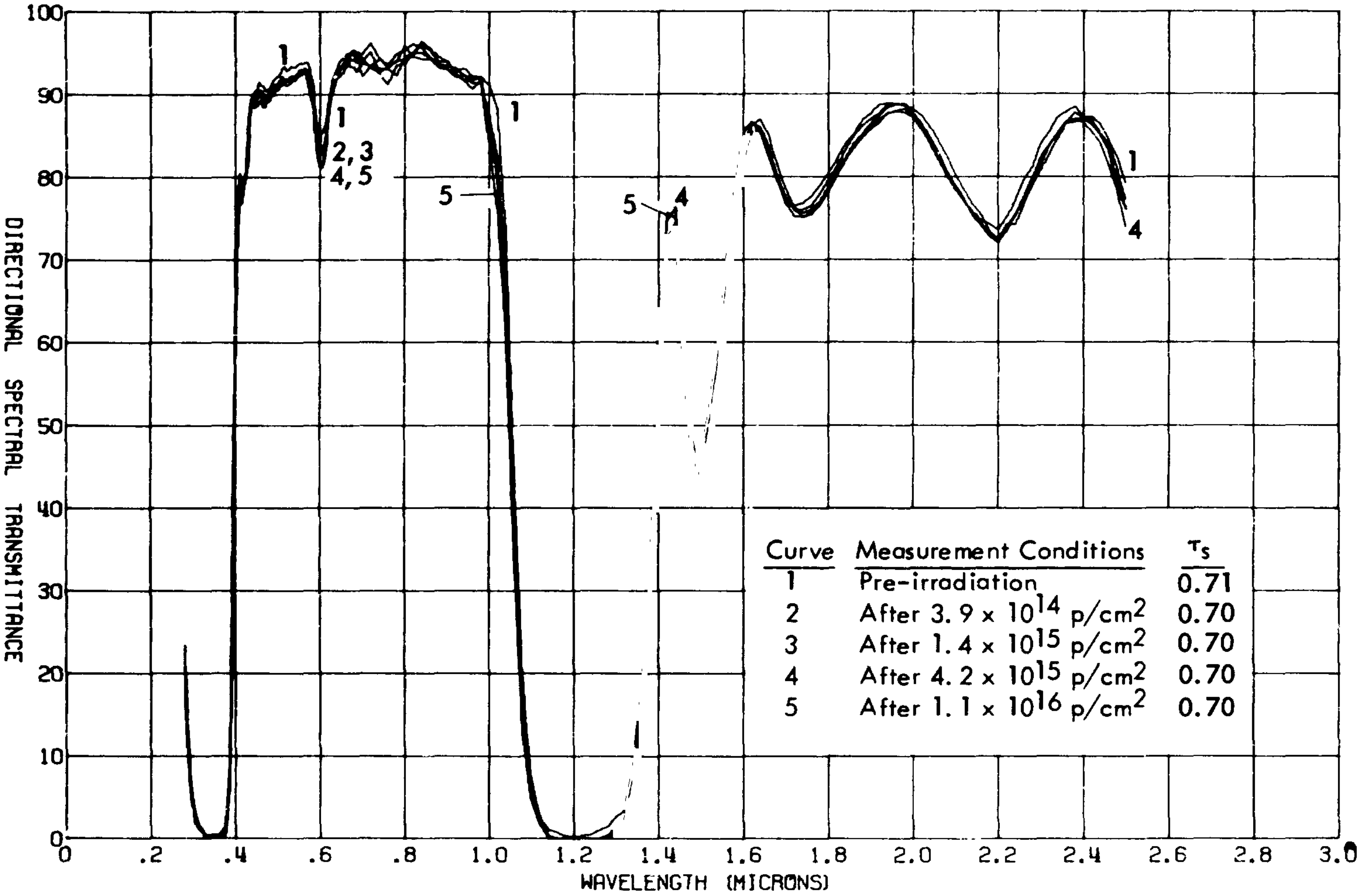

Curve	Measurement Conditions	τ_s
1	Pre-irradiation	0.71
2	After 3.9 x 10^{14} p/cm^2	0.70
3	After 1.4 x 10^{15} p/cm^2	0.70
4	After 4.2 x 10^{15} p/cm^2	0.70
5	After 1.1 x 10^{16} p/cm^2	0.70

FIGURE 57. IN SITU ULTRAVIOLET EFFECTS ON THE ABSORPTANCE OF J P L SAMPLE 2079 BLUE-RED FILTER 2400-HOUR TEST

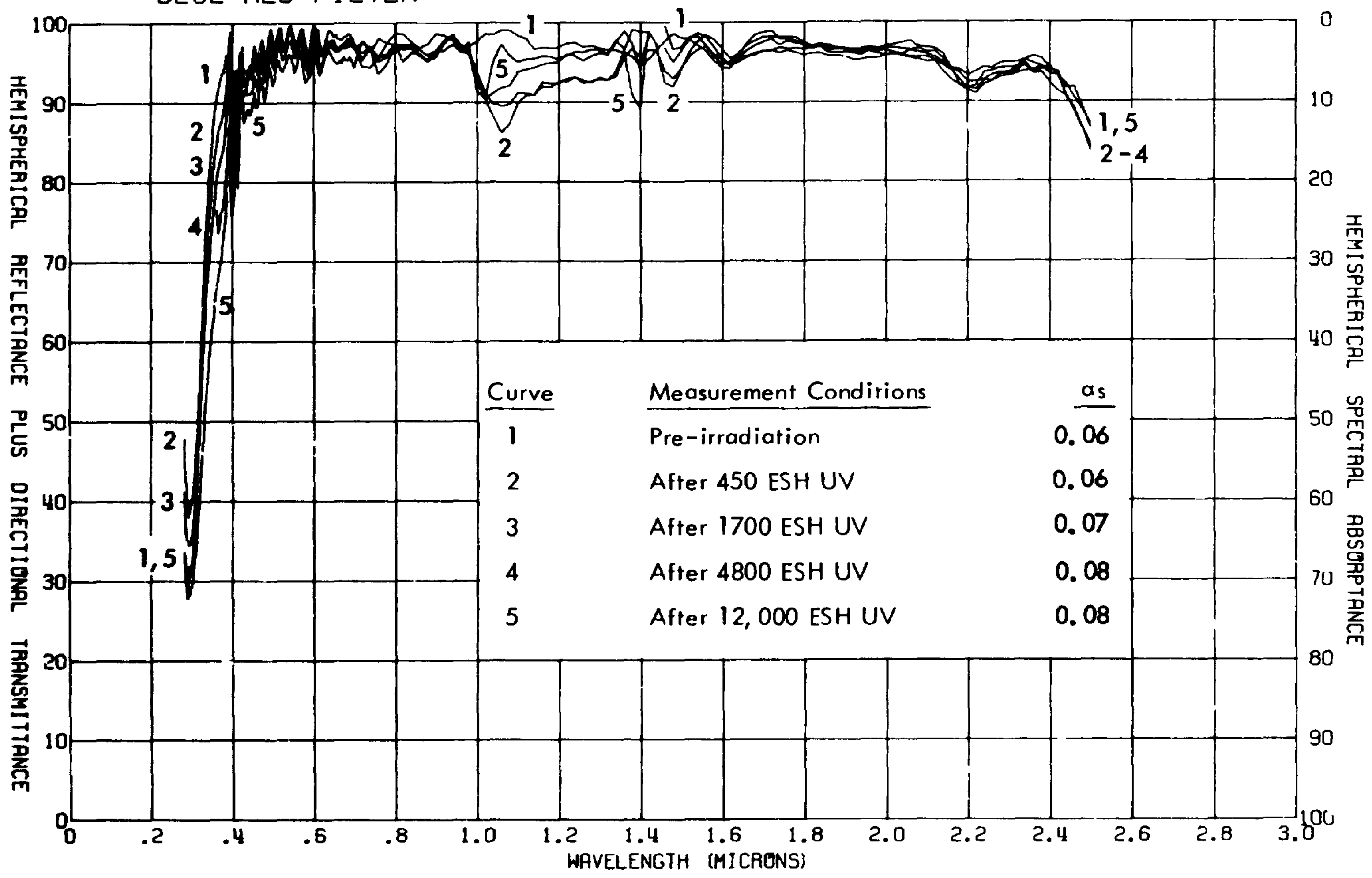

Curve	Measurement Conditions	α_s
1	Pre-irradiation	0.06
2	After 450 ESH UV	0.06
3	After 1700 ESH UV	0.07
4	After 4800 ESH UV	0.08
5	After 12,000 ESH UV	0.08

FIGURE 58.

IN SITU PROTON-ULTRAVIOLET EFFECTS ON THE ABSORPTANCE OF J P L SAMPLE 2088
BLUE-RED FILTER
2400-HOUR TEST

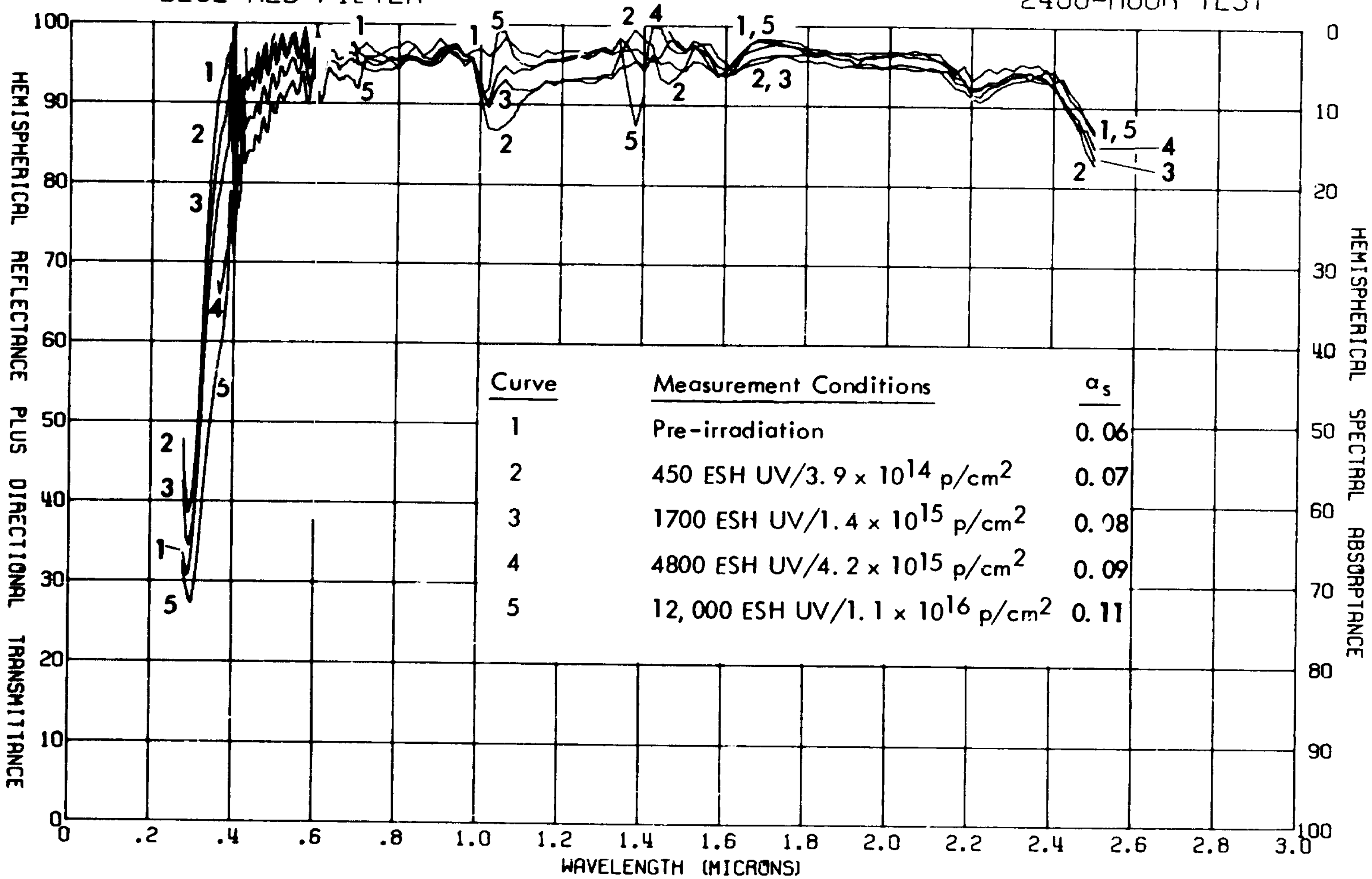

FIGURE 59. IN SITU PROTON EFFECTS ON THE ABSORPTANCE OF J P L SAMPLE 2097
BLUE-RED FILTER 2400-HOUR TEST

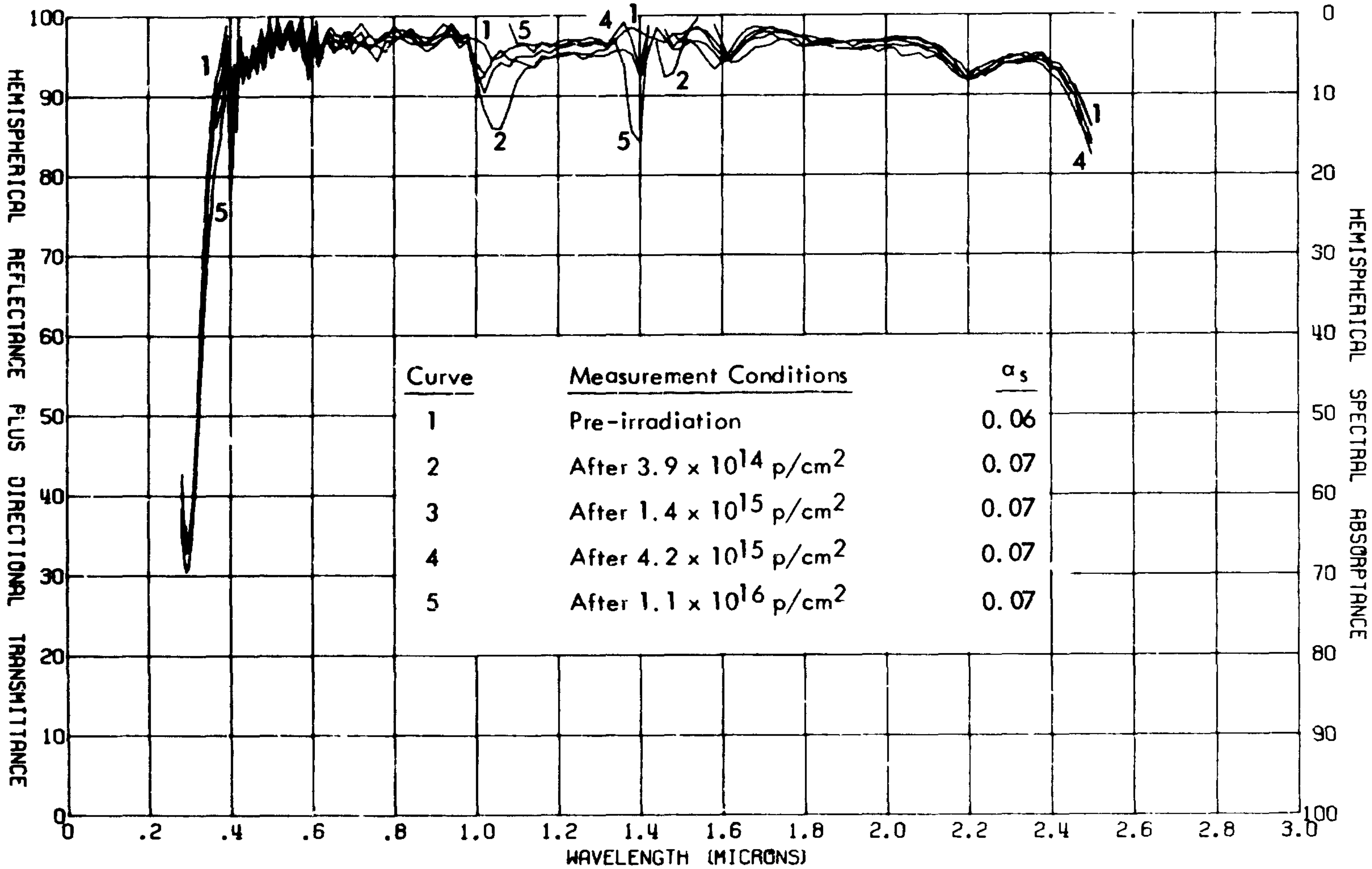

FIGURE 60. IN SITU ULTRAVIOLET EFFECTS ON THE REFLECTANCE OF J P L SAMPLE 2081
CLEAR GLASS - RTV 602 - POLISHED ALUMINUM 2400-HOUR TEST

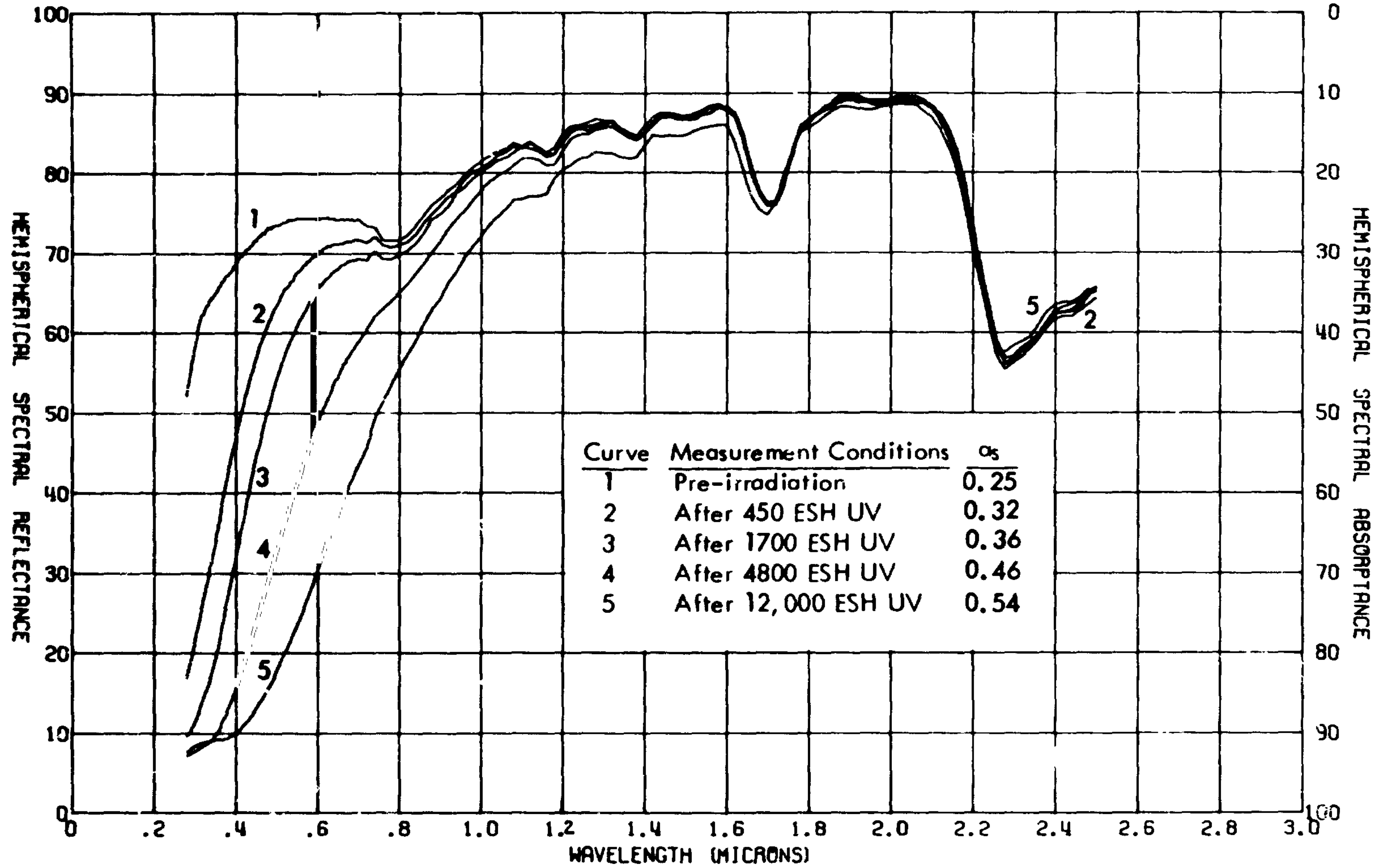

FIGURE 61.

IN SITU PROTON-ULTRAVIOLET EFFECTS ON THE REFLECTANCE OF J P L SAMPLE 2090
CLEAR GLASS - RTV 602 - POLISHED ALUMINUM 2400-HOUR TEST

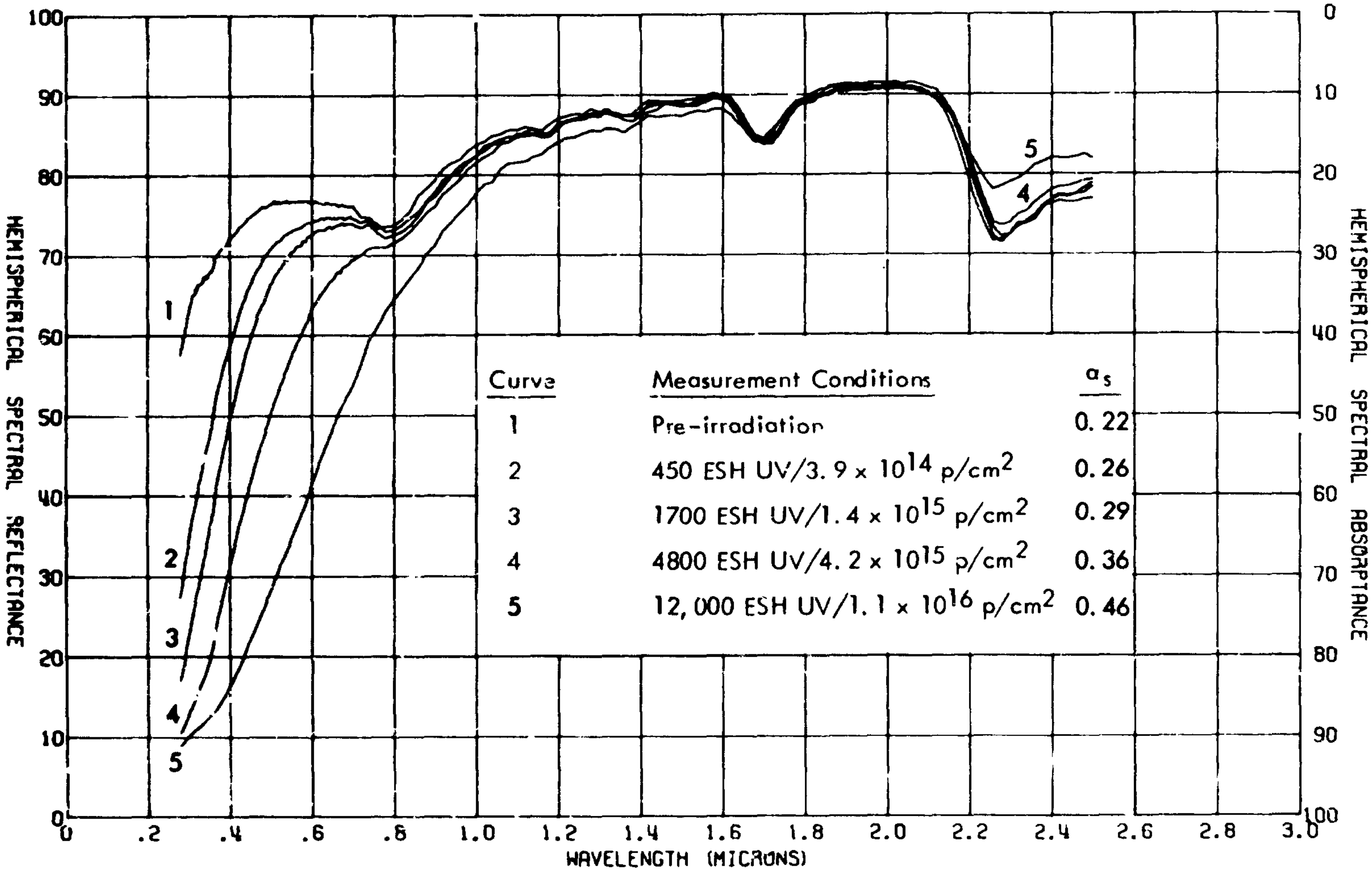

FIGURE 62. IN SITU PROTON EFFECTS ON THE REFLECTANCE OF J P L SAMPLE 2099
CLEAR GLASS - RTV 602 - POLISHED ALUMINUM 2400-HOUR TEST

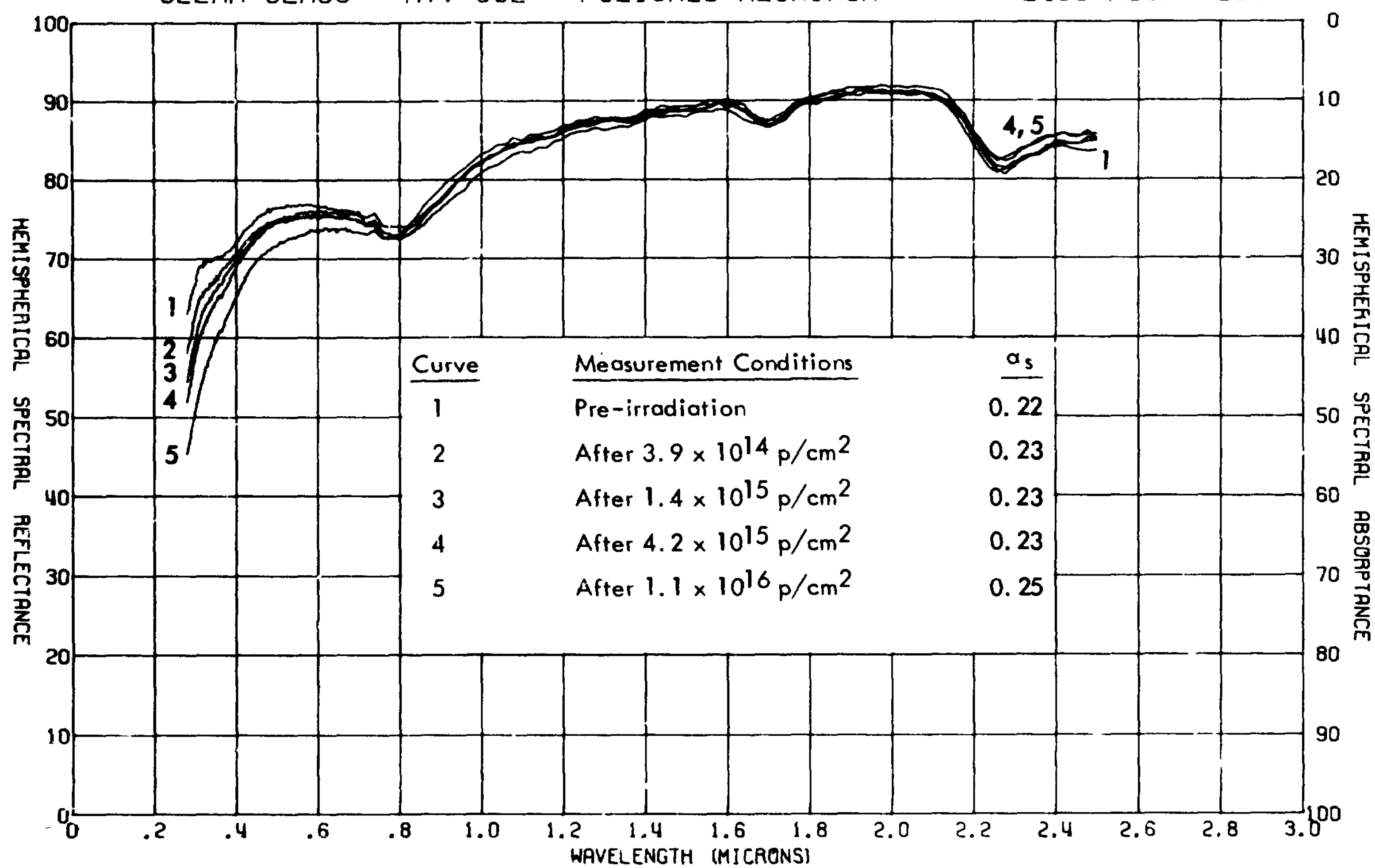

FIGURE 63. IN SITU ULTRAVIOLET EFFECTS ON THE REFLECTANCE OF J P L SAMPLE 2082
CLEAR GLASS - XR6-3489 - POLISHED ALUMINUM 2400-HOUR TEST

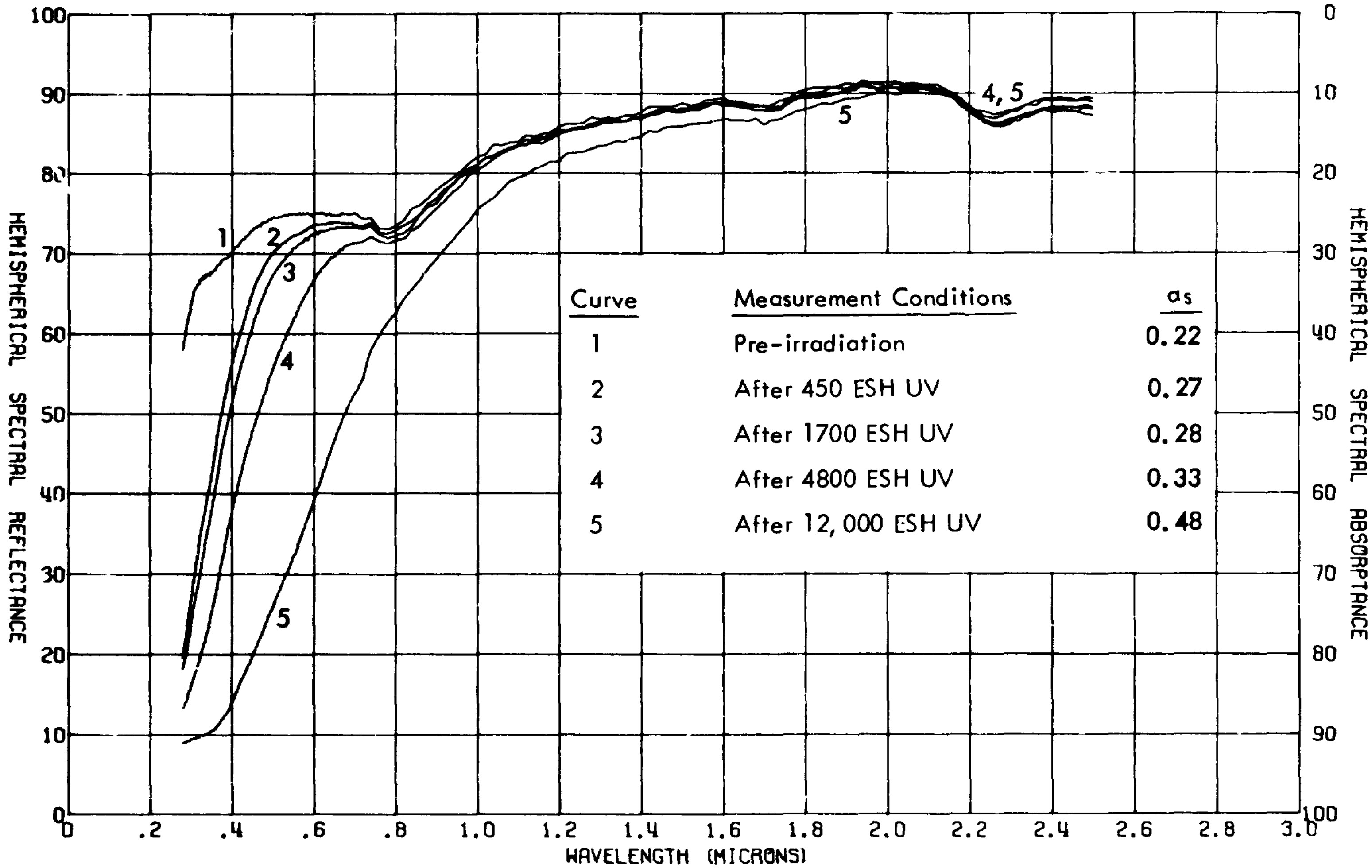

FIGURE 64.

IN SITU PROTON-ULTRAVIOLET EFFECTS ON THE REFLECTANCE OF J P L SAMPLE 2091
CLEAR GLASS - XR6-3489 - POLISHED ALUMINUM 2400-HOUR TEST

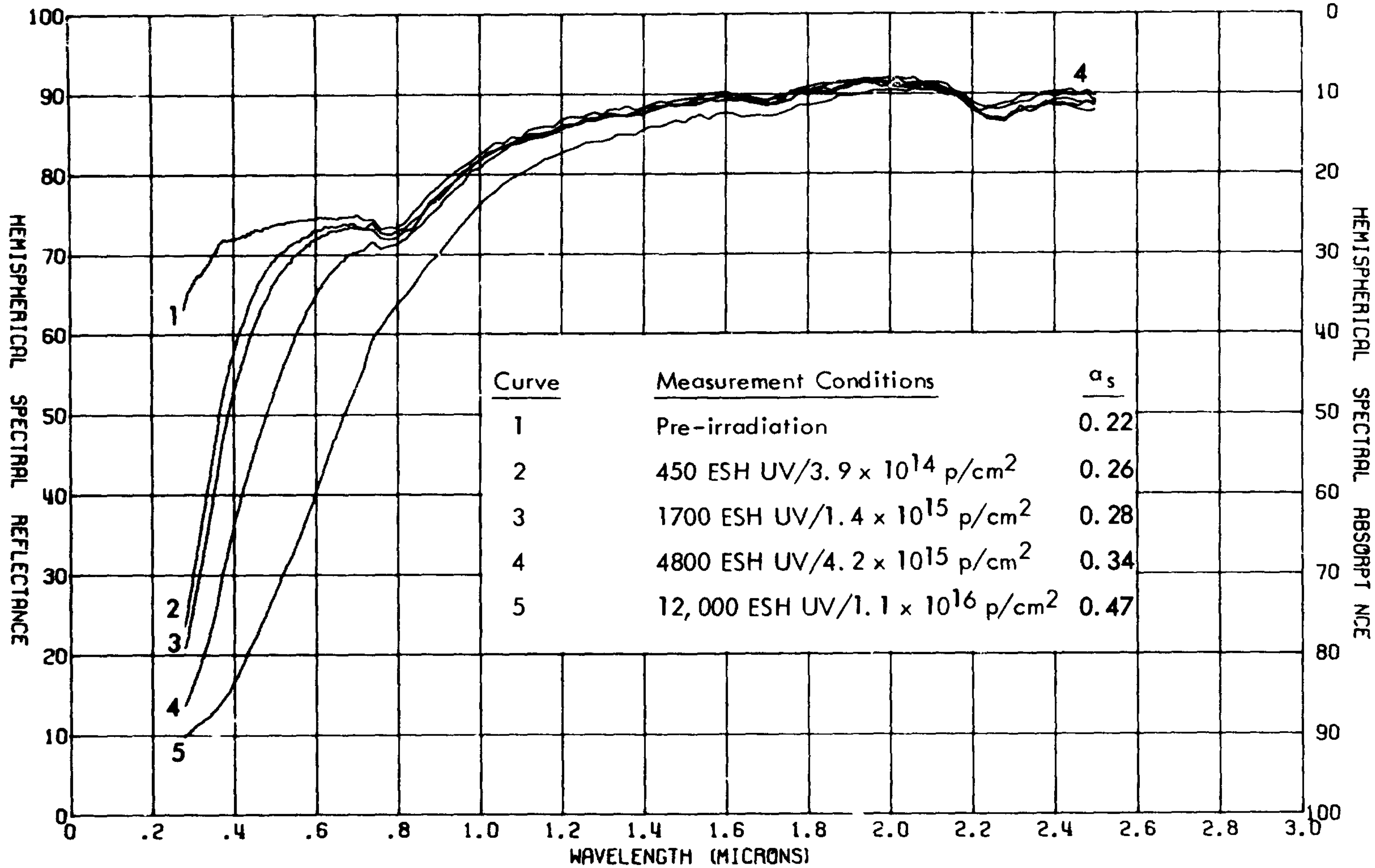

FIGURE 65. IN SITU PROTON EFFECTS ON THE REFLECTANCE OF J P L SAMPLE 2100 CLEAR GLASS - XR6-3489 - POLISHED ALUMINUM 2400-HOUR TEST

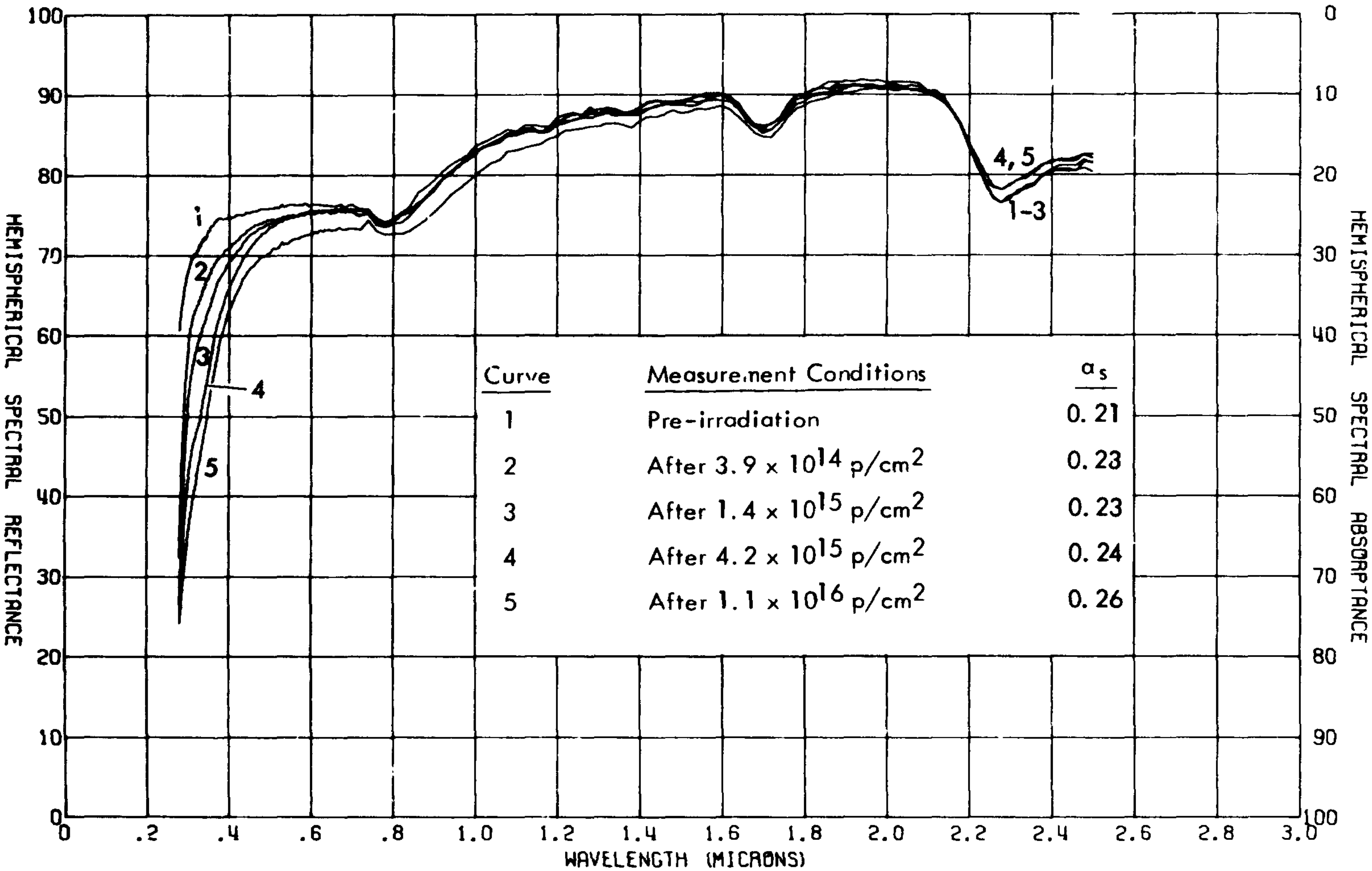

Curve	Measurement Conditions	α_s
1	Pre-irradiation	0.21
2	After 3.9×10^{14} p/cm^2	0.23
3	After 1.4×10^{15} p/cm^2	0.23
4	After 4.2×10^{15} p/cm^2	0.24
5	After 1.1×10^{16} p/cm^2	0.26

FIGURE 66. IN SITU ULTRAVIOLET EFFECTS ON THE REFLECTANCE OF J P L SAMPLE 2080 CLEAR GLASS (7940 FUSED SILICA) 2400-HOUR TEST

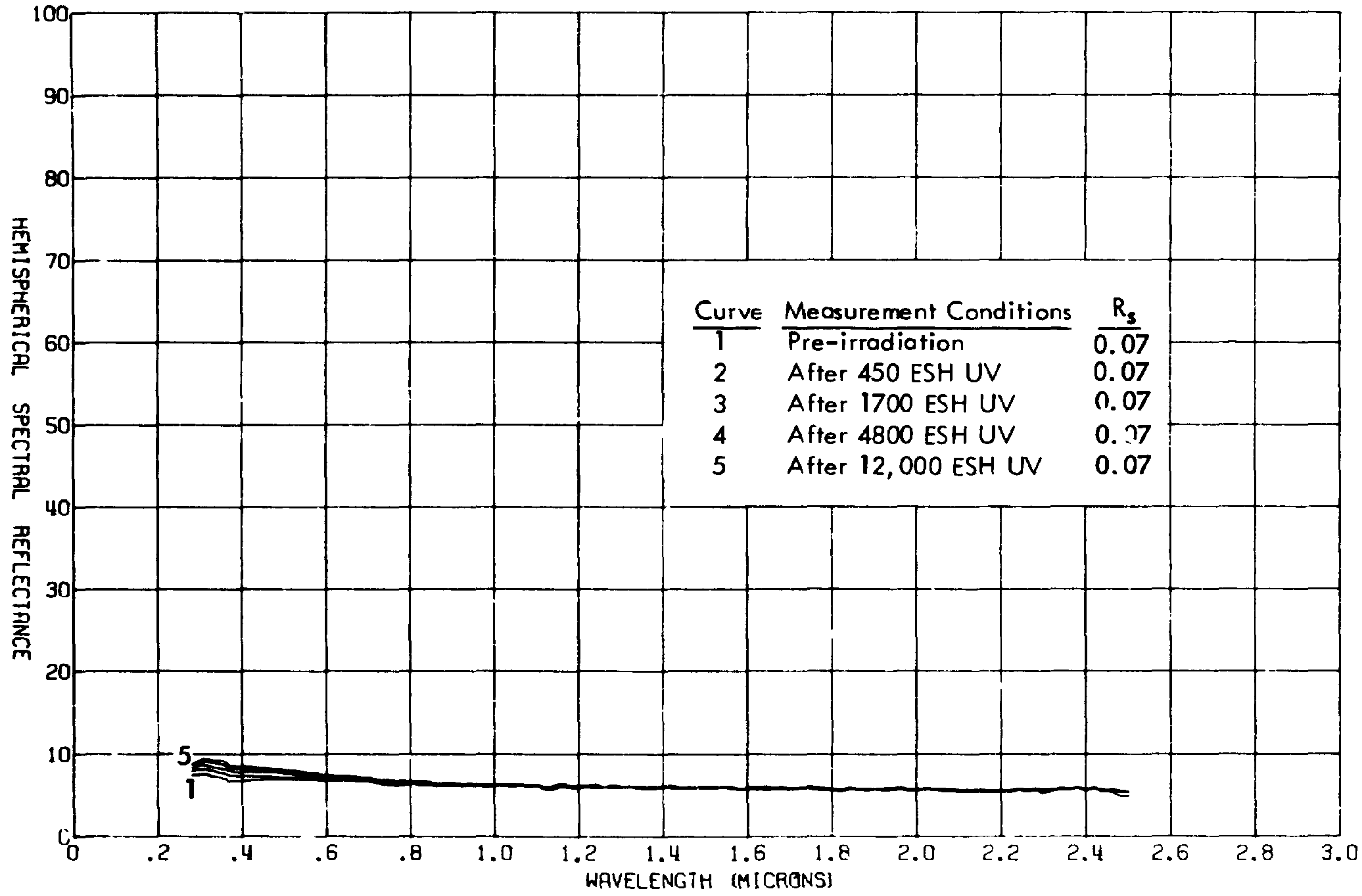

FIGURE 67.

IN SITU PROTON-ULTRAVIOLET EFFECTS ON THE REFLECTANCE OF J P L SAMPLE 2089
CLEAR GLASS (7940 FUSED SILICA) 2400-HOUR TEST

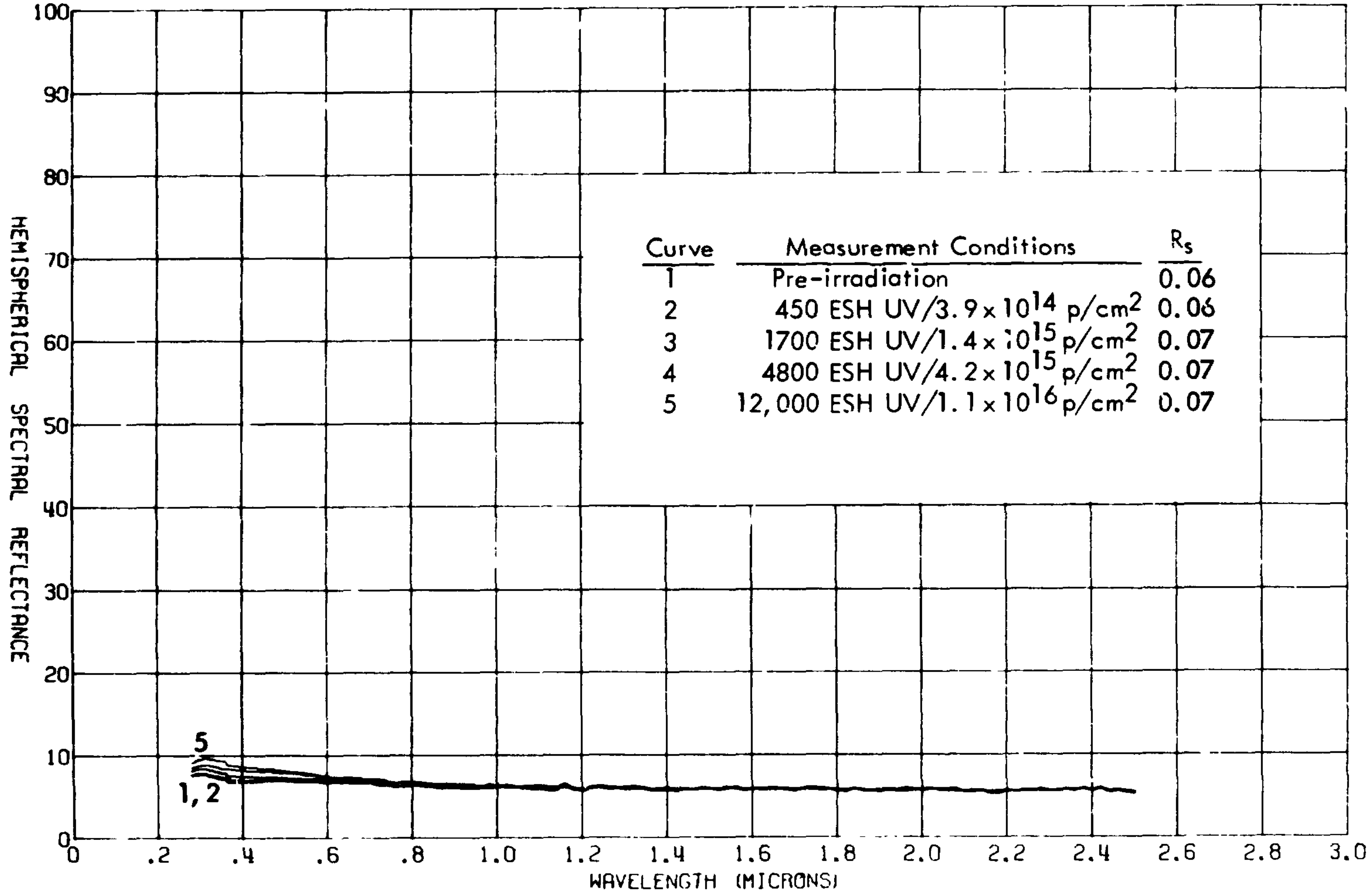

FIGURE 68. IN SITU PROTON EFFECTS ON THE REFLECTANCE OF J P L SAMPLE 2098 CLEAR GLASS (7940 FUSED SILICA) 2400-HOUR TEST

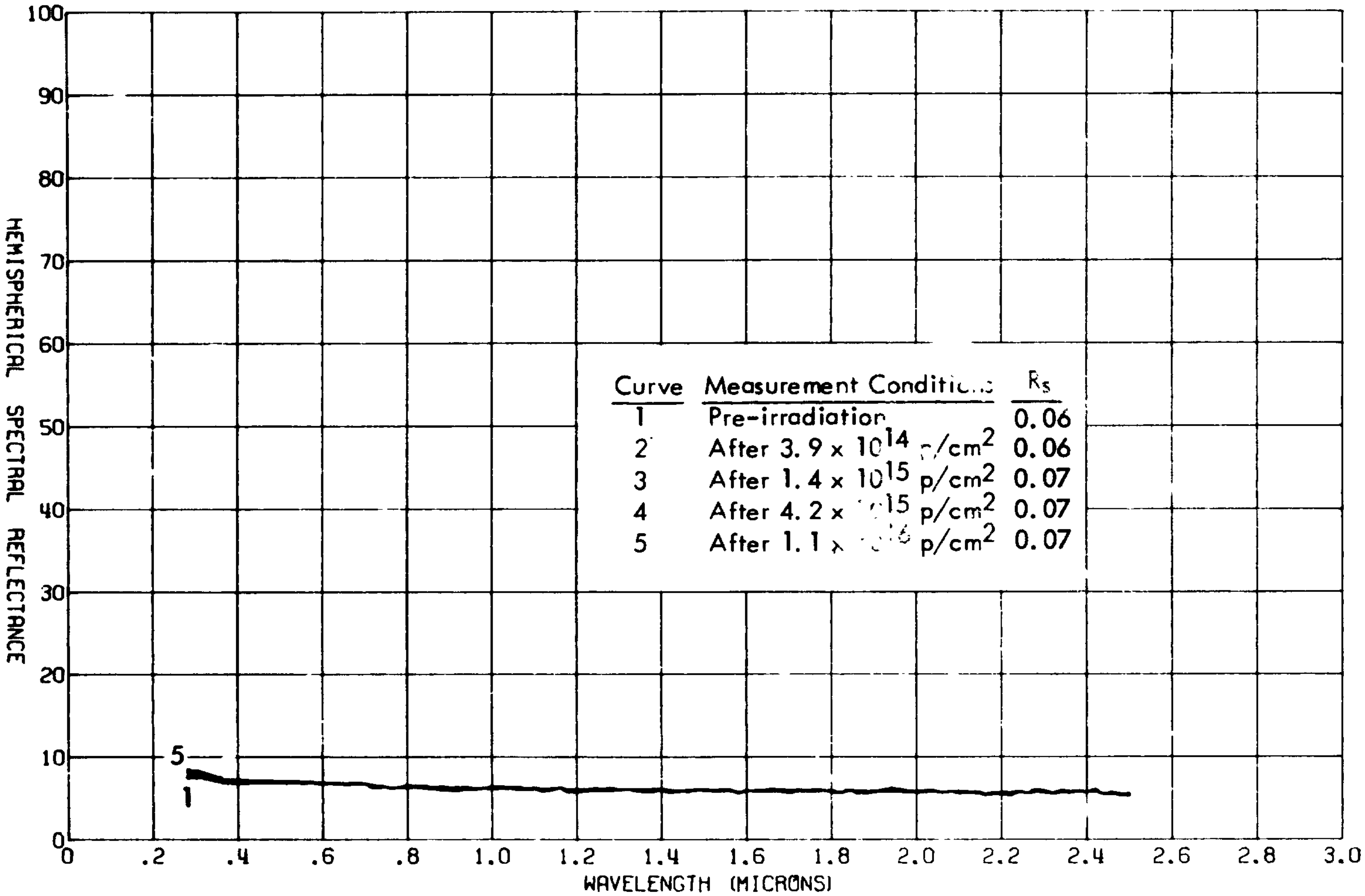

FIGURE 69. IN SITU ULTRAVIOLET EFFECTS ON THE TRANSMITTANCE OF J P L SAMPLE 2080 CLEAR GLASS (7940 FUSED SILICA) 2400-HOUR TEST

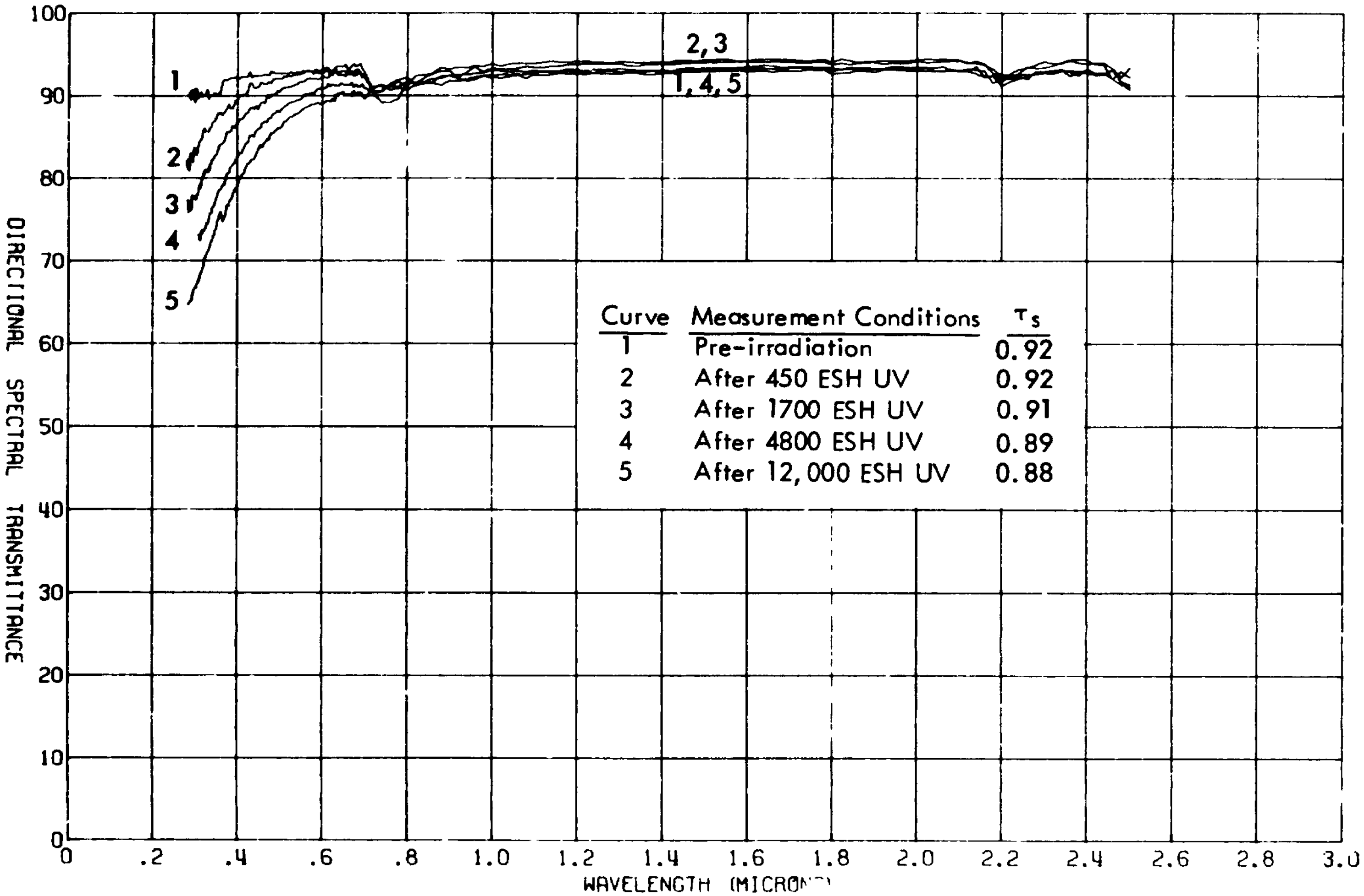

Curve	Measurement Conditions	τ_s
1	Pre-irradiation	0.92
2	After 450 ESH UV	0.92
3	After 1700 ESH UV	0.91
4	After 4800 ESH UV	0.89
5	After 12,000 ESH UV	0.88

FIGURE 70.

IN SITU PROTON-ULTRAVIOLET EFFECTS ON THE TRANSMITTANCE OF J P L SAMPLE 2089 CLEAR GLASS (7940 FUSED SILICA) 2400-HOUR TEST

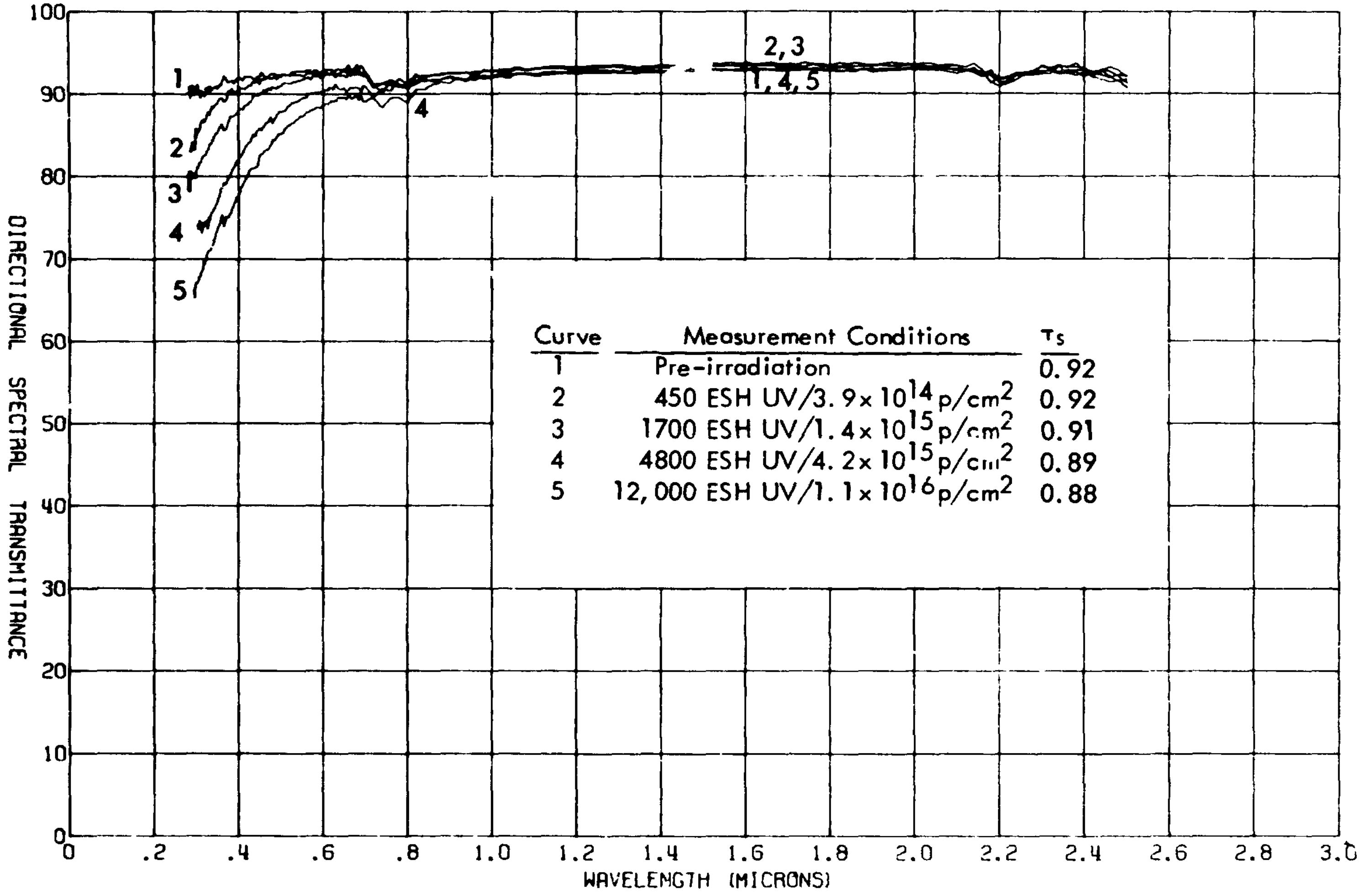

FIGURE 71. IN SITU PROTON EFFECTS ON THE TRANSMITTANCE OF J P L SAMPLE 2098 CLEAR GLASS (7940 FUSED SILICA) 2400-HOUR TEST

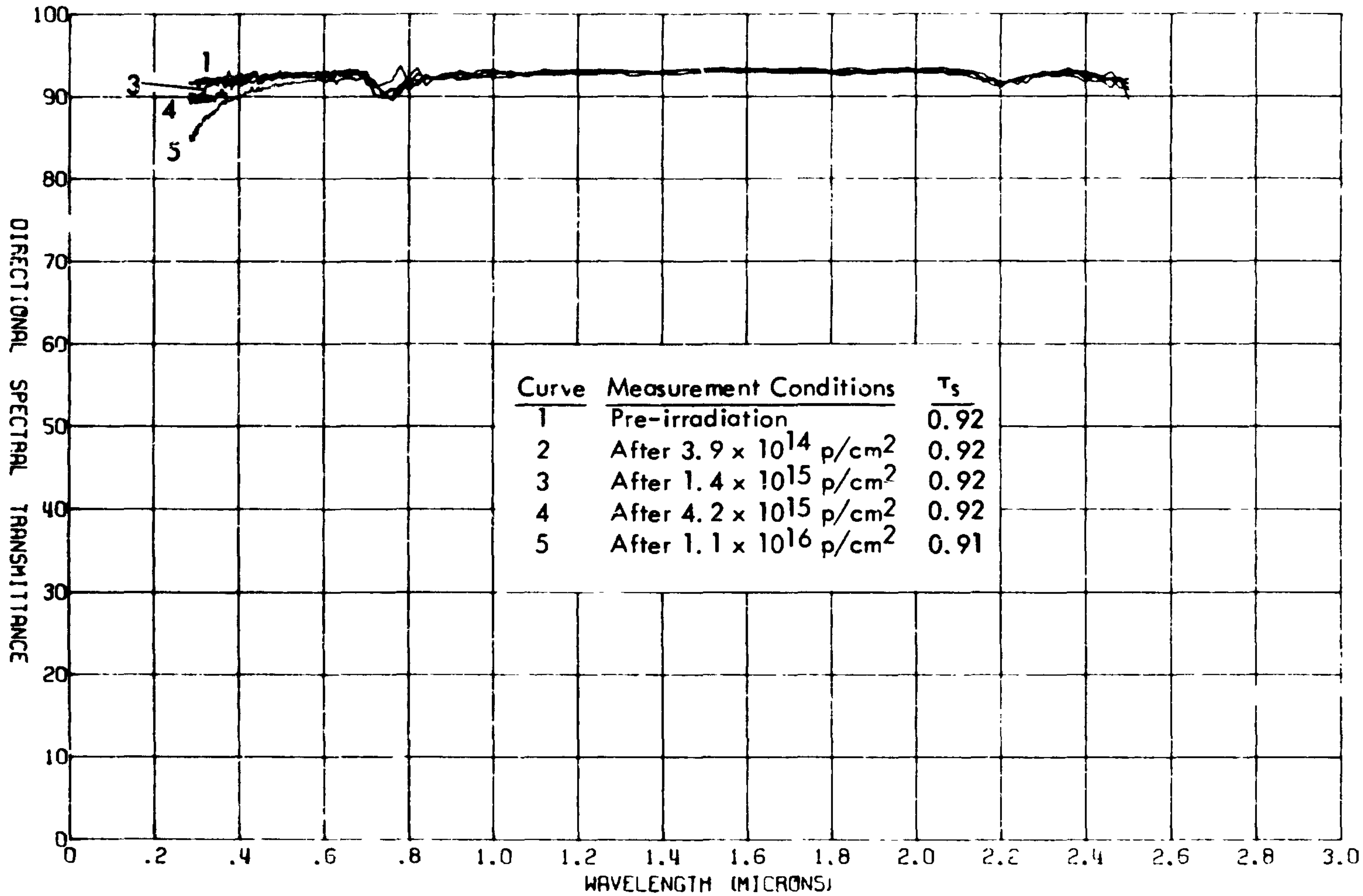

FIGURE 72. IN SITU ULTRAVIOLET EFFECTS ON THE ABSORPTANCE OF J P L SAMPLE 2080 CLEAR GLASS (7940 FUSED SILICA) 2400-HOUR TEST

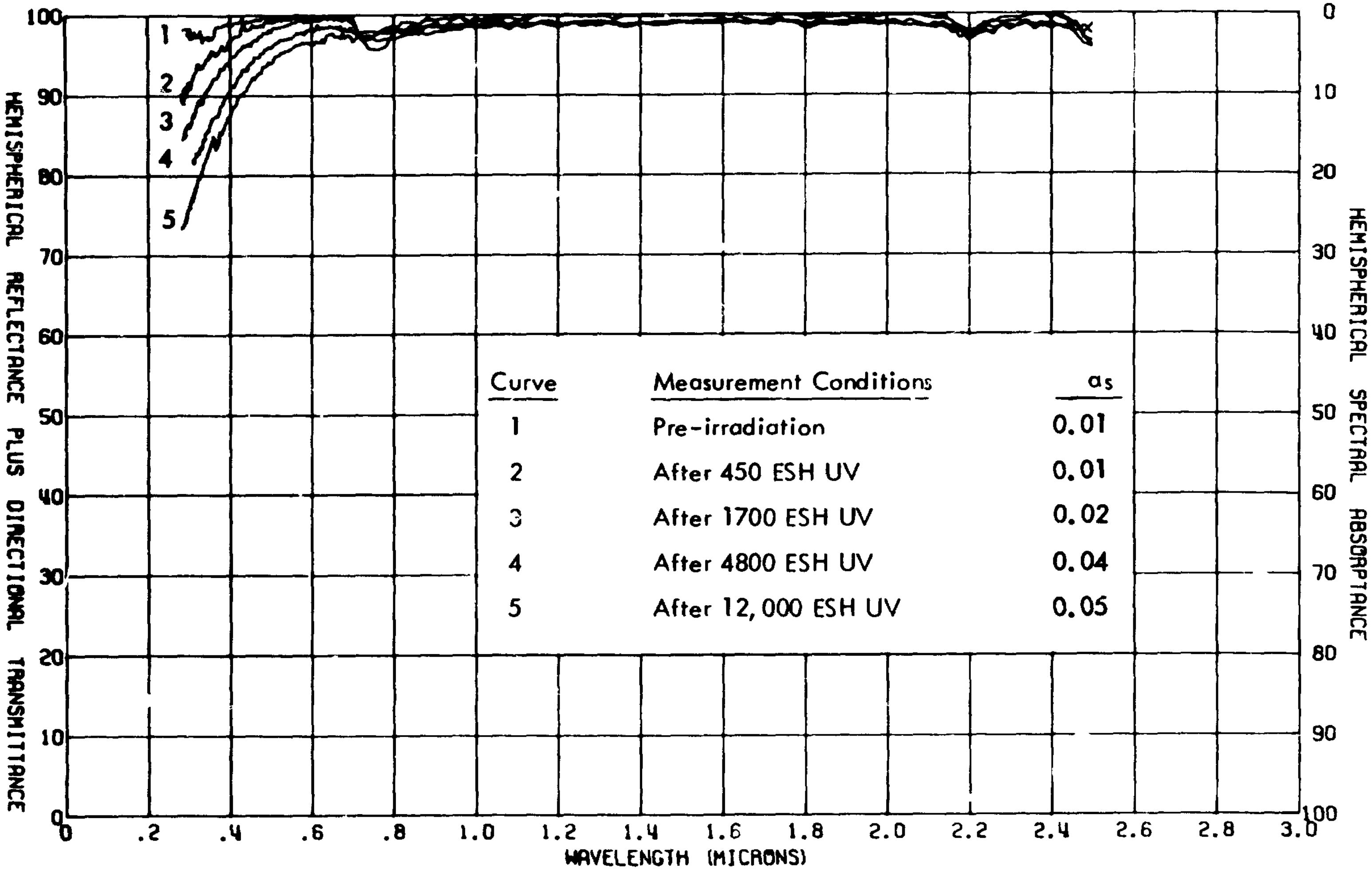

FIGURE 73. IN SITU PROTON-ULTRAVIOLET EFFECTS ON THE ABSORPTANCE OF J P L SAMPLE 2089 CLEAR GLASS (7940 FUSED SILICA) 2400-HOUR TEST

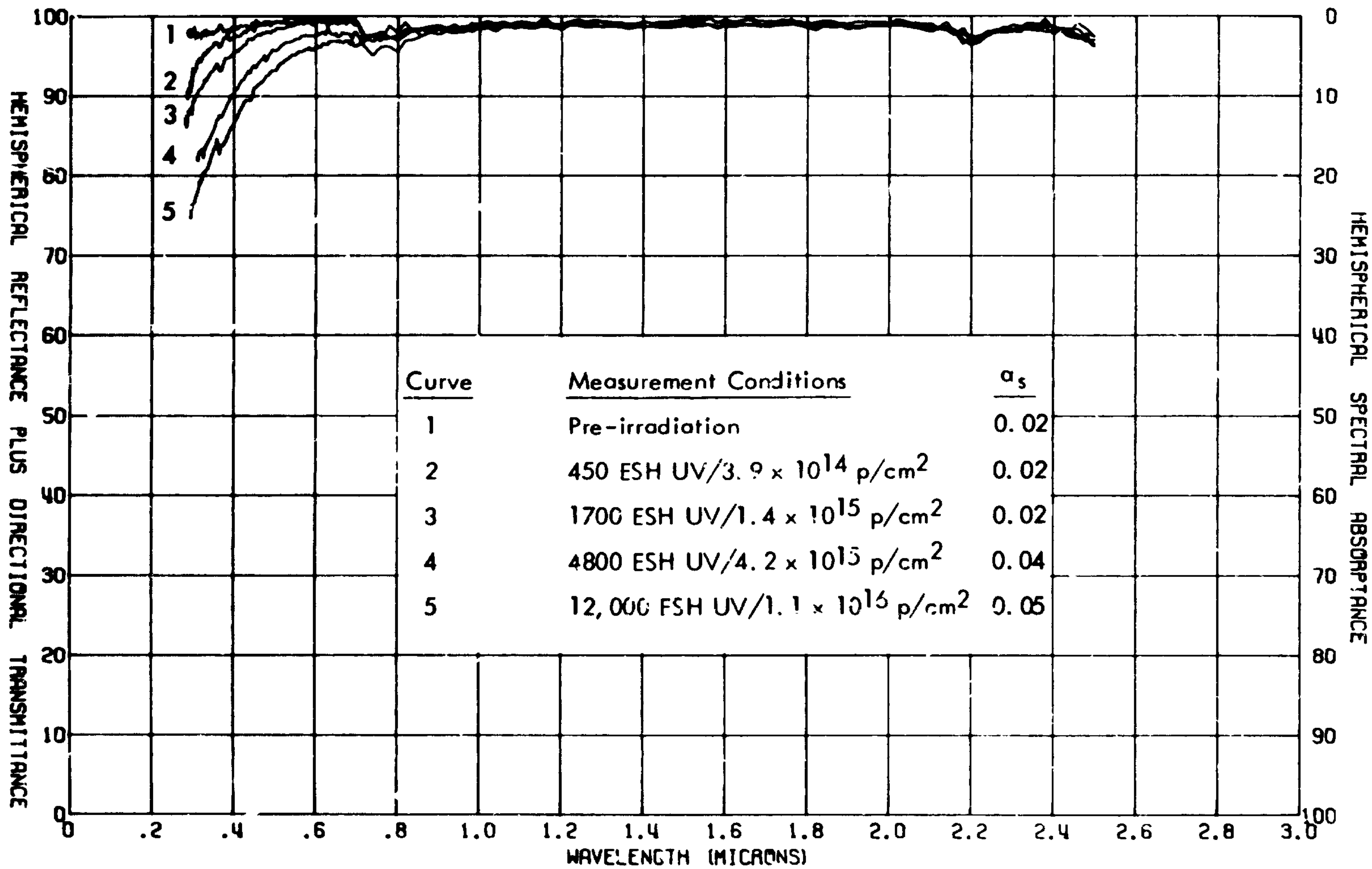

FIGURE 74. IN SITU PROTON EFFECTS ON THE ABSORPTANCE OF J P L SAMPLE 2098 CLEAR GLASS (7940 FUSED SILICA) 2400-HOUR TEST

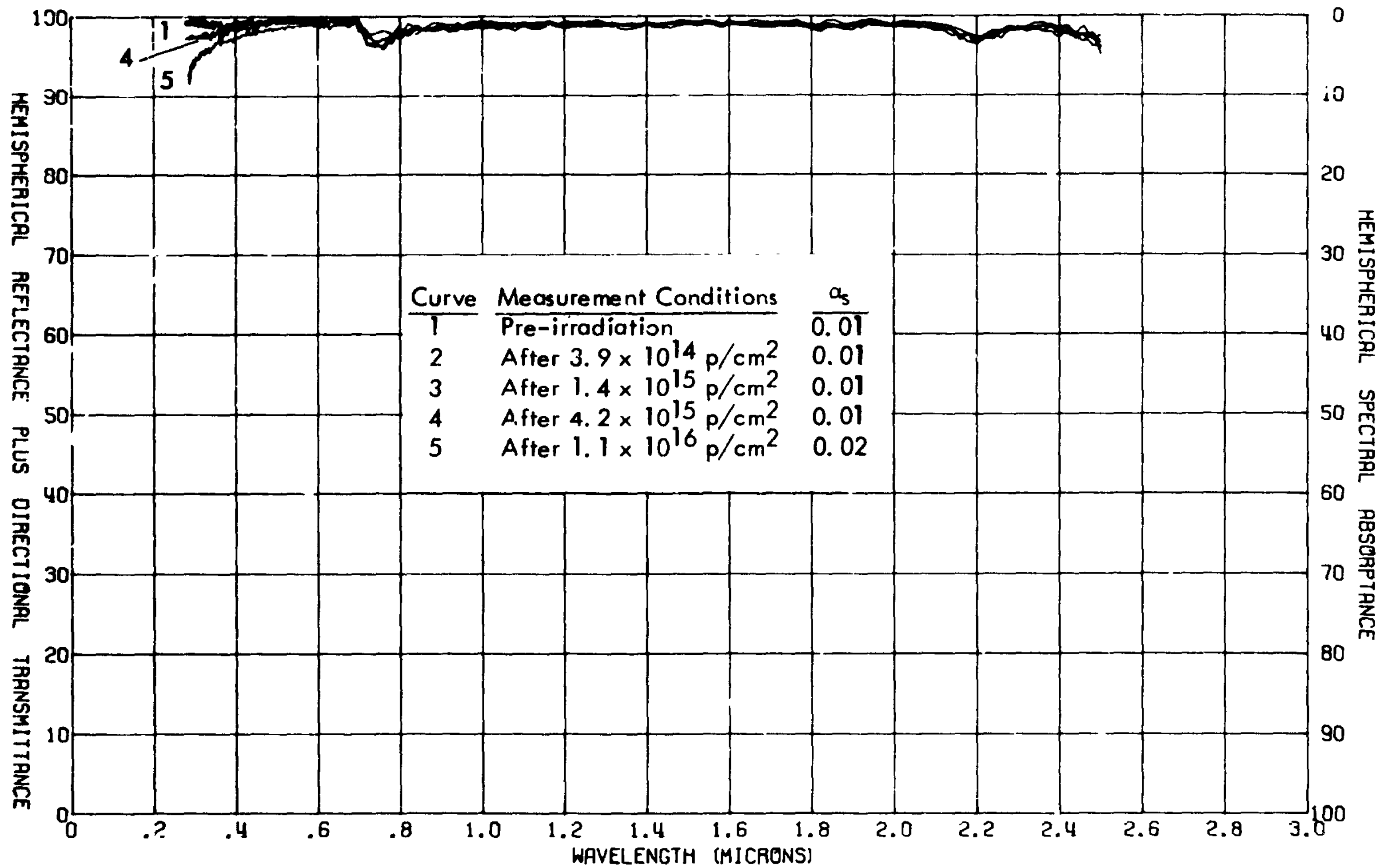

FIGURE 75. IN SITU PROTON-ULTRAVIOLET EFFECTS ON THE REFLECTANCE OF GOLD-BACKED KAPTON POLYIMIDE FILM 2400-HOUR TEST

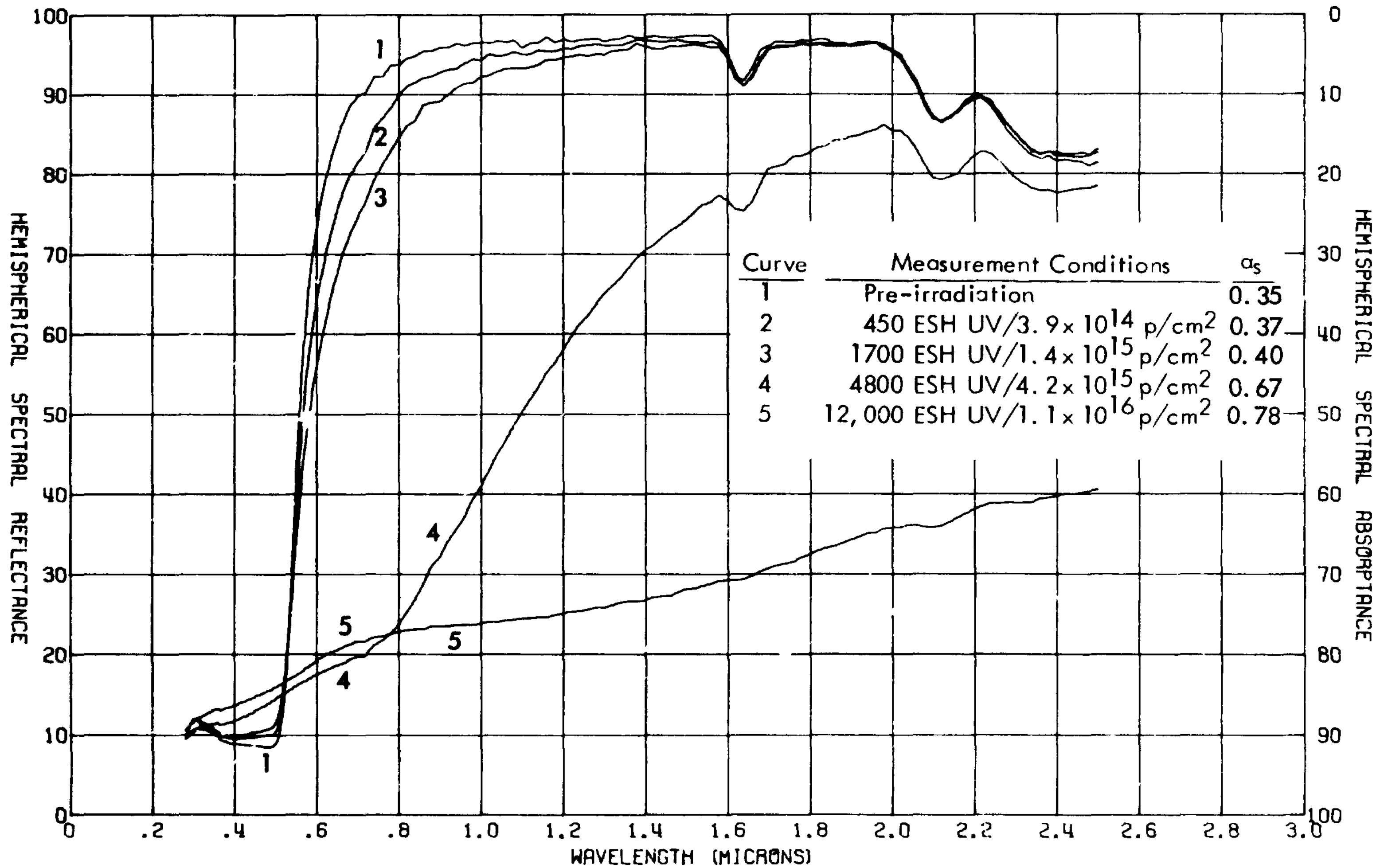

FIGURE 76. IN SITU PROTON EFFECTS ON THE REFLECTANCE OF GOLD-BACKED KAPTON POLYIMIDE FILM

2400-HOUR TEST

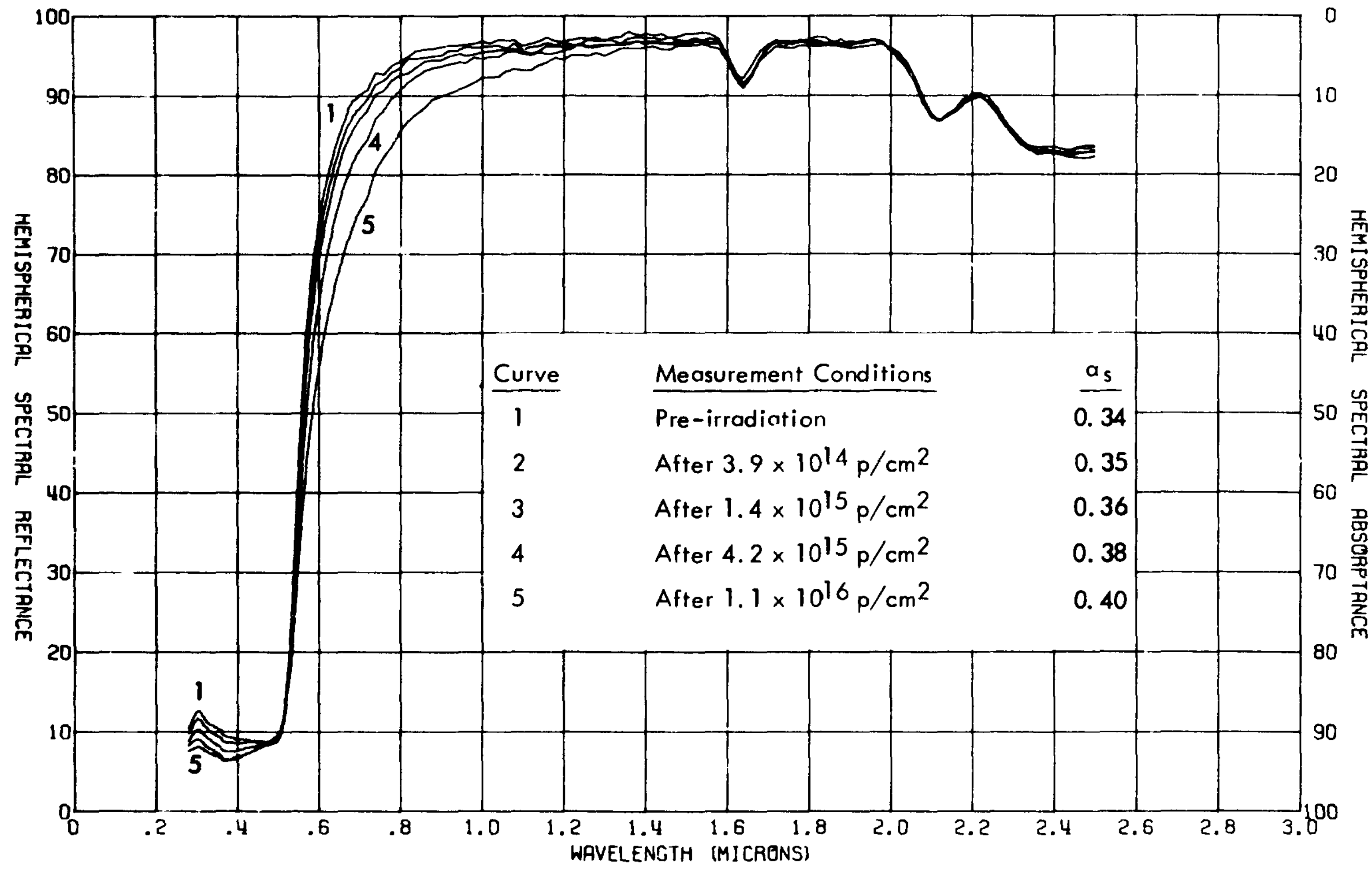

APPENDIX B

Introduction

This appendix presents spectral results obtained _in situ_ on 18 samples exposed to protons and ultraviolet radiation during a preliminary 500-hour test early in this program. Each spectral plot consists of reflectance, transmittance, and/or absorptance curves as a function of wavelength between 0.28 and 2.5 microns, each curve being numerically labelled to agree with certain exposure levels. In particular,

for those six samples exposed to ultraviolet radiation:

CURVE	MEASUREMENT CONDITIONS
1	Preirradiation; samples at +140°C
2	After 260 ESH (53 hours); + 140°C
3	After 700 ESH (140 hours); + 140°C
4	After 1600 ESH (316 1/2 hours) + 140°C
5	After 2500 ESH (500 hours) + 140°C

for those six samples exposed simultaneously to 3-keV protons and ultraviolet radiation:

CURVE	MEASUREMENT CONDITIONS
0	Preirradiation; samples at room temperature
1	Preirradiation; samples at +140°C
2	After 260 ESH and 2.3 x 10^{14} protons/cm^2; + 140°C
3	After 700 ESH and 6.0 x 10^{14} protons/cm^2; + 140°C
4	After 1600 ESH and 1.4 x 10^{15} protons/cm^2; + 140°C
5	After 2500 ESH and 2.2 x 10^{15} protons/cm^2; + 140°C

for those six samples exposed to 3-keV protons:

CURVE	MEASUREMENT CONDITIONS
1	Preirradiation; samples at +140°C
2	After 2.3 x 10^{14} protons/cm^2; +140°C
3	After 6.0 x 10^{14} protons/cm^2; +140°C
4	After 1.4 x 10^{15} protons/cm^2; +140°C
5	After 2.2 x 10^{15} protons/cm^2; +140°C

The spectral transmittance plot for the blue filter with sample number 2038 (Figure 83) represents anomalous data. In this figure, it is seen that spectral transmittance increases with exposure. Following the 500-hour test, a microscopic examination revealed small particle defects on one side of sample 2038. The curves in Figure 86 are also affected by the defects in this sample.

Solar absorptance and solar transmittance values for the 18 samples, before and after exposure, are given in Table 7. The 6 samples exposed simultaneously to protons and ultraviolet radiation were measured both at room temperature and at +140°C before irradiation. Pre-exposure thermophysical property values before exposure were identical at the two temperatures, except as indicated by footnotes.

Table 7. Solar Absorptance and Solar Transmittance Values of Samples Exposed in Preliminary 500-Hour Test and Measured at Temperature of +140°C

Kind of Exposure	Sample Type and Number	Parameter	Value Before Exposure	Value After Exposure for Duration of			
				53 hrs	140 hrs	316 hrs	500 hrs
Simultaneous Exposure to Protons and Ultraviolet Radiation	Blue Filter on Cell, 2041	α_s	0.78	0.79	0.79	0.79	0.79
	Blue Filter alone, 2044	α_s	0.02[a]	0.03	0.02	0.03	0.03
		τ_s	0.85[b]	0.84	0.85	0.84	0.84
	4026 Filter on Cell, 2042	α_s	0.30	0.31	0.31	0.30	0.31
	4026 Filter alone, 2045	α_s	0.05	0.05	0.05	0.06	0.06
		τ_s	0.29[c]	0.30	0.30	0.29	0.29
	Blue-red Filter on Cell, 2046	α_s	0.69	0.68	0.68	0.68	0.68
	Blue-red Filter/ Adhesive, 2043	α_s	0.20[d]	0.21	0.21	0.22	0.22

[a] 0.01 at room temperature
[b] 0.86 at room temperature
[c] 0.30 at room temperature
[d] 0.21 at room temperature

Table 7. Solar Absorptance and Solar Transmittance Values of Samples Exposed in Preliminary 500-Hour Test and Measured at Temperature of +140°C (continued)

Kind of Exposure	Sample Type and Number	Parameter	Value Before Exposure	Value After Exposure for Duration of			
				53 hrs	140 hrs	316 hrs	500 hrs
Exposed to Ultraviolet Radiation	Blue Filter on Cell, 2035	α_s	0.78	0.79	0.79	0.79	0.79
	Blue Filter alone, 2038	α_s	0.08	0.07	0.05	0.04	0.03
		τ_s	0.78	0.80	0.82	0.83	0.84
	4026 Filter on Cell, 2036	α_s	0.30	0.30	0.30	0.30	0.30
	4026 Filter alone, 2039	α_s	0.05	0.05	0.05	0.06	0.06
		τ_s	0.29	0.29	0.30	0.29	0.29
	Blue-red Filter on Cell, 2040	α_s	0.69	0.69	0.68	0.69	0.68
	Blue-red Filter/ Adhesive, 2037	α_s	0.20	0.21	0.21	0.22	0.22
Exposed to Protons	Blue Filter on Cell, 2047	α_s	0.78	0.78	0.78	0.78	0.78
	Blue Filter alone, 2050	α_s	0.03	0.03	0.02	0.03	0.03
		τ_s	0.84	0.84	0.85	0.84	0.83
	4026 Filter on Cell, 2048	α_s	0.29	0.29	0.30	0.29	0.30
	4026 Filter alone, 2051	α_s	0.05	0.05	0.05	0.06	0.05
		τ_s	0.29	0.30	0.30	0.29	0.29
	Blue-red Filter on Cell, 2052	α_s	0.69	0.69	0.69	0.69	0.68
	Blue-red Filter/ Adhesive, 2049	α_s	0.21	0.20	0.20	0.21	0.21

FIGURE 77. IN SITU ULTRAVIOLET EFFECTS ON THE REFLECTANCE OF J P L SAMPLE 2035 STANDARD M69/71 SOLAR CELL AND 415 BLUE FILTER 500-HOUR TEST

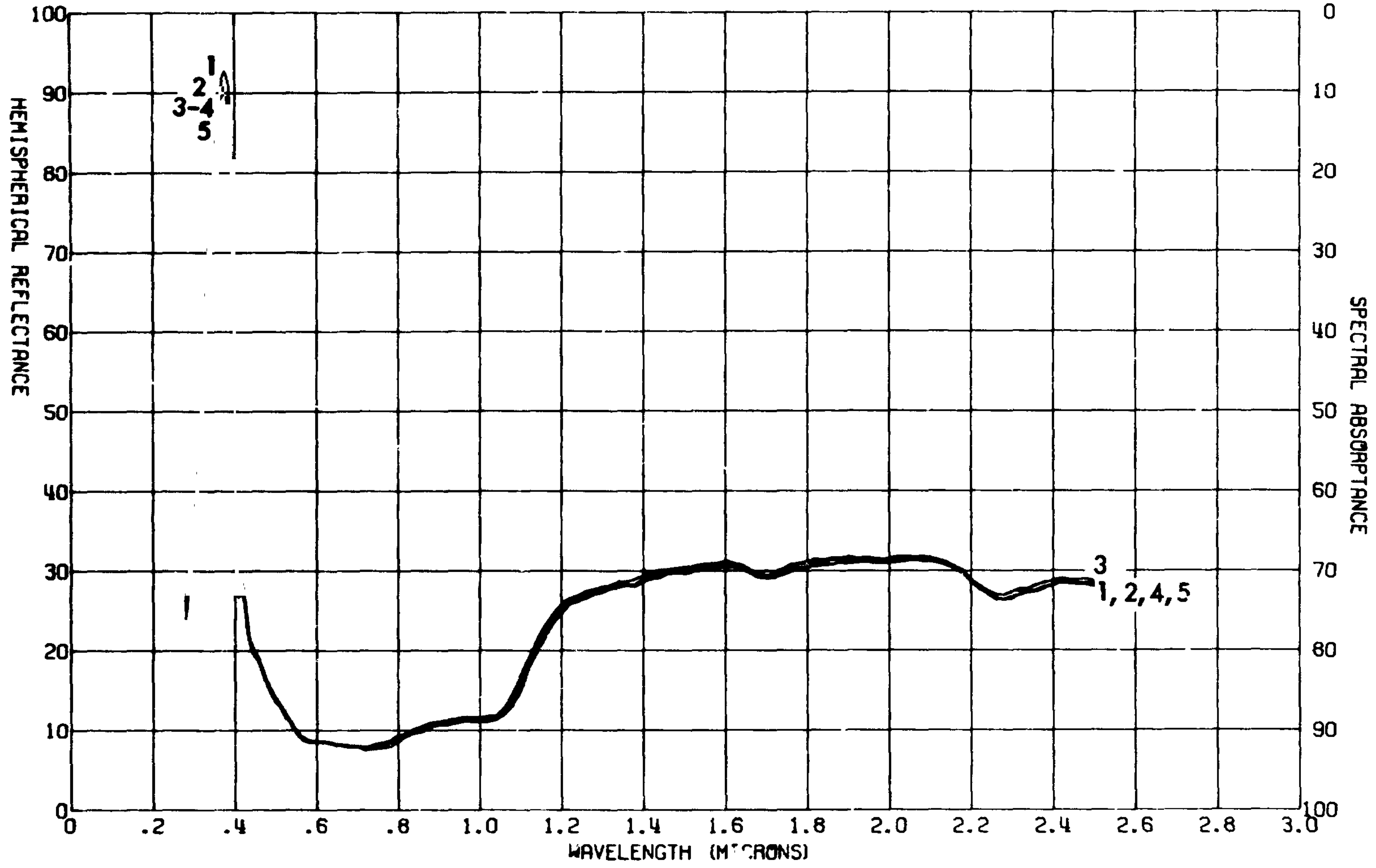

FIGURE 78.

IN SITU PROTON-ULTRAVIOLET EFFECTS ON THE REFLECTANCE OF J P L SAMPLE 2041
STANDARD M69/71 SOLAR CELL AND 415 BLUE FILTER

500-HOUR TEST

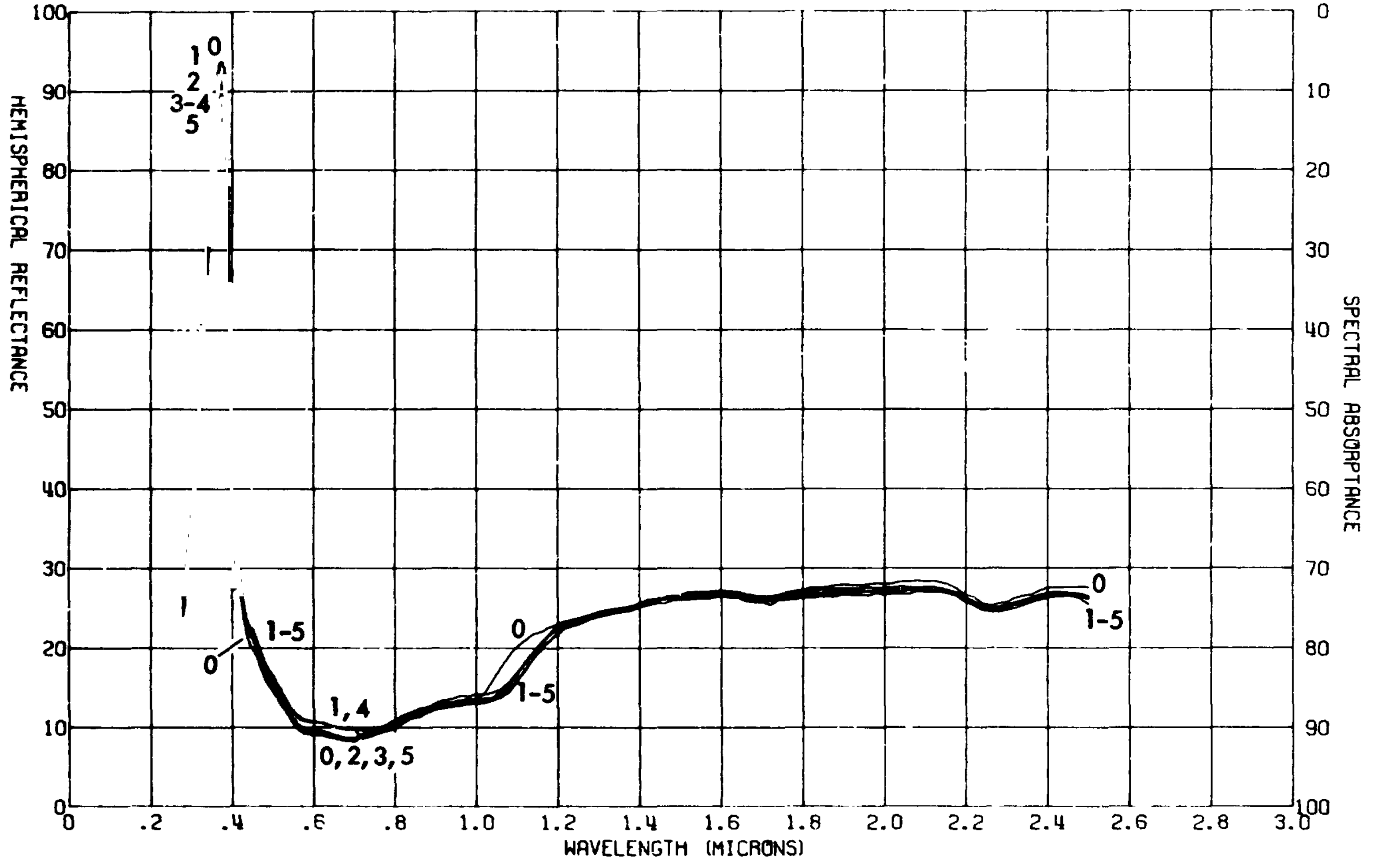

FIGURE 79. IN SITU PROTON EFFECTS ON THE REFLECTANCE OF J P L SAMPLE 2047 STANDARD M69/71 SOLAR CELL AND 415 BLUE FILTER 500-HOUR TEST

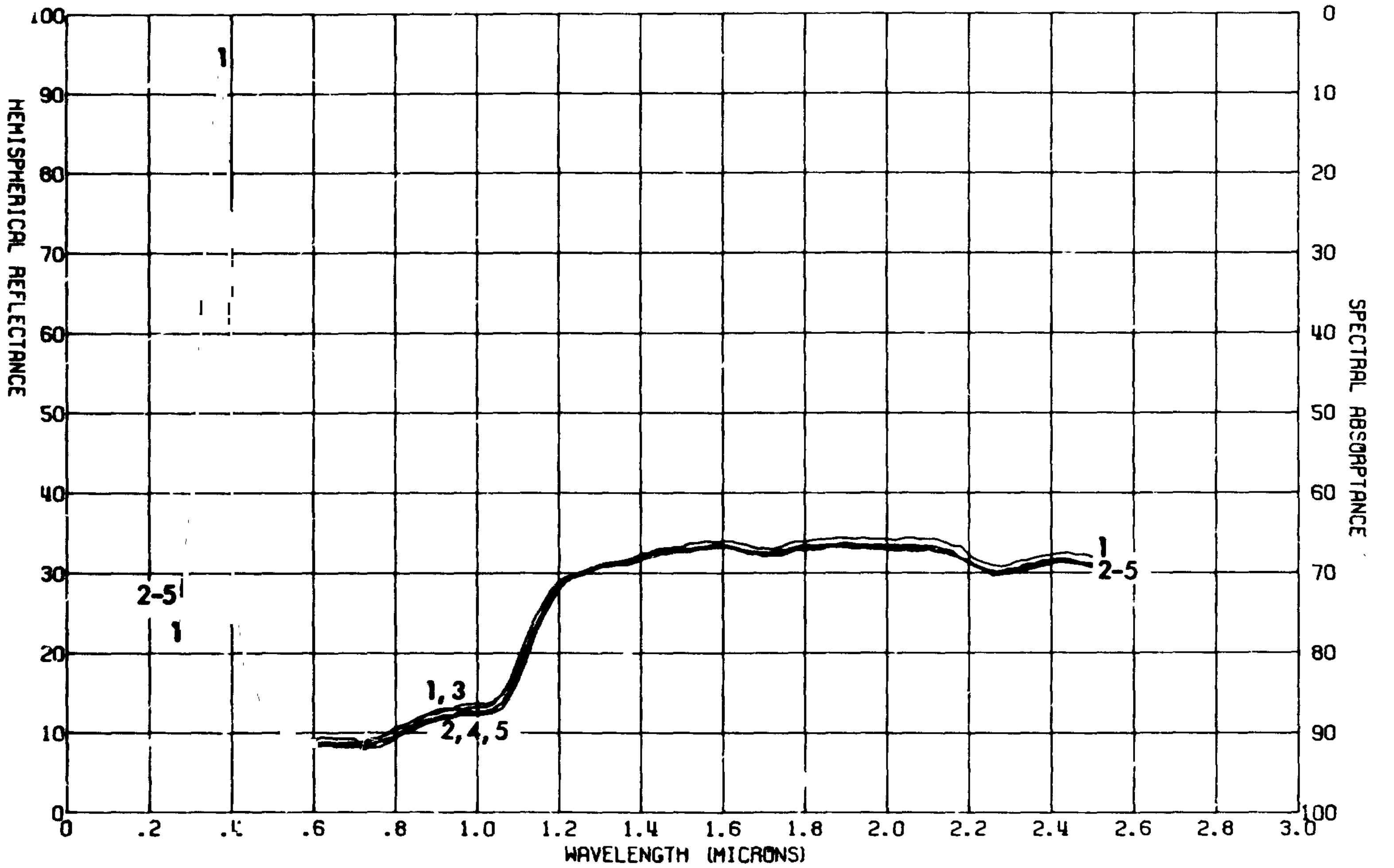

FIGURE 80. IN SITU ULTRAVIOLET EFFECTS ON THE REFLECTANCE OF J P L SAMPLE 2038
BLUE FILTER
500-HOUR TEST

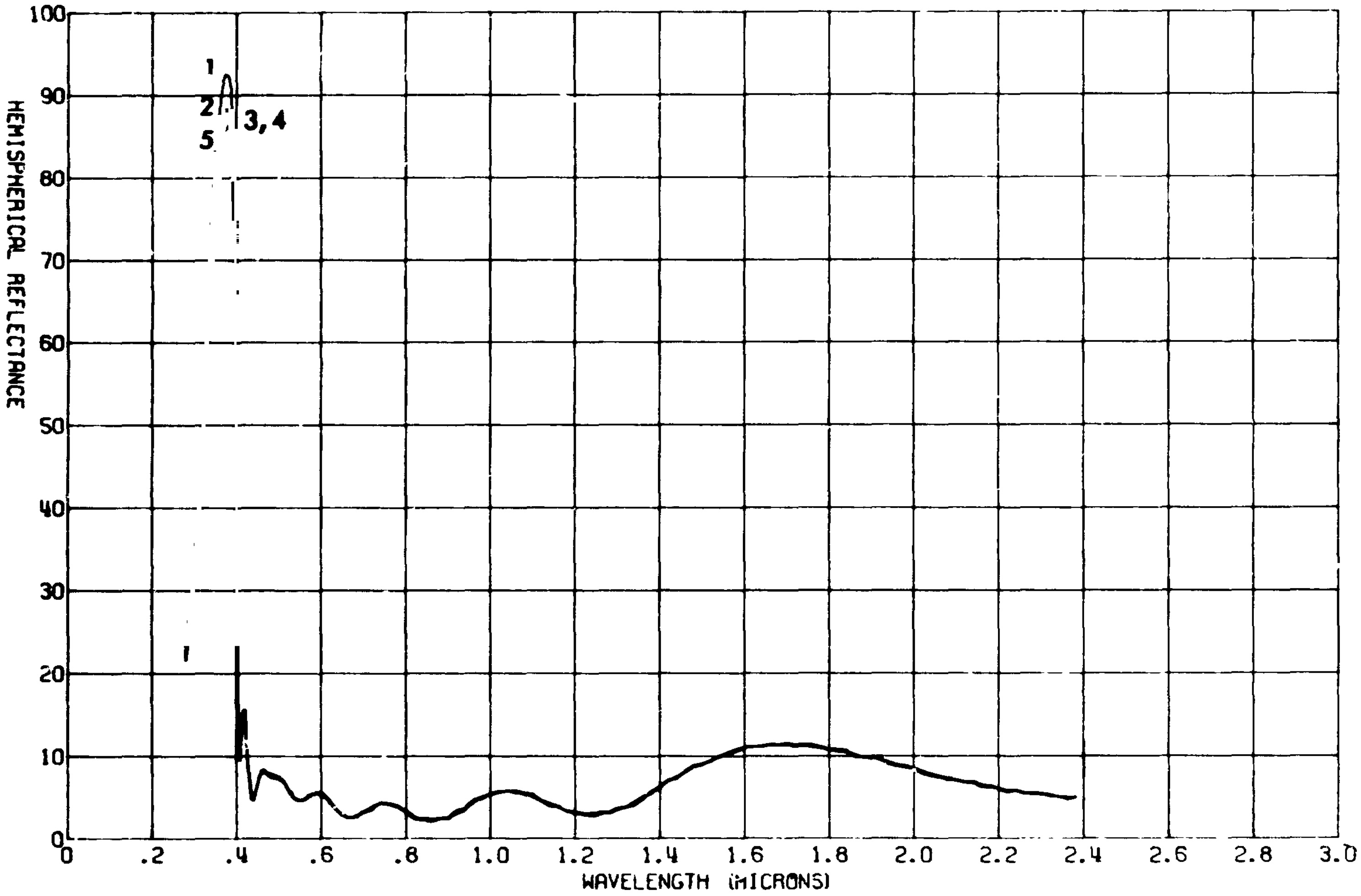

FIGURE 81. IN SITU PROTON-ULTRAVIOLET EFFECTS ON THE REFLECTANCE OF J P L SAMPLE 2044
BLUE FILTER 500-HOUR TEST

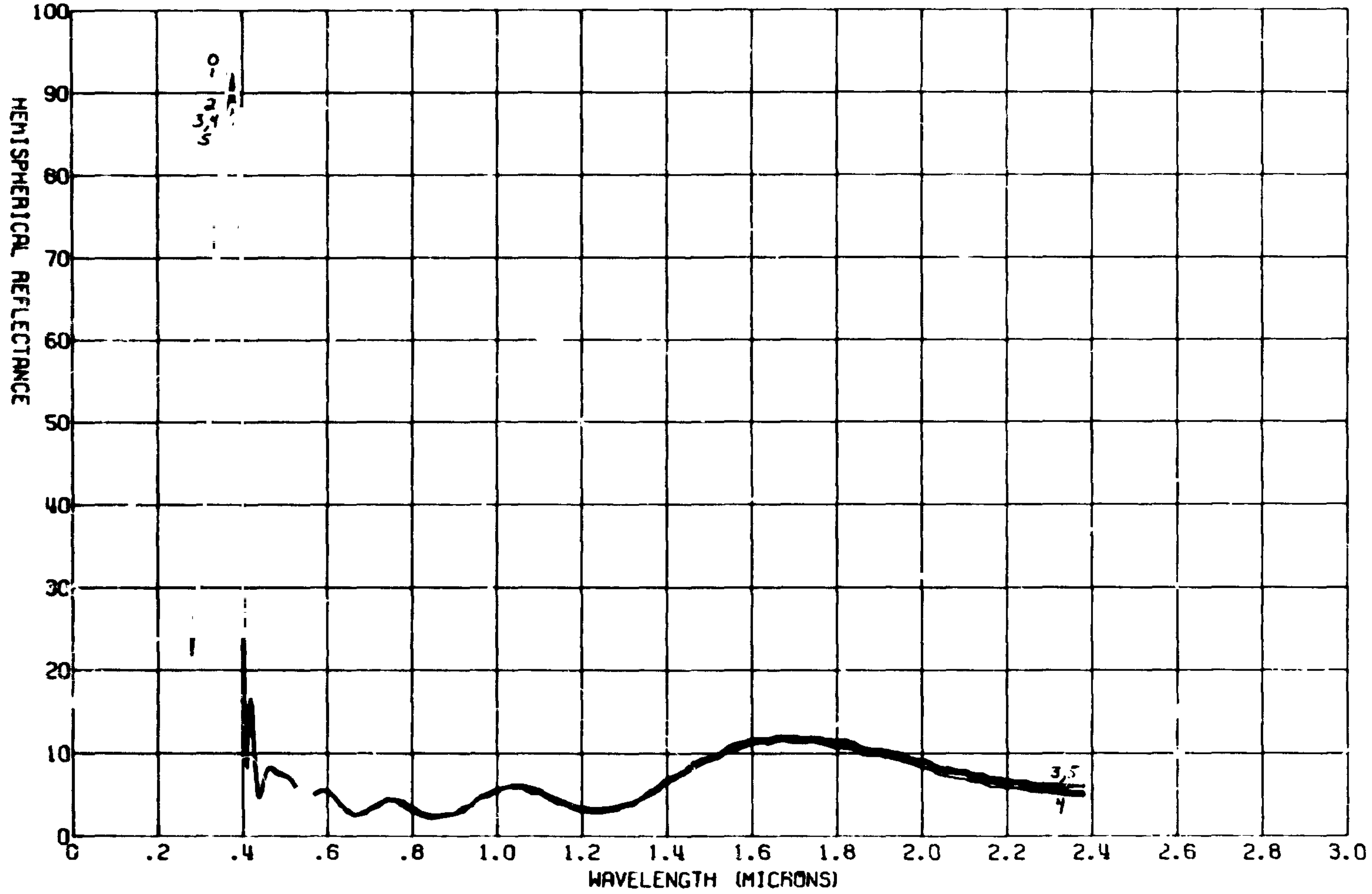

FIGURE 82. IN SITU PROTON EFFECTS ON THE REFLECTANCE OF J P L SAMPLE 2050
BLUE FILTER 500-HOUR TEST

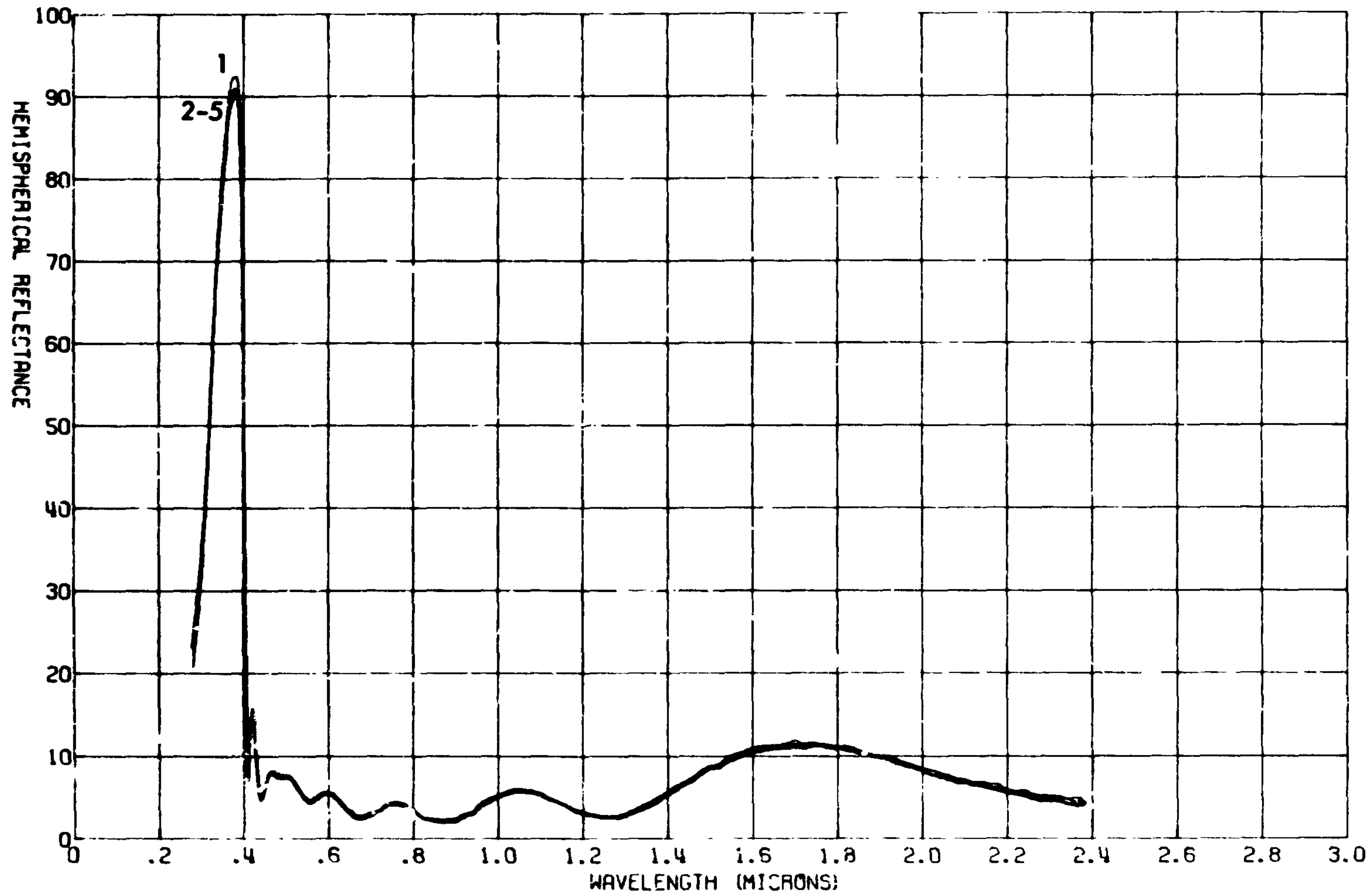

FIGURE 83. IN SITU ULTRAVIOLET EFFECTS ON THE TRANSMITTANCE OF J P L SAMPLE 2038
BLUE FILTER
500-HOUR TEST

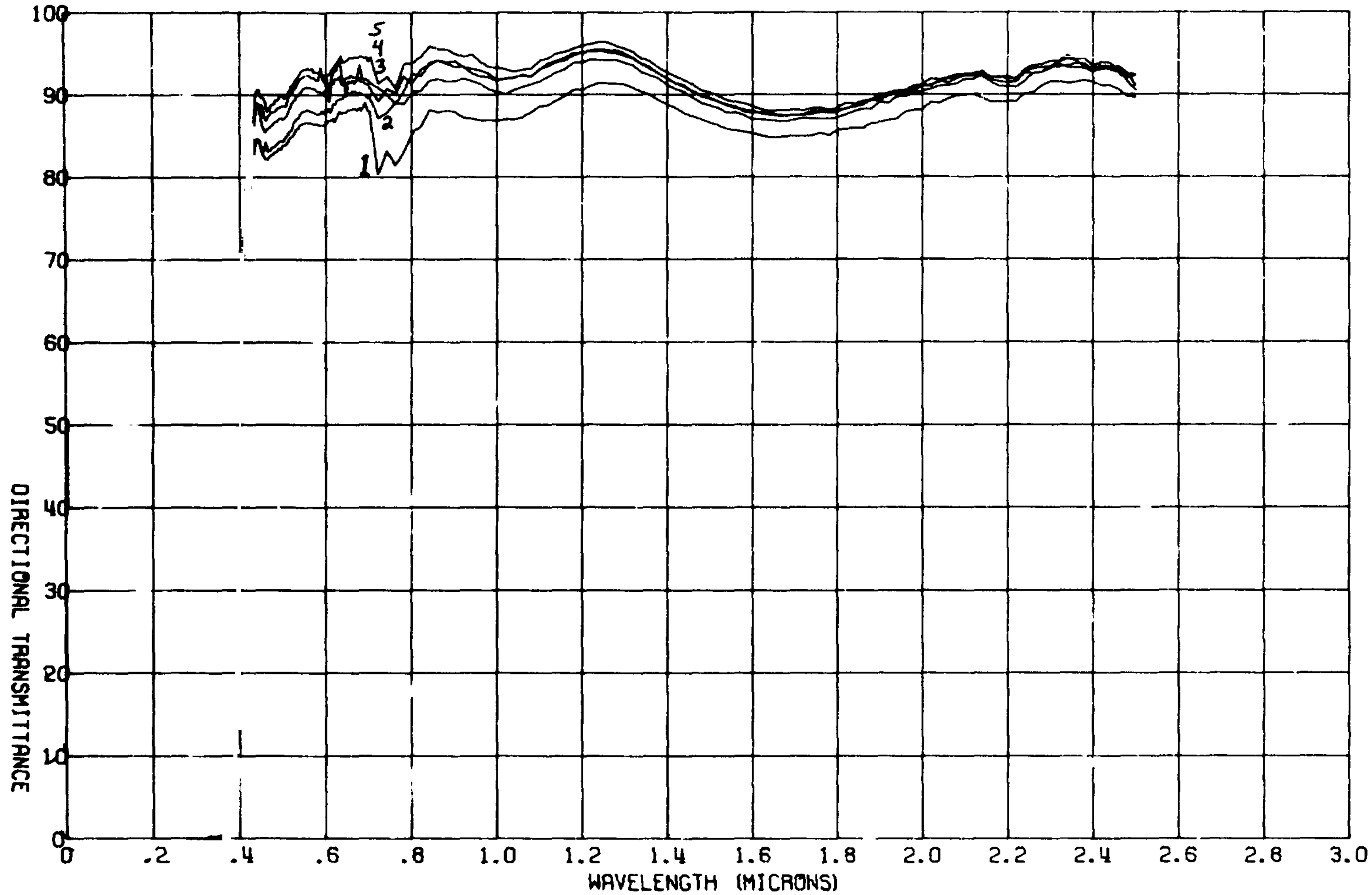

FIGURE 84.

IN SITU PROTON-ULTRAVIOLET EFFECTS ON THE TRANSMITTANCE OF J P L SAMPLE 2044
BLUE FILTER
500-HOUR TEST

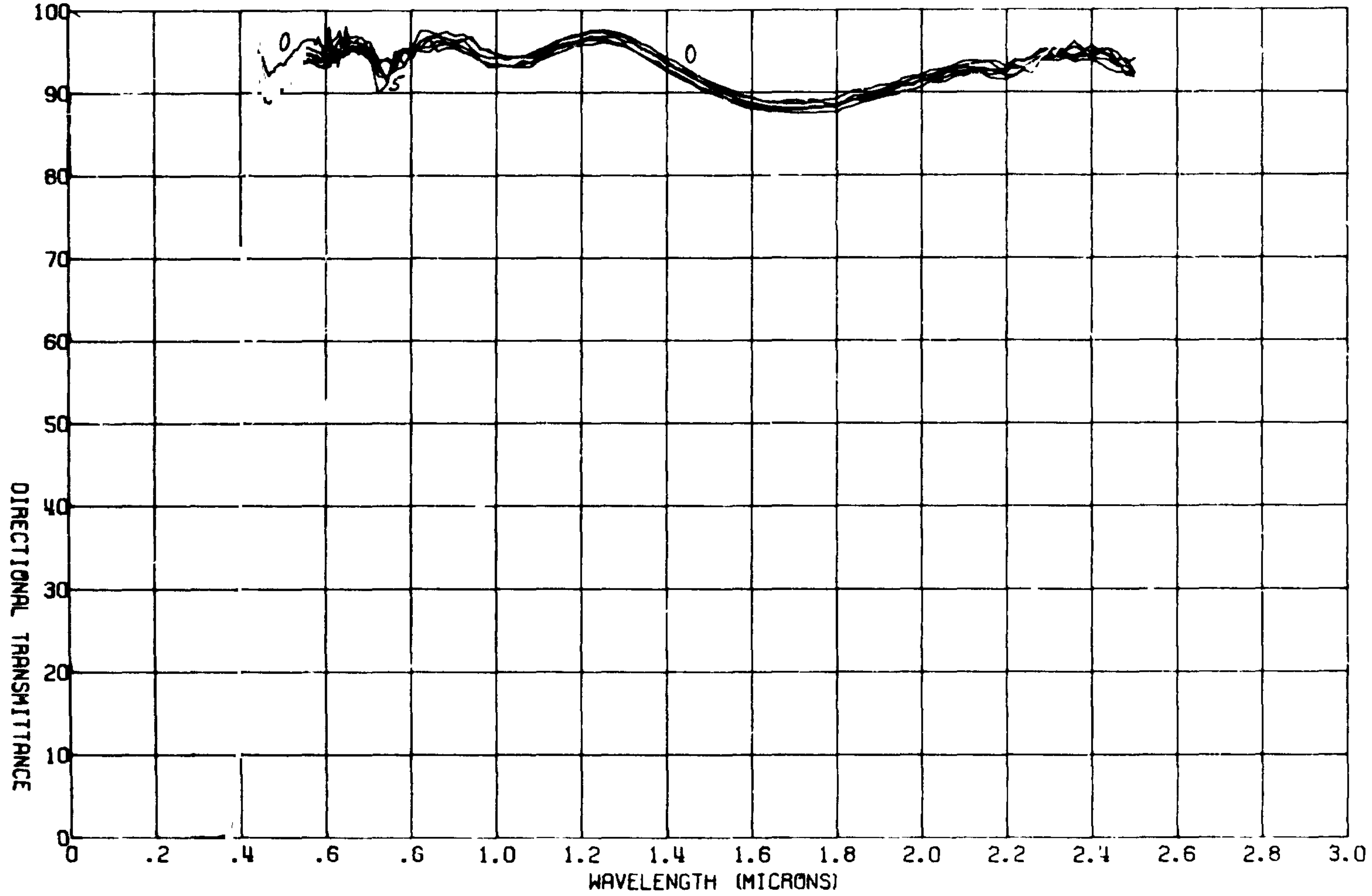

FIGURE 85. IN SITU PROTON EFFECTS ON THE TRANSMITTANCE OF J P L SAMPLE 2050
BLUE FILTER

500-HOUR TEST

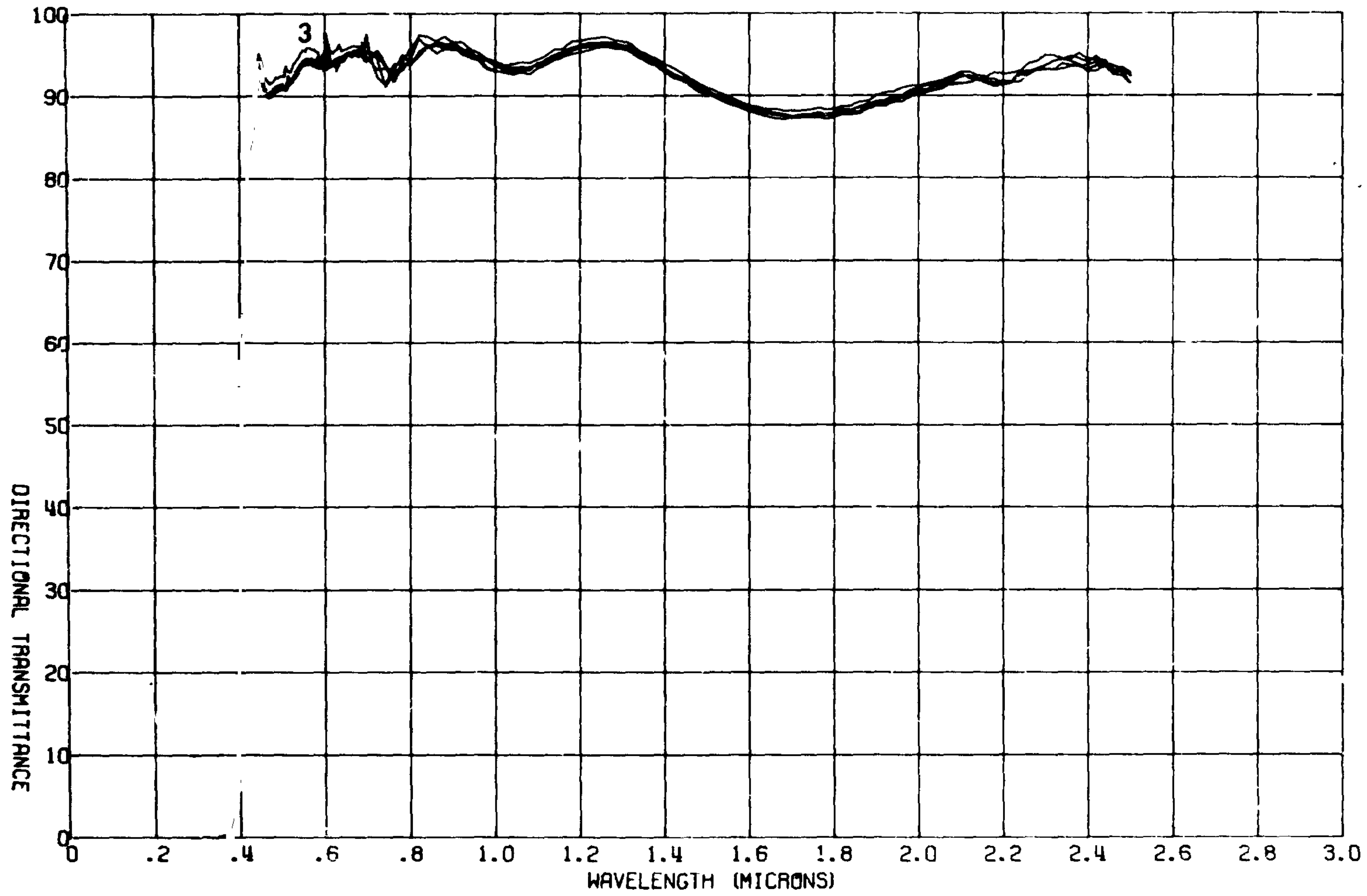

FIGURE 86. IN SITU ULTRAVIOLET EFFECTS ON THE ABSORPTANCE OF J P L SAMPLE 2038
BLUE FILTER
500-HOUR TEST

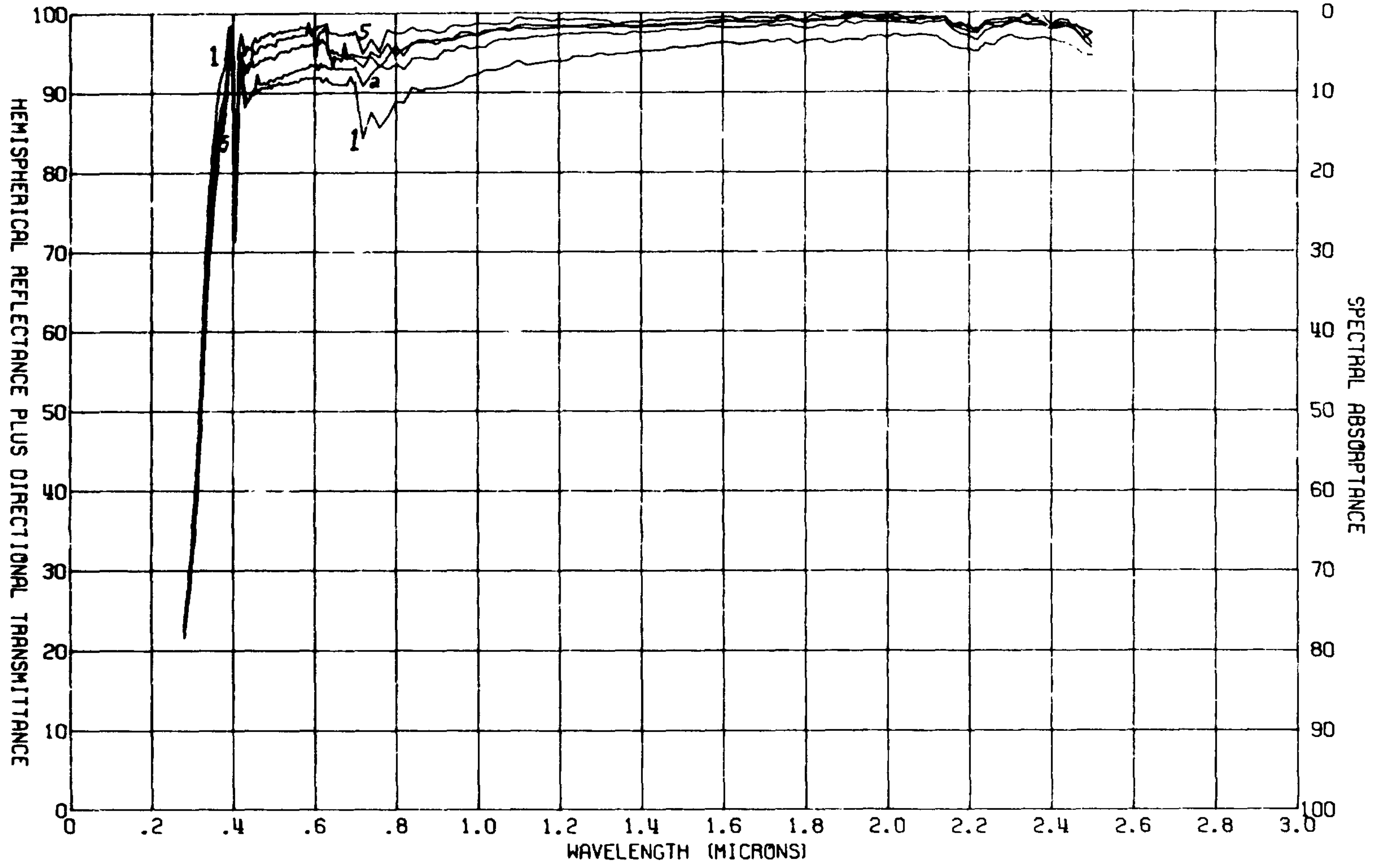

FIGURE 87.

IN SITU PROTON-ULTRAVIOLET EFFECTS ON THE ABSORPTANCE OF J P L SAMPLE 2044
BLUE FILTER
500-HOUR TEST

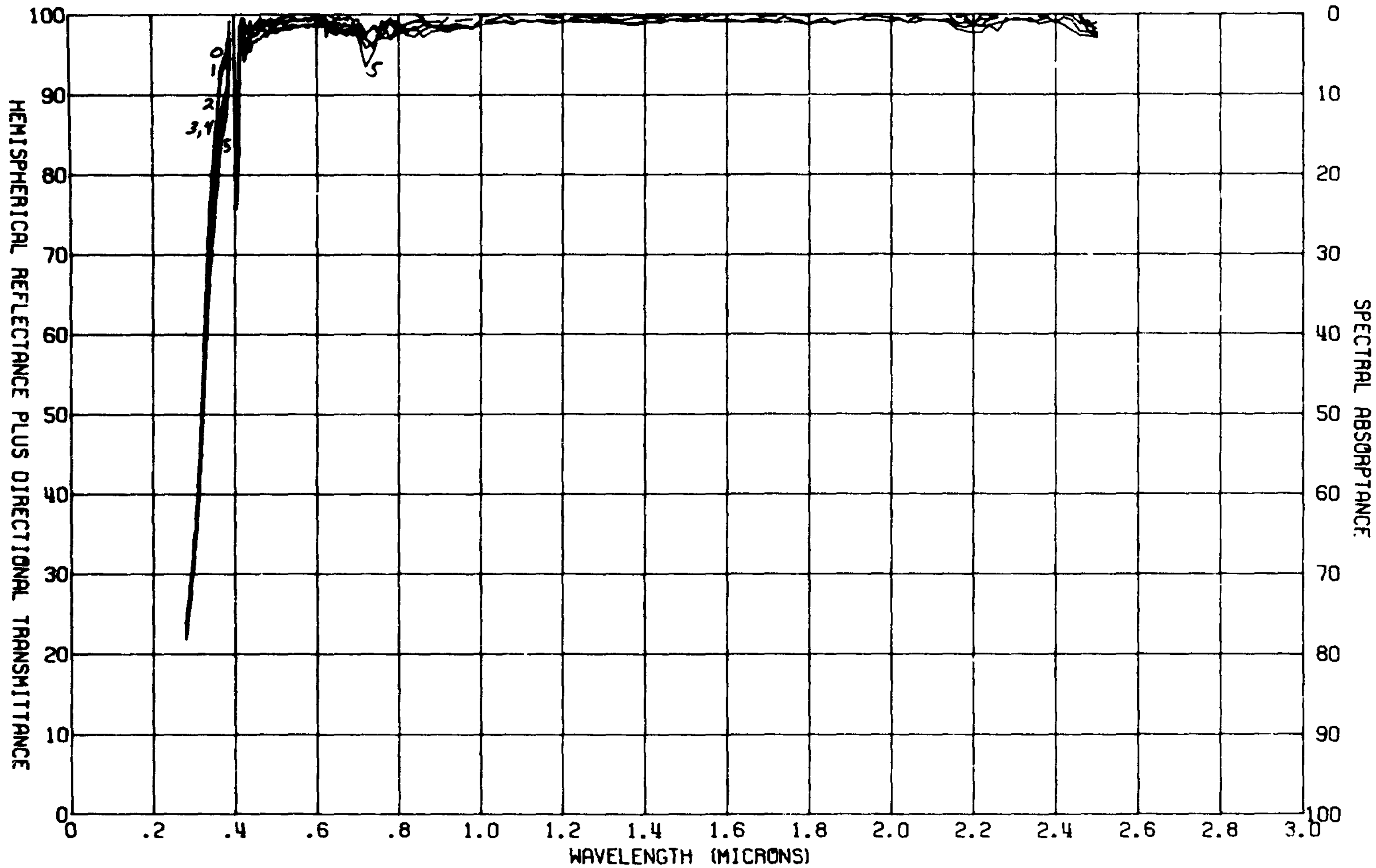

FIGURE 88. IN SITU PROTON EFFECTS ON THE ABSORPTANCE OF J P L SAMPLE 2050
BLUE FILTER
500-HOUR TEST

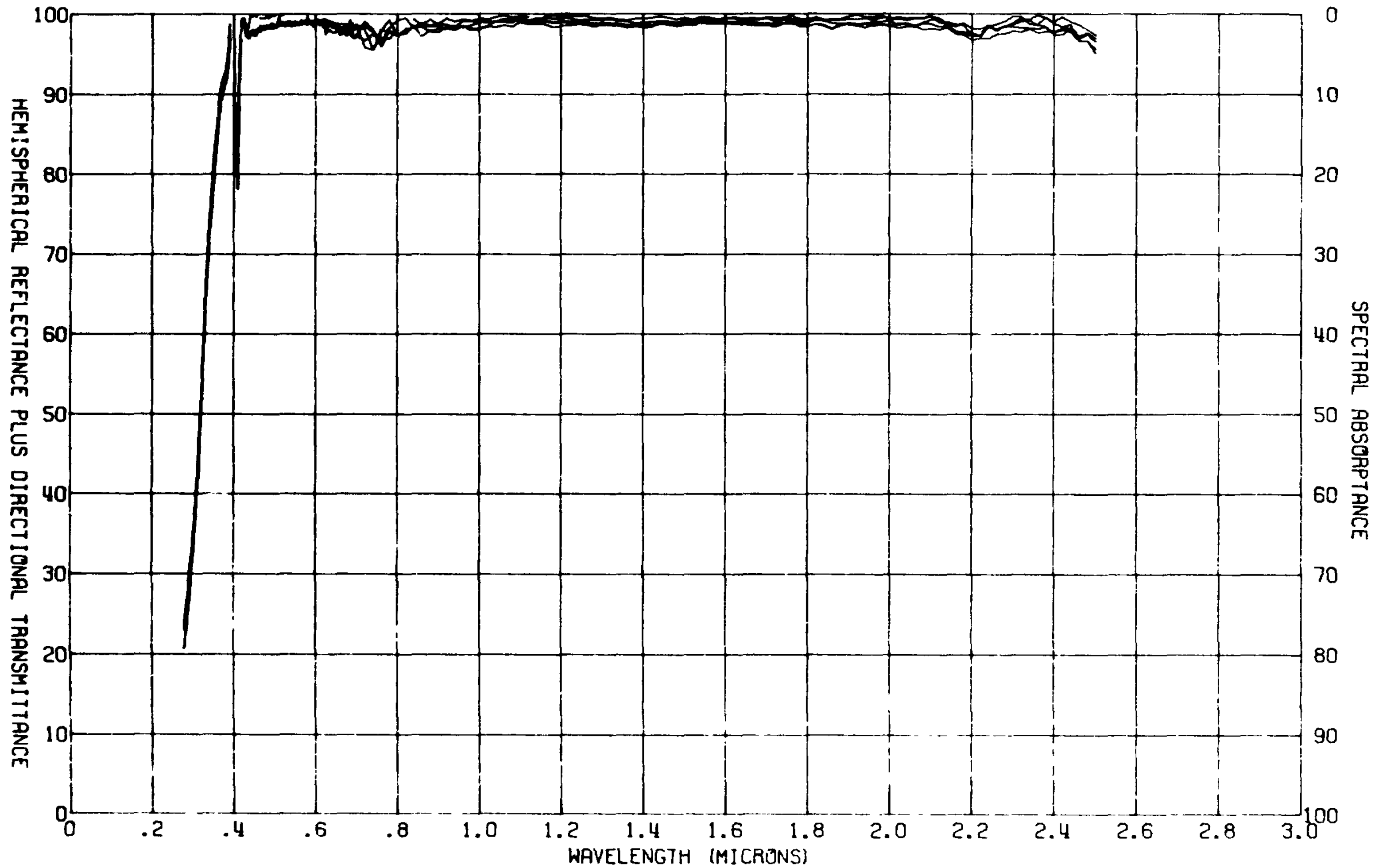

FIGURE 89. IN SITU ULTRAVIOLET EFFECTS ON THE REFLECTANCE OF J P L SAMPLE 2036 SOLAR CELL PLUS TYPE 4026 FILTER

500-HOUR TEST

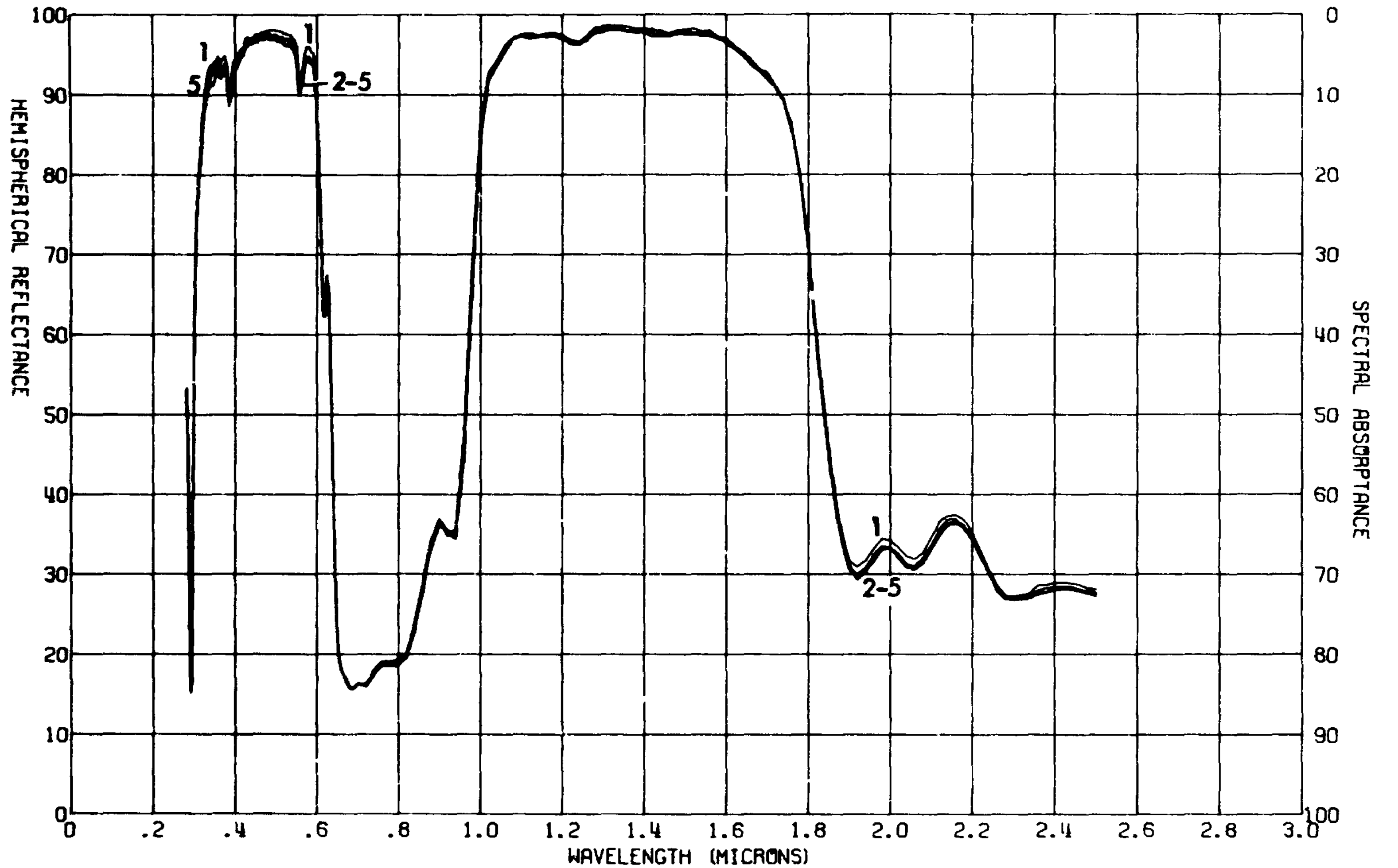

FIGURE 90.

IN SITU PROTON-ULTRAVIOLET EFFECTS ON THE REFLECTANCE OF J P L SAMPLE 2042
SOLAR CELL PLUS TYPE 4026 FILTER

500-HOUR TEST

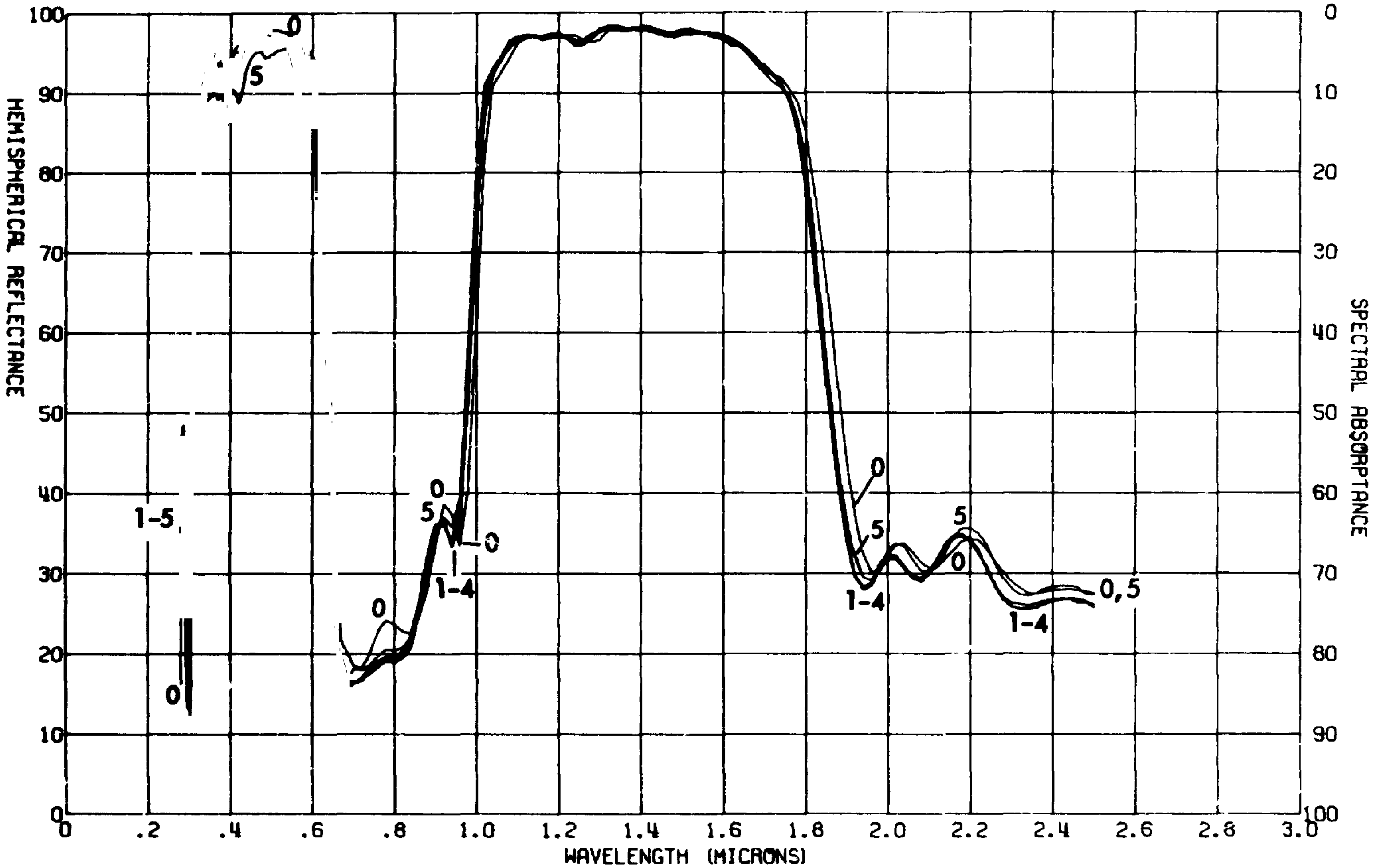

FIGURE 9-1. IN SITU PROTON EFFECTS ON THE REFLECTANCE OF J P L SAMPLE 2048 SOLAR CELL PLUS TYPE 4026 FILTER 500-HOUR TEST

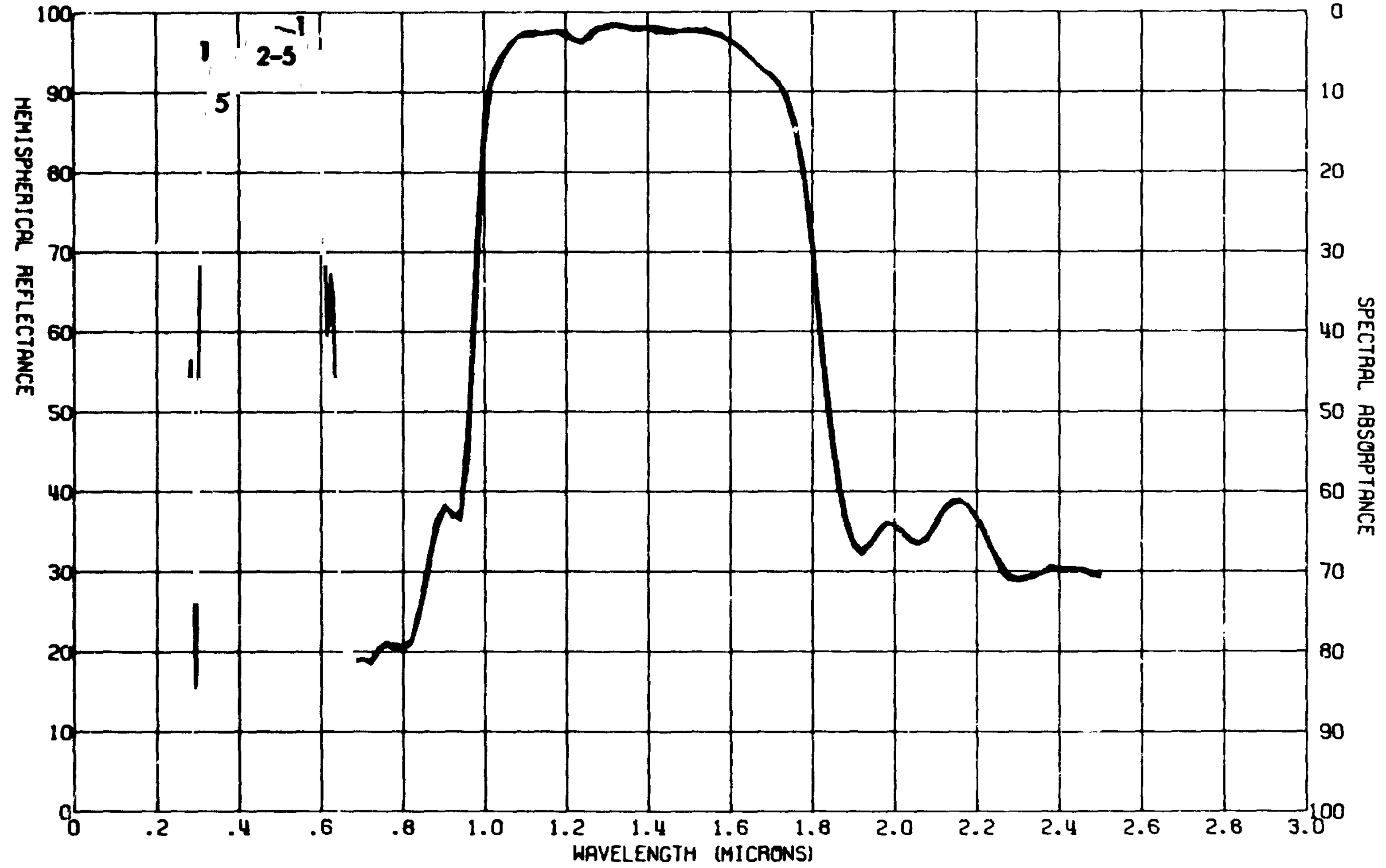

FIGURE 92. IN SITU ULTRAVIOLET EFFECTS ON THE REFLECTANCE OF J P L SAMPLE 2039
TYPE 4026 FILTER
500-HOUR TEST

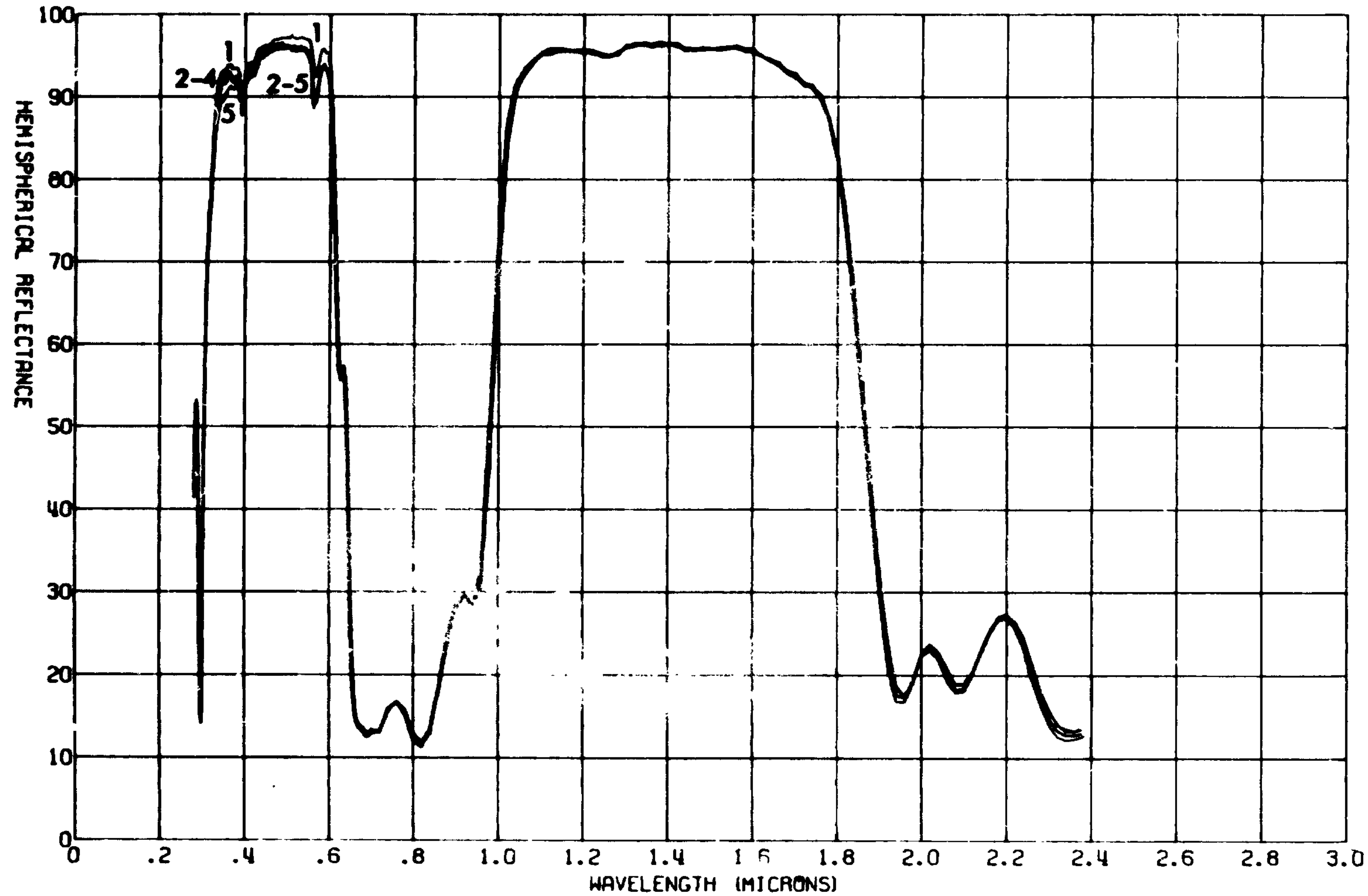

FIGURE 93. IN SITU PROTON-ULTRAVIOLET EFFECTS ON THE REFLECTANCE OF J P L SAMPLE 2045
TYPE 4026 FILTER 500-HOUR TEST

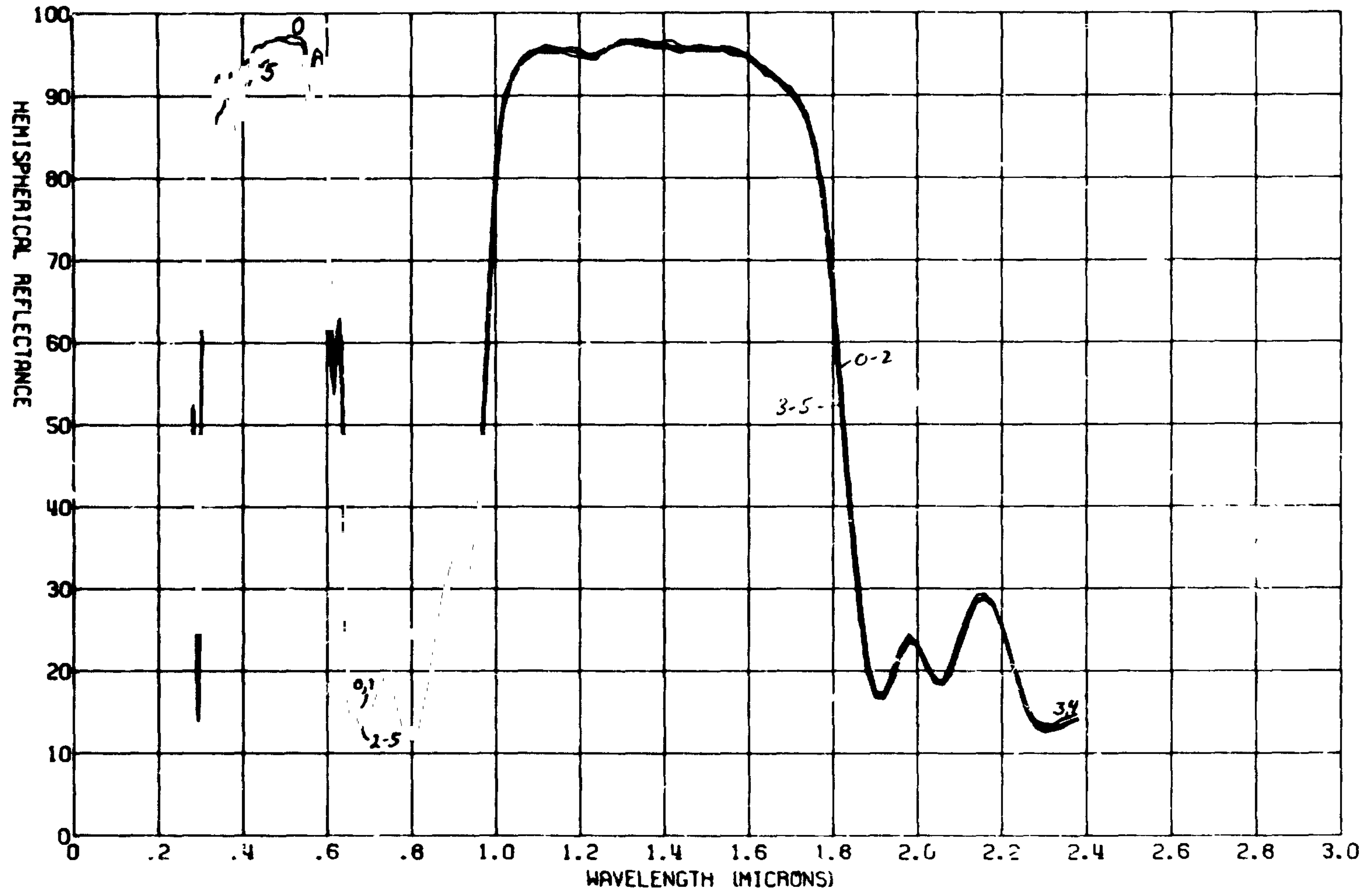

FIGURE 94. IN SITU PROTON EFFECTS ON THE REFLECTANCE OF J P L SAMPLE 2051
TYPE 4026 FILTER 500-HOUR TEST

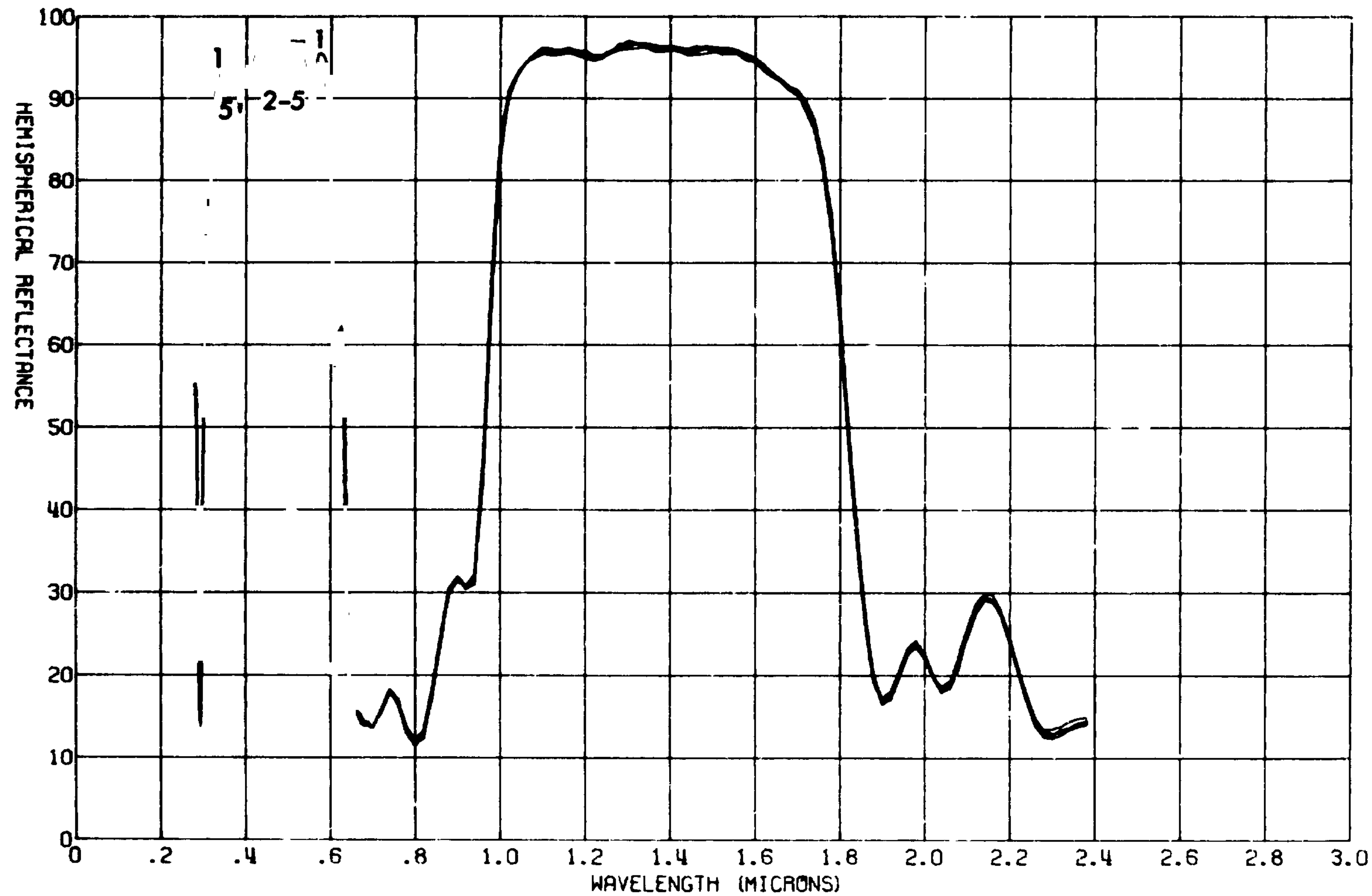

FIGURE 95. IN SITU ULTRAVIOLET EFFECTS ON THE TRANSMITTANCE OF J P L SAMPLE 2039
TYPE 4026 FILTER 500-HOUR TEST

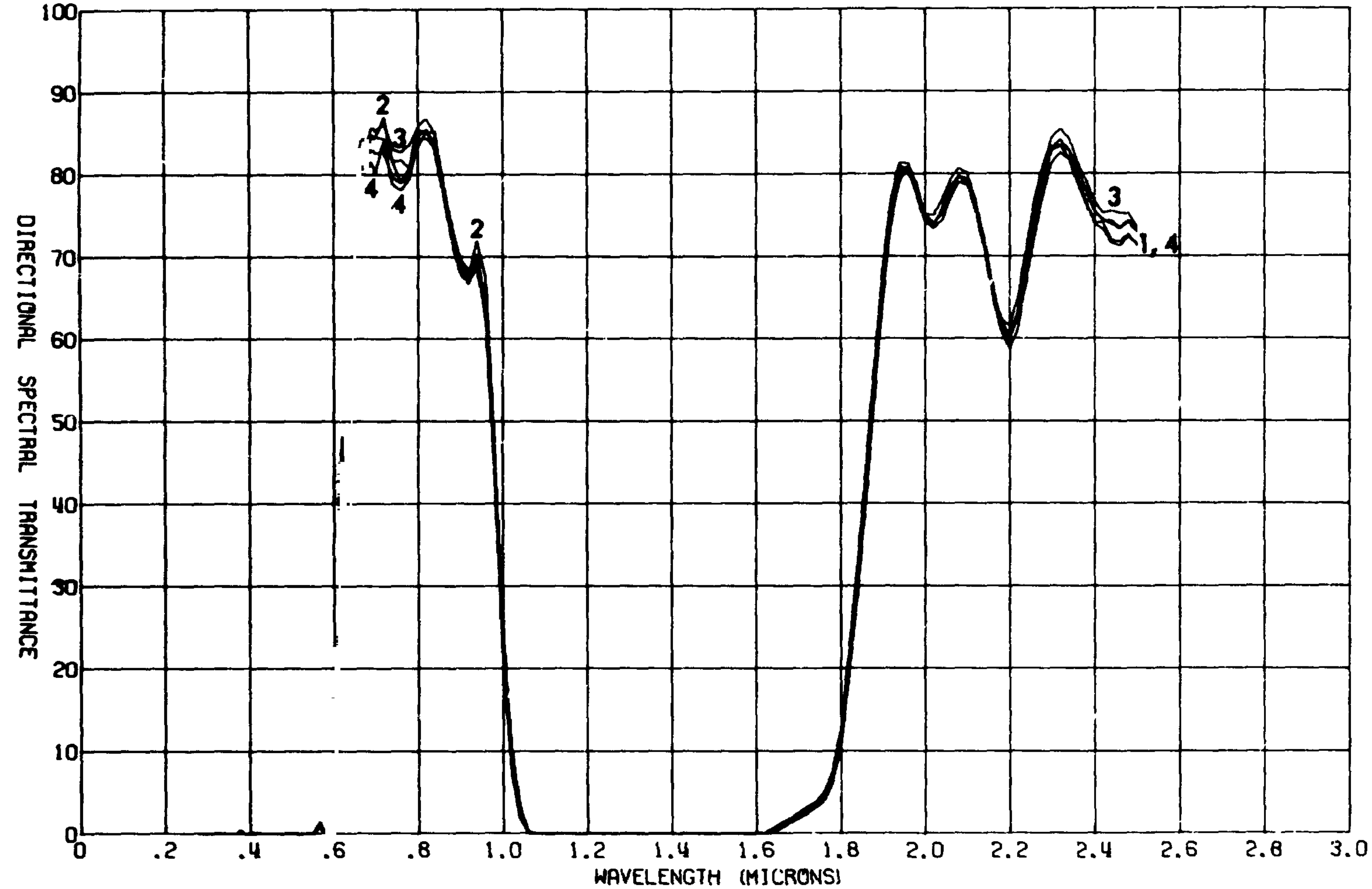

FIGURE 96. IN SITU PROTON-ULTRAVIOLET EFFECTS ON THE TRANSMITTANCE OF J P L SAMPLE 2045 TYPE 4026 FILTER 500-HOUR TEST

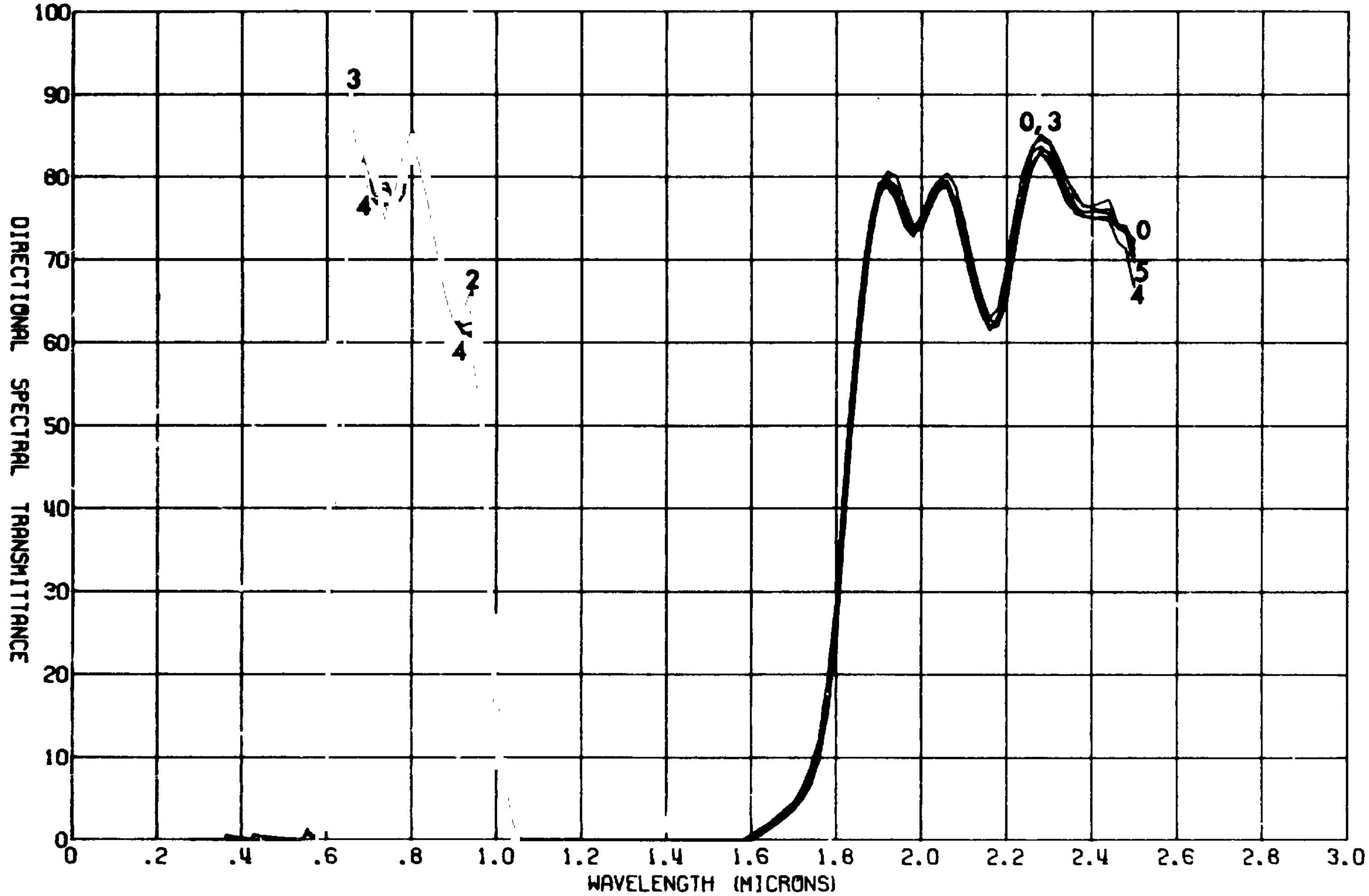

FIGURE 97. IN SITU PROTON EFFECTS ON THE TRANSMITTANCE OF J P L SAMPLE 2051
TYPE 4026 FILTER 500-HOUR TEST

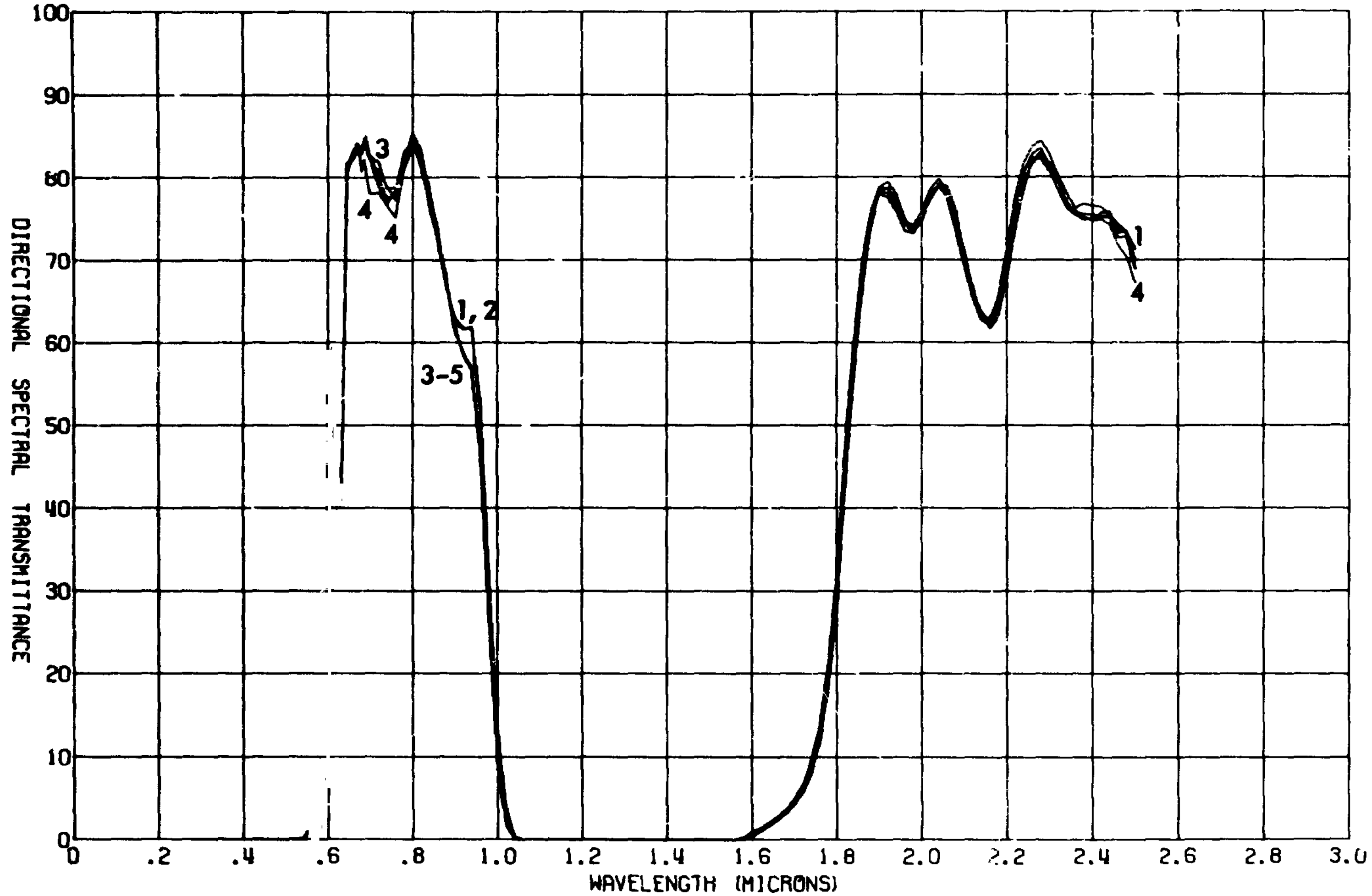

FIGURE 98. IN SITU ULTRAVIOLET EFFECTS ON THE ABSORPTANCE OF J P L SAMPLE 2039
TYPE 4026 FILTER

500-HOUR TEST

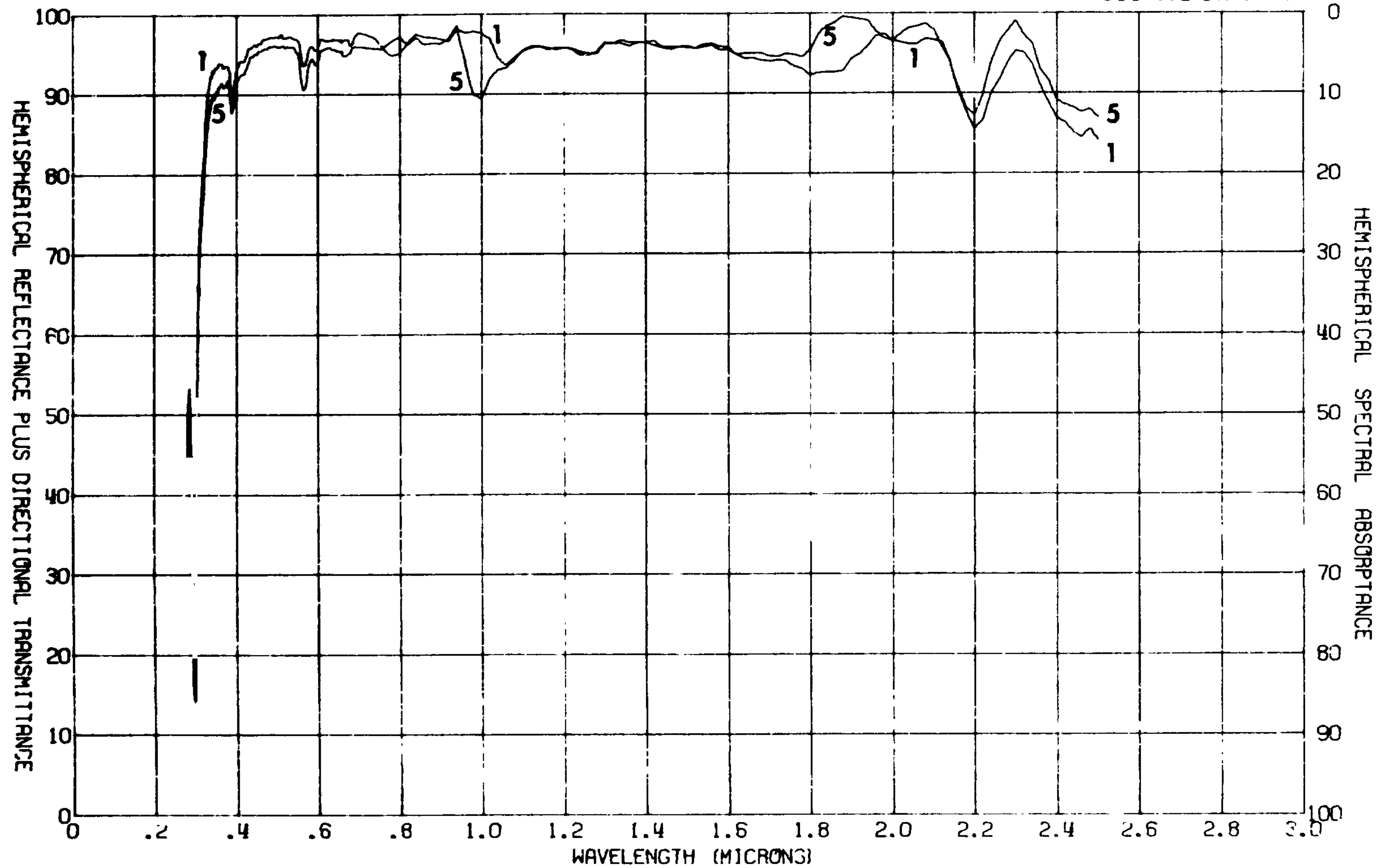

FIGURE 99.

IN SITU PROTON-ULTRAVIOLET EFFECTS ON THE ABSORPTANCE OF J P L SAMPLE 2045
TYPE 4026 FILTER

500-HOUR TEST

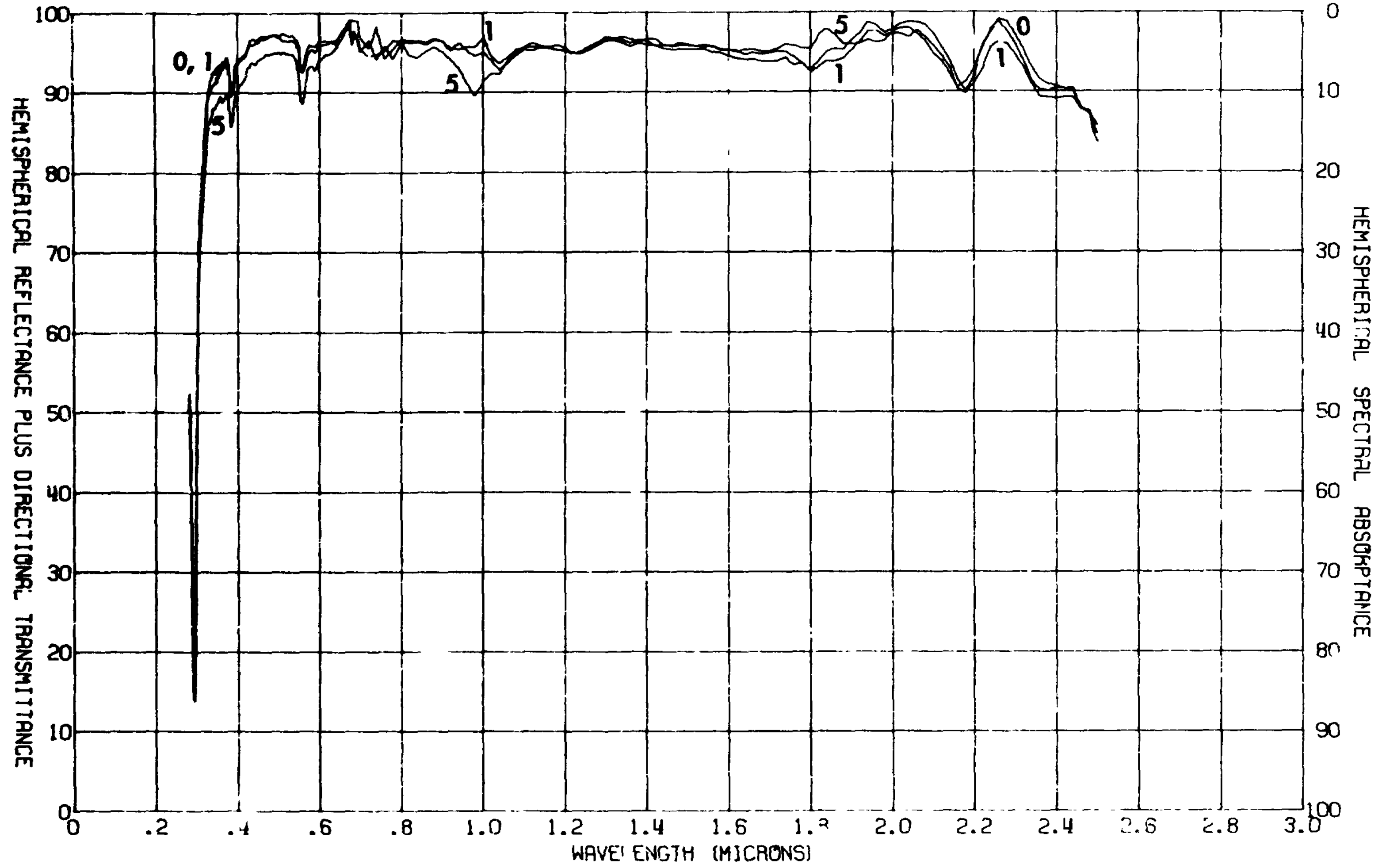

FIGURE 100. IN SITU PROTON EFFECTS ON THE ABSORPTANCE OF J P L SAMPLE 2051 TYPE 4026 FILTER

500-HOUR TEST

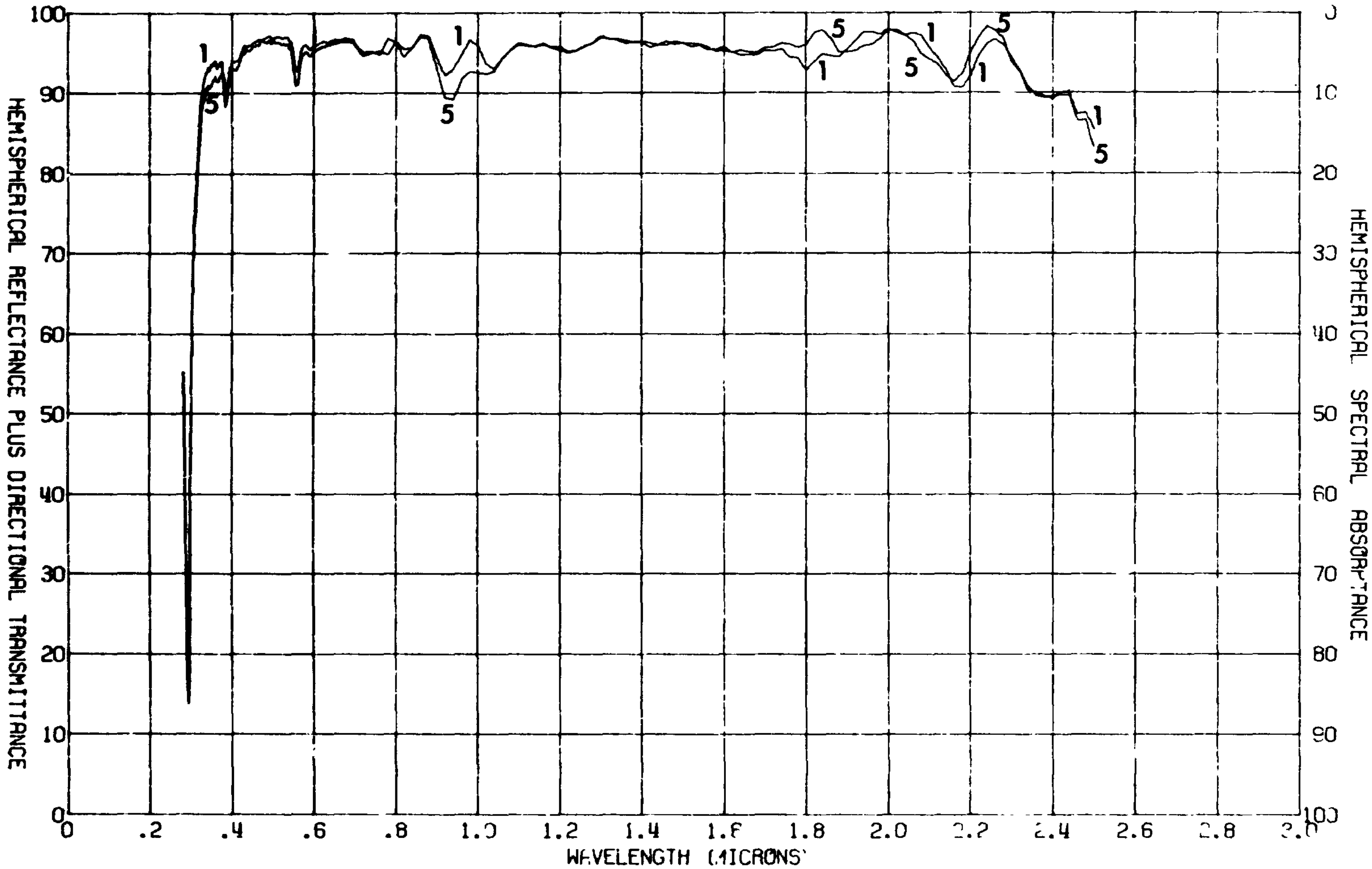

FIGURE 101. IN SITU ULTRAVIOLET EFFECTS ON THE REFLECTANCE OF J P L SAMPLE 2040 SOLAR CELL PLUS BLUE/RED FILTER

500-HOUR TEST

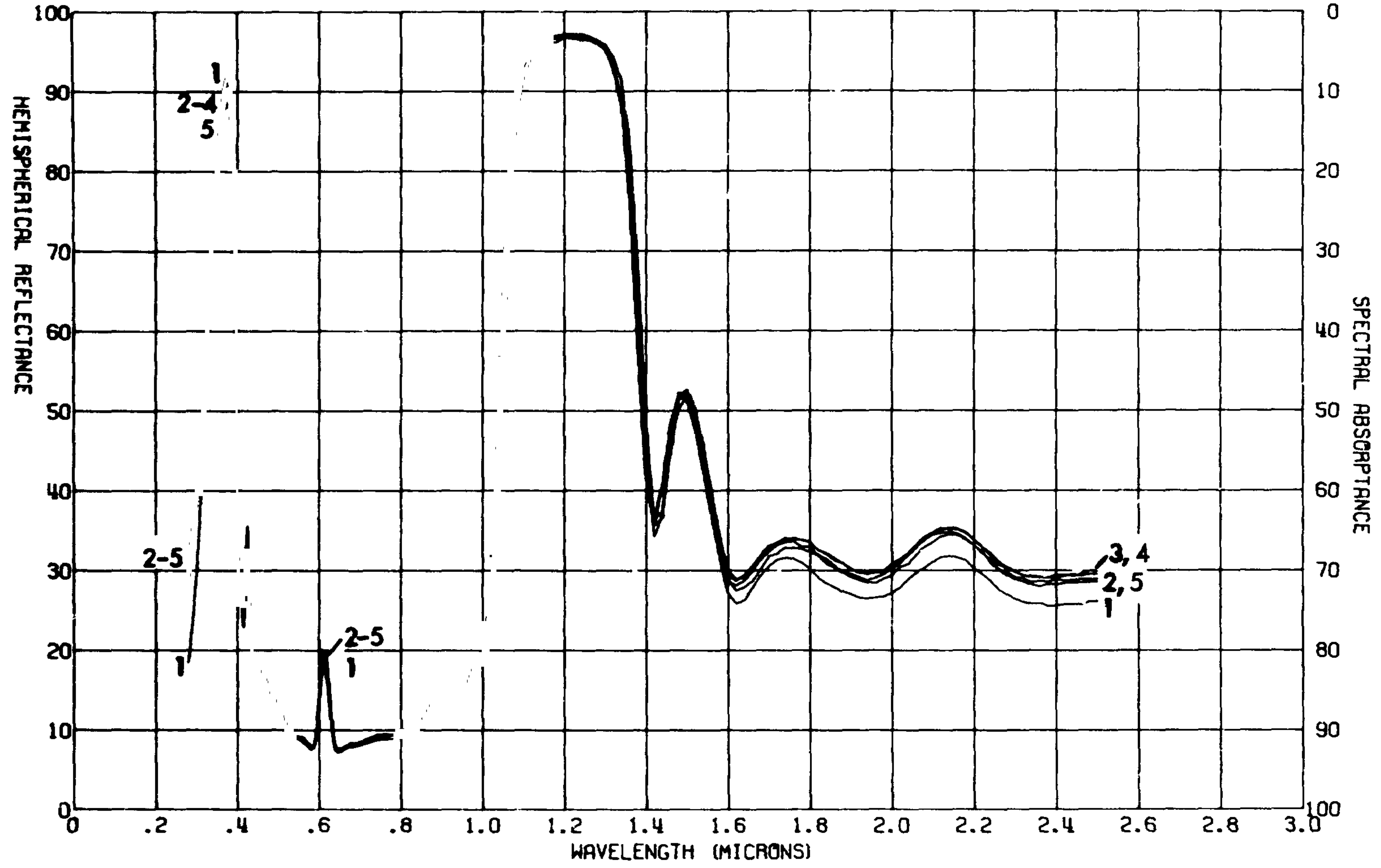

FIGURE 102.

IN SITU PROTON-ULTRAVIOLET EFFECTS ON THE REFLECTANCE OF J P L SAMPLE 2046
SOLAR CELL PLUS BLUE/RED FILTER

500-HOUR TEST

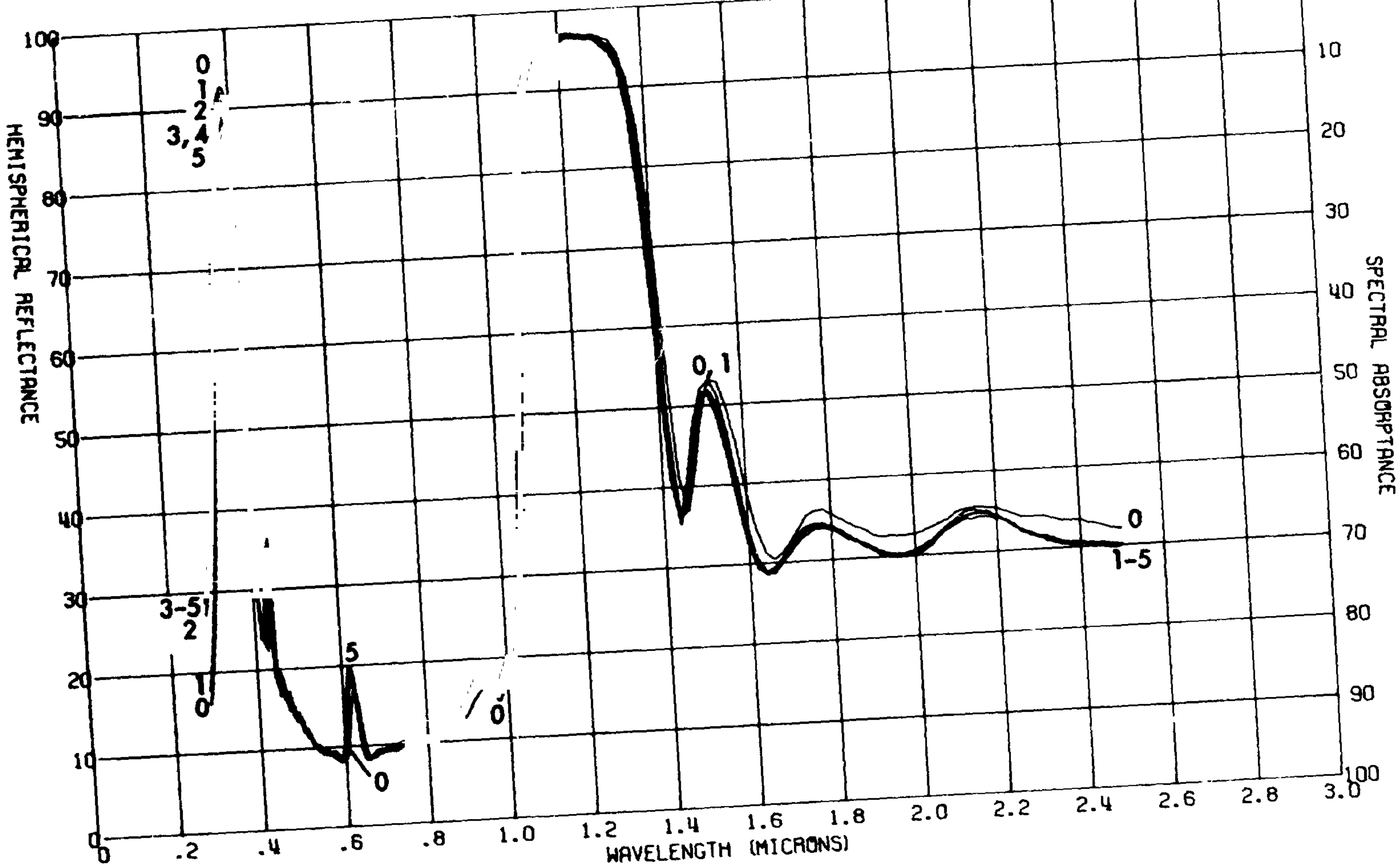

FIGURE 103. IN SITU PROTON EFFECTS ON THE REFLECTANCE OF J P L SAMPLE 2052
SOLAR CELL PLUS BLUE/RED FILTER
500-HOUR TEST

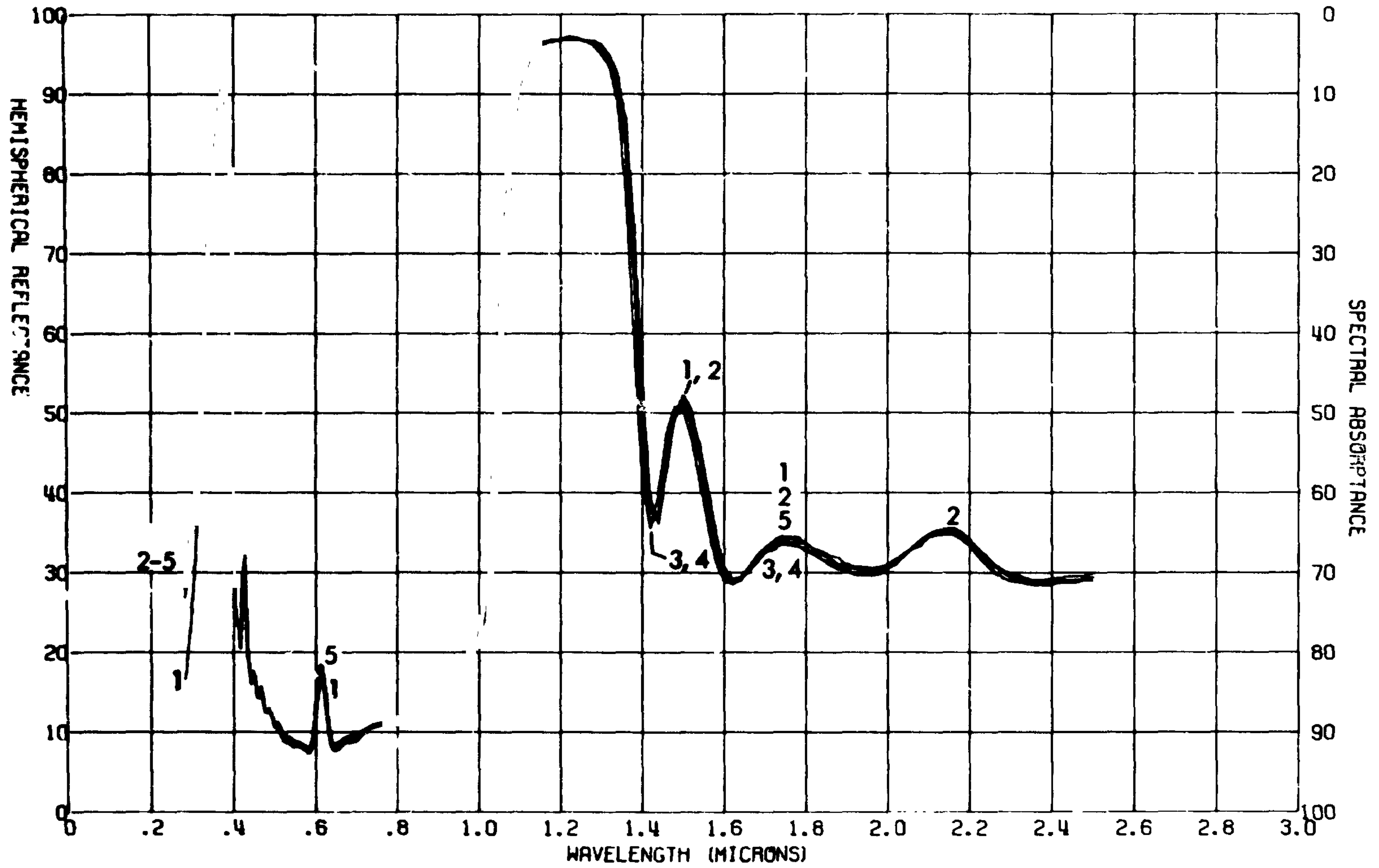

FIGURE 104. IN SITU ULTRAVIOLET EFFECTS ON THE REFLECTANCE OF J P L SAMPLE 2037
BLUE/RED FILTER - ADHESIVE - POLISHED ALUMINUM SUBSTRATE 500-HOUR TEST

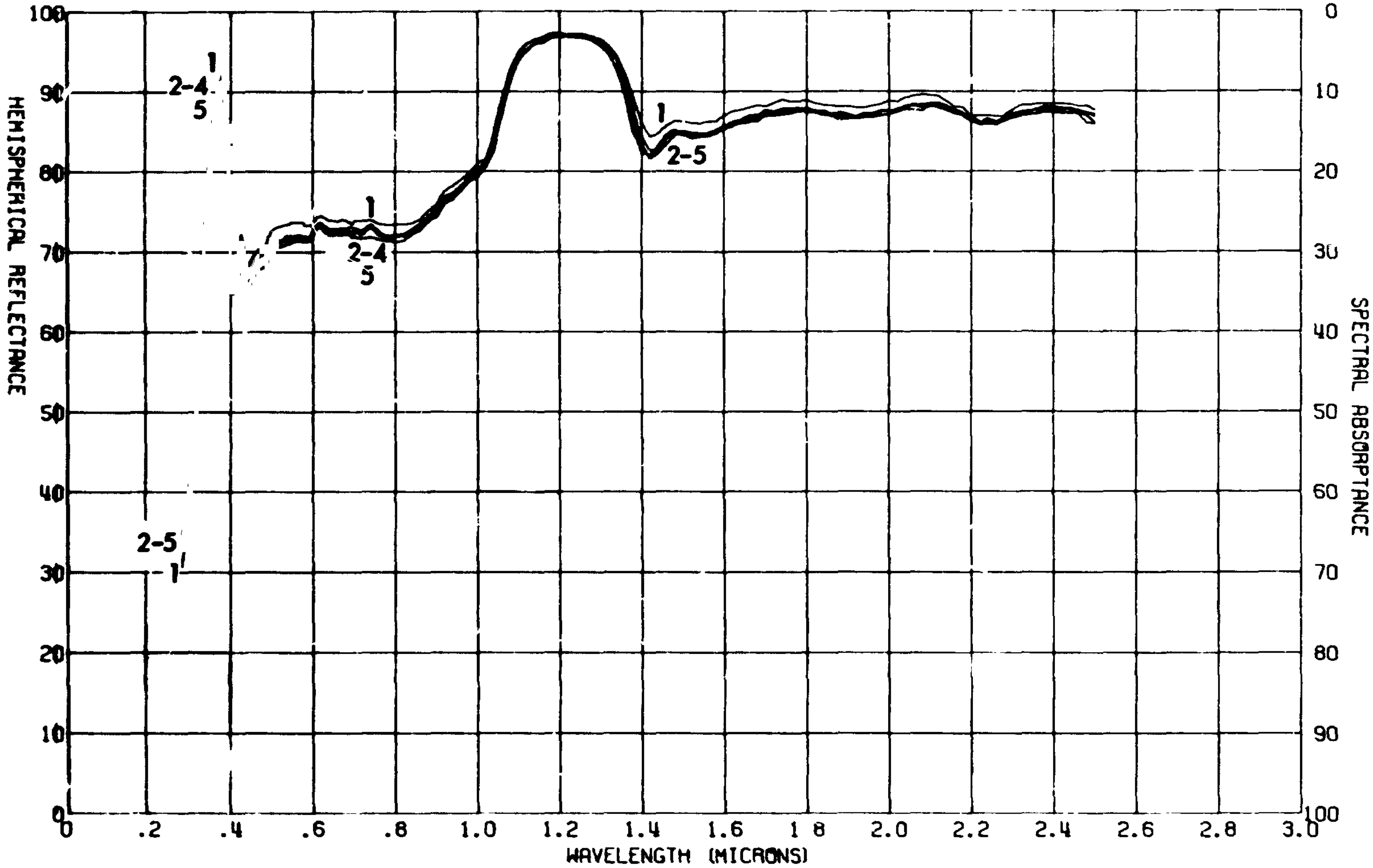

FIGURE 105.

IN SITU PROTON-ULTRAVIOLET EFFECTS ON THE REFLECTANCE OF J P L SAMPLE 2043

BLUE/RE FILTER - ADHESIVE - POLISHED ALUMINUM SUBSTRATE

500-HOUR TEST

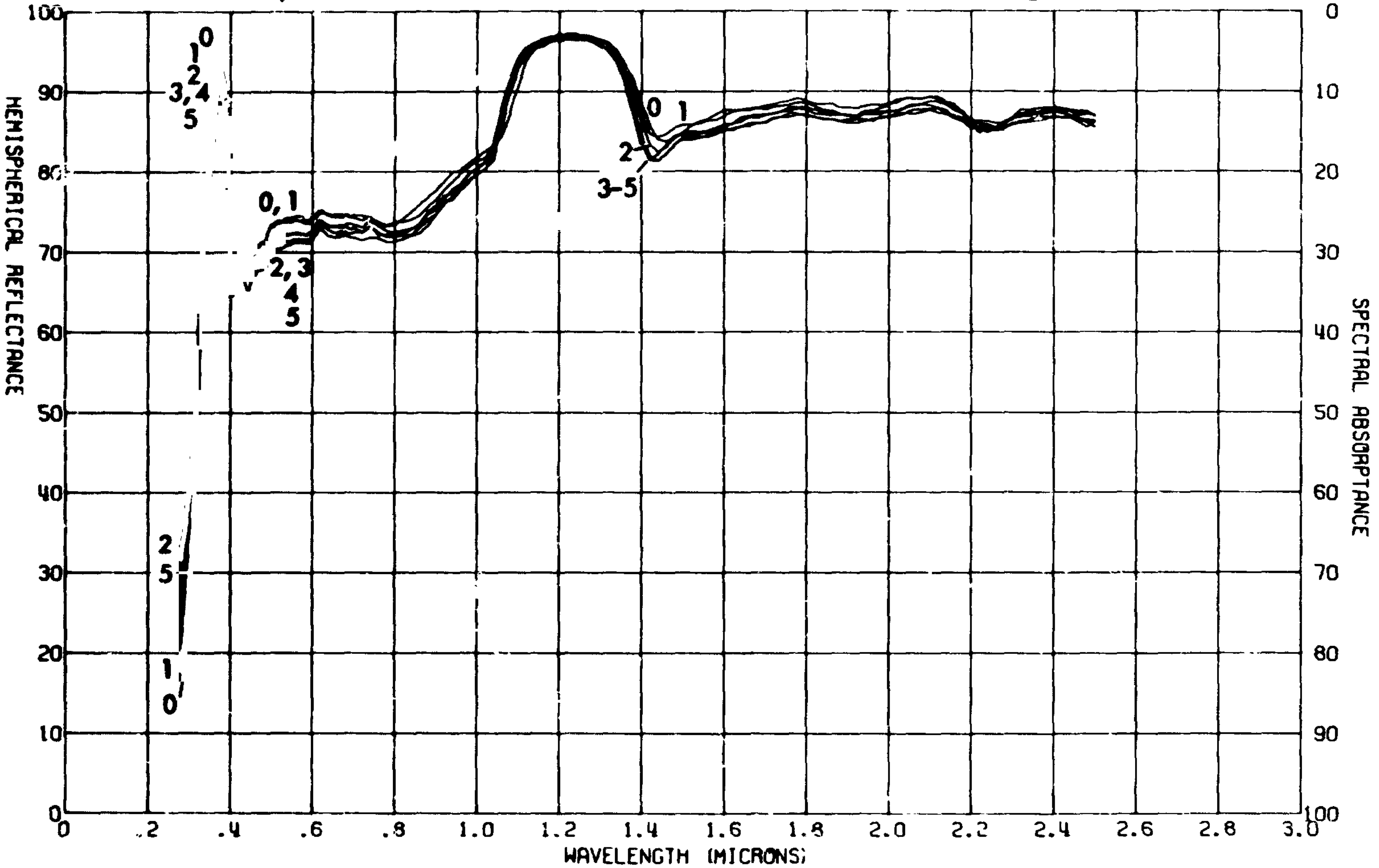

FIGURE 106. IN SITU PROTON EFFECTS ON THE REFLECTANCE OF J P L SAMPLE 2049

BLUE/RED FILTER - ADHESIVE - POLISHED ALUMINUM SUBSTRATE

500-HOUR TEST

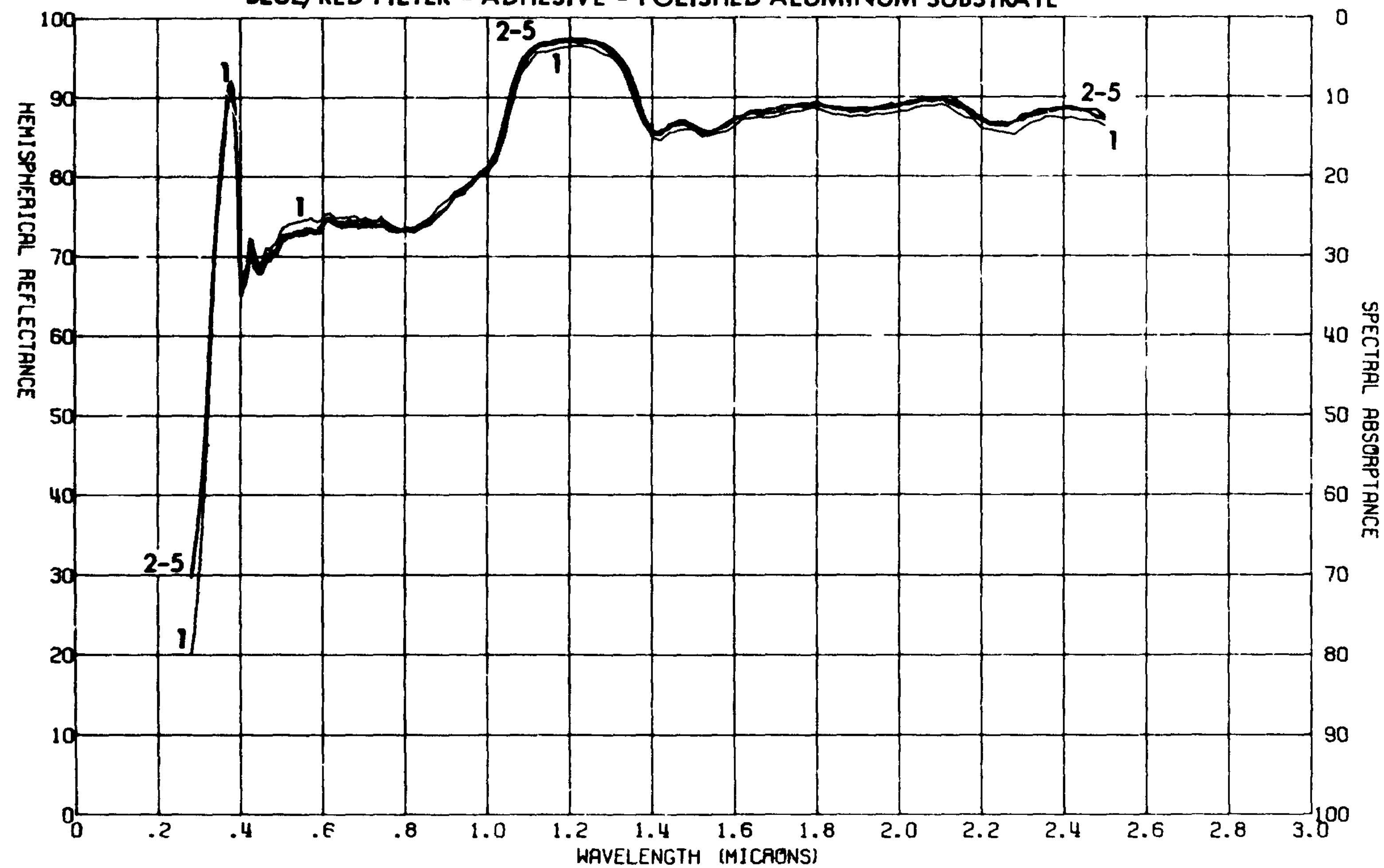

REFERENCES

1. Ross, Ronald G., Jr., "Solar-Panel Approaches for a Venus-Mercury Flyby", JPL paper presented at the Space Technology and Heat Transfer Conference, Los Angeles, June, 1970.

2. D. D. Abbott and R. R. Brown, "Experimental Results of Radiation Damage in Solar Cells", Boeing Document D2-36222-1, March, 1967.

3. A. C. Wilbur and D. L. Anderson, "An Exploratory Study of the Interplanetary Environmental Effects on Solar-Cell Cover Glasses", Conference Record of the Seventh Photovoltaic Specialists Conference, IEEE, November, 1968.

4. L. B. Fogdall and S. S. Cannaday, "Ultraviolet and Electron Radiation Effects on Reflectance and Emittance Properties of Thermal Control Coatings", Final Report AFML_TR-70-156, July, 1970.

5. L. B. Fogdall and S. S. Cannaday, "Proton and Electron Effects in Thermal Control Materials", Final Report for NASA-Goddard Contract NAS5-11219, May, 1970.

6. L. B. Fogdall, S. S. Cannaday, F. D. Reinke, and B. K. Madaras, "Experimental Study of Effects of Simulated Neutralized Solar Wind on White-Pigment Thermal Control Coatings", NASA CR 73389. Final Report for NASA-Ames Contract NAS2-5343, October, 1969.

BIBLIOGRAPHY

"Venus-Mercury Flyby Solar Cell Stack", D. D. Abbott and H. Oman, The Boeing Company. Final Report for JPL Program HF 525903, July, 1970.

Physics of Thin Films, Vol. 5, ed. Georg Hass and Rudolf E. Thun. New York: Academic Press, 1969.

"Optical Interference Coatings", P. Baumeister and G. Pincus. Scientific American, December, 1970.